Design, synthesis and evaluation of covalent inhibitors for tissue transglutaminase and factor XIIIa

Abdullah Akbar

A thesis submitted in partial fulfillment

of the requirements for the

Doctorate in Philosophy degree in

Bioorganic and Medicinal Chemistry

Department of Chemistry and Biomolecular Sciences

Faculty of Science

University of Ottawa

May, 2019

Abstract

Transglutaminases are a family of enzymes expressed in various tissues of our body. Some are expressed ubiquitously while others are specific to a tissue. Their primary catalytic activity is to crosslink substrates via an isopeptidic bond. The work described in this thesis focuses on two of these transglutaminases; human tissue transglutaminase (hTG2) and human factor XIIIa (FXIIIa). Divided into two projects for each enzyme, the main objective of this thesis was directed towards the discovery of potent and selective covalent inhibitors for each isozyme, namely hTG2 and hFXIIIa.

The first project was concentrated on the inhibition of hTG2 activity. Ubiquitously expressed in tissues, hTG2 is a multifunctional enzyme. Its primary activity is the formation of isopeptide bonds between glutamine and lysine residues found on the surface of proteins or substrates. In addition to its catalytic activity, hTG2 is also a G-protein, distinguishing it from other members of the transglutaminase family. Much evidence illustrates that hTG2's multifunctional abilities are conformationally regulated between its "open" and "closed" forms. Overexpression and unregulated hTG2 activity has been associated with numerous human diseases; however, most evidence has been collected for its association with fibrosis and celiac sprue. More recently, elevated hTG2 expression has been linked to cancer stem cell survival and metastatic phenotype in certain cancer cells. These findings call for the development of suitable and potent inhibitors that selectivity inactivate human hTG2 as a potential therapeutic target. Starting with previously designed acrylamide based peptidomimetic irreversible inhibitors, a structure-activity relationship (SAR) study was conducted. In this work, >20 novel irreversible inhibitors were prepared and kinetically evaluated. Our lead inhibitors allosterically inhibited GTP binding by locking the enzyme in its open conformation, as demonstrated both *in vitro* and

in cells. Furthermore, our most potent and efficient irreversible inhibitors revealed selectivity for hTG2 over other relevant members of the transglutaminase family (hTG1, hTG3, hTG6 and hFXIIIa), providing higher confidence towards our goal of developing an ideal drug candidate.

The second project was concentrated on the inhibition of hFXIIIa activity. In the blood, coagulation factor XIII (FXIII) is a tetrameric protein consisting of two catalytic A subunits (FXIII-A_2) and two carrier/inhibitory B (FXIII-B_2) subunits. It is a zymogen, which is converted into active transglutaminase (FXIIIa) in the final phase of coagulation cascade by thrombin proteolytic activity and Ca^{2+} binding. hFXIII is essential for hemostasis and thus its deficiency results in severe bleeding conditions. Further, hFXIIIa mechanically stabilizes fibrin and protects it from fibrinolysis. Due to the enzyme's involvement in the stability of blood clots, inhibition of hFXIIIa activity has been linked to thrombotic diseases. Furthermore, inhibitors of the enzyme have the therapeutic potential to be used as anticoagulant agents. The current number of selective and potent inhibitors of hFXIIIa are few, mainly due to the similarity between its catalytic pockets and hTG2. Inspired by a poorly reactive hTG2 inhibitor discovered in this work's hTG2 SAR study, we synthesized a small library of covalent inhibitors for hFXIIIa. Our kinetic results from this pioneering SAR study will pave the way for future hFXIIIa inhibitor SAR studies.

Keywords: transglutaminase, enzyme kinetics, isozyme selectivity, irreversible inhibition, covalent inhibition, acrylamide warheads, SAR study

Acknowledgements

To start, my gratitude is genuinely extended to my brilliant supervisor and mentor, Professor Jeffrey Keillor. The knowledge he shared was invaluable and I am enormously grateful for his consistent guidance. Beyond his intellect and amusing humor, Jeff offered his patience and understanding to ensure my mental, financial and physical well-being was never at risk. The memories we made during our professional and personal growth will always remain close to me.

My thanks further extend to the past and present members of the Keillor group that have overlapped with my time. Thank you for always finding the time in your day to help me and for making our lab such an enjoyable place to work. To the pioneering postdoctoral fellows of my work, Christophe Pardin and Christopher Clouthier, thank you for your significant findings and efforts towards TG2. To my postdoctoral friend, Nicole McNeil, thank you for the entertaining and successful collaborations. There were so many variables to mention, but it's best to focus on one variable for now. Mirka Strmiskova and Samuel Oteng-Pabi, you were both very generous with your time and without your help, I wouldn't be the biochemist I am today. Kim Apperley, although you were on the reversible inhibitor side, I always felt that our bond was irreversible (except during the TG2 crisis). Kelvin Tsao, you were a flamboyant evil spirit that I thankfully never needed help from. To all the undergraduate students I supervised – Viviane Ta, Josh Reed, Scott Foster, Arvind Grewal, and Rebecca Mailloux – thank you for the extra hands that assisted the completion of my thesis and/or paved the way for future projects. I am grateful for all the pioneers from the Keillor group that provided us with the appropriate assays and SAR studies that led to our lead compound, **NC9**. Likewise, I am appreciative of all the collaborators who showed interest in my work. Our collaborations flourished into fruitful discoveries that advanced our knowledge in the field of TG2.

To my family and friends, thank you for helping me maintain a balance between life and work. To my hardworking father, thank you for setting an example, I can't wait till I contribute to your early retirement. To my sisters, Bashayer and Batool, thank you for your support, kindness and care. To my girlfriend, Sofia, thank you for your genuine love, you've been a positive influence and strong support since day one.

Table of Contents

List of Tables

List of Figures

List of Schemes

List of Symbols, Abbreviations and Nomenclature

Symbol	Definition
% v/v	percent by volume
°C	degrees Celcius
Å	Angström
A_{405}	Absorbance units at 405 nanometres
A101	Abz-NE(CAD-DNP)EQVSPLTLLK-OH trifluoroacetate
Abz	2-aminobenzoyl
Ac	acetyl
ACN	acetonitrile
Acr	acryloyl
AD	Alzheimer's Disease
AL5	*N*-Cbz-Glu(γ-*p*-nitrophenylester)Gly
aq	aqueous
anh.	anhydrous
Arg	arginine
Asp	aspartic acid
ATP	adenosine 5'-triphosphate
AU	absorbance units
b	y-intercept
Boc	tert-butyloxycarbonyl

BODIPY	boron-dipyrromethene
br	broad
BTK	Bruton's tyrosine kinase
Ca	calcium
$CaCl_2$	calcium chloride
CAD-DNP	N-(2,4-dinitrophenyl)cadaverine
calcd	calculated
Cbz	carboxybenzyl
cDNA	complementary DNA
CE	capillary electrophoresis
Cys	cysteine
d	doublet
Da	dalton
DABCO	1,4-diazabicyclo[2.2.2]octane
Dap	2,4-diaminopropanoic acid
DCM	dichloromethane
dd	doublet of doublets
DIPEA	*N*,*N*-diisopropylethylamine
DMAP	4-(dimethylamino)pyridine
DMF	*N*,*N*-dimethylformamide
DMSO	dimethylsulfoxide
DON	6-diazo-5-oxo-L-norleucine
E	enzyme
EC	enzyme commission

EC_{50}	concentration of a drug that gives half-maximal response
EDC	1-ethyl-3-(3-dimethylaminopropyl)carbodiimide
ECS cells	epidermal cancer stem cells
EDTA	ethylenediaminetetraacetic acid
EGTA	ethylene glycol-bis(β-aminoethyl ether)-*N*,*N*,*N*′,*N*′-tetraacetic acid
EI	electron impact
Em	emission
EMT	epithelial–mesenchymal transition
eq.	equation
equiv	molar equivalent
ESI	electrospray ionization
ESI-TOF	electrospray ionization – time of flight
Ex	excitation
FDA	Food and Drug Administration
FRET	Förster resonance energy transfer
FRET-FLIM	Förster resonance energy transfer – fluorescence lifetime measurement
FXIII	factor XIII
FXIIIA	factor XIII A-subunit
FXIIIA2	factor XIII A-subunit dimer

FXIIIa	activated fXIII
FXIIIB	factor XIII B-subunit
GDP	guanosine 5'-diphosphate
Gln	glutamine
Glu	glutamic acid
Gly	glycine
GmbH	*Gesellschaft mit beschränkter Haftung* (company with limited liability)
gplTG2	guinea pig liver tissue transglutaminase
GSH	glutathione, reduced form
GTP	guanosine 5'-triphosphate
GTPγS	guanosine 5'-*O*-(3-thio)triphosphate
h	hour
HCl	hydrogen chloride
His	histidine
hFXIIIa	human activated factor XIII
HOBt	hydroxybenzotriazole
hTG1	human transglutaminase 1
hTG2	human tissue transglutaminase
hTG3	human epidermal transglutaminase
hTG3a	activated human epidermal transglutaminase
hTG6	human transglutaminase 6
HPLC	high-performance liquid chromatography
HRMS	high-resolution mass spectrometry

hTG2	human tissue transglutaminase
Hz	hertz
hν	UV light
I	inhibitor
IC_{50}	concentration of inhibitor required to decrease the enzyme's activity to 50%
J	coupling constant
k_{cat}	enzyme turnover number
kDa	kilodaltons
K_{eq}	equilibrium constant
K_I	irreversible inhibitor inhibition constant
K_i	reversible inhibitor inhibition constant
k_{inact}	inactivation rate constant
K_M	Michaelis-Menten constant
k_{obs}	observed rate constant
LC	liquid chromatography
Leu	leucine
Lys	lysine
m	multiplet
M	molar
MeOH	methanol
MgCl2	magnesium chloride
MgSO4	magnesium sulfate
MHz	mega hertz

mL	millilitres
mM	millimolar
MOE	Molecular Operating Environment
mol	mole
mp	melting point
min	minute
MOPS	3-(*N*-morpholino)propanesulfonic acid
mRNA	messenger RNA
MS	mass spectrometry
mU	enzyme activity in milliunit
m/z	mass to charge ratio
n.d.	not detected
NHS	*N*-hydroxysuccinimide
nm	nanometre
NMR	nuclear magnetic resonance
nPAGE	native polyacrylamide gel electrophoresis
o/n	overnight
obt.	obtained
P	product
PAGE	polyacrylamide gel electrophoresis
PDB	Protein Data Bank
Pd/C	palladium on carbon
pH	negative logarithm of the hydronium concentration

pK_a	negative logarithm of the acidity constant K_a
pNP	*p*-nitrophenolate
q	quadruplet
QTOF	quadrupole time-of-flight
Rf	retention factor
RFU	relative fluorescent units
RNA	ribonucleic acid
RT	room temperature
S	substrate
s	singlet
SAR	structure-activity relationship
SDS-PAGE	sodium dodecylsulfate polyacrylamide gel electrophoresis
SAXS	small-angle X-ray scattering
t	time
t	triplet
tBu	tertiary butyl
TCEP	tris(2-carboxyethyl)phosphine
tert	tertiary
TFA	trifluoroacetic acid
TG1	transglutaminase 1, keratinocyte transglutaminase
TG2	transglutaminase 2, tissue transglutaminase
TG3	transglutaminase 3, epidermal transglutaminase
TG4	transglutaminase 4, prostate transglutaminase

TG5	transglutaminase 5
TG6	transglutaminase 6
TG7	transglutaminase 7
TGase or TG	transglutaminase
THF	tetrahydrofuran
TLC	thin layer chromatography
Tris	tris(hydroxymethyl)aminomethane
Trp	tryptophan
Tyr	tyrosine
UV	ultraviolet
v	rate
v_0	initial rate in the absence of inhibitor
Val	valine
VEGFR-2	vascular endothelial growth factor receptor 2
V_{max}	maximum rate
α	Substrate competition factor ($\alpha=1+[S]/K_M$)
δ	chemical shift
μM	micromolar

Epigraph

“I've missed more than 9000 shots in my career. I've lost almost 300 games. 26 times,

I've been trusted to take the game winning shot and missed.

I've failed over and over and over again in my life. And that is why I succeed.”

– Michael Jordan

Chapter One: **Introduction**

1.1 Medicinal Chemistry

Medicinal chemistry is a branch of chemistry that serves to design, synthesize and evaluate biologically active compounds that interact with distinct targets to combat diseases. Moreover, it is a discipline that connects synthetic chemists, biochemists, pharmacologists and biologists, to create a collaborative environment towards the development of a drug. The drug discovery process begins with the collection of data in a research setting to validate a hypothesis that states the inhibition or activation of a protein or pathway will result in a therapeutic effect towards an illness. The selected target is screened against a library of compounds to identify a 'hit' molecule that interacts with the target to provide the desired biological activity. Chemical synthetic manipulations follow to improve the potency, selectivity, physicochemical and pharmacokinetic properties, with the hopes of generating a 'lead' compound that sustains the therapeutic effect. Once a small organic molecule or a biological therapeutic with drug-like properties is engineered, often termed a drug candidate, it will be evaluated in clinical trials, and if successful, ultimately become a marketed medicine.

1.1.1 Target Identification

Identifying and validating a biological target associated with a disease is a central initial step in the drug discovery process. A target is a broad term used for a biomolecule involved in the disease process, which includes proteins (i.e. enzymes, receptors and ion channels) and nucleic acids. A target may also pertain to the association or disturbance of a specific protein-protein or protein-gene interaction. Ideally a target needs to be efficacious, safe and accessible to

the drug[1]. In addition, the biological target must have an activity assay to evaluate the binding of the drug *in vitro* and *in vivo*. Furthermore, validation of the target is essential and can be acquired by target modifications, to observe loss or decrease of disease's phenotype through the appropriate *in vivo* model (e.g. transgenic mice studies).

One valuable identification method to find novel drug targets is done through accessing relevant literature published and shared by researchers worldwide. Another target identification approach includes examining mRNA/protein levels to determine whether expression is linked to cause or progression of disease. Descriptive studies can provide direction through evaluation of mRNA/protein expression in diseased versus healthy tissues. Genetic association is another tactic used to identify valid targets. For example, familial Alzheimer's Disease (AD) patients often have mutations in the amyloid precursor protein or presenilin gene which further leads to the increased production of the amyloid beta peptide in the brain, characteristic of AD[2]. The use of chemical probes to profile the genomic or proteomic activity of specific target classes has also helped in the identification of targets in disease versus healthy models. Proteomic based techniques for target discovery include mass spectrometry approaches[3] and non-mass spectrometry approaches, such as reverse phase protein microarrays[4] and peptide arrays[5]. Furthermore, an alternative approach can be done using phenotypic screening to identify applicable disease targets. Kurosawa and coworkers used a phase-display antibody library to isolate human monoclonal antibodies that bind to the surface of tumour cells[6]. Immunostaining identified preferred and strong binding of monoclonal antibodies to the malignant cells and the recognized antigens were isolated and were beneficial for identifying targets for cancer therapeutics. It is very important that the identified targets are validated experimentally with a proposed mode of action towards the disease. Target validation techniques range from *in vitro*

experimentation, to reveal characteristics of the target and its pathways in which it is involved, to *in vivo* modification of a desired target in animal models. Many techniques exist to validate a target; however, confidence is gained when multiple approaches are employed to show similar results.

1.1.2 Hit Identification

Once a target has been identified and validated with confidence, a hit compound is sought after. Like a target, a hit compound must also be identified and validated. The purpose of a hit compound is to elicit the desired activity towards a biological target to ultimately effectively treat a disease. Early drug discovery has mainly relied on naturally occurring substances for medicinal purposes. Natural products, particularly in plants, played a leading medical role against various human pathologies. In the early 1900s, scientists began to examine natural substrates more closely with the hope of identifying and isolating the natural ingredient that was medically useful. The serendipitous discovery of penicillin's antibacterial property by Fleming in 1929[7] and its isolation by Chain and Florey in 1940[8] is one defining example that paved the way for modern antibacterial drugs. However, pharmaceutical companies have reduced their research and investments towards medicinally active natural products in the past two decades[9]. Justification for the reduced interest of natural products as hits for drug discovery been reviewed[9]; justifications include the fact that hit identification from natural products is a slow process in comparison to the pace of high throughput screening of many existing compound libraries, and also that the structural complexity of natural products leads to difficult synthesis.

Advances within the drug development sector have led to a variety of screening approaches to identify hit molecules. One widely used approach is high throughput screening,

where various available compound libraries are assayed directly against the desired drug target[10]. This type of screening requires a target specific activity assay to identify a hit compound from a large library of approximately 100,000 compounds. With the use of complex automated machinery, high throughput screening can identify a hit molecule without prior knowledge of target structure, allowing for a time efficient process. Unlike high throughput screening, fragment based screening[11] involves the screening of a smaller library (thousands of compounds) of low molecular weight compounds in hopes of finding a hit. Typically, hit fragments will have low affinity to the target but will provide a structural basis for further modifications. Through computational and crystallographic analysis of hit fragment with target, the fragments that form high quality interactions with target are then optimized to possess high affinity and selectivity. Alternatively, a more qualitative phenotypic screening can be done using a tissue based approach[12], which looks for a response more aligned with the final desired *in vivo* effect as opposed to targeting one specific molecular component.

With the explosion of genomic, proteomic, and structural information of hundreds of targets, an alternative approach to drug discovery has emerged, known as structure-based drug design[13]. In fact, a combination of the above screening approaches can be combined with a structure-based approach. Primarily, structural data of the target, deriving from X-ray crystallography, NMR or possible homology models, must be available to use. Using computer algorithms, compounds or fragments of compounds from rational design, a database or hits from a screen are positioned into a selected region of the structure. These compounds are virtually scored and ranked based on their steric and electrostatic interactions with the target site, and the best compounds are prepared and tested with biochemical assays to identify a hit or validate a hit from a screen. Structure determination of the target in complex with the identified hit will reveal

structural moieties of the compound that can be optimized to increase potency. Potency can be improved by studying the structure-activity relationship (SAR) of the hit compound towards its target. An SAR study aims to understand the 3D structural interaction of a hit with its biological target, which allows researchers to rationally understand the available chemical space. The optimized compounds usually show marked improvement in binding and, often, specificity for the target.

Within this broad field of medicinal chemistry, the Keillor group focuses on the development of inhibitors for transglutaminases. More specifically, we design, synthesize and evaluate inhibitors of tissue and plasma transglutaminases.

1.2 Transglutaminases

Transglutaminases (TGases, EC 2.3.2.13) are a family of calcium (Ca^{2+}) dependent enzymes that post-translationally modify their respective substrates by introducing an isopeptidic N_{ε}-(γ-glutaminyl)lysine bond. The introduction of the isopeptic covalent bond occurs between a glutamine containing protein or peptide and a primary amine such as a lysine residue found on the surface of a protein. Some transglutaminases are known to be multifunctional proteins; however, they share one general mechanism depicted in Scheme 1.1 The TGase family is composed of nine isoforms: TGases 1 through 7, Factor XIII, and the catalytically inactive erythrocyte membrane protein band 4.2. Throughout the catalytically active TGases members, a conserved catalytic triad is found consisting of the residues cysteine, histidine and aspartate. The human isoforms are described individually below.

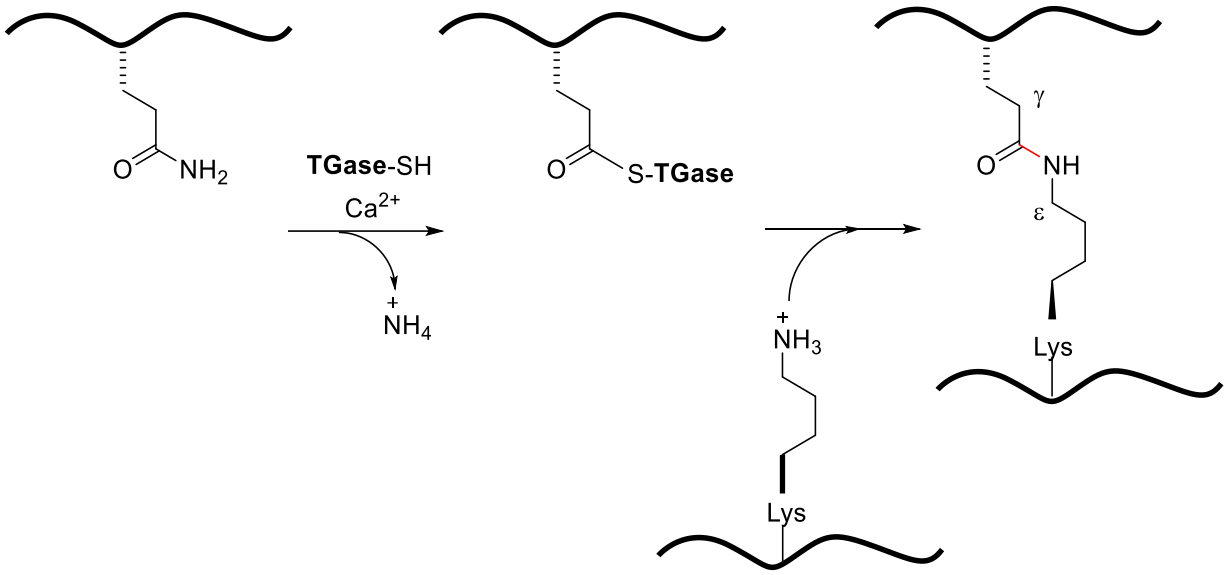

Scheme 1.1.1. Transamidation reaction catalysed by TGases.

Reproduced with permission from Keillor et al., Bioorganic Chemistry (2014)[14]

1.2.1 Keratinocyte Transglutaminase (TG1)

TG1, also known as keratinocyte TGase[15], is 90-kDa enzyme that is found as a protein anchored to the keratinocyte membrane in the epidermis via fatty acyl linkages. As intracellular Ca^{2+} levels rise in suprabasal epithelial cells of the epidermis, TG1 crosslinks the appropriate proteins to assemble the cornified envelope, a protective layer replacing the plasma membrane of keratinocytes. Pathogenetically, TG1 is associated with lamellar ichytosis, a disorder of cornification that affects the epidermis.

1.2.2 Tissue Transglutaminase (TG2)

Among the most studied of the TGases, tissue transglutaminase or TG2 is a 78-kDa protein that structurally consists of four domains; an N-terminal β-sandwich, a catalytic domain

harbouring the active site Cys277, and two C-terminal β-barrels[16]. Ubiquitously expressed in tissues, TG2 is predominantly found in the cytosol, but it is also localised in the nucleus, membrane, cell surface and extracellular matrix[17]. TG2 is a multifunctional enzyme that has been demonstrated to have transamidation, deamination and GTP binding activity[14]. To avoid nonspecific crosslinking in the intra- and extracellular environment, regulation of TG2 activity is tight. Three well understood physiological regulators of its enzymatic activity are Ca^{2+} ions, guanine nucleotides, and protein redox regulation by thioredoxin. TG2's transamidation activity is activated by Ca^{2+} and inhibited by GTP, an allosteric regulator[18]. When bound to guanine nucleotides, such as GTP or GDP, TG2 adopts a compact (closed) conformation, where substrate access to Cys277 is obscured by two loops of the first β-barrel domain[19]. Studies showed that TG2 activity is also affected by redox potential of its environment[20,21]. More specifically, TG2 is susceptible to reversible inactivation by the formation of an intramolecular disulfide bond between cysteine residues Cys370/Cys371. Unregulated TG2 activity has been associated with Celiac disease, fibrosis, Alzheimer's disease and cancer[18]. Further detail on TG2 is found in section 1.3 since it is the subject of significant study presented in this thesis.

1.2.3 Epidermal Transglutaminase (TG3)

Similar to TG1, TG3 (epidermal TGase) is expressed in keratinocytes and is a cytosolic protein found in the upper epidermal layers, with a role in cornified envelope assembly[15]. TG3 is structurally similar to TG2 as evident from its crystal structure (PDB code 1L9N), also possessing a Cys-His-Asp catalytic triad[17]. TG3 is expressed as an inactive 77-kDa zymogen, which is proteolytically cleaved into a 50-kDa active enzyme (TG3a). Moreover, the cleaved 27 kDa fragment remains associated with the activated protein[22]. Like other TGases, TG3 requires Ca^{2+} for its

catalytic transamidation activity. The zymogen binds a single calcium ion and upon proteolytic activation, the active enzyme weakly binds two additional Ca^{2+} ions. As with TG2, guanine nucleotides also inhibit TG3 activity[23]. Physiologically, while gluten sensitivity typically known as Celiac disease is associated primarily with TG2, TG3 has been suggested[15] to serve as the auto-antigen responsible for the skin phenotype in dermatitis herpetiformis, a blistering skin disease in response to gluten sensitivity.

1.2.4 Prostate Transglutaminase (TG4)

TG4, also known as the prostate transglutaminase, is an enzyme found to be expressed predominately in the prostate gland[24]. The exact function of TG4 in humans is not entirely known, and neither is the structure of this 77-kDa protein. Physiologically, TG4 knockout mice exhibited reduced fertility due to defects in copulatory plug formation, preventing oocyte fertilization[25]. It has also been found that the elevated expression of TG4 has a role in the aggressiveness of prostate cancer[24]. More specifically, TG4 was involved in the adhesion of cancer cells to the extracellular matrix via interaction with the β1 subunit of integrin. Increased levels of TG4 have been linked to increased tumour aggressiveness, making TG4 a possible biological target in devising treatment for prostate cancer.

1.2.5 TG5

In comparison, TG5 was a later discovery in the TGase family[26]. Although its function has not been fully characterized, it is known to be expressed in the upper spinous and granular layer of the human epidermis and in hair follicles[15]. Like TG3, TG5 is an 80-kDa zymogen which, upon proteolytic cleavage, produces a 53-kDa fragment comprised of the shared TGase

catalytic domain. TG5 contains a GTP binding site, and both GTP and ATP inhibit its activity *in vitro*[27], and the role of its GTP binding activity in regulating cell function is not fully understood. Like TG2 and TG3, the presence of Ca^{2+} can out compete guanosine nucleotide binding and restore transamidation activity. Physiologically, intracellular overexpression of TG5 has been linked to apoptosis, a distinguishing consequence from other TGases found in the epidermis[28]. In addition, mutations in the TG5 gene are known to cause acral peeling skin syndrome, an autosomal recessive skin disorder[29].

1.2.6 TG6

TG6 is another recently identified member of the TGase family[30]. Its descriptive characterization[31] suggests that the expression of TG6 is unique to specific tissues rather than having a ubiquitous expression like TG2. Evidence of TG6 expression in an adult mouse brain was observed, more specifically in the septal region, basal ganglia, hypothalamus and brainstem[32]. The enzyme consists of 706 amino acids and has a calculated molecular mass of about 79 kDa. Structurally, TG6 displays high amino acid sequence conservation to TG3 (50% overall and 59% within the Cys-His-Asp catalytic core domain). However, similarly to TG2, TG6 is sensitive to oxidative inactivation and is inhibited by guanine nucleotides in a manner that suggests that it may also act as a guanine exchange factor[31]. Furthermore, TG6 is a protein that can be detected in the cell cytosol as well as at the cell surface, which might allow it to have independent intra- and extracellular functions, where the enzyme might function based on the availability to bind GTP or Ca^{2+}. TG6 has been associated with ataxia-like deficits in mice and it is hypothesized that TG6 may play an important role in motor control[31].

1.2.7 TG7

In terms of physiological function, little is known about TG7. The enzyme was first identified at the transcriptional level through deeper analysis of the transglutaminase gene cluster[30]. TG7 is composed of 710 amino acids and has a molecular mass of 80 kDa. Peptide screens have identified peptidic substrates for TG7[33] that provide direction to measuring TG7's transamidation activity to further understand its physiological function. So far, no reports associate TG7 with any known disease.

1.2.8 Plasma Transglutaminase (FXIII)

Plasma TGase or Factor XIII (FXIII) is a 320-kDa tetrameric enzyme complex consisting two A subunits (FXIIIA) and two B subunits (FXIIIB)[34]. Factor XIII exists as a homodimer of the A subunits in extracellular matrix, while plasma FXIII circulates in the blood as an A_2B_2 heterotetramer. FXIIIA is a zymogen that possesses the catalytic domain responsible for transamidation, while FXIIIB is an inhibitory glycoprotein subunit with no enzymatic function[35]. Although the full FXIII complex has not yet been crystallized, the structure of the 83-kDa A_2 homodimer subunit has been solved by X-ray crystallography (PDB 1GGU). Like TG3 and TG5, FXIIIA is a zymogen that is activated (FXIIIa) by proteolytic cleavage, more specifically by thrombin, allowing the catalytic cysteine in the active site to be accessible. FXIIIa lacking the inhibitory B subunits can be activated upon elevation of intracellular calcium concentrations, independent of proteolysis[17]. FXIIIa is mainly known for polymerizing fibrin in the blood clotting cascade (further detail in section 1.4.1); however, expression in other tissues has been reported[35]. Several protein substrates for FXIIIa have been identified, including proteins involved in blood coagulation, such as adhesive proteins and cytoskeletal proteins. These classes

of substrates correlate with the three functional roles for FXIIIa, namely its involvement in fibrinolytic system, wound healing, and other less well-defined cellular functions. Further detail on FXIII is found in section 1.4 since it is one of the enzymes contributing to the work in this thesis.

1.2.9 Erythrocyte membrane protein band 4.2

Unlike other members of the TGase family, erythrocyte membrane protein band 4.2 (band 4.2) has no catalytic activity. High sequence homology is observed between band 4.2 and the active site region of other TGases containing the following amino acid sequence: Gly-Gln-Cys-Trp-Val, which includes the active site cysteine[36]. However, band 4.2 has an alanine residue in the place of the catalytic cysteine, a substitution that is no doubt responsible for the lack of transamidation activity. Band 4.2 is mainly present in erythrocytes, bone marrow, fetal liver, and spleen[37]. Band 4.2 is a major component of the erythrocyte membrane cytoskeleton and plays an important role in maintenance of membrane integrity and regulation of cell stability[37]. Band 4.2 null mice show alterations in red blood cell function, including spherocytosis and altered ion transport[38].

1.3 Human Tissue Transglutaminase

Tissue transglutaminase (TG2) is the primary focus of the inhibitor development program in the Keillor group and one of two transglutaminases studied over the course of this thesis work, the other being factor XIII. TG2 was the first member of the TGase family to be discovered and remains the most studied. TG2 has been associated with several diseases; however, for this work, it is considered as a medicinal target involved in tumour invasion, migration and growth. Details

of its mechanism, allosteric and conformational regulation, physiology, associated diseases and current inhibitors are presented below.

1.3.1 Mechanism

TG2 has been demonstrated to act as an acyl transferase using a ping-pong mechanism to catalyse its crosslinking or transamidation reactions. Transamidation occurs as a double displacement reaction; initially, the active site cysteine (C277) thiolate attacks the amide side chain of a glutamine residue, resulting in the formation of a thioester acyl enzyme intermediate and the release of ammonium. Consequently, a primary amine (such as the amine side chain of a lysine residue) acts as a nucleophile, resulting in the formation of an isopeptidic bond and the liberation of the enzyme. Accordingly, transamidation reactions result in posttranslational modifications of glutamine acyl donors in the presence of a suitable primary amine that can serve as acyl acceptor substrate. When this primary amine is the lysine side-chain of a second protein, cross-linking occurs. In the absence of a primary amine substrate, water can assume the role of an acyl acceptor 'substrate', resulting in the deamidation of the glutamine residue to glutamate. Mechanistically, hydrolysis has been observed to be much slower than aminolysis, and deacylation appears to be rate-limiting over acylation[39]. A more detailed representation of the mechanism is shown below in Scheme 1.2. While additional acyl transfer reactions have been proposed for other TGases, limited evidence exists in support of TG2 mediated intramolecular transamidation (i.e. cyclisation)[40] or transesterification[41,42]. In addition, TG2 can reversibly cleave isopeptide bonds with its isopeptidase activity[43].

The active site consists of a catalytic triad of Cys277, His335 and Asp358 that are located at the end of a hydrophobic tunnel made up of Trp241, Trp332 and Thr360. The mutation of

tryptophan residues Trp241 and Trp332 to alanine results in a protein with no detectable activity[16], thus confirming that these tunnel-lining residues have a role in catalysis. Furthermore, Thr360 is also involved in the transamidation activity[16]; the T360A mutant displays a marked preference for hydrolysis over aminolysis.

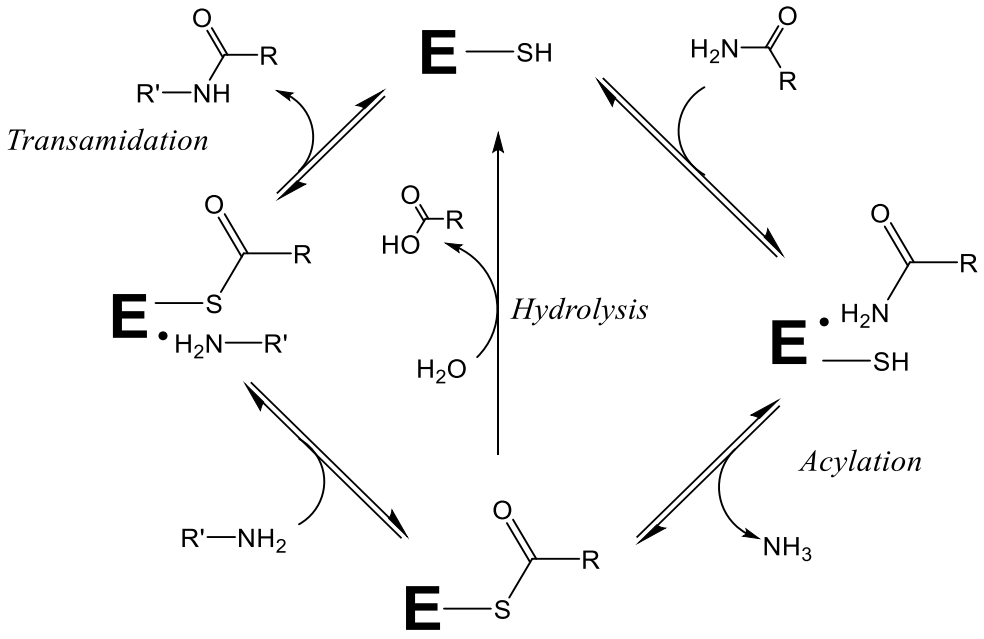

Scheme 1.2. Acyl transferase activities of TG2.

Reproduced with permission from Keillor et al., Bioorganic Chemistry (2014)[14]

TG2 is relatively selective regarding which Gln residues are modified by acyl transfer reactions, but much less selective towards lysine residues or primary amines. Early studies with guinea pig liver TGase (gplTG) by Folk and Cole reported that Gln alone does not serve as a substrate, nor do the peptides Gln-Gly and Gly-Gln-Gly; however, Cbz-Gln-Gly, Cbz-Gln-GlyOEt, and benzoyl-Gly-Gln-Gly are functional[44]. From this work it was noted that the N-terminal Cbz group plays an important role in conferring affinity for small peptidic substrates.

Additional insight was provided in a kinetic study that featured a series of synthetic dipeptides bearing an N-terminal Cbz or Boc group[45]. All Cbz-peptides displayed similar K_M and k_{cat} values, whereas the Boc-dipeptides did not appear to act as donor substrates, showing no reactivity with gplTG. Given its simple structure, reasonable affinity and commercial availability, Cbz-Gln-Gly has been the most commonly used non-protein acyl donor substrate.

1.3.2 Allosteric regulation

The acyl transfer reaction of TG2, including transamidation, is allosterically activated by binding of Ca^{2+} ions. In contrast, binding guanine containing nucleotides inhibits transamidation activity[46]. Several potential calcium binding sites have been tentatively identified[47], whereas the nucleotide binding pocket of TG2 associated with GTP/GDP binding has been shown by X-ray crystallography to include residues 476–482 and 580–583 of the first and last strand of β-barrel 1 (see TG2 structure in figure 1.1). In its active form, TG2 binds up to six Ca^{2+} ions and its transamidation activity is decreased or lost when specific Ca^{2+} binding sites are mutated[47]. Additionally, the binding of GTP may be abolished by an arginine point mutation (R580A) found in the proposed GTP/GDP binding pocket[48]. TG2's ability to bind guanine nucleotides also led to the realization that it was also known as the G-protein Ghα, which mediates the activation of phospholipase C by the α_{1B}-adrenergic receptor[49].

In the cytosol, the transamidation activity is likely dormant, due to the low concentration of Ca^{2+} and the high concentration of GTP. However, extracellularly, the higher concentration of Ca^{2+} results in an increase of its transamidation activity. To regulate its extracellular activity, studies have shown that TG2 forms a disulfide bond between Cys370 and Cys371 through the oxidation of residue Cys230, initiating a cascade of intramolecular disulfide bond formation to render it inactive[16,20]. More recently, characterization of the physiological mechanism for the switch

between the (active) reduced state and the (inactive) oxidized state of TG2 has been linked with the protein thioredoxin, as a specific activator of oxidized TG2[21]. Moreover, TG2 is protected from oxidation in the presence of high calcium ion concentration[20], suggesting that TG2 activation is not simple. In summary, Ca^{2+}, guanine nucleotides, and the redox potential combine to regulate TG2 in three distinct states, depending on the physiological conditions the enzyme faces.

1.3.3 Conformational regulation

Different from other TGases, TG2 undergoes a large conformational change that is allosterically regulated. TG2 adopts an extended or open conformation upon binding of Ca^{2+} and folds into a compact or closed conformation once bound to GTP/GDP. In the closed, inactive form, TG2 assumes a compact conformation (Figure 1.1 A) that displays considerable interaction between the catalytic domain and the two C-terminal β-barrels, thus reducing the accessibility to and the activity of the catalytic site. However, in the open form (Figure 1.1 B), the active site is solvent exposed.

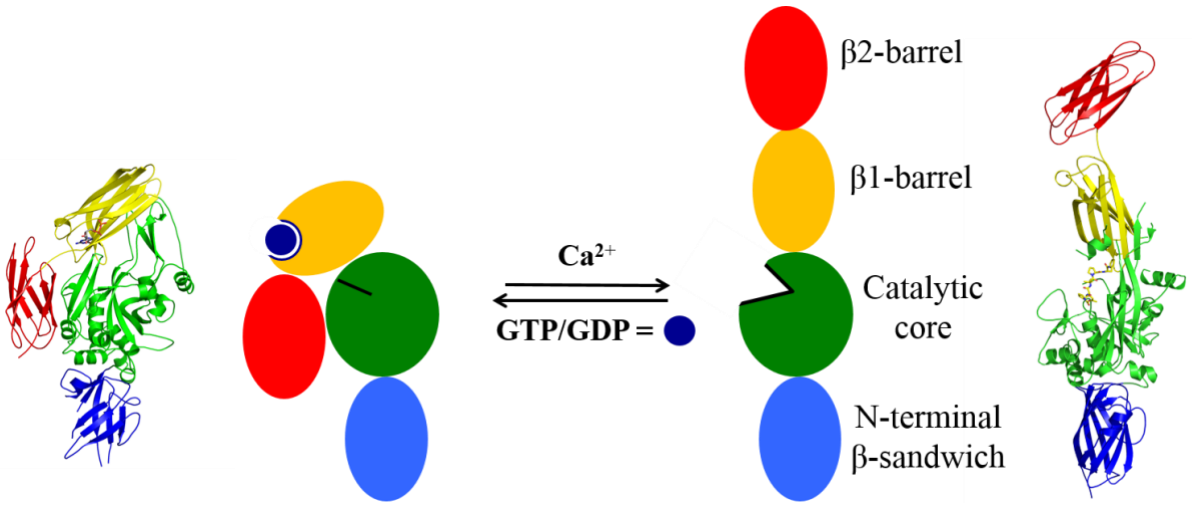

Figure 1.1. Conformations of TG2: A) closed GDP bound[19] conformation and B) open substrate mimicking inhibitor bound[16] conformation.

Originally, the conformational change was observed by small-angle X-ray scattering (SAXS) in the form of a considerable increase in the radius of gyration of the activated enzyme in solution[50]. Solved x-ray crystal structures of the enzyme demonstrate that two dramatically different structures exist, as seen in Figure 1.1, which are allosterically regulated to cause a large conformational change. The distance between the termini increases from less than 10 Å in the closed form to approximately 150 Å in the open form[51]. During this conformational change, the C-terminal β-sandwich domains are displaced, while the N-terminal and catalytic domains remain mostly unchanged, thus suggesting that the closed form blocks substrate binding, while the open form reveals the active site for catalytic activity. This conformational regulation is therefore not involved in the spatial orientation of the catalytic machinery for activity. Furthermore, native polyacrylamide gel electrophoresis (nPAGE) confirms[16] the presence of two conformations in solution, as does kinetic capillary electrophoresis (CE)[52]. The latter experiment showed that the interconversion rates between the open and closed forms are slower than k_{cat}, suggesting that the conformational changes do not occur during the catalytic cycle, but rather as part of the tight functional regulation of TG2. Finally, FRET[53] and FRET-FLIM[51] experiments *in cellulo* have confirmed the effect of Ca^{2+} in promoting the open form of the enzyme.

1.3.4 Physiological roles

Since the discovery of TG2 in 1957[54] a large number of putative substrates have been proposed for the enzyme in the intra- and extracellular component of various tissues. At the extracellular surface, TG2 uses its transamidation activity to crosslink proteins such as collagen, fibronectin and elastin to aid in extracellular matrix assembly and stabilization[55]. Moreover, TG2 has been reported to act as a non-enzymatic scaffold protein, non-covalently interacting with

extracellular proteins to enhance cell adhesion[56]. Using its transamidation activity, TG2 can incorporate amines such as serotonin, histamine, dopamine and norepinephrine to monoaminate substrate proteins[57]. TG2 has also been observed to promote cell survival through a signalling role associated with its conformation, protecting cells from apoptosis[58]. In the absence of suitable amine substrate or at relatively low pH, TG2 can also hydrolyse peptide-bound glutamines to glutamic acids via its deamidation reaction. Besides its classical transamidation/deamination activity, TG2 possess a poor GTPase activity and a non-enzymatic GTP binding function[59,60]. Its GTP binding activity allows intracellular TG2 to link transmembrane adrenergic, thromboxane A2, and oxytocin receptors to cytoplasmic signalling targets such as phospholipase C.

1.3.5 Associated Diseases

1.3.5.1 General

Pathogenicity of TG2 can arise from its unregulated transamidation and deamination activity. More so, its GTP binding ability has also been proposed to evoke certain signalling pathways that lead to a disease state. TG2 has been implicated in the pathogenesis of a number of diseases, such as neurodegenerative disorders[61], diabetes[62], renal disease[63], fibrosis[64], celiac sprue[65] and certain types of cancers[66]. Overall, the greatest potential for the treatment of TG2-related disease at the moment appears to be centred around celiac disease, fibrosis and tumour progression, due to the specific nature of the enzyme's role in their pathologies. Therefore, inhibition of TG2 activity may offer a potential strategy to therapeutically treat these diseases. Before examining the scope of TG2 inhibitors, a brief examination of the role TG2 in celiac sprue, fibrosis, and tumour growth will help illustrate the potential benefits these inhibitors may offer.

1.3.5.2 Celiac disease

Celiac sprue, also known as celiac disease, is a T-cell mediated inflammatory disorder of the small intestine caused by a class of proteins called prolamins found in wheat, barley, and rye[65]. Prolamins intrinsically have a high glutamine content (approximately 30%) and some of these glutamine residues are recognized by TG2. Intestinal TG2 deamidates specific glutamine residues in the prolamin peptides to glutamate residues, thereby increasing their affinity for the disease-associated HLA-DQ2 and HLA-DQ8 proteins, which in turn trigger the T cell immune response leading to inflammation and destruction of intestinal architecture[67]. Celiac patients also generate an antibody autoimmune response against TG2[68], creating anti-TG2 antibodies that can be found in both the small intestine, where they have been shown to colocalize with extracellular TG2[69], and in the blood, where they are currently being used as a diagnostic tool for the disease[70].

1.3.5.3 Fibrosis

Damage to tissues prompts a repair process typically involving two distinct stages: a regenerative phase, in which injured cells are replaced by cells of the same type and a phase known as fibroplasia or fibrosis, in which connective tissues replaces normal parenchymal tissue[71]. Although initially beneficial, the repair process becomes pathogenic when it is not controlled appropriately, resulting in substantial deposition of extracellular matrix components in which normal tissue is replaced with permanent scar tissue. Fibrotic disease can affect vital organs including the lungs, liver, heart, and kidneys. Recent studies suggest that TG2 is involved in tissue fibrosis due to its role in stabilization and crosslinking of the extracellular matrix. In

pulmonary fibrosis, TG2 knockout mice experiments showed significantly less fibrosis phenotype compared with wild-type mice[64]. In kidney fibrosis, it has been shown that in rats induced to undergo renal scarring, treatment with the transglutaminase inhibitors lead to reduction in kidney scarring with preservation of kidney function[72,73]. In liver fibrosis, TG2 has been shown to be involved in the increase in production of protein crosslinks, furthermore, liposome based delivery of TG2 inhibitors to the liver has minimised and reversed the scarring associated with fibrosis[74]. With these associations and further studies to dissect the mechanism of TG2 involved in fibrotic diseases, the development of TG2 specific drug candidates may be valued towards therapeutic options.

1.3.5.4 Tumour progression

Tumours are heterogeneous cells, made up of mainly two components: the parenchyma (neoplastic cells) and the stroma (microenvironment)[75]. The components of the complex microenvironment, which includes several tumour supporting cells, modulate cancer cell growth and regulate their malignant biological behaviours through numerous intracellular signalling transduction pathways[76]. Cancer cells recruit tumour supporting cells from nearby endogenous host stroma and encourage events such as tumour angiogenesis, proliferation, invasion, and metastasis, as well as mediate mechanisms of therapeutic resistance[77]. Tumour stromal cell composition is known to vary between tissues, which adds to the complexity of cancer therapeutics. Metastasis is a leading cause of poor prognosis and high mortality rate among many malignancies and epithelial-mesenchymal transition (EMT) is a major biological process promoting the invasive and metastatic abilities of cancer cells. Many studies have shown that elevated and unregulated TG2 expression is associated with formation of aggressive and

metastatic tumours that are resistant to conventional therapeutic intervention[78]. TG2 has been shown to be a breast cancer cell survival factor, and overexpression in the tumour's stroma is associated with high risk of cancer recurrence[79]. TG2 is highly expressed in advanced breast cancer and in drug-resistant breast cancer cells and TG2 knockdown restores drug sensitivity[80]. In glioblastoma, TG2 expression is elevated in tumour regions where fibronectin assembles in the extracellular matrix, and knockdown of TG2 results in a loss of this assembly[81]. Treatment with a TG2 inhibitor, reduces matrix remodelling both *in vitro* and *in vivo*, and resensitizes glioma tumours to chemotherapeutic treatment[81]. Moreover, a GTP-binding competent and transamidation defective TG2 mutant confers resistance to doxorubicin, suggesting that GTP binding activity, but not TG2 crosslinking activity, is required for this response[82]. Epidermal squamous cell carcinoma tumours possess a subpopulation of cells that display a different potential for proliferation and differentiation called epidermal cancer stem cells (ECS cells)[83]. These ECS cells have shown to form fast growing, aggressive, invasive, and highly vascularized tumours in immune-compromised mice[83]. Elevated expression of TG2 is observed in ECS cells and TG2 knockdown or irreversible inhibition of TG2, reduces ECS cell survival, invasion and migration[84]. Furthermore, using the appropriate TG2 mutants, the mechanism inducing the metastatic behaviour of ECS cells was linked to the GTP binding activity and not the transamidation activity of the enzyme[78]. TG2 has also been associated with ovarian[85], breast[79,86], pancreatic[87], liver[88], lung[89] and colon cancer[84]. These findings suggest that TG2 holds therapeutic significance in the fight against cancer.

1.3.6 Current Inhibitors

As discussed above, TG2 is a potential therapeutic target and selective and potent TG2 inhibitors, to alter one or all its activities, are sought after clinically. Depending on the disease state, the pathogenic role of TG2 has been linked to its protein crosslinking, deamidation or GTP binding activity, thus inhibitors are designed to inactivate the enzyme based on the disease associated activity. Moreover, TG2 knockout mice appear developmentally and reproductively normal, mainly displaying delayed wound healing and poor response to stress[90]. Due to the lack of serious and fatal deficiencies observed in TG2 knockout mice with respect to normal biological functions, as well as its involvement in a wide range of diseases, TG2 has been proposed as a safe therapeutic target.

Early research towards inhibition of TG2 was achieved through the use of primary amines[91], which can 'inhibit' the native function of the enzyme by competing as substrates in the crosslinking reaction. Cystamines are still used as 'inhibitors'[92], based on the well-known deactivation of TGases by disulfide compounds[93], despite their lack of selectivity, particularly when applied in biological settings, thus lessening the potential of this class of inhibitors. However, the field of TG2 inhibitors has focused on designing competitive acyl donor inhibitors.

1.3.6.1 Reversible Inhibitors

The first reported reversible inhibitors were based on a thieno[2,3-*d*]pyrimidin-4-one acylhydrazides scaffold, where **compound 1** and **LDN-27219** (Figure 1.3) were the most potent, with IC_{50} values of 0.8 μM and 0.6 μM[94,95]. A more recent study showed that these compounds were better inhibitors of TG3 than of TG2[96]. **LDN-27219** was kinetically evaluated and was shown to act as a reversible inhibitor that does not bind at the active site. Furthermore, **LDN-**

27219 was originally proposed to compete with GTP binding; however, recent literature shows otherwise[96].

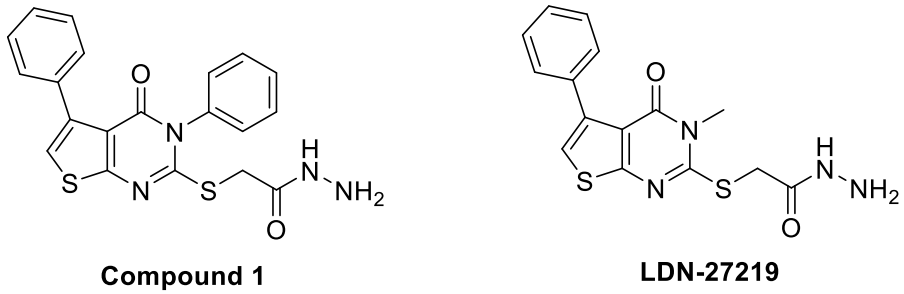

Figure 1.2. Reversible allosteric inhibitors of TG2.

Following these initial inhibitors, the Khosla group recently developed acylideneoxoindoles as another scaffold for reversible TG2 inhibitors[97], inspired by the structure of isatin (indoline-2,3-dione), whose analogs are widely used as reversible inhibitors of Cys dependent protease[98]. In their SAR study, the 4-chloro analogue (**compound 10**, Figure 1.3) had the highest potency, with a K_i of 0.7 mM and was competitive with the acyl donor substrate. The Keillor group has also played a critical role in designing reversible inhibitors for TG2, using a *trans*-cinnamoyl scaffold. Rationale for the choice of scaffold was based on previous studies which illustrated that the Cbz protecting group, in peptidic substrates conferred affinity to the enzyme[45]. From their series of inhibitors, the most potent inhibitor (K_i = 1.0 μM) was termed **CP4d** (Figure 1.4) and the mode of inhibition was reported as a reversible competitive[99]. However, due to the electrophilic nature of **CP4d**'s alkene moiety, this class of inhibitors was susceptible to nucleophilic attack by glutathione, a key element in cellular metabolism and toxicity response. To address this issue, several modifications to the inhibitor scaffold were made, ultimately

showing that a bis(triazole) scaffold increased resistance to nucleophilic attack, with **compound 27d** (Figure 1.3) being the most potent (K_i = 10 μM). Furthermore, FRET FLIM experiment with **CP4d** has illustrated reversible binding that favours the closed form of the enzyme[51].

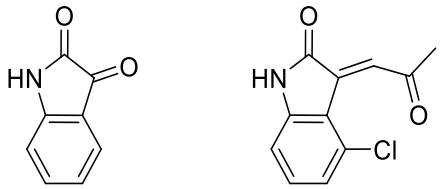

Figure 1.3. Reversible inhibitor with isatin scaffold optimised by the Khosla group.

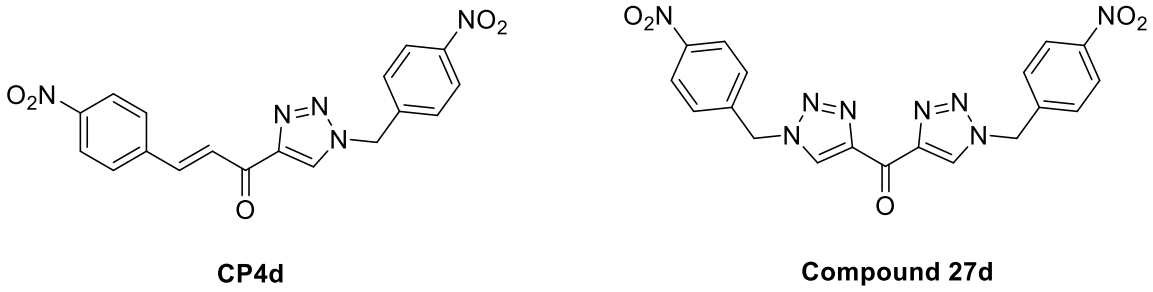

Figure 1.4. Reversible inhibitors with cinnamoyl scaffold optimised by the Keillor group.

1.3.6.2 Irreversible Inhibitors

Many irreversible inhibitors have been developed against TG2. Recently, review articles regarding the development of TG2 inhibitors have been published[18,100]. As such, for the irreversible inhibitors, the recent work of two of the more active groups in this field, namely the Khosla and Keillor groups will be highlighted. Using a 3-halo-4,5-dihydroisoxazole group as a reactive electrophilic 'warhead', the Khosla group developed compound **KCC009** (Figure 1.5), an irreversible inhibitor (k_{inact}/K_I = 2.00 x 10^3 M^{-1} min^{-1}, k_{inact} = 1.3 min^{-1}, K_I = 0.74 mM) with

high specificity for TG2 and effectiveness *in vivo* (mouse model)[101]. Further optimisation of this scaffold led to compound **ERW1041E** (k_{inact}/K_I = 16.9 x 10^3 M^{-1} min^{-1}, k_{inact} = 0.110 min^{-1}), which is more efficient and has also been shown to inhibit the activity of TG2[102] in the small intestine of a mouse[103].

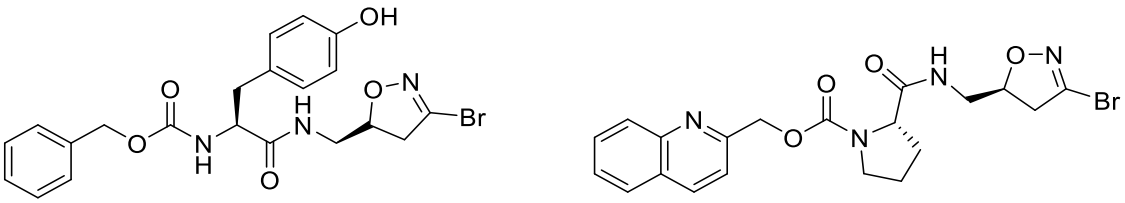

Figure 1.5. Key irreversible TG2 inhibitors from the Khosla group.

The Keillor group inhibitor design was based on the dipeptidic substrate Cbz-Gln- Gly, where the glutamine side chain was replaced with a lysine based acrylamide 'warhead', resulting in Cbz-Lys(Acr)- Gly as their most efficient irreversible inhibitor (k_{inact}/K_I = 3.0 x 10^6 M^{-1} min^{-1}, K_I = 150 nM against guinea pig liver TGase (gplTG), used as a model for TG2)[104]. Derivative **NC9** (Figure 1.6) has a lower efficiency[104] (k_{inact}/K_I = 1.4 x 10^4 M^{-1} min^{-1}, K_I = 29 μM against gplTG) but its fluorescent dansyl group allows its use as a probe in cellular studies for TG2 localisation. Included in this thesis, is the kinetic re-evaluation of the above inhibitors against human TG2 and design, synthesis and kinetic evaluation of novel irreversible inhibitors of human TG2.

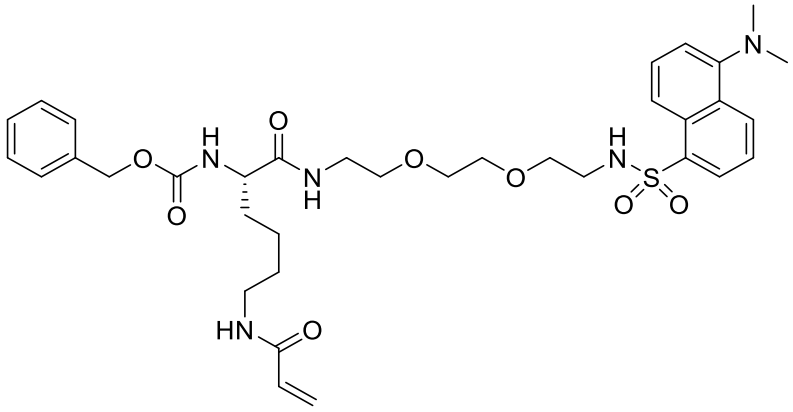

NC9

Figure 1.6. NC9, a key irreversible inhibitor crafted by the Keillor group.

Recently, Zedira GmbH have brought an irreversible inhibitor to phase II clinical trials for attenuating the immune response to gluten in celiac patients. Compound ZED1227 (Figure 1.7) is the first direct-acting transglutaminase blocker to reach clinical trials.

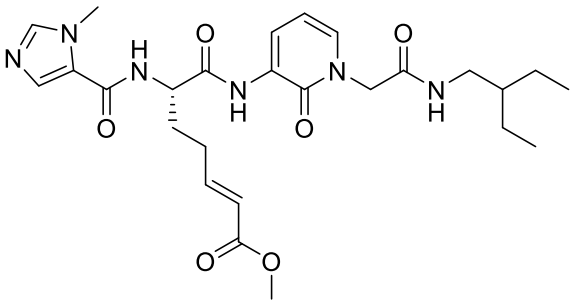

ZED1227

Figure 1.7. Compound ZED1227, the first TGase inhibitor to reach clinical trials.

1.4 Factor XIII

Fibrin stabilizing factor or factor XIII (FXIII) is the second enzyme studied in this thesis work. FXIII is well known for its involvement in the blood coagulation cascade, though it is also

involved in certain cellular activity[34]. Due to its crucial involvement in hemostasis, in this work, we consider FXIII as a medicinal target for thrombosis. The development of selective FXIII inhibitors is another interest in the Keillor group and a subject that pertains to the work of chapter 4 of this thesis. Details of its mechanism, physiology, associated diseases and current inhibitors will be discussed below.

1.4.1 Mechanism

FXIII is a zymogen that circulates in the plasma as a heterotetrameric protein complex, consisting of two homodimer A-subunits ($FXIIIA_2$, 83 kDa) and two homodimer B-subunits ($FXIIIB_2$, 80 kDa)[105]. The A-subunit is a transglutaminase zymogen and the B-subunit is an inhibitory glycoprotein with no enzymatic function[35]. Although the full complex has not yet been crystallized, the structure of the A_2 homodimer has been solved by x-ray crystallography[106]. The structure of a single FXIII A-subunit (FXIIIA) resembles that of the other transglutaminases, especially TG2, consisting of N-terminal β-sandwich followed by the catalytic domain, that harbours the active site Cys314, and two C-terminal β-barrels[107]. In contrast to TG2, the N-terminus carries a 37 amino acid peptide sequence that is proteolytically cleaved during activation[34]. The X-ray structure revealed that the catalytic cysteine residue is completely buried by the activation peptide, where an electrostatic interaction between Arg11 from the activation peptide and Asp 343 found within the catalytic domain places the activation sequence in a position that makes Cys314 inaccessible towards its substrates[35]. Cleavage occurs via thrombin mediated hydrolysis of the Arg37-Gly38 peptide bond found in the N-terminus of FXIIIA. This proteolytic event considerably weakens the interaction between the FXIII A-subunits from the inhibitory FXIII B-subunits. In the presence of Ca^{2+}, the separation of the $FXIIIA_2$ homodimers

into an active transglutaminase (FXIIIa) takes place. Like other TGases, FXIIIa can crosslink proteins/peptides via its transamidation activity to form isopeptide bonds and can also perform the reverse isopeptidase activity. Interestingly, without proteolytic cleavage and in the presence of high Ca^{2+} concentration in the cellular environment, the B-subunits can be removed from the heterotetrameric complex ($FXIIIA_2B_2$) thus liberating the FXIIIA zymogen with its activation sequence bound (FXIIIA')[107]. Unlike TG2, FXIII does not possess a GTP/GDP binding site that allosterically regulates the enzyme's activity[107]. However, the homologous residues of FXIIIA interact with the FXIIIB subunit. Furthermore, the redox regulation by the vicinal cysteine residues in TG2 are substituted by Arg408 and Cys409 in FXIIIA and form the central core of the dimeric interface of $FXIIIA_2$ homodimer[107]. This suggests that these two homologous regions may have regulatory functions for either enzyme, although the biochemical nature of the binding partner is different for the two transglutaminases.

1.4.2 Physiology

FXIII circulates the plasma as a heterotetramer protein complex composed of two A-subunits and two B-subunits. The A-subunit contains the active site of the transglutaminase, and is synthesized by hepatocytes, monocytes, and megakaryocytes[108]. The B-subunit serves as an inhibitory carrier of the A-subunit in the plasma, and it is synthesized in the liver[108]. $FXIIIA_2$ is expressed primarily in cells of bone marrow origin, where platelets have a high concentration of $FXIIIA_2$[35]. The heterotetrameric FXIII complex is converted to an active plasma transglutaminase that participates in the final stage of the coagulation cascade. Thrombin activated FXIII (named FXIIIa), in the presence of Ca^{2+}, catalyzes the formation of covalent crosslinks between γ-glutamyl and ε-lysyl residues on adjacent soluble polymerized fibrin chains

into insoluble crosslinked polymerized fibrin clots[109]. FXIIIa also crosslinks α2-antiplasmin, a plasmin inhibitor, to fibrin clots to make the developing fibre more resistant to fibrinolysis[109].

The coagulation cascade is part of the wound healing response that begins after the wound is formed. Inflammatory cells such as macrophages and neutrophils migrate to the wounded area by a chemotactic effect induced by cytokines. Angiogenesis then starts under the influence of growth factors such as vascular endothelial growth factor (VEGF), fibroblast growth factor, and transforming growth factor-G. The newly synthesized small vessels, together with fibrin, will form the granulation tissue. Besides the significant role of FXIII in fibrin chain crosslinking, FXIIIa crosslinks with proteins such as fibronectin and vitronectin, which adhere to the integrin of inflammatory cells[110]. As a result, adhesion of the inflammatory cells is enhanced, and the integrin related signal pathway is activated. It is found that fibronectin plays a potential role in the activation of macrophage[111], and crosslinked vitronectin can inhibit apoptosis of neutrophils[112]. FXIIIa supports platelet adhesion to integrins on the surface of the platelet cells, a process independent of its transglutaminase activity, to stabilize the provisional extracellular matrix at the very early stage of wound healing[110]. FXIII also plays an important role in angiogenesis. VEGF receptor-2 (VEGFR-2) and $\alpha_v\beta_3$ integrin on the surface of vascular endothelial cells are both signal molecules in angiogenesis, which can be activated by fibronectin and vitronectin when crosslinked with FXIIIa[113]. VEGFR-2/$E_v\beta_3$ complex formation mediated by FXIII further activates the signal pathway towards a proangiogenic effect[114].

1.4.3 Associated Diseases

1.4.3.1 General

Unregulated crosslinking activity of FXIIIa can lead to pathogenicity, mainly creating a disruption in the coagulation and wound healing processes. Moreover, disturbance in FXIII-protein interactions can induce negative biological outcomes, resulting in affected signalling pathways of a disease state. FXIII has been implicated in the pathogenesis of diseases such as thrombosis[115] and an autosomal recessive FXIII deficiency[116].

1.4.3.2 FXIII deficiency

Factor XIIIA deficiency is a rare bleeding disorder inherited as an autosomal recessive disease. FXIIIA deficiency can be due to a reduction in FXIIIA synthesis (Type I) or decreased FXIIIA function (Type II)[116]. Affected individuals experience severe, lifelong bleeding, characteristically from the umbilical cord at birth, and intracranial bleeding[117]. In addition, delayed wound healing in some patients and recurrent miscarriages have been reported[117]. Plasma FXIII has a long half-life (9-14 days), and levels of greater than 3-5% of plasma FXIII are sufficient to prevent spontaneous bleeding[116]. FXIII deficiency is often treated with cryoprecipitate or fresh frozen plasma. However, the risks of blood infection or systemic reaction are possible. Recombinant FXIIIA concentrate is also used for treatment and is free of any human products, making it safer than the plasma derived FXIII. Patients are regularly injected with the clotting factor concentrate to prevent bleeding. Continuous prophylactic therapy every month is recommended for patients with severe FXIII deficiency to prevent life threatening spontaneous bleeding[116].

1.4.3.3 Venous thrombosis

Thrombosis, the obstruction of blood flow due to the formation of clot, which may result in tissue anoxia and damage, is a major cause of morbidity and mortality in a wide range of arterial and venous diseases. Unregulated hemostasis can promote blood clotting which can cause a pathologic thrombosis, leading to arterial or venous occlusions. Three factors are involved in the induction of a thrombus; the vessel wall, coagulation proteins, and platelets[118]. Moreover, pathways regulating thrombus formation are similar to those that regulate hemostasis. Arterial thrombosis is highly dependent on the state of the vessel wall, the platelet, and factors related to blood flow[118]. In contrast, venous thrombosis arises from defects in the proteins governing coagulation and/or fibrinolysis, such as FXIII[118].

Growing evidence has suggested that fibrin clot morphology plays an important role in venous thrombosis. A study investigating the morphology of clots has demonstrated that patients with venous thrombosis tend to form clots that are denser and have increased resistance to fibrinolysis[119]. Following that conclusion, it was illustrated that crosslinking activity of FXIIIa increases clot density and further increases its resistance fibrinolysis[120]. Plasmin is an important serine protease that is involved in fibrinolysis and its activity on a fibrin clot is inhibited by α2-antiplasmin. FXIIIa crosslinking of α2-antiplasmin to the fibrin clot can evoke a prothrombotic effect[109].

One notable polymorphism of FXIIIA is an amino acid exchange of Val34Leu, which is located on the activation peptide. This polymorphism has been associated with thrombosis due to an increased activity of FXIII Val34Leu during blood coagulation[121]. Since the polymorphism is located just 3 amino acids before the thrombin cleavage site, it is not surprising that Val34Leu substitution influences the effect of thrombin on FXIII activation[120]. It was demonstrated with

both cellular FXIII and plasma FXIII that in the case of the Leu34 variant, the cleavage of the activation peptide proceeds at an approximately 2.5-fold higher rate than in the case of Val34 variant[122]. The relationship between FXIII Val34Leu polymorphisms and thrombosis has been reviewed with a conclusion that the polymorphism association is conflicting between studies[123]. Thus, additional studies are required to explore the effect of FXIII Val34Leu polymorphism on the risk of thrombotic diseases.

1.4.4 Current inhibitors

As noted above, patients with a disrupted hemostasis, more specifically fibrinolysis, are at risk of developing venous thrombosis. More so, the level of fibrinolysis is associated to fibrin clot stability. This suggests that treatment can be carried out by modulating FXIIIa activity to normalize the fibrinolytic rates in patients with thrombotic tendency, by reducing crosslinking of fibrin clot and addition of inhibitory proteins (ex. α2-antiplasmin). Thus, the design of a selective and potent FXIIIa inhibitor can be used as a therapeutic tool for thrombosis patients by acting as an antifibrinolytic agent. Also, inhibitors that target coagulation factors can disrupt hemostasis and may be used as anticoagulants in a therapeutic setting. Furthermore, selective irreversible inhibitors with or without a "tag" (i.e. fluorophore, bioorthogonal moiety, radioisotope) can be used in a biological setting to further understand the mechanistic pathway, localization, known substrates, and distribution of FXIIIa in both healthy and disease states. Like TG2, the field of FXIIIa inhibitors has focused on designing competitive acyl donor inhibitors.

To date, only a few inhibitors have been reported for FXIIIa. Tridegin, a 66-amino acid peptide was isolated from the salivary gland of the leech *Haementeria ghilianii* and reported as a potent reversible inhibitor of FXIIIa, with a reported IC_{50} of approximately 9 nM[124]. Other

research groups have contributed to the drug discovery process by providing substrate sequence information to aid in the design of peptidic or peptidomimetic inhibitors for FXIIIa[124,125]. In the early 90s, researchers developed a few pharmacophores, such as 2-[(2-oxopropyl)thio]imidazolium[126] and 5-methylthiazolo-[2,3]-1,3,4-thiadiazolium[127] (depicted in Figure 1.8) that demonstrated inhibitory activity towards FXIIIa. In addition, both pharmacophores showed selective reactivity towards the enzyme over glutathione, a thiol molecule found at high concentration (~5 mM) in the cell that can interfere with enzyme binding[126]. These discoveries provide insight on the reactivity of warhead towards the enzyme, but no selectivity over other cysteine proteases, making these inhibitors nonspecific.

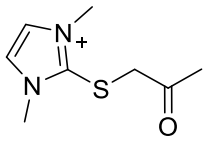

2-[(2-oxopropyl)thio]imidazolium derivative

k_{inact}/K_I = 2.1 x 10^5 M^{-1} min^{-1}

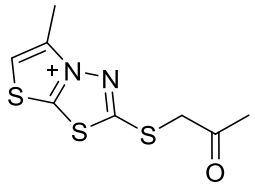

5-methylthiazolo-[2,3]-1,3,4-thiadiazolium derivative

k_{inact}/K_I = 13.8 x 10^6 M^{-1} min^{-1}

Figure 1.8. Reactivity of FXIIIa pharmacophores.

Other series of small molecules that irreversibly inhibit FXIIIa, which bear electrophilic pharmacophores, such as 3-substituted bicyclic [1,2,4]-thiadiazole[128] and mono-substituted cyclopropenone[129] were explored through individual SAR studies. In SAR studies[129] with the mono-substituted cyclopropenones, compound 5 (Figure 1.9) was obtained as the most potent inhibitor; however, no test of selectivity with other TGases or cysteine proteases was conducted. From the 3-substituted bicyclic [1,2,4]-thiadiazole SAR study[128], compound 16 (Figure 1.10)

was obtained as the most potent inhibitor, with a 76-fold selectivity towards FXIIIa over guinea pig liver TG2.

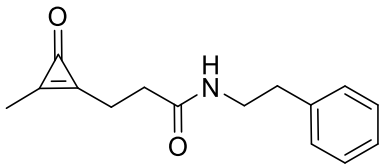

Compound 5

k_{inact}/K_I = 3.0 x 10^5 M^{-1} min^{-1}

Figure 1.9. Cyclopropenone based irreversible FXIIIa inhibitor.

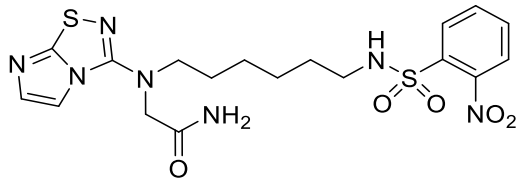

Compound 16

k_{inact}/K_I = 2.7 x 10^5 M^{-1} min^{-1}

Figure 1.10. 3-substituted bicyclic [1,2,4]-thiadiazole based irreversible FXIIIa inhibitor.

Due to the structural homology between TG2 and FXIIIa, unfortunately, many TG2 inhibitors have been claimed or advertised as selective FXIIIa inhibitors. To date, Zedira GmbH has been able to successfully obtain an X-ray crystal structure of FXIIIa with a peptidic irreversible inhibitor[130] (**ZED1301**, Figure 1.11), whose design was based on a selective FXIIIa peptidic substrate (DQMMLPWPAVL) discovered through a phage-displayed peptide library[125].

Inhibitor ZED1301 binds at the surface of the catalytic domain of FXIIIa with an IC_{50} value of 0.1 µM and a 30-fold selectivity over human TG2 (IC_{50} = 3 µM).

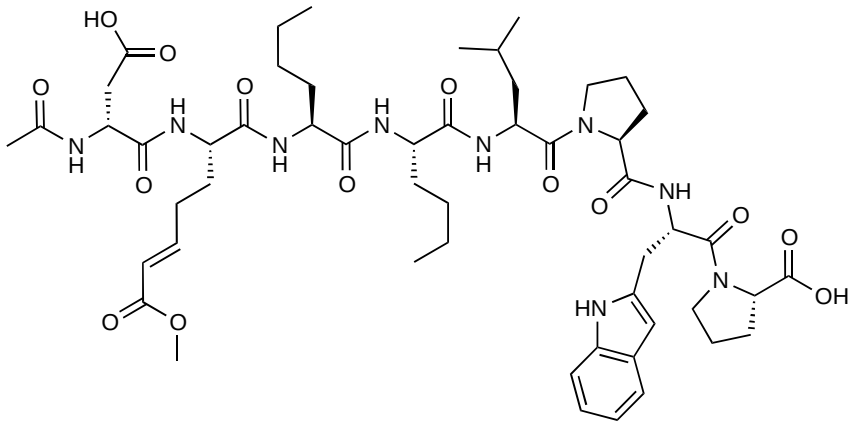

Figure 1.11. Compound ZED1301, a peptidic irreversible FXIIIa inhibitor.

1.5 Irreversible enzyme inhibitors

Enzyme binding can occur through irreversible or reversible interactions, where enzyme binds with the appropriate substrate or inhibitor. Affinity-based irreversible enzyme inhibitors inactivate the enzyme by forming a covalent bond with the enzyme and filling the suitable binding pocket. This inactivation is a result of a chemical reactivity between the inhibitor molecule and enzyme, creating a covalently bound inhibitor enzyme complex. Irreversible inhibitors rely on the reactivity of the enzyme's active site, such as having an electrophilic moiety directed towards a nucleophilic residue.

For all irreversible inhibitors, the inactivation of the target enzyme occurs through a covalent bond. Over a range of irreversible inhibitor concentrations, the rate of covalent bond formation will be slow on the time scale of enzyme turnover. Therefore, the reaction progress

curve will be nonlinear, displaying time-dependent inhibition in the presence of an irreversible enzyme inhibitor. Also, when the concentration of inhibitor is equal to or exceeds the enzyme concentration, the progress curve may reach a plateau value, with steady state velocity of zero, prior to consumption of substrate. The rate at which the system is inactivated can be assessed by calculating the pseudo-first order rate constant k_{obs}. Furthermore, the mechanism of an irreversible inhibitor can proceed through either a single-step or a two-step mechanism (scheme 1.3). Non-specific inhibitors can covalently bind to any amino acid residue on the enzyme and not every modification will lead to an inactivation. In single-step non-specific covalent modification, the dependence of k_{obs} on the inhibitor concentration will appear as linear and non-saturating. With regards to two-step covalent inactivation, reversible binding to enzyme happens first under a rapid equilibrium followed by a covalent bond formation. With two-step irreversible inhibitors, a plot of k_{obs} as a function of inhibitor concentration will show saturation, reaching a plateau value at high values of inhibitor concentrations (Figure 1.13), related to the rate constant of covalent inactivation (k_{inact}). The slope of the linear fit will have units of a second order rate constant ($M^{-1}\ s^{-1}$) and is the best measure of relative inactivator efficiency and is usually reported in the literature as k_{inact}/K_I. The data, as illustrated in figure 1.9, for these target specific irreversible enzyme inhibitors will fit to the following equation:

$$k_{obs} = \frac{k_{inact}[I]}{K_I + [I]}$$

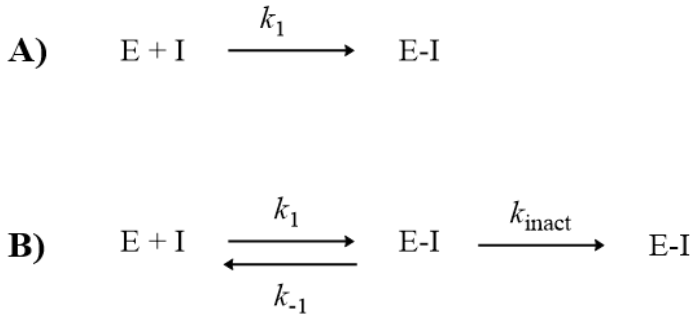

Scheme 1.3. Mechanisms of irreversible enzyme inhibitors. (A) Nonspecific inhibition, (B) Affinity-based inhibitor.

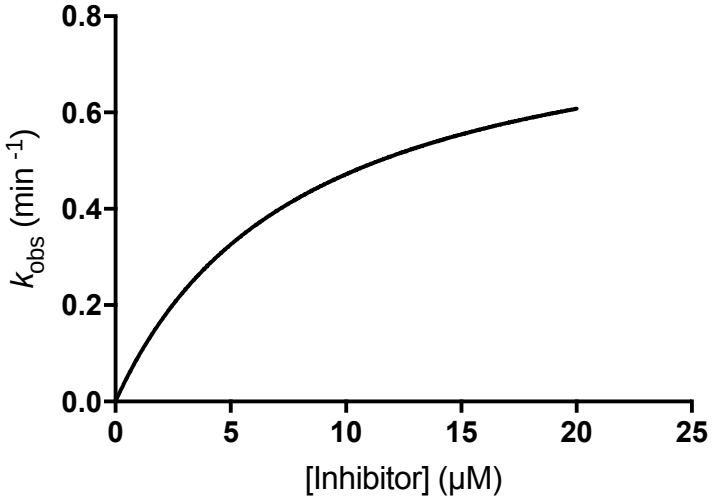

Figure 1.12. Plot of k_{obs} as a function of inhibitor concentration for a two-step mechanism of inactivation.

For reversible inhibitors, IC_{50} values are highly relative and depend upon the assay used to measure activity, the concentration of substrate used, and the mode of inhibition, to name just a few factors[131]. For irreversible inhibition, IC_{50} values may be useful within one study, but not meaningful when used to compare two separate studies. Irreversible inhibitor activity depends on

the time of incubation, temperature, concentration of enzyme and competing substrate inhibitors[132]. Thus, irreversible inhibitors are best compared using the second order rate constant or efficiency parameter, k_{inact}/K_I.

1.6 Thesis overview and goals

The primary aim of the research presented herein was to gain more knowledge of irreversible inhibitors of human TG2, by understanding their mode of inhibition, and/or to optimize their potency using a SAR approach and the appropriate kinetic evaluations. Most of the work was done starting from the lead irreversible chemical probe **NC9** (Figure 1.6), where the carboxylbenzyl extremity is designated as the 'West end', connected to a dansyl fluorophore end, called the 'East end', by a polyethylene glycol linker. **NC9** also carries a lysine-based acrylamide warhead that reacts covalently with the enzyme.

Using the scaffold of a very poor TG2 inhibitor from our initial SAR study and a published FXIIIa crystal structure bound to a peptidic irreversible inhibitor, a second project emerged with the goal of designing a novel small molecule FXIIIa irreversible inhibitor. An SAR approach and the appropriate kinetic evaluations will be used to understand inhibitor's potency and mode of inhibition.

Overall, the research presented may be grouped into two enzyme inhibitor design and evaluation projects, as described in greater detail in the upcoming chapters.

Chapter Two: **Design and synthesis of TG2 inhibitors**

2.1 Targeted covalent inhibitors as drug candidates

Targeted covalent inhibitors (TCIs) reversibly associate with a biological target and then react to form a covalent attachment. The scaffold holding the electrophilic group confers affinity for the target enzyme. At the site of inhibitor association, the electrophilic group reacts with the nucleophilic residue within its proximity. The covalently attached scaffold will block the site of association and permanently shut down enzyme activity, protein-protein interaction and/or signalling pathway. The development and use of these class of inhibitors as drugs has been reviewed recently[133,134].

Due to the covalent attachment of TCIs on their targets, their duration of action is greater than that of reversible inhibitors. This covalent attachment to the target provides TCIs with a higher overall efficacy in comparison to their non-covalent reversible analogues. Ultimately, the duration of action of TCIs is dependent on the protein target's turn over. Hence, covalent inhibitors provide a prolonged duration of action for biological targets with slow turnovers. This can be both beneficial and a risk during drug discovery. Longer duration of target inhibition allows for a lower dosage (meaning less risk of toxicity), but if the target has a physiologically important function and a slow rate of resynthesis, then risks are introduced.

The major concern with covalent inhibitors as drug candidates is the possibility for non-specific target binding. The warhead's reactivity to other off-target proteins can lead to toxic events leading to undesired side effects. This concern can be reduced by attenuating the reactivity of the warhead and increasing the selectivity towards the target. The latter can be challenging when the target is a member of a family of proteins with similar binding pockets. In

comparison to non-covalent inhibitors, covalent inhibitors with electrophilic warheads are more likely to be cleared by the liver as they can react with the thiol group of glutathione found in cells, lowering the drug's bioavailability[135]. Thus, a lower reactivity of the warhead towards glutathione can slow its clearance and increase the probability of the interaction of the inhibitor with its intended target. Although glutathione has been the medicinal chemist's standard for warhead reactivity within the cell, one should also consider other potential cellular nucleophiles such as amines, cysteine, γ-glutamylcysteinlysine and cysteamine[136].

More recently, a higher number of TCIs have been developed as drugs due to their selectivity and higher efficacy during therapy. For example, ibrutinib (Figure 2.1) is a potent and selective inhibitor of Bruton's tyrosine kinase (BTK), a cancer target linked to mantle cell lymphoma[134]. This FDA approved drug carries an acrylamide warhead that is reportedly selective towards Cys481 found in the ATP binding pocket of BTK[137]. This class of inhibitors has produced promising drug candidates and current development is focussed on their selectivity, efficacy, and toxicity.

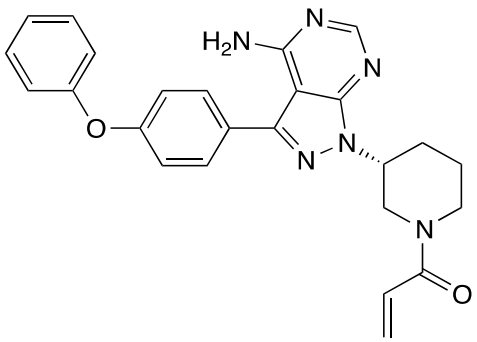

Figure 2.1. Chemical structure of ibrutinib, a potent inhibitor of Bruton's tyrosine kinase (BTK).

2.2 Previous work done by Keillor group on TG2 covalent inhibitors

Many covalent inhibitors for TG2 have been developed in the Keillor group. The design of these covalent inhibitors was based on two peptidic scaffolds, Cbz-Gln-Gly and Cbz-Phe-Gln, that are known to be TG2 donor substrates[101,138]. Each scaffold was functionalized with an electrophilic group that can covalently attach to the nucleophilic cysteine thiolate found in the enzyme's active site, rendering the enzyme inactive. To avoid cytotoxicity, the electrophilic moiety should be stable outside of the enzyme's binding pocket and reactive within, thus avoiding unwanted covalent attachment to other biological components (i.e. other cysteine proteases). Within the Keillor group a variety of electrophilic groups, or 'warheads', were used in the design of TG2 covalent inhibitors. These included chloromethyl amides[139], 1,2,4-thiadiazoles[140], maleimides[141], epoxides[142] and α,β-unsaturated amides[142]. The inhibitors bearing the prementioned warheads were evaluated for their activity against purified guinea pig liver TG2, using a continuous transamidation assay[143]. The efficiency of these covalent inhibitors was evaluated through the hyperbolic Kitz and Wilson equation (Chapter 1, Section 1.5) and expressed as the ratio of k_{inact}/K_I (analogous to k_{cat}/K_M used to express the efficiency of an enzyme substrate). Highly efficient covalent inhibitors of purified guinea pig liver TG2 from various SAR studies conducted by the Keillor group are depicted in Figure 2.2 with their k_{inact}/K_I ratio.

From these SAR studies, a few distinguishing results were noted regarding affinity, efficiency and reactivity of inhibitors towards guinea pig liver TG2. The affinity (K_I) of most inhibitors was found to lie in the sub-micromolar range, where the Cbz-Gln-Gly scaffold inhibitors displayed higher affinity than the Cbz-Phe-Gln scaffold inhibitors. Overall, the reactivity rate of electrophilic groups towards the enzyme were similar with an inactivation rate

constants (k_{inact}) ranging from 0.5 – 1.0 min^{-1}. Thus, giving inhibitor efficiencies of (k_{inact}/K_I) of approximately 10^5-10^6 M^{-1} min^{-1}. The maleimide-based inhibitors were not as efficient, with lower values of approximately 10^3 M^{-1} min^{-1}. Using the Cbz-Gln-Gly scaffold, inhibitor activity was increased with a longer side chain bearing their respective warheads. Studies by the Keillor group and others[45,104,144] have shown that the removal of the Cbz group presented a lower affinity towards the TG2. Furthermore, the acrylamide warhead showed to be stable *in vitro*, against 1.6 mM of glutathione at physiological condition (pH = 7.0 and 37 ˚C)[139]. After 24 hours, only 10% of the Cbz-Lys(Acr)-Gly inhibitor was consumed by glutathione.

As illustrated in Figure 2.1, the most efficient inhibitor from pioneering work in the Keillor group was Cbz-Lys(Acr)-Gly (k_{inact}/K_I = 3.0 x 10^6 M^{-1} min^{-1}), which also had a low K_I value of 0.15 µM. The Cbz-Lys(Acr)-Gly inhibitor was synthetically modified with a PEGylated linker bonded to a dansyl fluorophore moiety. The inhibition activity of the designed chemical probe, NC9 (Figure 1.6), was tested against guinea pig liver TG2 with an efficiency value of k_{inact}/K_I = 1.4 x 10^4 M^{-1} min^{-1}. To further understand the physiological behaviour of TG2 in biological contexts, numerous research collaborations with the Keillor group used NC9 as a chemical probe to explore the enzyme's role in selected disease states[60,145,146] and/or understand the enzyme's conformation in a cellular context[51,52,147].

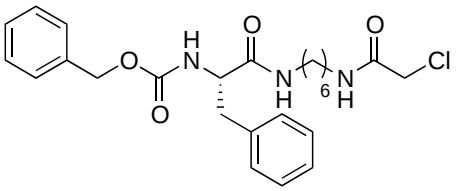

k_{inact}/K_I = 5.3 x 10^5 M^{-1} min^{-1}

JWK-1

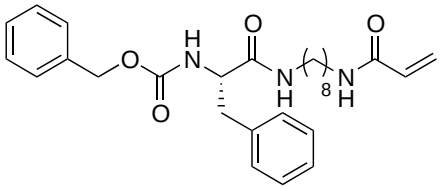

k_{inact}/K_I = 1.1 x 10^5 M^{-1} min^{-1}

JWK-2

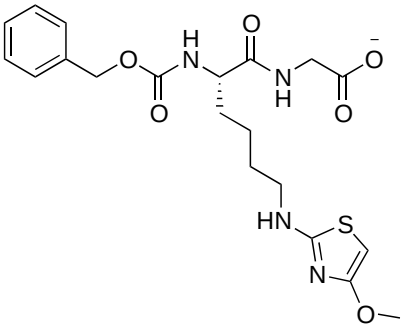

k_{inact}/K_I = 7.2 x 10^5 M^{-1} min^{-1}

JWK-3

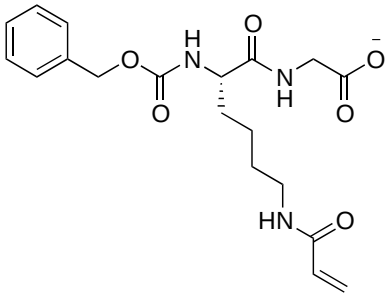

k_{inact}/K_I = 3.0 x 10^6 M^{-1} min^{-1}

JWK-4

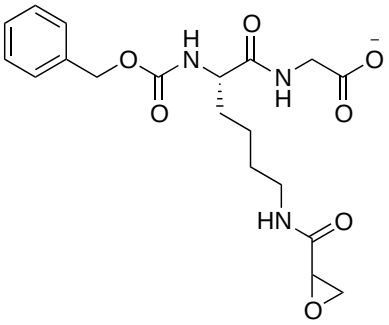

k_{inact}/K_I = 2.0 x 10^6 M^{-1} min^{-1}

JWK-5

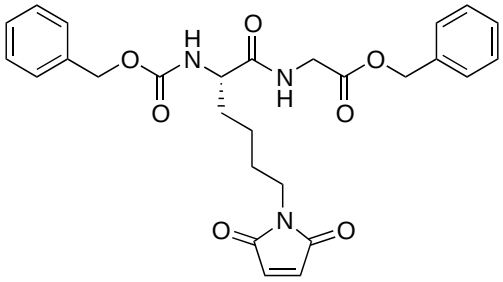

k_{inact}/K_I = 17.1 x 10^3 M^{-1} min^{-1}

JWK-6

Figure 2.2. Most efficient covalent inhibitors against guinea pig liver TG2 from the various SAR studies conducted by Keillor group. For simplicity, Keillor inhibitor in this figure are arbitrarily labelled from JWK-1 to JWK-6. Covalent inhibitors in this figure were synthesized and evaluated in various SAR studies conducted by the Keillor group[139–142]**.**

2.3 Inhibitor design

A crystal structure of the extended form of human TG2 (PDB code 2Q3Z) in complex with a covalent inhibitor has been reported by the Khosla group[16]. The covalent inhibitor, Ac-P(DON)LPF-NH_2, was bound to the active site cysteine via its 6-diazo-5-oxo-L-norleucine (DON) warhead. The active site was described as a hydrophobic binding groove with a hydrophobic tunnel leading to catalytic cysteine and its histidine base. In contrast to an earlier crystal structure of human TG2 bound to GDP[19], which depicted the enzyme in a folded or 'closed' conformation, Khosla's covalent inhibitor locked the extended TG2 structure in its 'open' conformation.

In Figure 2.3, NC9 was docked into the structure of extended conformation of human TG2 (PDB code 2Q3Z) in place of Khosla's covalent inhibitor. In the lowest energy poses, the acrylamide warhead was placed next to the active site nucleophile, the Cbz group was bound in Pocket 1 and the dansyl group occupied Pocket 2. Similar to the C-terminus Phe of Khosla's inhibitor, which formed hydrophobic interactions with Pocket 2, NC9 shared a similar hydrophobic interaction through its dansyl group.

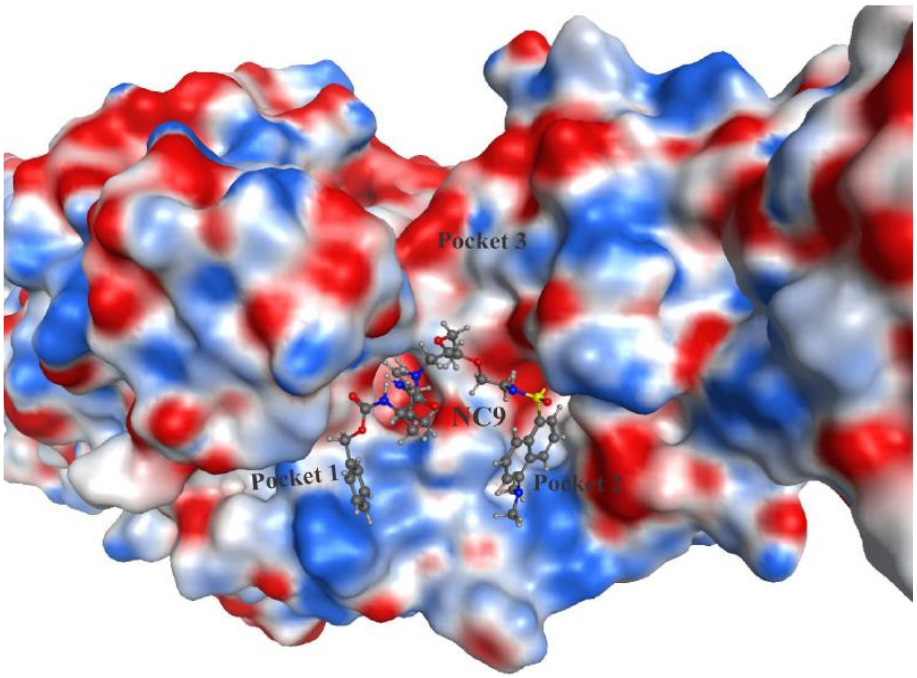

Figure 2.3. Putative binding model of NC9 with human TG2. Using the default parameters of the Molecular Operating Environment (MOE) software, NC9 was energetically minimized and docked into the structure of 'open' conformation hTG2 (PDB code 2Q3Z). The observed binding pockets in the active site of hTG2 were labelled from pocket 1-3 for reference.

As mentioned above, previous inhibition studies based on the Cbz-Phe[45,101]and Cbz-Lys[99,144] scaffolds have shown that the N-terminal Cbz protecting group confers affinity to these covalent inhibitors. It was also noted, that the acrylamide warhead demonstrated an ideal balance between its stability against glutathione and reactivity towards TG2. As such, the Cbz group and the acrylamide warhead were maintained throughout the SAR study in this thesis. While maintaining the prementioned groups, we systematically varied the length of the side chain, the peptide backbone spacer, and the C-terminal R group (Figure 2.4), seeking to optimize inhibition efficiency.

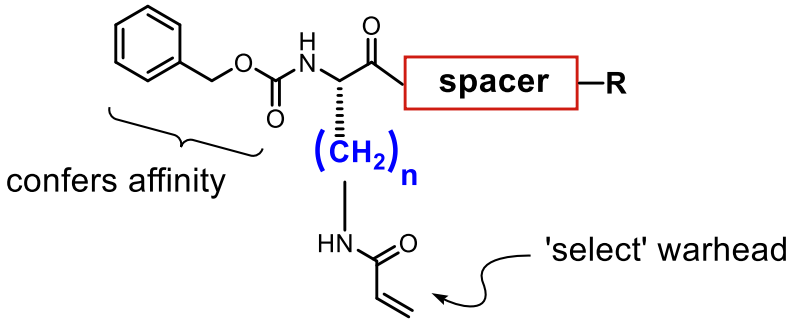

Figure 2.4. Proposed structural modifications for this work's SAR study with human TG2.

2.4 Inhibitor synthesis

As mentioned in section 2.2 above, the most potent inhibitor developed by the Keillor group was prepared using a Cbz-Lys scaffold with an attenuated acrylamide warhead. More specifically, Keillor and co-workers found that Cbz-Lys(Acr)-Gly was a very potent inhibitor of guinea pig liver TG2. In this thesis, the Cbz-Lys scaffold served as a starting point scaffold for the SAR study. Furthermore, the subsequent SAR study for this dissertation evaluated synthesized compounds against human TG2. The N-terminal Cbz protecting group, on the 'West end' of the inhibitors, was maintained as it confers affinity. Our investigation started with modification of the spacer (Figure 2.4) which links the 'East end' of the inhibitors to the N-terminal Cbz-Lys scaffold bearing the acrylamide warhead. Also, to focus on the effect of spacer length variation only, the 'East end' was maintained as an aromatic and hydrophobic dansyl group, which may provide favourable association with the hydrophobic binding pocket of hTG2. Different diamine spacers were rationally chosen to connect the east and west ends of our covalent inhibitors via amide bonds that mimic peptidic backbones, which may provide beneficial intermolecular interactions with the enzyme (Figure 2.4). Keeping Lipinksi's[148] and

Veber's[149] rules in mind, we reduced the number of rotatable bonds and polar surface area (PSA) by systematically decreasing the length of the diamine spacer. The monodansylated alkylamines shown in Figure 2.5 were synthesized and coupled to activated carboxylic acid of Cbz-Lys(Acr) to give our first inhibitor series. To ease with the purification of the monodansylated alkyl amines, a Boc group was added to the free amine, making it more hydrophobic and easier to elute from a chromatography silica-based column. The addition of the Boc group also increased the yield of reaction by increasing solubility in the organic phase during aqueous washes and avoiding diamine coupling during synthesis.

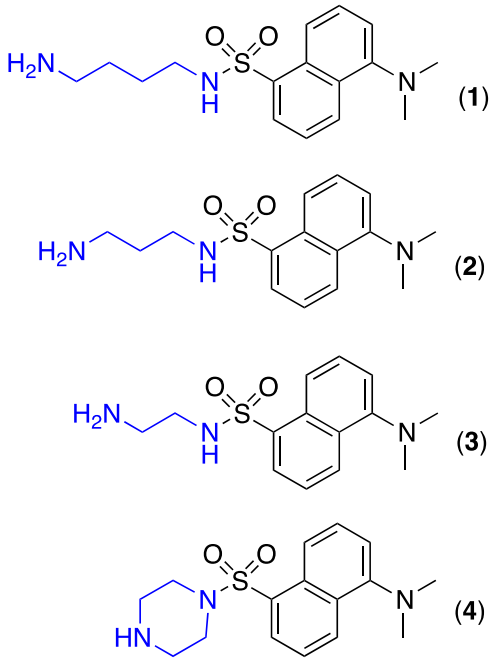

Figure 2.5. Monodansylated alkylamine spacers.

Depending on the kinetic evaluations of the spacer series, additional inhibitors were prepared maintaining the Cbz group and dansyl group, while systematically varying the side

chain length bearing the acrylamide warhead. These inhibitors were synthesized using commercially available Cbz protected amino acids such as Z-Dap-OH, Z-Dab-OH and Z-Orn-OH. The acrylamide derivatives used with the various amine side chains are depicted in Figure 2.6.

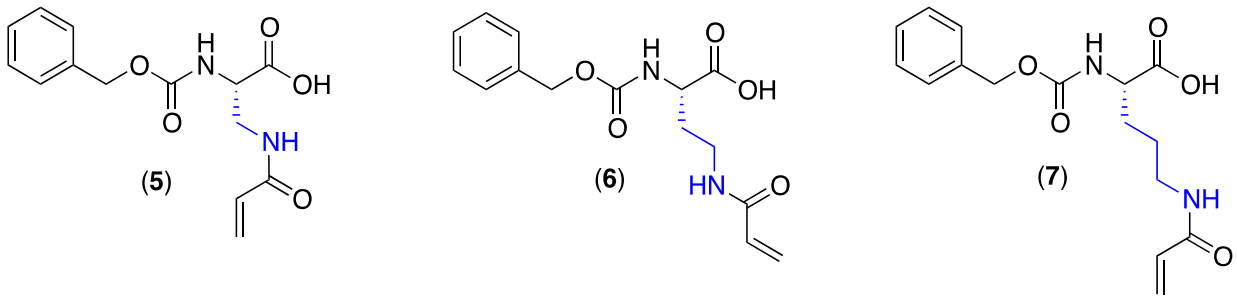

Figure 2.6. Cbz protected amino acids bearing an acrylamide warhead on their side chain with varying length.

Once the appropriate spacer and sidechain length was found for optimal inhibitory activity against human TG2, the SAR study shifted its focus to the dansyl group. The SAR study on the 'East end' series of inhibitors replaced the dansyl group with various aromatic and aliphatic derivatives. The goal was to probe the interaction with the putative hydrophobic binding pocket of human TG2. Furthermore, the hydrophobic derivatives on the 'East end' were linked in two ways to the spacer; via a sulfonamide or a carboxamide group. The variation in the linkage was expected to possibly orient the C-terminal hydrophobic group slightly differently due to the conformational difference between a carboxamide and a sulfonamide. For the work of this thesis, the focus was synthesizing and evaluating three carboxamide linked aromatic derivatives; 1-naphthyl, 2-naphthyl and a phenyl group.

The general procedures and details for the synthesis of intermediates and final compounds can be found in Chapter 7. Presented below are brief discussions of any noteworthy anomalies or improvements from the synthetic procedures we used (Scheme 2.1).

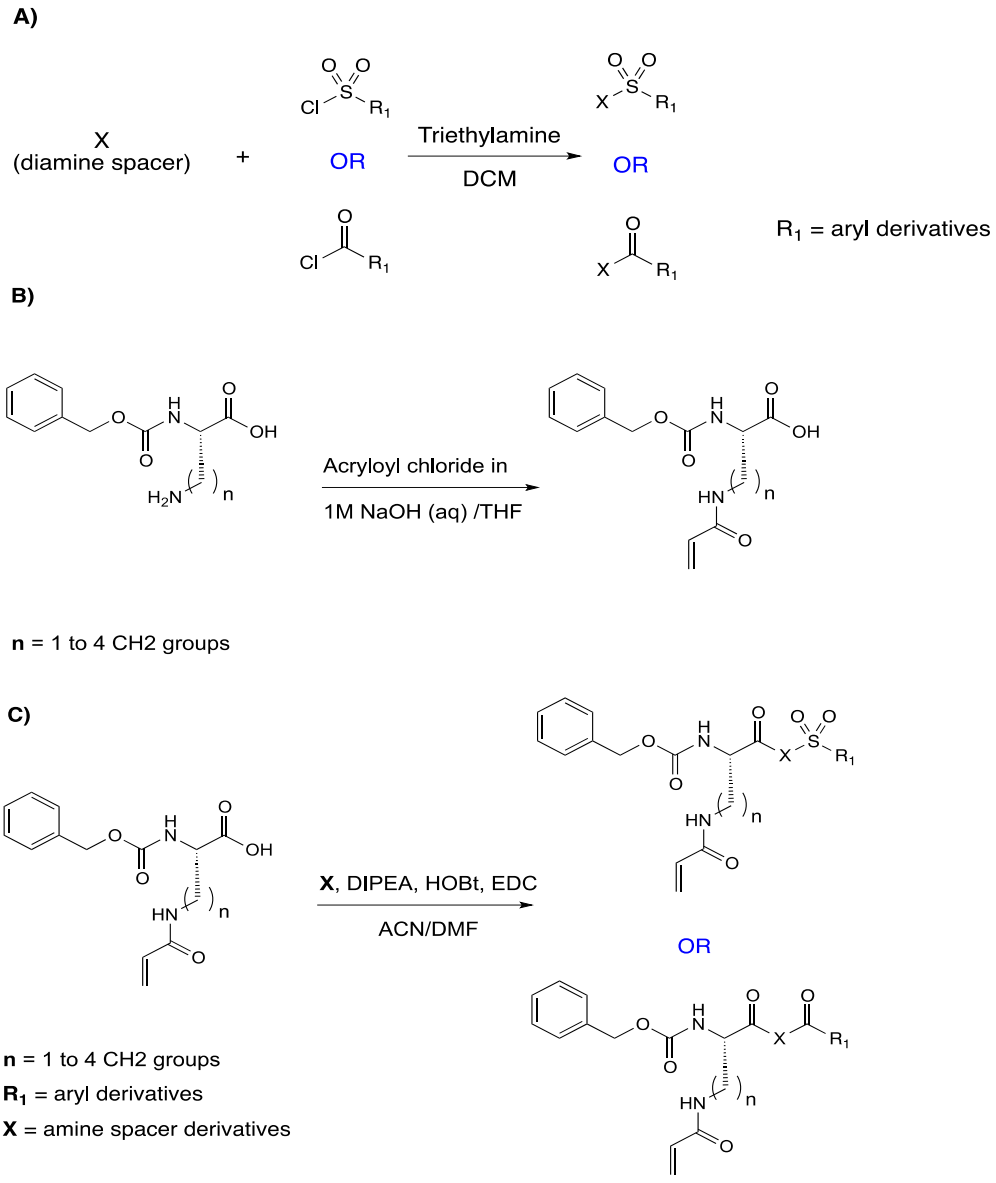

Scheme 2.1. General scheme for the convergent synthesis of this work's hTG2 covalent inhibitors, where the products of scheme A and B are combined to make final inhibitors in C.

2.4.1 Addition of warhead

The attachment of an acrylamide group on the side chain of Cbz protected amino acid derivatives was adapted from a previous method[144]. The amine groups of commercially available Cbz protected amino acids were reacted with acryloyl chloride to afford the desired acrylamide, as illustrated in Scheme 2.1 A. The reaction took place in a basic aqueous medium with THF and was completed anywhere from 30 minutes to 2 hours. The reported yield for this reaction using 4-bromoanaline was 90%, while this work reports yields ranging from approximately 62-82% using Cbz protected amino acids. Pure intermediates were isolated through multiple extraction with ethyl acetate to remove acrylic acid, an impurity in this reaction. Extraction of acrylamide products with DCM, provided an impure mix with acrylic acid (identified with 1H NMR). The highest yield was afforded with Cbz-Lys (82%) where the side chain possessed 4 methylene units followed by the nucleophilic amine. A loss of 1 methylene unit from Cbz protect amino acid (Cbz-Orn) decreased the yield to 70%. A similar pattern occurred with the loss of 2 and 3 methylene units from the Cbz protected amino acid, giving a yield of 62% and 64%, respectively. This observation can be linked to higher solubility of Cbz protected amino acids in the aqueous layer due to the loss of methylene units and thus a decrease in quantity is found in the organic layer.

2.4.2 Amide coupling to afford final compounds

The Cbz protected amino acids, bearing the warhead, and the amine linker derivatives, were coupled via an amide bond to afford the final compounds (Scheme 2.1 C). The carboxylic acid was activated into a better electrophile using 1-ethyl-3-(3-

dimethylaminopropyl)carbodiimide (EDC) and 1-hydroxy-1H-benzotriazole (HOBt). Nucleophilic primary or secondary amines then react with the activated esters to form an amide bond. Originally, O-(benzotriazol-1-yl)-1,1,3,3-tetramethyluronium hexafluorophosphate (HBTU) was used to perform the amide coupling synthesis; however, due to difficulty of removing its urea by-product, a combination of HOBt/EDC was used. A more water soluble carbodiimide was chosen (EDC), since its urea by-product can be readily washed away through multiple aqueous washes. The yield for these coupling reactions using primary amines ranged from 56% to 49% while the yield for amide coupling using secondary amines was lower in comparison, yielding around 41% to 32%. The overall low yield of this reaction can be attributed to formation of by-products such as N-acyl urea and formation of guanidium salts. In addition, activated esters are in lower concentration in hygroscopic solvents, which converts them back to carboxylic acids. Therefore, using anhydrous DMF/ACN as a solvent system can help increase the yield of amide product.

As mentioned above, inhibitors are rationally designed using information extracted from the inhibitor bound crystal structures, docking models and previous SAR studies. Following the synthesis of our acrylamide bearing inhibitors, they were kinetically evaluated for their affinity and efficiency to inactivate hTG2.

Chapter Three: **Evaluation of TG2 inhibitors**

3.1 Kinetic evaluation of transglutaminase activity in the presence of covalent inhibitors

A covalent inhibitor's potency can be evaluated through two parameters; K_I and k_{inact} (see Chapter 1, section 1.5 for introductory discussion). The equilibrium constant K_I is a measure of the covalent inhibitor's ability to dissociate from the enzyme-inhibitor complex (EI), thus providing a parameter that measures affinity to the target enzyme. Like the Michaelis-Menten equilibrium constant (K_M) for substrate binding to enzyme, K_I also considers all rate constants associated with the dissociation of enzyme-inhibitor complex (Figure 3.1). Therefore, K_I values reported hereafter are defined according to the following equation:

$$K_I = \frac{k_{-2} + k_{inact}}{k_2}$$

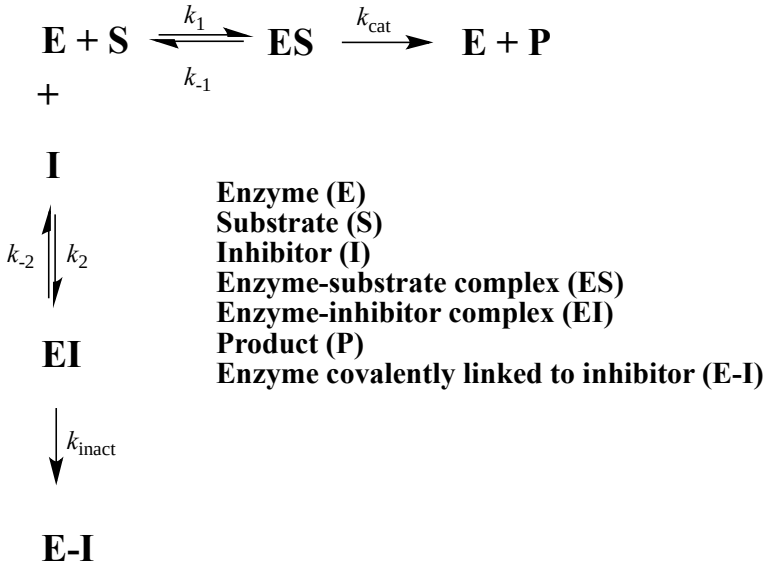

Figure 3.1. Irreversible inhibition via a two-step reaction; first forming a reversible complex (EI), followed by transformation to an irreversible complex (E-I). This irreversible inactivation competes with substrate and enzyme reaction.

where k_{inact} is the rate constant for the conversion of the reversible EI complex to the irreversibly inhibited enzyme E-I (Figure 3.1).

Transglutaminases (TGases) are known to catalyze reactions via a ping-pong mechanism (see Chapter 1.3, Scheme 1.2)[150]. At the active site, a thiol found on the nucleophilic cysteine residue is acylated by the γ-carboxamide group of peptide-bound glutamine (acyl donor). This acylation step results in the formation of a thioester acyl enzyme intermediate. Deacylation occurs through either hydrolysis or aminolysis of the intermediate thiolester acyl enzyme, resulting in the regeneration of free enzyme. In the absence of a primary amine acceptor, water is capable of regenerating free enzyme. Using a colorimetric assay[39] developed by the Keillor group, we can monitor the progress of the TGase reaction with a substrate mimic; *N*-Cbz-L-Glu(γ-*p*-nitrophenyl ester)Gly (**AL5**). The kinetics for the hydrolysis of the thiolester acyl enzyme intermediate can be monitored with **AL5**, as an increase of absorbance at 405 nm due to the release of p-nitrophenolate (Scheme 3.1).

Scheme 3.1. A general illustration of transglutaminase (TGase) reacting with AL5 to form a thiolester acyl enzyme intermediate that is observed spectrophotometrically at 405 nm.

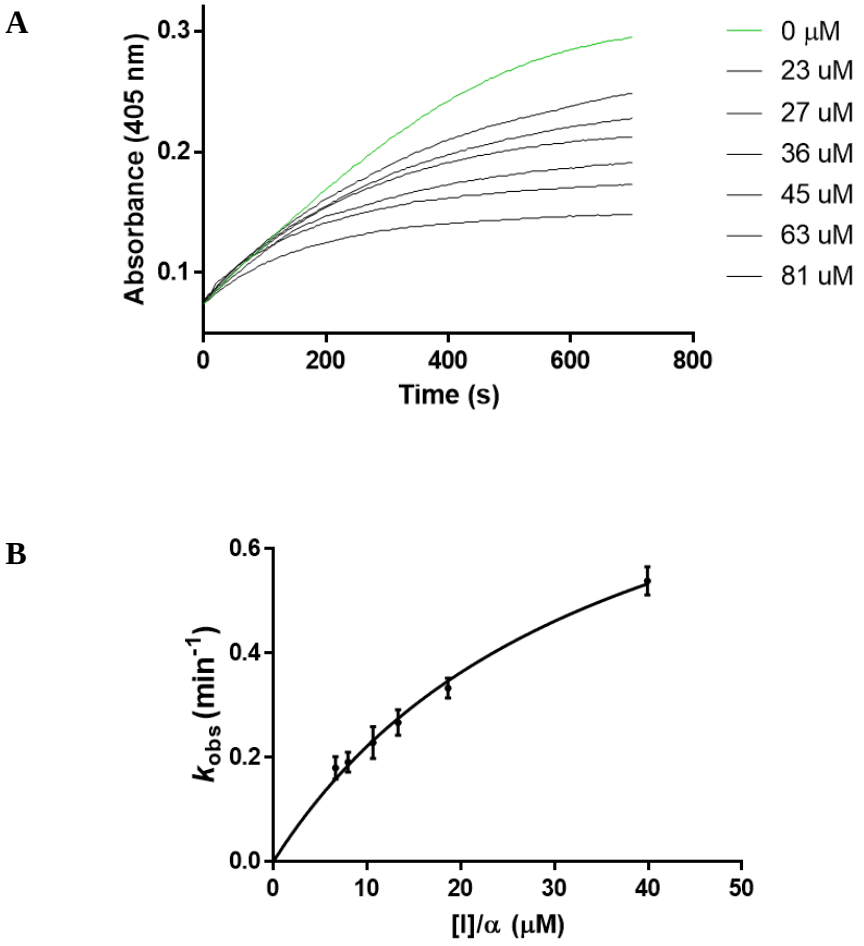

Figure 3.2. Determination of covalent inhibition parameters using a previously reported continuous colorimetric assay. (A) Time-dependent inactivation curves of enzymatic reaction in the presence of various concentrations of inhibitor 9. (B) Nonlinear regression to a hyperbolic equation of k_{obs} versus varying concentrations of inhibitor 9.

The data presented in Figure 3.2 A can be fit to a series of first-order exponential curves, from which one can measure the rate constant for inactivation of the enzyme (k_{obs}) by a given concentration of an inhibitor. For time-dependent irreversible inhibitors the value of k_{obs} is expected to increase over a certain range of inhibitor concentration and then exhibit saturation at higher concentrations of inhibitor as shown in Figure 3.2 B. Kitz and Wilson[151] have shown that the dependence of k_{obs} on inhibitor concentration for a time-dependent irreversible inhibitor is described by a hyperbola from which the values of k_{inact}, the maximal rate constant for inactivation of the enzyme by the inhibitor, and K_I, the apparent concentration of inhibitor displaying half-maximal rate of inactivation, can be extracted by the fitting the hyperbola to the Kitz and Wilson equation as follows:

$$k_{obs} = \frac{k_{inact}[I]}{\alpha K_I + [I]}$$

where α represents the competition between substrate and inhibitor towards the free enzyme. This reversible competition can follow this equation:

$$\alpha = 1 + \frac{[S]}{K_M}$$

The TG2 inhibitors presented herein are classified as covalent inhibitors, as they all are bearing an electrophilic acrylamide warhead. The efficiency of a covalent inhibitor is typically expressed as the ratio k_{inact}/K_I, derived from the hyperbolic Kitz and Wilson equation above, which is analogous to the k_{cat}/K_M used to express the efficiency of a substrate in an enzyme catalyzed reaction. As a point of reference, a k_{inact}/K_I ratio equal to or greater than 10^6 M^{-1} min^{-1}

may be considered as a highly efficient covalent inhibitor[18]. All kinetic parameters mentioned can be used to measure affinity and reactivity of different inhibitors and substrates, provided that key differences in experimental conditions (such as pH, temperature, and enzyme source) are taken into account. The covalent inhibitors kinetic evaluation against human TG2 were compared under the same experimental conditions.

3.1.1 Kinetic evaluation of spacer derivatives

We started our search for a potent and selective inactivator of human TG2 (hTG2) with a previously reported covalent inhibitor developed by our group; Cbz-Lys(Acr)-OH (**8**)[142]. Compound **8** was evaluated against guinea pig liver TG2 (gplTG2) and displayed exceptional kinetic inhibition parameters with K_I value of 0.52 μM and efficiency constant (k_{inact}/K_I) of 1.3 x 10^6 M^{-1} min^{-1}. Although gplTG2 may be homologous to hTG2, we re-evaluated Cbz-Lys(Acr)-OH and found that its affinity and efficiency constant were 2 orders of magnitude worse (see Table 3.1)[152]. Interestingly, we observed by extending the carboxylate group, through the addition of a glycine linker in between Cbz-Lys(Acr) and C-terminal (compound **9**), there was a gain in the inhibition efficiency[152]. This may be due to the extension of the negative charge from possible unfavourable interactions in the binding pocket. Furthermore, Replacing the carboxylic acid groups of **8** and **9** with a neutral terminal amide in **10** or a methyl ester in **11** results in minor gains in affinity and efficiency, building a case for the possibility of unfavourable interaction with the negative charge. We also kinetically re-evaluated **NC9**, a previous compound from the Keillor group, on hTG2. **NC9** is structurally composed of the Cbz-Lys(Acr) scaffold with a polyethylene glycol linker and dansyl group extending out the C-terminal end or the 'East end' of the molecule. In comparison we found that **NC9** has a comparable inhibition constant for

hTG2 as it did for gplTG2 (K_I ~30 μM). However, **NC9** displayed a quicker inactivation of hTG2 due to its higher k_{inact} value of 2.60 min^{-1} compared to 0.483 min^{-1} for gplTG2. The observed increase in k_{inact} with respect to hTG2 may be due to a different binding mode that places the acrylamide warhead closer to the active site Cys277 residue. When considering both affinity and reactivity, the overall efficiency (k_{inact}/K_I) of **NC9** is 5-fold higher for inhibition of hTG2 versus gplTG2. From our kinetic re-evaluation of past inhibitors tested on gplTG2, we found that **NC9** was one of the most efficient inhibitors of hTG2.

Table 3.1. Kinetic Parameters of Substituted Cbz-Lys(Acr)-R.

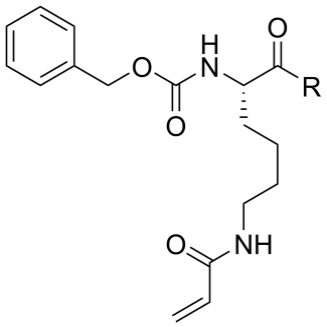

Inhibitor	R group	K_I (μM)	k_{inact} (min^{-1})	k_{inact}/K_I (10^3 M^{-1} min^{-1})
8b		60.3 ± 18.6	0.796 ± 0.13	13.2 ± 4.6

9 [b]	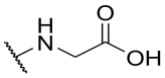	48.1 ± 10.3	1.26 ± 0.17	26.1 ± 6.6
10 [a]		35.1 ± 15.1	1.08 ± 0.46	30.7 ± 2.5
11 [b]	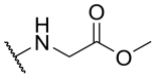	40.0 ± 5.9	1.45 ± 0.12	36.2 ± 6.1
NC9	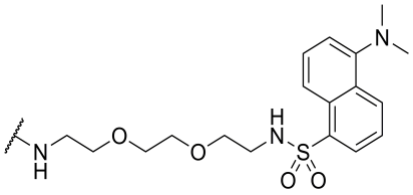	33.9 ± 3.4	2.60 ± 0.17	76.4 ± 9.1

a) kinetic parameters for compound #**14** were determined using a double reciprocal method of data analysis (see Appendix III).

b) Compounds **8**, **9** and **11** were synthesized and kinetically evaluated by N. M. R. McNeil.

Although originally designed as a fluorescent probe, the dansyl group on **NC9** may be associating with hTG2 rather than extending away from the enzyme pocket via its PEG spacer. From our kinetic results shown in Table 3.1, we see that the addition of a hydrophobic and aromatic dansyl group may be providing beneficial contact with a distal binding pocket of hTG2 that the truncated compounds **8**-**11** cannot access. Furthermore, docking **NC9** into an open conformation of hTG2 (PDB code 2Q3Z)[16] suggests that the dansyl group may be bound in the hydrophobic pocket on the surface of hTG2 in which the Phe side chain of Ac-P(DON)LPFNH$_2$ was bound in the cocrystal structure. This putative binding model also shows that the PEG spacer forms a long flexible loop, where there are few productive interactions with binding pocket of

hTG2. To this end, we first sought to systematically decrease the length of the diamine spacer between the Cbz-Lys(Acr) and the dansyl aromatic group of **NC9**.

As presented in Table 3.2, decreasing the diamine spacer length from eight atoms in **NC9** to four atoms in compound **12** resulted in a minor change with respect to the kinetic parameters. However, we were able to reduce the number of rotatable bonds and polar surface area (PSA), respecting Veber's rules[153]. A further decrease in the number of methylene units in the diamine linker from four to three resulted in a lower inhibitor efficiency. This was due to a drop in k_{inact} from 2.19 min^{-1} in compound **12** to 0.85 min^{-1} in compound **13**. Decreasing the spacer length to two methylene units (**14**) restored the reactivity of the covalent reaction back to a k_{inact} value of 1.45 min^{-1}. Keeping a two methylene unit spacer length, we rigidified our linker with a piperazine group as seen in compound **15**, also known as **VA4**. The introduction of the piperazine spacer increased the efficiency constant (k_{inact}/K_I) to 1.07 x 10^5 M^{-1} min^{-1}, displaying the best inhibition in the spacer modification series. Compound **VA4** exceeded the overall inhibition efficiency of **NC9** and showed more than two-fold reduction in the inhibition dissociation constant (K_I). The affinity increase with a rigid piperazine spacer suggests more favourable interactions with the binding pocket of hTG2 compared to a more flexible PEG spacer.

Table 3.2. Kinetic parameters of irreversible inhibitors with varying backbone spacers.

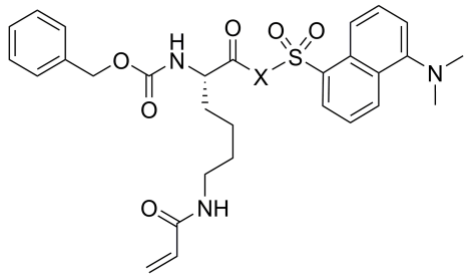

Inhibitor	X group	K_I (μM)	k_{inact} (min^{-1})	k_{inact}/K_I ($10^3\ M^{-1}\ min^{-1}$)
NC9	NH-$(CH_2CH_2O)_2$-CH_2CH_2NH	33.9 ± 3.4	2.60 ± 0.17	76.4 ± 9.1
12	HN-$(CH_2)_4$-NH	27.1 ± 11.9	2.19 ± 0.94	80.8 ± 4.7
13	HN-$(CH_2)_3$-NH	30.5 ± 9.4	0.85 ± 0.25	27.6 ± 1.7
14	HN-$(CH_2)_2$-NH	23.5 ± 3.1	1.45 ± 0.12	61.5 ± 9.6
15 (VA4)	piperazine	12.9 ± 2.6	1.40 ± 0.13	107 ± 23.8

3.1.2 Kinetic evaluation of side chain derivatives

For the next series of inhibitor derivatives, we chose to systematically vary the side chain of the Cbz-Lys(Acr) scaffold holding the acrylamide warhead. We started this series with a SAR study using **VA4** as the new parent compound. Similar to the spacer modification, we chose to reduce the number of rotatable bonds in inhibitors **16-18**, with the hope of increasing the

probability of good bioavailability as recommended by Veber's rules. Time-dependent inhibition of hTG2 within a reasonable inhibitor concentration range was only observed for compound **18**, which consisted of 3 methylene units on the side chain. Reducing the methylene units in the side chain to one (**16**) or two (**17**) did not illustrate sufficient time-dependent inhibition of hTG2 and thus, we were unable to determine the kinetic parameters for these compounds. The efficiency of compound **18** dropped an order of magnitude due to a significant loss in affinity, as the K_I increased from approximately 13 μM to 48 μM (see Table 3.3). As a comparison, we measured the observed rate constant (k_{obs}) for the inactivation of hTG2 in the presence of inhibitors **16**-**18** and **VA4**, as shown in Figure 3.3. We used our colorimetric assay to monitor the time-dependent inactivation curves and it was obvious that reducing the number of methylene units of the side chain below four resulted in a significant loss of inhibitor activity.

Table 3.3. Kinetic parameters of derivatives having varied side chain length.

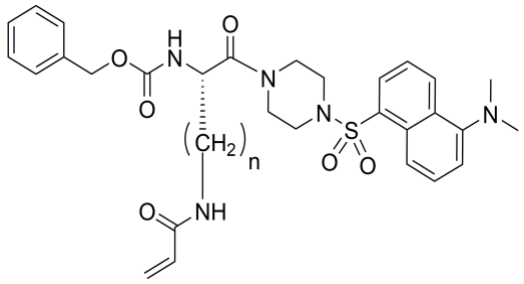

Compound	$(CH_2)_n$	K_I (μM)	k_{inact} (min^{-1})	k_{inact}/K_I (10^3 M^{-1} min^{-1})
16	n = 1	n.d.	n.d.	n.d.
17	n = 2	n.d.	n.d.	n.d.
18 [a]	n = 3	47.7 ± 37.8	1.18 ± 0.93	24.7 ± 2.2
15 (VA4)	n = 4	12.9 ± 2.6	1.40 ± 0.13	107 ± 23.8

n.d = not detectable.

a) kinetic parameters for compound **18** were determined using a double reciprocal method of data analysis (see Appendix III).

Figure 3.3 shows that a side chain length of one or two methylene units is not long enough for the inhibitors to inactivate hTG2 efficiently. Similar results have been reported with the Cbz-Phe-X and Cbz-X-Gly scaffolds, where fewer methylene units in the side chains showed poor inhibition as well[154]. In the crystal structure of 'open' conformation hTG2 (PDB code 2Q3Z)[16], the active site's C277 is located at the bottom of a hydrophobic tunnel. Since one and two methylene unit side chain inhibitors showed a poor rate of covalent inactivation, we presume the acrylamide warhead was not positioned in the proximity C277 to favour nucleophilic attack,

and therefore no significant enzyme inactivation was observed. The inhibition reappeared with three methylene units (**18**) but was the most efficient with four methylene units in **VA4**. Regardless, from this series of inhibitors, it was evident that the side chain length is a critical component for successful inactivation of hTG2.

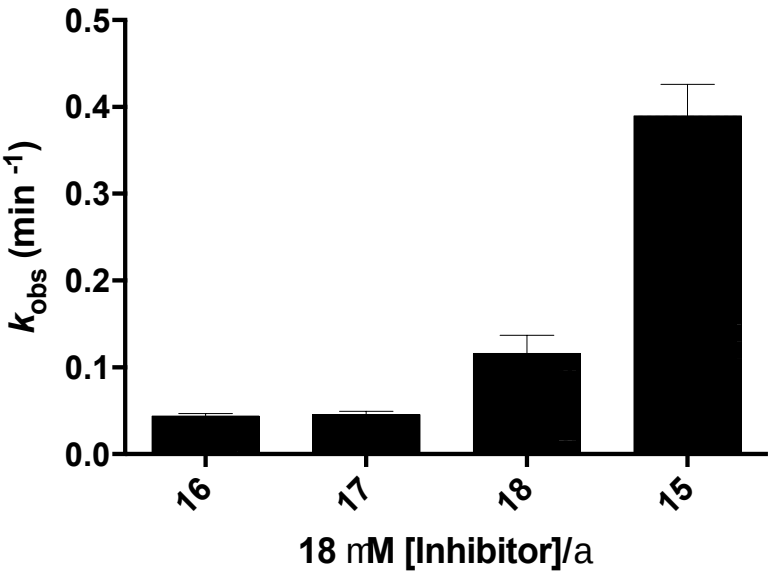

Figure 3.3. Observed rate constants (k_{obs}) of inactivation of hTG2 with 18 µM of inhibitors 15-18.

3.1.3 Kinetic evaluation of 'East end' derivatives

So far, we noted that a more rigid piperazine linker and four methylene units on the side chain (**VA4**) provided beneficial interactions that enhanced both affinity and reactivity of our inhibitors towards inactivation of hTG2. Having established appropriate lengths with spacer and side chain, we relocated our attention to the modification of the dansyl group found on the 'East end' of **VA4**. As mentioned earlier, we believe binding of the dansyl group is occurring in a

hydrophobic pocket, thus we sought to replace it with various aromatic and aliphatic functional groups, hoping that the chosen derivatives would help us understand the necessary interactions at the binding pocket. The first set of derivatives for the 'East end' modification SAR study maintained a sulfonamide connection with the piperazine spacer. As a way of understanding the binding associated with the dansyl group, we removed the dimethylamino group on the naphthalene ring to make compound **19** and then kinetically compared it to **VA4** (see Table 3.4). Although both inhibitors **19** and **VA4** had similar affinity constants (K_I), compound **19** had a rate constant of inactivation (k_{inact}) that is 3.5-fold less than **VA4** and resulted in an overall lower inhibition efficiency. Changing the orientation from a 1-naphthyl to a 2-naphthyl moiety in compound **20** also gave a low rate constant of inactivation (k_{inact}), with a small increase in affinity. Reducing the size of the aromatic ring from naphthyl to phenyl in compound **21** resulted in slight increase in the rate constant of inactivation (k_{inact}), from 0.38 min^{-1} to 0.47 min^{-1}. However, the overall inhibitor efficiency was similar to compound **20**. Furthermore, we saw that aromaticity is not necessary to achieve modest inhibition efficiency with the sulfonamide linked series[152]. Derivatives such as cyclohexyl, isopropyl, ethyl, and methyl sulfonamides all gave comparable inhibition values to those of the aromatic derivatives[152].

Table 3.4. Kinetic parameters of piperazine sulfonamide derivatives.

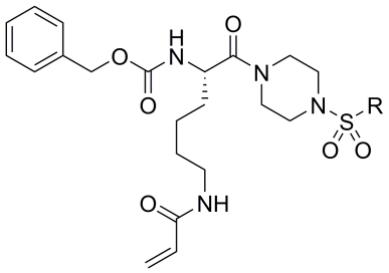

Inhibitor	R group	K_I (μM)	k_{inact} (min^{-1})	k_{inact}/K_I (10^3 M^{-1} min^{-1})
15 (VA4)	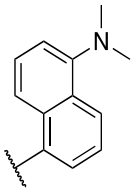	12.9 ± 2.6	1.40 ± 0.13	107 ± 23.8
19	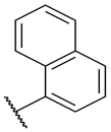	10.4 ± 1.8	0.39 ± 0.03	37.2 ± 7.1
20	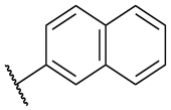	6.7 ± 1.1	0.38 ± 0.03	57.3 ± 10.6
21	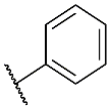	8.8 ± 1.5	0.47 ± 0.04	53.3 ± 9.8

The final set of derivatives for the 'East end' modification series maintained the Cbz-Lys(Acr)-pip-X scaffold, but the linkage to the piperazine spacer was changed from sulfonamide to an amide. We hypothesized that a switch from a tetrahedral to a trigonal planar geometry at the spacer linkage would possibly orient the C-terminal hydrophobic groups differently, thus we

retested amide linked derivatives; 1-naphthyl (**22**), 2-naphthyl (**23**), and phenyl (**24**). Direct comparison of amide derivatives, compounds **22**-**24**, in Table 3.5 to their corresponding sulfonamide derivatives, compounds **19**-**21,** in Table 3.4 suggests that the presence of an amide functional group in place of the sulfonamide is beneficial for the inhibition of hTG2. All three of these aromatic derivatives (**22**-**24**) show approximately a 2-fold increase in overall inhibition efficiency compared to their sulfonamide counterparts (**19**-**21**). From the amide linked series, compound **22** (also called **AA9**) has the best affinity constant with a K_I value of 8.9 µM. Also, in comparison to the more efficient inhibitor in the sulfonamide linked series (**VA4**), **AA9** has a slightly better affinity to hTG2. Compound **24** did show the highest inhibitor efficiency; however, it demonstrated the worst affinity within the series with a K_I value of 36.6 µM. Upon consideration of inhibitor affinity and efficiency, we considered compound **15** (**VA4**) and compound **22** (**AA9**), to be the best lead compounds from the sulfonamide and amide piperazinyl linked derivatives. Both compounds are highly efficient irreversible inhibitors with a k_{inact}/K_I of approximately 10^5 M^{-1} min^{-1}.

Table 3.5. Kinetic parameters of piperazine amide derivatives.

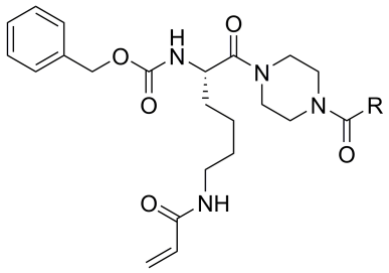

Inhibitor	R group	K_I (μM)	k_{inact} (min^{-1})	k_{inact}/K_I (10^3 M^{-1} min^{-1})
22 (AA9)	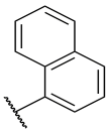	8.9 ± 1.0	0.90 ± 0.05	101 ± 12.8
23	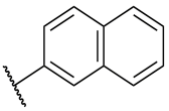	13.4 ± 2.3	1.21 ± 0.13	90.3 ± 18.0
24	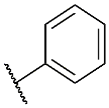	36.6 ± 4.8	4.77 ± 0.46	130 ± 21.2

3.2 Assessment of TG2 GTP binding activity in the presence of covalent inhibitors

TG2 has been shown to have allosteric binding sites for both Ca^{2+} and guanosine nucleotides [155]. More specifically, Ca^{2+} binding activates the acyl transfer catalysis of TG2, and guanosine nucleotide binding deactivates this activity. A crystal structure of hTG2 bound to GDP demonstrated a dramatic conformational change, where the two C-terminal β-barrel domains

were folded over the catalytic core[19]. In addition, TG2 is unique amongst its isozymes, in that when bound to GTP, it functions as a G-protein [156]. Originally, TG2 was reported as a GTP binding protein called G_h and was involved in coupling the α1-adrenergic agonists for the stimulation of the phosphoinositide lipid metabolism[156]. Later, studies demonstrated that G_h was identical to TG2[49]. More recently, studies have shown that the GTP-binding ability (and by extension, presumably the G-protein activity) of hTG2 is involved in certain types of cancer[37,84,157]. Other than the diseases associated with hTG2's acyl transfer activity, targeting and abolishing its GTP binding activity can also offer potential therapeutics toward treatment of linked diseases.

Our covalent inhibitors are competitive with respect to the acyl-donor substrate (**AL5**) of hTG2. With increased **AL5** concentration, the value of k_{obs} at a constant inhibitor concentration decreases, demonstrating that the binding of both substrate and inhibitor is competing at the active site of the free enzyme. Furthermore, we have observed by mass spectrometry that one equivalent of **NC9** and **23** is covalently incorporated into irreversibly inhibited hTG2[158], presumably through reaction with the active site cysteine. Thus, our inhibitors target the substrate binding pocket and should not be competing with the GTP binding pocket. Interestingly, through collaborate work, we have shown through FRET-FLIM[51,147] and by CE-MS[52,158] that our acrylamide-based irreversible inhibitors (at micromolar concentrations) can lock hTG2 in its open conformation. Thus, not allowing an irreversibly locked and extended conformation of hTG2 to bind GTP. To further solidify this conclusion, we tested two of our lead compounds (**VA4** and **AA9**) for their ability to abolish GTP binding. For this assessment we used a GTP binding assay (Scheme 3.2) that uses a fluorescent nonhydrolyzable GTP analogue (GTPγS FL BODIPY) whose fluorescence increases when bound to a GTP-binding protein[159].

After incubating hTG2 with our lead covalent inhibitors, **VA4** and **AA9**, hTG2 showed significant loss in GTP binding ability (see Figure 3.4). Thus, in addition to their ability to covalently inhibit the acyl transfer activity of hTG2 and locking the enzyme in its extend/open conformation, **VA4** and **AA9** are also capable of almost completely abolishing GTP binding.

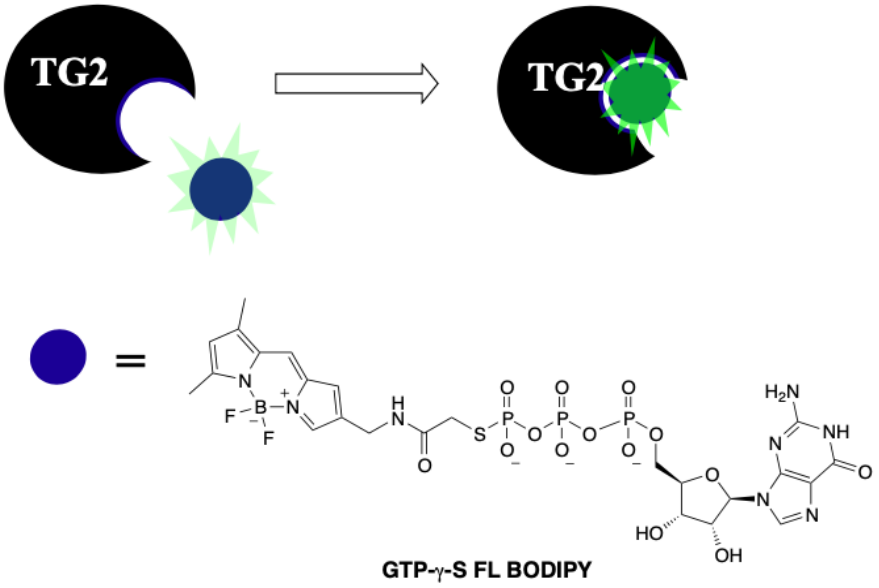

Scheme 3.2. A general illustration of tissue transglutaminase (TG2) binding a fluorescent nonhydrolyzable GTP analogue (GTPγS FL BODIPY) whose fluorescence increases when bound.

Having access to a library of covalent inhibitors from our SAR library, we decided to gain more insight into the structural requirements for inhibition of GTP binding. We chose to test inhibitor **10** which lacks two key structural components: namely the C-terminal functional group and the piperazine spacer. Even without these structural features, inhibitor **10** was still capable of

abolishing hTG2's GTP binding activity (see Figure 3.5). Before we ruled out a possible structural requirement for exclusive GTP binding abolishment over inhibition of acyl transfer activity, we decided to evaluate the GTP binding using iodoacetamide; a non-specific irreversible inhibitor known for TG2 and many other cysteine proteases[160]. Incubation with iodoacetamide did not perturb its GTP binding ability (see Appendix IV), suggesting that covalent inhibition of acyl transfer activity does not always lead to abolishment of GTP binding. Furthermore, the covalent addition of the acetamide group does not prevent the enzyme from adopting its closed conformation and therefore, allows for a conformation suitable for guanosine nucleotide binding. These findings with inhibitor **10** and iodoacetamide do not give a complete understanding of the structural requirements needed for exclusive inhibition of acyl transfer activity. However, these preliminary results may lead to future systematic structural modification of our covalent inhibitor to develop an exclusive acyl transfer inhibitor that does not alter hTG2's GTP binding. Regardless, we have developed efficient inhibitors that abolish both acyltransferase and GTP-binding activities *in vitro*, namely **VA4** and **AA9**. This represents a novel allosteric mechanism for inhibiting GTP binding, without the use of GTP analogues, an approach that may suffer from the lack of selectivity.

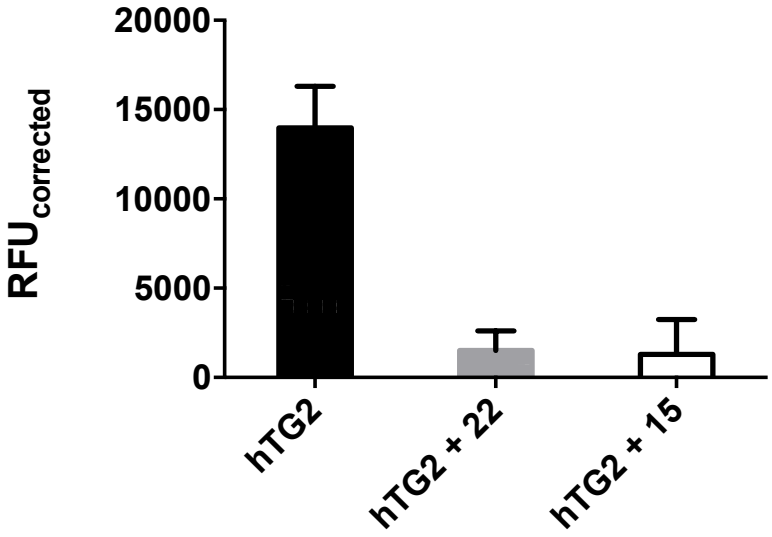

Figure 3.4. Suppression of GTP binding activity using 3 µM GTP-γ-S FL BODIPY after inhibition of hTG2 with VA4 (15) and AA9 (22).

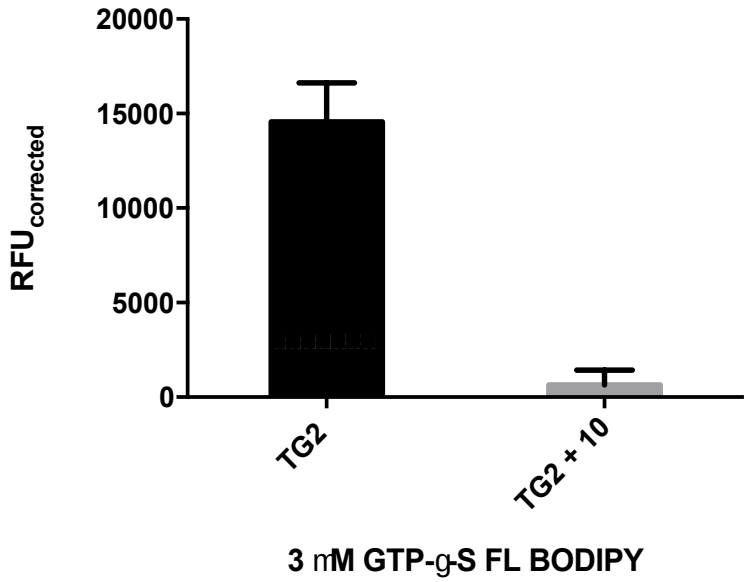

Figure 3.5. Suppression of GTP binding activity using 3 µM GTP-γ-S FL BODIPY after inhibition of hTG2 with compound 10.

3.3 Cellular target and evaluation

hTG2 has been shown to be highly elevated in epidermal cancer stem (ECS) cells[84]. In addition, hTG2 knockdown or inactivation with 20 μM **NC9** reduced ECS cell proliferation and survival[84], the expression of epithelial−mesenchymal transition (EMT) transcription factors and markers[157], and metastatic phenotype[84]. In TG2 knockout ECS cells, treatment with **NC9** had no effect, suggesting that the inhibitor's biological activity is not related to off-target interaction[147]. Furthermore, administration of **NC9** by intraperitoneal injection at 20 mg/kg reduced the growth of mouse xenograft tumours initiated by injection of cancer stem cells[146]. Through these biological assays, **NC9** was found to be surprisingly effective against human squamous cell carcinoma, which is the reason we sought to optimize it further to create a more drug-like candidate.

Extracellular basement membranes composed of collagens, laminins, and proteoglycans, form thin and sheet-like structures that separate epithelial tissues from adjacent connective tissues[161]. The crossing of cancer cells through this membrane is a crucial aspect of metastasis. It has been shown previously that ECS cells invade efficiently and migrate rapidly relative to non-stem cancer cells and that these properties are associated with enhanced tumour formation[83]. As optimizations were taking place in this SAR study, we decided to compare the migrating ability of ECS cells in the presence of **VA4** and **NC9**. To determine the relative potency of **NC9** and **VA4**, we monitored the ability of ECS cells to migrate through collagen membrane-like polymer called Matrigel[161] treated with either of these inhibitors over a concentration range of 1-50 μM. As can be seen in the dose-response data shown in Figure 3.6, both inhibitors are capable of inhibiting ECS cell migration. Due to a higher potency, the migration data for **VA4** could be

fitted to provide an EC_{50} value of 3.9 μM[152], while **NC9** did not provide enough data points to extrapolate a precise EC_{50} value.

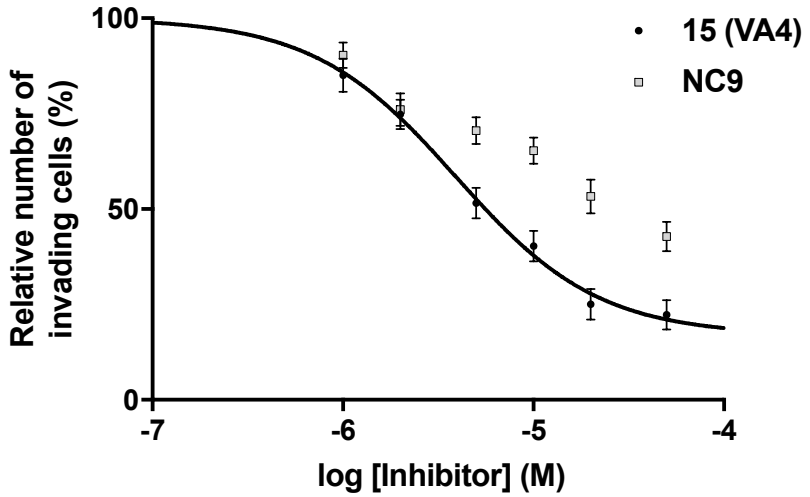

Figure 3.6. Dose-response data for inhibition of ECS invasion by 15 (VA4) and NC9. The solid line was fitted through the data for 15 (VA4), providing an EC_{50} value of 3.9 μM. Experimental data was obtained from Dr. Gautam Adhikary[152].

3.4 Isoenzyme selectivity

We next assessed the selectivity of our most studied inhibitors, **NC9** and **VA4**, for their reaction with hTG2 over other members of the TGase family. We chose to test these covalent inhibitors against four therapeutically relevant isoforms of human transglutaminase: FXIIIa, hTG3a, hTG1, and hTG6. The activities of hTG2, hTG1 and hTG6 were measured using our previously reported continuous colorimetric assay[39], using Cbz-Glu(γ-p-nitrophenyl ester)Gly or **AL5** as a substrate (see Scheme 3.1). As for the other TGases, FXIIIa and hTG3a, a

commercially available continuous fluorescent assay[43,162] that utilizes a peptidic FRET-quenched substrate called **A101** was used (see Scheme 3.3). For all enzymatic reactions, we measured the respective kinetic parameters (K_M and V_{max}) with their appropriate substrate; **AL5** or **A101** (see Appendix II for data).

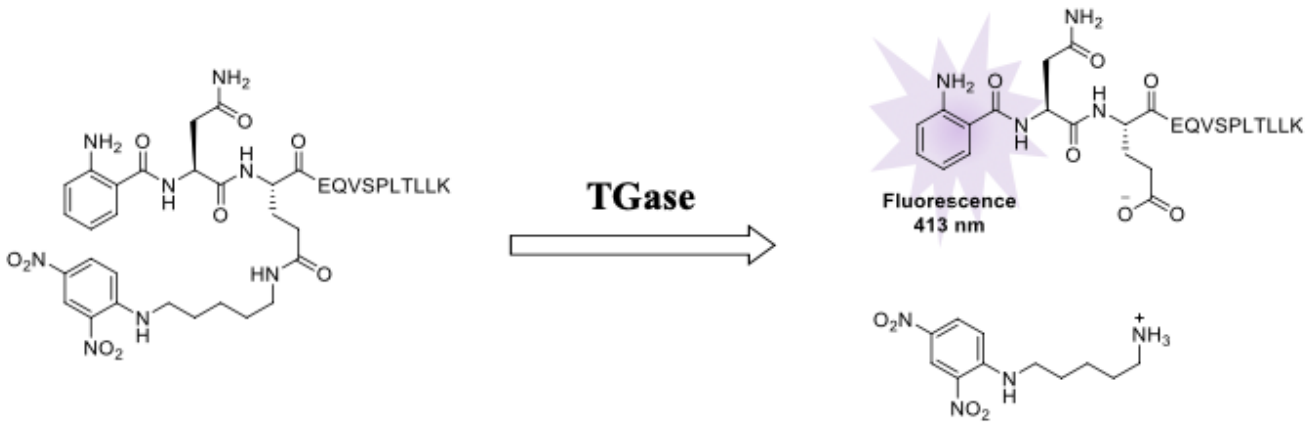

Scheme 3.3. A general illustration of transglutaminase (TGase) reacting with a peptidic FRET-quenched substrate via its isopeptidase activity. Once the N-(2,4-dinitrophenyl)cadaverine is cleaved off and the enzyme forms a thiolester acyl intermediate, the N-terminal fluorophore 2-aminobenzoyl (Abz) group is observed spectrophotometrically at 413 nm[162].

At a specific inhibitor concentration, we obtained the rate constant of inactivation (k_{obs}) for each of the selected TGase isozymes (see Appendix V for data). Furthermore, these inhibitor concentrations were chosen to account for competition with substrates in each enzymatic reaction. In general, our potent irreversible inhibitors showed excellent selectivity toward hTG2 over the other isozymes (see Table 3.5).

Both **VA4** and **NC9** demonstrated superior selectivity toward hTG2 over hTG3a by about 390-fold. **VA4** was 48-fold less reactive with hTG1, 97-fold less reactive with FXIIIa, and no inhibition was observed with hTG6 compared to inhibition of hTG2. In addition, **VA4** generally illustrated a lower reactivity toward other TGase isozymes compared to **NC9**. The subsequent *in vitro* selectivity over homologous TGases bodes well for *in vivo* selectivity.

Table 3.5. Selectivity of VA4 and NC9 against TGase isoforms.

Compound #	k_{obs} **(10** $^{-3}$ **min** $^{-1}$**)**				
	TG2	**TG1**	**TG3a**	**TG6**	**FXIIIa**
NC9	390 ± 49	78.9 ± 5.9	1.01 ± 0.09	6.16 ± 0.14	5.91 ± 1.59
15 (VA4)	394 ± 37	8.27 ± 0.76	0.65 ± 0.21	n.d.	4.08 ± 0.77

n.d = not detected

Chapter Four: **Design, Synthesis and Kinetic Evaluation of FXIIIa inhibitors**

4.1 Recent work on FXIIIa inhibitors

As mentioned in Chapter 1 section 1.4.4, research directed towards designing selective human FXIIIa (hFXIIIa) inhibitors is limited. To date, the most promising selective hFXIIIa reported was by the Zedira, a biotechnology company specializing in transglutaminase research. Zedira introduced **ZED1301** (Figure 4.1), a peptidic irreversible hFXIIIa inhibitor bearing an acrylate methyl ester warhead. **ZED1301** demonstrated a 30-fold selectivity for hFXIIIa compared to hTG2. Furthermore, a crystal structure was solved with **ZED1301** bound in the active site pocket of hFXIIIA$_2$ (calcium activated homodimeric proenzyme)[130]. The peptidic sequence found in **ZED1301**, was derived from the 12-mer peptidic substrate (**pepF11KA**: DQMMLPWPAVAL) discovered to be selective for hFXIIIa over hTG2 via a phage-display selection[125]. The irreversible inhibitor was shown to bind covalently to the catalytic C314 residue with its glutamyl-like acrylate methyl ester warhead. With the emergence of this crystal structure demonstrating the complexation of a peptidic inhibitor with the active site, researchers can begin to include implicit binding interactions within their structure-based design of future hFXIIIa inhibitors.

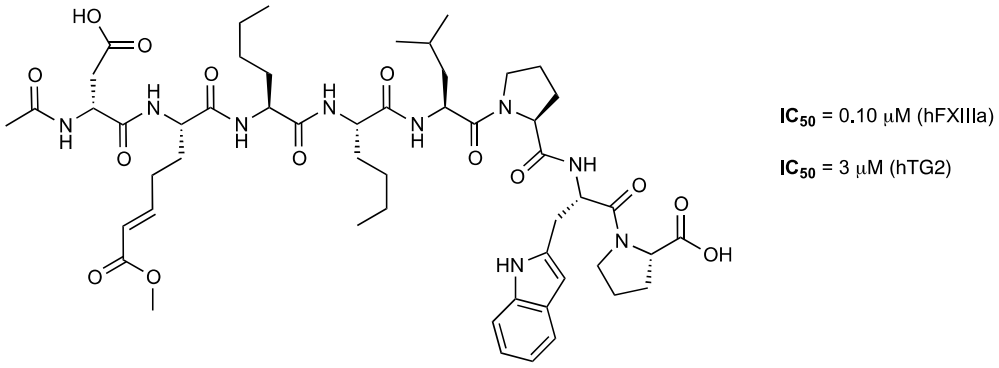

Figure 4.1. Zedira's ZED1301, a covalent peptidic inhibitor bearing an acrylate methyl ester with a 30-fold selectivity for hFXIIa over hTG2.

hFXIIIa is an enzyme involved in the last step of the coagulation pathway, and inhibition of the enzyme can provide another direction for anticoagulant therapy. For decades, vitamin K antagonists were the only available anticoagulants. Vitamin K antagonist's anticoagulant effect is due to the inhibition of vitamin K epoxide reductase which inhibits the synthesis of vitamin K-dependent protein involved in coagulation[163]. These anticoagulants have a small therapeutic index and unpredictable dose-response relationship, giving rise to frequent bleeding complications or insufficient anticoagulation[163]. More recently, a new generation of anticoagulants has emerged targeting directly or indirectly serine proteases that are upstream of the coagulation pathway such as thrombin and factor Xa[164]. Since hFXIIIa is linked to the mechanical stability, half-life, and lysis rate of clots[120] and acts downstream of thrombin and factor Xa, it can be a potential therapeutic for a safer and more selective anticoagulant. From our knowledge within the transglutaminase field, a hFXIIIa inhibitor that selectively discriminates against hTG2 is highly sought-after for research related biological evaluations. Furthermore, selectivity against hTG2 over the other TGase members is important since tissue transglutaminase is distributed ubiquitously. With that, we decided to start our search for a hFXIIIa inhibitor that has poor affinity for hTG2. Once a lead compound is found, selectivity against other TGase isoforms will follow.

4.2 Inhibitor design and synthesis

Originally, like Zedira, we proposed to modify the glutamine residue in the reported **pepF11KA** peptide (DQMMLPWPAVAL) to incorporate our lysine-borne acrylamide warhead.

We also observed that the pentamer and heptamer peptide substrate, DQMML and DQMMMAF, was enough to show selectivity towards hFXIIIa over hTG2 by 570-fold and 2686-fold, respectively[165]. In Zedira's crystal structure of hFXIII, the active site was noted to appear differently than hTG2, with a wider opening for binding of the acyl amine acceptor[130]. In addition, a space resembling pocket 1 (see Chapter 2, Figure 2.3) was described as being more distinguished between hFXIIIa and hTG2. In this region, we observed an electrostatic interaction between the aspartate residue in **ZED1301** and arginine residue (R223) in pocket 2. Moreover, from phage-displayed selection library that found **pepF11KA** peptide, about 35% of the preferred peptide sequences for hFXIIIa had a negatively charged carboxylate side chain in the -1 position to the glutamine, while none of the preferred peptides for hTG2 had a negatively charge residue at the -1 position to the glutamine. Like hTG2, hFXIIIa also has a hydrophobic pocket 2 that prefers non-polar motifs[16,130].

From our SAR study results in Chapter 3, we discovered that inhibitor **16** (Figure 4.2 A), with one methylene unit on the side chain bearing our warhead, exhibited very poor reactivity with hTG2. More specifically, compound **16** was about 10-fold less reactive towards inhibition of hTG2 (Figure 4.2 B) than **VA4** (a compound that has four methylene units on the side chain bearing the acrylamide warhead). In fact, there was a trend of decreasing reactivity towards hTG2 as we systematically decreased the number of methylene units in the Lys(Acr) side chain. Having this low reactivity for the inactivation of hTG2, we thought to select a one methylene unit acrylamide side chain or Dap(Acr) for our SAR study of hfXIIIa inhibitors, with the hope of selective inhibition of hFXIIIa over hTG2.

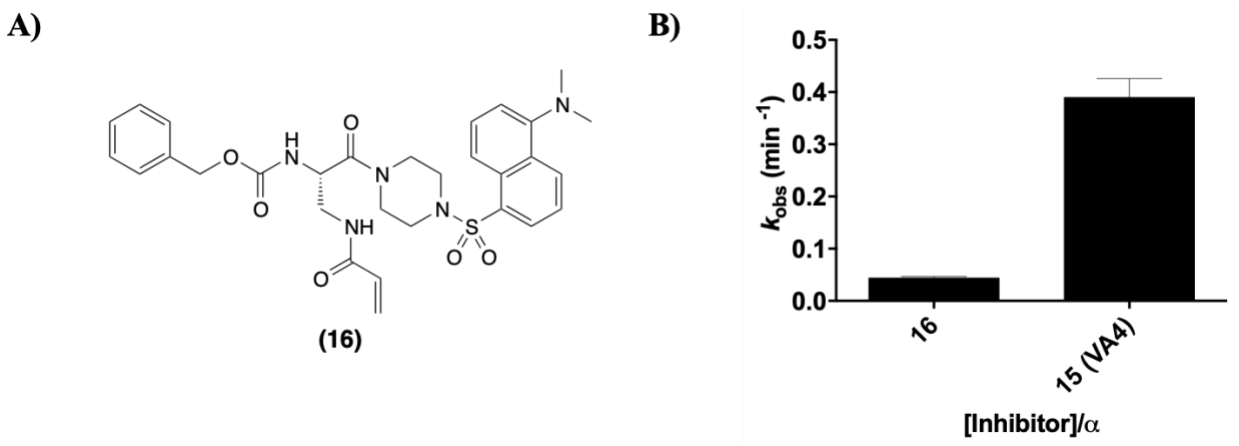

Figure 4.2. A) Chemical structure of compound 16. B) Rate constant for the covalent reactivity (k_{obs}) of 16 versus 15 (VA4) against hTG2 at a concentration of 18 μM.

As previously tested with our TG2 studies, the acrylamide warhead showed stability against glutathione, while maintaining reactivity with the active site cysteine[139]. Further, an acrylamide warhead held via one methylene unit demonstrated low reactivity towards hTG2. The latter result can potentially allow for isozyme selectivity, with the possibility for sufficient reactivity towards the active site cysteine of hFXIIIa. With that, we decided to start our pioneering SAR study on inhibitors for hFXIIIa with Dab(Acr), with the understanding that other warheads may allow for more efficient inhibitors. Similar to what we have done in our hTG2 SAR study, we systematically varied the spacer length with the same diamine spacers to explore their binding towards hFXIIIa. Moreover, to focus on the effect of spacer length variation only, the 'East end' was maintained as an aromatic and hydrophobic dansyl group, which may provide favourable association with the hydrophobic binding pocket of hFXIIIa. Once an optimal spacer length was found, we then sampled a few aryl derivatives linked via a sulfonamide and carboxamide, for a preliminary evaluation of their binding strength towards hFXIIIa. As

mentioned earlier, the binding in pocket 1 was noted to be different between hFXIIIa and hTG2. More specifically, as seen in the crystal structure of FXIIIA bound with **ZED1301**, a negative residue may show favourable interaction. Thus, we tried replacing the Cbz group on the 'West end' of the inhibitors with an N-acyl-L-aspartate residue. Scheme 4.1 summarizes our goals for our initial SAR study towards finding a selective and efficient covalent inhibitor of hFXIIIa.

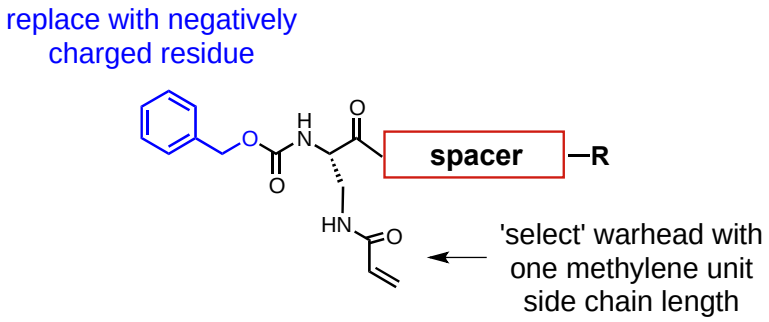

Scheme 4.1. Proposed structural modifications for this work's SAR study with human FXIIIa.

The synthesis of inhibitors for this SAR study can be divided into two scaffolds; Cbz-Dap and Boc-Dap(Cbz). The Cbz-Dap scaffold was used to synthesize the spacer and 'East end' derivatives, while the Boc-Dap(Cbz) scaffold was used to synthesize the 'West end' derivates. As explained above, both scaffolds used our acrylamide warhead. Through a similar convergent synthesis used to make our hTG2 inhibitors, Cbz-Dap(Acr)-OH and various aryl monosubstituted alkyldiamine spacers were coupled to give us on set of our final inhibitors (see Scheme 2.1 in Chapter 2 for a general synthesis scheme). The monosubstituted alkyldiamine spacers ranged from 2 to 4 methylene units linked to a maintained dansyl group. To ease purification of the monodansylated alkyl amines, a Boc group was added to the free amine,

making it more hydrophobic and easier to elute from a silica-based column. The addition of the Boc group also increased the yield of reaction by increasing solubility in the organic phase during aqueous washes and avoiding diamine coupling during synthesis. Once an optimal spacer length was discovered, the dansyl group was replaced with a 1-naphthalene derivative linked via sulfonamide or carboxyamide.

For the 'West end' derivatives, a different synthetic route was designed and the general scheme for this route is depicted in Scheme 4.2. The Boc-DapCbz) scaffold was used to synthesize our 'West end' derivatives. It offered a late Boc protected intermediate that can easily be functionalized with various derivatives via a simple dilute acidic deprotection. More importantly, the trifluoracetic acid (TFA) deprotection did not alter the existing functional groups. If the Cbz-Dap scaffold was used to make the same later intermediate, then we would be affecting the electrophilic alkene group found on the acrylamide warhead. Cbz deprotection conditions such as hydrogenation would reduce our warhead alkene to an alkane. We also were not able to devise a convergent synthesis, where Boc-Dap(Acr)-OH is coupled to various aryl compounds with a spacer. This was because we did not obtain a high yield for the addition of the acrylamide warhead using Boc-Dap, rather than Cbz-Dap. The Boc protected scaffold was very soluble in the aqueous phase and did not allow us to follow our acrylamide warhead addition reaction conditions.

Consequently, the Boc-Dap(Cbz)-OH scaffold was directly coupled to the spacer and the 'East end' of the inhibitor in the early steps of the synthesis, rather than at the end. A common hydrogenation reaction was used to remove the Cbz-group from the β-amine and subsequently followed by the acrylation of the amine to afford our acrylamide warhead. A mild acidic Boc-deprotection was used to free up the α-amine, which was then used to couple to a negatively

charged residue. For this thesis's SAR study, we used N-acyl-L-aspartic acid as our negatively charged residue. The general procedures and details for the synthesis of intermediates and final compounds can be found in Chapter 6.

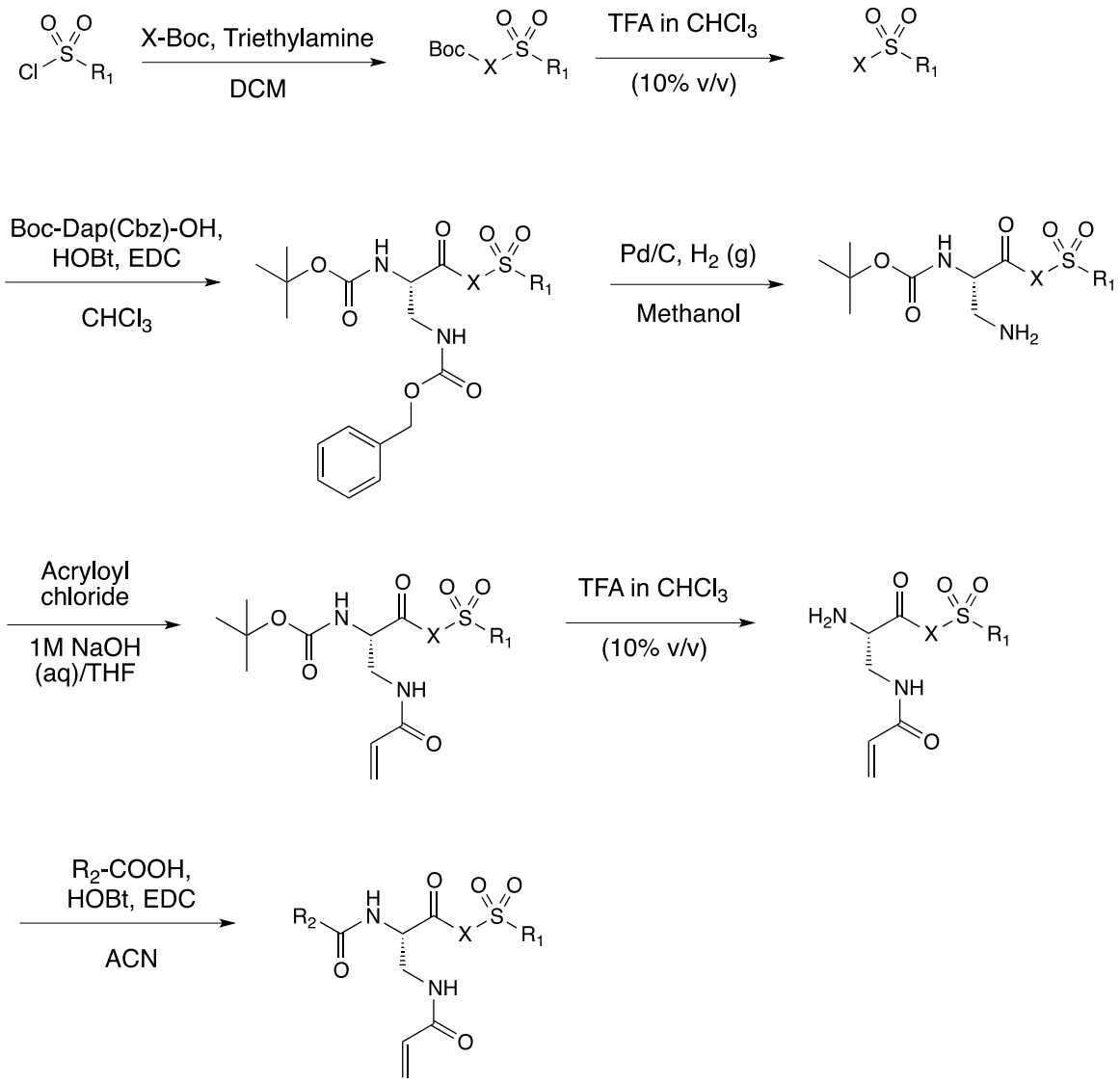

X = diamine spacer derivates

R_1 = aryl derivatives

R_2 = negatively charged derivatives

Scheme 4.2. General scheme for the synthesis of this work's hFXIIIa 'West end' derivatized covalent inhibitors.

4.3 Kinetic evaluation of FXIIIa inhibitors

As described in Chapter 3, a covalent inhibitor's potency can be evaluated through two parameters; K_I and k_{inact}[132]. Moreover, these kinetics parameters are measured under Kitz and Wilson conditions[151], where the dependence of k_{obs} versus inhibitor concentration will show a hyperbolic relationship that fits under equation 3.1 from Chapter 3. The rate constant k_{obs} is a measure of covalent enzyme inactivation and it can be measured graphically when the enzyme is saturated with substrate. During this substrate saturation, the curvature of enzymatic reaction rate is solely due to the inhibitor's activity and thus we can measure the rate constant of inactivation (k_{obs}). However, if the efficiency of the enzyme-substrate reaction (k_{cat}/K_M) is greater the enzyme-inhibitor efficiency (k_{inact}/K_I), then a pseudo-first order regression for the inhibitor exclusively is not observed. Consequently, we are observing both the substrate depletion and inhibition reaction. This scenario was observed with our Dap(Acr) hFXIIIa inhibitors. Another method to solve for k_{obs} is possible and would require a more rigorous experimental set up. The k_{obs} can be measured graphically by plotting percent residual activity versus time. Experimentally, a researcher would measure both the initial rate of enzymatic activity in the presence and absence of inhibitor. Aliquots are obtained at various time intervals to measure percent inhibitions of one inhibitor concentration. The aliquots must be significantly diluted to avoid competitive binding of inhibitor with substrate, which will allow for the measurement of only covalent inactivation or the k_{obs} over time. As a preliminary screen for this pioneering study, we chose to examine initial rates to obtain an inhibition constant for the competitive reversible reaction. Given the cost of the enzyme and assay, this approach was a better use of our resources.

Our approach used a fluorescent assay that utilizes a peptidic FRET-quenched substrate called **A101**[43,162], the same one used for the isozyme selectivity assay in our hTG2 SAR study

(see Scheme 3.3 in Chapter 3). Moreover, our hFXIIIa inhibitors are competitive with respect to the substrate (**A101**) of hFXIIIa. With increased **A101** concentration, the initial rate of the enzymatic reaction at a constant inhibitor concentration increases, demonstrating that the binding of both substrate and inhibitor is competing at the active site of the free enzyme. With that, we can measure the initial rate of hFXIIIa's isopeptidase activity in the presence of various inhibitor concentration (see Figure 4.3 A) and use a Dixon plot[166] to measure the equilibrium constant for inhibitor's binding affinity (K_i). The relationship between K_i, inhibitor concentration and initial rate of enzymatic reaction is represented in the linear equation below:

$$\frac{v_0}{v_i} = \frac{K_M}{V_{max}[S]K_i}[I] + \frac{K_M+[S]}{V_{max}[S]}$$

By plotting the inverse value of the initial rate versus inhibitor concentration, we obtain a slope containing the K_i value. With the linear equation 3.1, we can isolate for the x-intercept, which equals to the following:

$$x - intercept = \frac{-\frac{K_M + [S]}{V_{max}[S]}}{\frac{K_M}{V_{max}[S]K_i}}$$

With further algebraic manipulation, we obtain the following:

$$x - intercept = -K_i(1 + \frac{[S]}{K_M}) = -K_i\alpha$$

Through this manipulation, we see that the x-intercept provides an equilibrium constant for the dissociation of the enzyme-inhibitor complex multiplied by the equation that accounts for substrate competition or α parameter (Equation 3.3 in Chapter 3). Thus, obtaining the x-intercept of a Dixon plot and dividing by α, we obtain the K_i value. A graphical example is shown for the inhibition of hFXIIIa with compound **16** in Figure 4.3. Our Dixon plot is normalized for two variables; the substrate competition is accounted for by dividing our inhibitor concentrations by α and all our initial rates are divided by the initial rate of our enzymatic reaction in the absence of inhibitor. The former gives us an x-intercept value corresponding to K_i and the latter gives us a y-intercept of 1 for all inhibitors and allows for simultaneous comparison between inhibitors throughout our SAR study. Moreover, the normalization of the initial rates and substrate competition account for variations in enzyme concentration and substrate affinity between assays, more importantly between enzymes. With that, we decided to compare only the affinity of our hFXIIIa inhibitors by comparing K_i values between hTG2 and hFXIIIa.

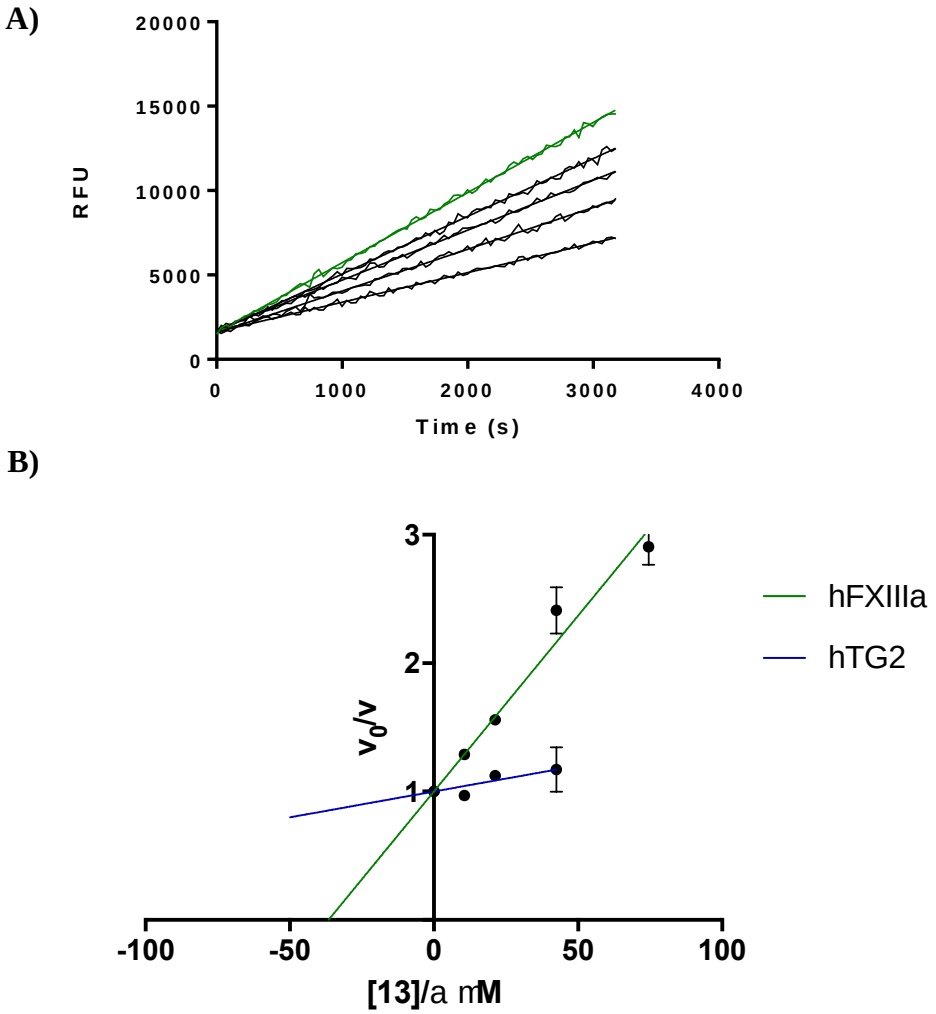

Figure 4.3. Determination of inhibitor affinity constant (K_i) using a previously reported continuous fluorescent assay. (A) Initial rates of the enzymatic reaction were measured by monitoring the relative fluorescent units (RFU) versus time in the absence (green line, v_0) and presence of increasing inhibitor concentrations (black line, v). (B) A Dixon plot fitted to a linear regression for various concentration of inhibitor 16 with hFXIIIa (green line) and hTG2 (blue line). The plot was normalized for substrate competition and the initial rates between two enzymes.

4.3.1 Kinetic evaluation of spacer derivatives

Our kinetic evaluation started with compound **16**, which connected both the East and West ends of the molecule via a piperazine spacer. We found that compound **16** had a K_i value of approximately 37 μM for hFXIIIa and 250 μM for hTG2, with a 7-fold selectivity preferring hFXIIIa (Table 4.1). Although a rigid piperazine spacer provides our inhibitor with a higher probability for greater bioavailability, we decided to explore the affinity of inhibitors towards hTG2 and hFXIIIa with a more extended spacer. Moreover, we wanted to steer away from the piperazine spacer, as it had favourable interaction with hTG2. Increasing the methylene units in the spacer to four (**25**) and three (**26**) did not show higher affinity towards hFXIIIa. However, as seen previous with hTG2, having four or three methylene unit spacers reduced inhibitor's affinity to hTG2. A more conformationally restricted compound **27** with a two-methylene diamine spacer, we observed a slight increase in the affinity for hFXIIIa and about 20-fold selectivity towards hFXIIIa over hTG2. With all this, we decided to continue our SAR study with compound **27**, also known as **AA27**, since it showed the highest affinity for hFXIIIa with a sufficient selectivity from binding to hTG2.

Table 4.1. Kinetic Parameters of Substituted Cbz-Dap(Acr)-R.

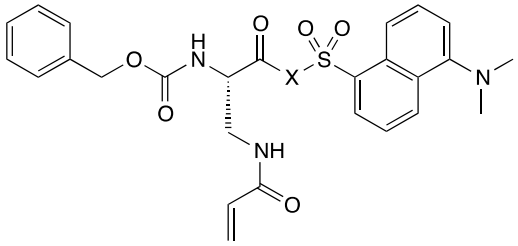

Inhibitor	X group	K_i (μM)	
		hFXIIIa	**hTG2**
16	piperazine	36.5 ± 2.1	248 ± 60.7
25	HN-$(CH_2)_4$-NH	44.4 ± 2.2	1197 ± 192
26	HN-$(CH_2)_3$-NH	63.6 ± 5.7	n.d.
27 (AA27)	HN-$(CH_2)_2$-NH	25.5 ± 1.2	514 ± 96.6

n.d = not detected

4.3.2 Kinetic evaluation of 'East end' derivatives

Having established an appropriate length with the spacer, we relocated our attention to the modification of the dansyl group found on the 'East end' of **AA27**. With a pioneering approach, we investigated two linkages for the attachment of our 'East end' via a sulfonamide (**28**) and a carboxamide (**29**) bond. Both bonds maintained a 1-napthalene 'East end' derivative, allowing us to analyse the influence of the two different connections on enzyme affinity (see Table 4.2). With respect to hFXIIIa, sulfonamide linked inhibitor **28** had a K_i value of 103 μM and amide linked inhibitor **29** had a K_i value of 75 μM. The removal of the dimethyl amino group from the dansyl moiety decreased the affinity of the inhibitor to hFXIIIa by about 4-fold,

while sustaining the selectivity away from hTG2. We also noticed that with the amide linkage there was an increase in affinity for hTG2 by about 4-fold. From these results, we demonstrated that an amide linkage for the 'East end' of our inhibitors does not provide favourable selectivity towards hFXIIIa over hTG2.

Table 4.2. Kinetic parameters of 'East end' derivatives

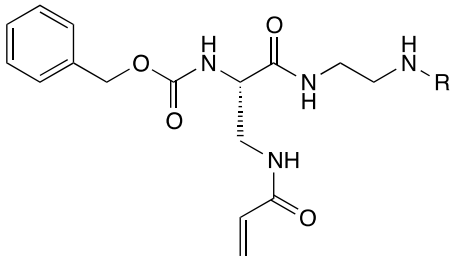

Inhibitor	X group	K_i (μM)	
		hFXIIIa	**hTG2**
27 (AA27)	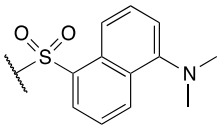	25.5 ± 1.2	514 ± 96.6
28 (AA21)	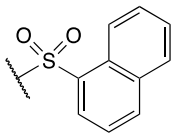	102.6 ± 3.3	438 ± 81.8
29 (AA20)	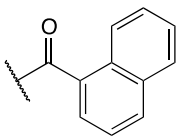	74.4 ± 6.3	144 ± 31.1

4.3.3 Kinetic evaluation of 'West end' derivative

Continuing this preliminary SAR study on hFXIIIa, we placed a negatively charged N-Acyl-L-aspartic acid residue on the 'West end' of **AA27**. As discussed in our inhibitor design section, we hoped that placement of a negative charge on the 'West end' of our inhibitor would increase the affinity with hFXIIIa by interacting with nearby positively charged arginine residue. Unfortunately, replacing the N-terminal Cbz group with a N-Acyl-L-aspartic acid residue resulted in a lower affinity to hFXIIIa relative to compound **AA27**. However, the affinity for hTG2 was still poor with a K_i value of 371 μM maintaining that sought after selectivity for hFXIIIa. Prospective derivatives for the 'West end' will be further discussed in chapter 5. Overall, these results showed that **AA27** is superior to all inhibitors in this work's SAR study through its affinity and selectivity for hFXIIIa.

Table 4.3. Kinetic parameters of 'West end' derivatives

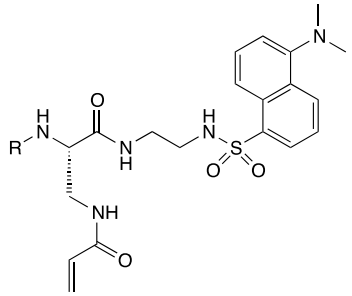

Inhibitor	R group	K_i (μM)	
		hFXIIIa	**hTG2**
30	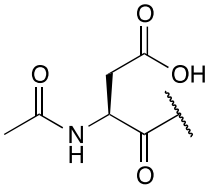	72.5 ± 1.8	371 ± 57.7

Chapter Five: **Conclusion and perspectives**

5.1 Human tissue transglutaminase inhibitors

5.1.1 Goal of the project

The main project for this thesis was to develop a potent and selective covalent inhibitor of hTG2 based on our previously reported Cbz-Lys(Acr) scaffold. Starting with our lead inhibitor **NC9**, an inhibitor bearing an acrylamide warhead, we decided to develop a library of inhibitors. Our SAR study maintained the Cbz group for affinity reasons and the 'select' acrylamide warhead for its balance between stability and reactivity. We systematically varied the length of the side chain, the peptide backbone spacer, and the C-terminal 'East end' group (see Figure 5.1) on **NC9**. The goal was to develop an efficient covalent inhibitor that blocks the acyl transferase activity of hTG2. Additionally, we wanted to investigate how our covalent inhibitors can affect the GTP binding ability of hTG2. Inhibitors that provided high potency and selectivity were carried forward as potential drug candidates that can inactivate overexpressed and unregulated hTG2 activity that has been associated with numerous human diseases, including cancer stem cell survival and metastatic phenotype.

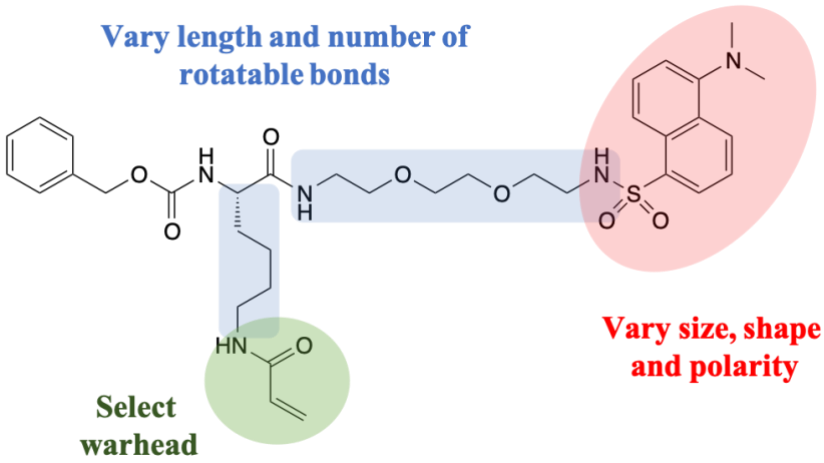

Figure 5.1. Strategic SAR approach on previously reported acrylamide based peptidomimetic irreversible inhibitor, NC9.

5.1.2 Results

From the spacer derivatives within our SAR study, we found that the piperazine spacers gave the highest inhibitor efficiency within the series. In addition, the piperazine spacer allowed us to reduce the spacer length from eight atoms in **NC9** to two atoms in compound **15** (**VA4**), resulting in a dramatic reduction in the number of rotatable bonds. On the contrary, reducing the length of the side chain reduced the number of rotatable bonds in inhibitors **17-19**, but drastically reduced the efficiency of the inhibitors in return. Thus, reducing the number of methylene units of the side chain below 4 resulted in a loss of inhibitor activity. Upon consideration of affinity and reactivity, we judged inhibitors **15** (aka **VA4**) and **22** (aka **AA9**) (Figure 5.2) to be the best lead compounds from the sulfonamide and amide piperazinyl linked derivatives. Both compounds are highly efficient irreversible inhibitors with an efficiency (k_{inact}/K_I) of approximately 10^5 M^{-1} min^{-1}. Furthermore, these two lead compounds (**VA4** and **AA9**) were tested further for their ability to abolish GTP binding. This evaluation showed that hTG2 significantly lost its GTP binding ability after incubation with our **VA4** and **AA9**. Finally, we assessed the selectivity of **NC9** and **VA4** for their reaction with

hTG2 over four therapeutically relevant isoforms of human transglutaminase: FXIIIa, hTG3a, hTG1, and hTG6. In general, our potent covalent inhibitors showed excellent selectivity toward hTG2 over the other isozymes.

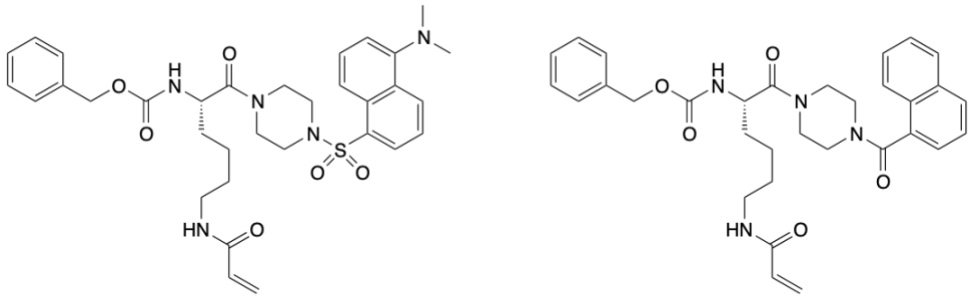

VA4

K_I = 8.9 μM

k_{inact}/K_I = 1.0 x 10^5 M^{-1} min^{-1}

AA9

K_I = 13 μM

k_{inact}/K_I = 1.1 x 10^5 M^{-1} min^{-1}

Figure 5.2. Structures and kinetic inhibition parameters of VA4 and AA9 towards hTG2.

5.1.3 Perspectives

Looking forward, our first step will be to continue our hTG2 SAR study. We will add various derivatives on the 'West end' of our lead inhibitors and determine their efficiency towards inactivation of hTG2. Another potential SAR project will focus on rigidifying the Lys side chain carrying the acrylamide warhead. Once a suitable inhibitor efficiency is determined, the focus of this project will be redirected towards pharmacokinetics. We would study common pharmacological factors such as absorption, distribution, biotransformation and elimination of lead inhibitors. These pharmacokinetic studies will be conducted on an *in vitro* level to start, then moving to *in vivo* mouse models and eventually concluding at the clinical level. Simultaneously, we must always ensure our potent inhibitors are selective to hTG2 rather than being promiscuous to similar protein pockets. Beyond an *in vitro* evaluation, we will design a clickable probe to test the selectivity of our potent

inhibitors in a cellular context. We will hope to create a selective and efficient inhibitor, with therapeutically benefical pharmacokinetic properties.

5.2 Human factor XIIIa inhibitors

5.2.1 Goal of the project

The secondary project for this work was a pioneering study aimed towards developing a high affinity hFXIIIa small molecule inhibitor that will possess selectivity against hTG2. The inhibitor design was based on a Dap(Acr) scaffold that was shown to be poorly reactive towards hTG2. Starting with our lead inhibitor **16**, we rationally developed a library of inhibitors. Our SAR study maintained the acrylamide warhead, as it previously demonstrated a beneficial balance of stability and reactivity with hTG2. We also decided to maintain the one methylene unit side chain, as we believe it is a key structural basis for selectivity for hFXIIIa over hTG2. Like our hTG2 SAR study, we explored the spacer length on compound **16** (see Figure 5.3) and systematically increased the number of methylene units to study both its effect on affinity and its selectivity between hTG2 and hFXIIIA. Additionally, we evaluated a few simple variations on the 'East end' and 'West end' of inhibitor **16**, as illustrated in Figure 5.3. With this small inhibitor SAR study, our goal was to provide preliminary data to allow for the development of an efficient and selective inhibitor that blocks the acyl transferase activity of hFXIIIa.

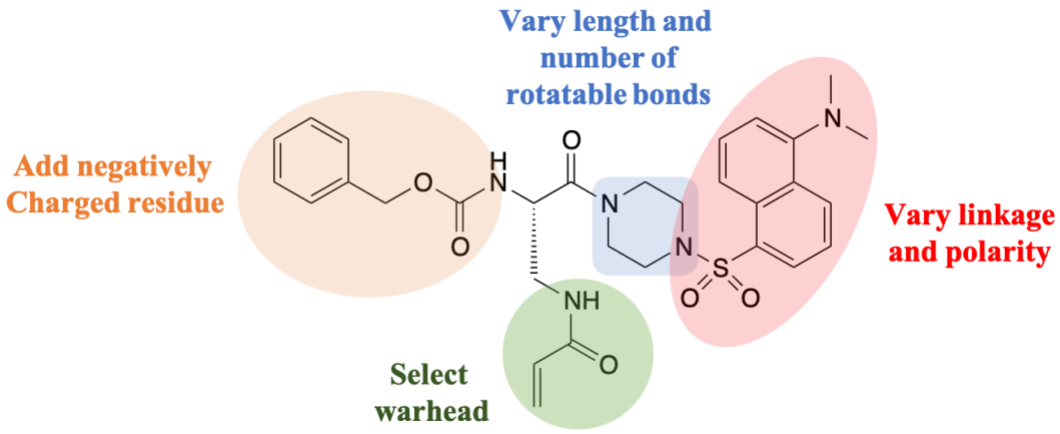

Figure 5.3. Strategic SAR approach on acrylamide based covalent inhibitor 16.

5.2.2 Results

After kinetic evaluation of our spacer derivatives, we found that the two methylene unit diamine spacer, **AA27**, had the highest affinity for hFXIIIa and sufficient selectivity over hTG2. The piperazine spacer was comparable in its affinity; however, it showed lower selectivity over from hTG2. The two methylene unit spacer was 20-fold more selective for hFXIIIa, while the piperazine spacer was only 6-fold selective. Further investigation into our SAR study showed that removal of the dimethyl amine on the dansyl group of **AA27** decreases the affinity towards hFXIIIa by 4-fold. Additionally, an amide linked 1-naphthalene on the 'East end' of our Dap(Acr) scaffold displayed a drop in selectivity for hFXIIIa relative to hTG2. Modification of the 'West end' of compound **AA27** with a negatively charged aspartate residue reduced the affinity towards hFXIIIa and kept a comparable selectivity for hTG2. This preliminary SAR study allowed us to discover a reasonably potent inhibitor, **AA27**, with a K_i value of 26 μM towards hFXIIIa and a 20-fold selectivity away from hTG2. This serves as an excellent starting point for further development of an inhibitor that is specific for hFXIIIa.

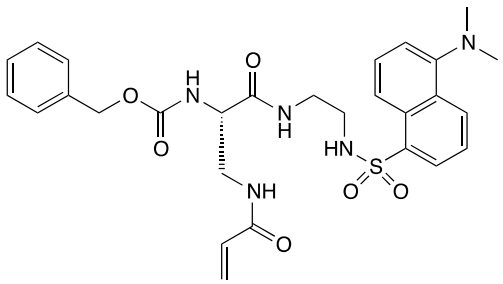

AA27

K_i = 26 μM (hFXIIIa)

K_i = 514 μM (hTG2)

Figure 5.4. Structure and inhibitor dissociation constants for compound 26 (AA27) interacting with hTG2 and hFXIIIa.

5.2.3 Perspectives

Our novel findings during our SAR study with hFXIIIa provided us with a structural framework to use for future inhibitor designs. With the knowledge that a Dap(Acr) scaffold provides selectivity for hFXIIIa over hTG2, we can further elaborate both the *N*- and *C*-termini with appropriate derivatives. We would start at the *N*-terminal or 'West end' of the inhibitor and try other negatively charged residues, such as one to three methylene unit extensions with a carboxylic acid group. By testing these flexible carboxylate groups, we can explore the space needed to create a sought-after favourable electrostatic interaction in the pocket of hFXIIIa. Another potential plan can focus on the acrylamide warhead, as it did not show much covalent reactivity with hFXIIIa. One option can be to reduce the alkene in the acrylamide warhead and conceivably test a new generation of *reversible* hFXIIIa inhibitors. Alternatively, we can test the reactivity of different warheads towards hFXIIIa, while trying to retain inhibitor selectivity. Our

near-future focus will be maintained on the SAR study, with hopes of discovering the first selective and potent small molecule hFXIIIa inhibitor.

Chapter Six: **General comments and procedures**

6.1 General comments

Chemicals and solvents were obtained from Sigma-Aldrich or Fisher Scientific and used without further purification, as were deuterated solvents obtained from Cambridge Isotope Laboratories. NMR spectra were recorded on Bruker AVANCE 300, 400 and 500 MHz instruments, and chemical shifts were reported in ppm referenced to the deuterated solvent peak. High resolution mass spectra results were obtained from the John Holmes Mass Spectrometry facility of the University of Ottawa, using a quadrupole time-of-flight (QTOF) analyzer and electrospray ionization (ESI). Melting points were recorded for solid compounds on a Stanford Research Systems EZ. Final compounds used for *in vitro* analysis were of ≥ 95% purity as judged by the HPLC chromatogram obtained using a Phenomenex C18 reversed phase column, 4.6 mm × 150 mm; solvent, acetonitrile/water. An isocratic elution of 40:60 acetonitrile/water or a gradient elution of 75:25 to 30:70 acetonitrile/water over 20 min or 80:20 to 30:70 acetonitrile/water with 0.1% TFA over 15 min was used depending on compound. All compounds were eluted with a flow rate of 1.0 mL/min and monitored with a UV detector at 260 nm.

6.1.1 General procedures

6.1.1.1 Addition of acrylamide

The commercially available *N*-terminal Cbz protected amino acid (1 equiv) was dissolved in THF/1.0 M NaOH (1.2 equiv) (1:1 v/v) and cooled to 0 °C. Acryloyl chloride (1.2 equiv),

dissolved in THF, was slowly added concurrently. The solution was stirred for 10 min and quenched by the addition of saturated NaCl solution. The mixture was acidified to pH 1 with 1.0 M HCl and extracted three times with dichloromethane. The organic extracts were combined and washed with water, brine, dried with $MgSO_4$, filtered, and concentrated to afford clear, colourless oils.

6.1.1.2 Synthesis of monodansylated amine intermediates

The commercially available diamine (6 equiv) was dissolved in cooled DCM followed by the addition of dansyl chloride (1 equiv). The yellow solution was allowed to warm to room temperature and left stirring for 30 min. The solution was washed three times with saturated $NaHCO_3$ solution, and the organic phase was washed with brine, dried with $MgSO_4$, filtered, and evaporated under reduced pressure to provide a green/yellow oil. The crude product was purified by flash chromatography over silica gel (elution with gradient of 1−4% MeOH in CH_2Cl_2) to afford the desired products as yellow/green oils.

6.1.1.3 Synthesis of sulfonamide intermediates (using unprotected amines)

Commercially available diamine (6 equiv) was dissolved in DCM and cooled to 0 °C. The sulfonyl chloride (1 equiv) was dissolved in dichloromethane and added slowly via dropping funnel, typically resulting in an opaque solution. The yellow solution was allowed to warm to room temperature and left stirring for 1.5 hours. Dilution in DCM followed by addition of saturated $NaHCO_3$ solution gave a clear, colourless solution. The DCM was separated, washed with brine, dried with $MgSO_4$, filtered, and concentrated under reduced pressure to afford typically white or yellow solids. The crude product was purified by flash chromatography over

silica gel (elution with gradient of 1−4% MeOH in CH_2Cl_2) to afford the desired products as white solids.

6.1.1.4 Synthesis of amide intermediates (using protected amines)

Commercially available Boc protected diamines (1 equiv) were dissolved in DCM. Triethylamine (2.5 equiv) and the acid chloride (3 equiv) were added slowly via dropping funnel. The solution was stirred at room temperature for either 1 h or overnight. The solution was concentrated under reduced pressure and the residue was dissolved in DCM. The solution was washed with water, saturated $NaHCO_3$ solution and brine, dried with $MgSO_4$, filtered, and concentrated under reduced pressure to afford a white sticky foam.

6.1.1.5 Boc-deprotection of intermediates

Boc protected amine intermediates (1 equiv) were dissolved in $CHCl_3$ with 10% v/v trifluoroacetic acid. The solution was stirred at room temperature and monitored via TLC (Solvent system: 5% CH_3OH/DCM with 0.5% triethylamine). Starting material was no longer detected after approximately 2 h, and the $CHCl_3$ was concentrated under reduced pressure. The residue was triturated with diethyl ether and the TFA salt was dissolved in 5 mL of ACN containing 1 equiv of trimethylamine and carried forward without further purification.

6.1.1.6 Coupling using EDC/NHS

The carboxylic acid (1 equiv) was dissolved in ACN, and EDC·HCl (1 equiv) and NHS (1 equiv) were added. The solution was stirred at room temperature for 16 h. The solution was diluted with ethyl acetate and washed with water, saturated $NaHCO_3$ solution, and brine. The ethyl acetate solution was dried with $MgSO_4$, filtered, and concentrated to afford the crude NHS

ester typically as a white solid. The NHS ester was carried forward without further purification. Crude NHS ester (1.1 equiv) was dissolved in 10 mL of ACN. Triethylamine (1 equiv) and the desired amine intermediate (1 equiv) were added, and the reaction was left to stir at room temperature for 3 h or kept overnight. The solution was diluted with ethyl acetate, washed with saturated $NaHCO_3$ solution and brine, dried with $MgSO_4$, filtered, and concentrated to afford white sticky foams or oil (dansylated final compounds were yellow/green).

6.1.1.7 Coupling using EDC/HOBt

The carboxylic acid (1 equiv) was added to a solution of EDC·HCl (1.2 equiv), HOBt (1.2 equiv), and N,N-diisopropylethylamine (1.2 equiv) in ACN and stirred at room temperature for 30 min. The amine intermediate (1.2 equiv) was added, and the solution was left stirring at room temperature for 20 h. The ACN was evaporated under reduced pressure, and the residue was dissolved in $CHCl_3$. The $CHCl_3$ was washed with water, saturated $NaHCO_3$ solution, 1 M HCl, and brine. The organic phase was dried with $MgSO_4$, filtered, and concentrated under reduced pressure to afford the crude product, typically as an oil. The crude products were purified by flash chromatography over silica gel (elution with a gradient of 0−3% MeOH in CH_2Cl_2) to afford the desired products mostly as sticky foams (dansylated final compounds were yellow/green).

6.1.1.8 Cbz deprotection (hydrogenation)

Cbz protected compounds were dissolved in dry MeOH under nitrogen atmosphere. Pd/C (20 mol %) was added and the flask was evacuated and flushed with nitrogen three times. The flask was subsequently evacuated and flushed with hydrogen three times with vigorous stirring.

After 2 h, starting material was still present and fresh Pd/C was added to ensure reaction completion. After 8 h, the solution was filtered over celite and the collected MeOH was put under nitrogen atmosphere and Pd/C (20 mol %) was added. The mixture was left stirring vigorously overnight. Starting material was not observed via TLC (Solvent system: 5% CH_3OH/DCM). The solution was filtered over celite and washed with methanol. The methanol solution was concentrated to afford the deprotected product as a sticky foam.

6.2 Experimental section for Chapter 2

Syntheses and characterization data for intermediate/final compounds used in Chapter 2 are described below. General procedures used for syntheses are denoted for each compound; modifications will be described.

6.2.1 Intermediate synthesis

6.2.1.1 N-(4-aminobutyl)-5-(dimethylamino)naphthalene-1-sulfonamide (**1**)

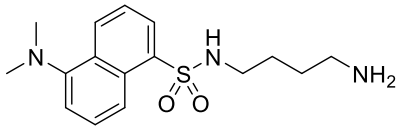

Compound **1** was synthesized using general procedure 6.1.1.2. Yielded 71 % of compound as a green oil. ^{1}H NMR (400 MHz, $CDCl_3$) δ 8.46 (d, *J* = 8.5 Hz, 1H), 8.33 (d, *J* = 8.6 Hz, 1H), 8.17 (d, *J* = 7.2 Hz, 1H), 7.45 (m, 2H), 7.10 (d, *J* = 7.5 Hz, 1H), 2.81 (br s, 8H), 2.64 (m, 2H), 1.43 (m, 4H), ^{13}C NMR (100 MHz, $CDCl_3$) δ 151.9, 135.2, 130.1, 129.9, 129.7, 129.3, 128.2, 123.3, 119.2, 115.2, 45.5, 42.9, 40.8, 28.8, 27.2; HRMS (ESI-QTOF) m/z $[M + H]^+$ calcd for $C_{16}H_{24}N_3O_2S$ 322.1576; found 322.1576.

6.2.1.2 N-(3-aminopropyl)-5-(dimethylamino)naphthalene-1-sulfonamide (**2**)

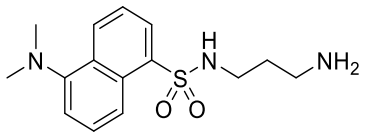

Compound **2** was synthesized using general procedure 6.1.1.2. Yielded 78 % of compound as a green oil. ^{1}H NMR (400 MHz, $CDCl_3$) δ 8.50 (d, *J* = 8.5 Hz, 1H), 8.30 (d, *J* = 8.6 Hz, 1 H), 8.21 (d, *J* = 7.3 Hz, 1H), 7.50-7.48 (m, 2H), 7.15 (d, *J* = 7.0 Hz, 1H), 2.99 (m, 2H), 2.85 (s, 6H), 2.69 (m, 2 H), 1.49 (m, 2H) , ^{13}C NMR (100 MHz, $CDCl_3$) δ 152.1, 135.0, 130.3, 130.1, 129.8, 129.7, 128.2, 123.4, 119.2, 115.3, 45.6, 43.1, 40.7, 30.7; HRMS (ESI-QTOF) m/z $[M + H]^+$ calcd for $C_{15}H_{21}N_3O_2S$ 308.1433; found 308.1407.

6.2.1.3 N-(2-aminoethyl)-5-(dimethylamino)naphthalene-1-sulfonamide (**3**)

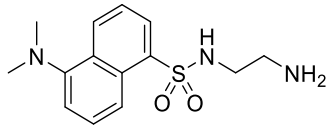

Compound **3** was synthesized using general procedure 6.1.1.2. Yielded 70 % of compound as a green oil. ^{1}H NMR (400 MHz, $CDCl_3$) δ 8.49 (d, J = 8.4 Hz, 1H), 8.30 (d, J = 8.6 Hz, 1 H), 8.20 (d, J = 7.2 Hz, 1H), 7.51-7.45 (m, 2H), 7.12 (d, J = 7.5 Hz, 1H), 2.93 (m, 2H), 2.84 (s, 6H), 2.77 (m, 2H)., ^{13}C NMR (100 MHz, $CDCl_3$) δ 152.1, 134.8, 130.5, 130.0, 129.8, 129.7, 128.6, 123.3, 119.0, 115.4, 45.6, 44.9, 40.9; HRMS (ESI-QTOF) m/z $[M + Na]^+$ calcd for $C_{14}H_{20}N_3O_2SNa$ 316.1096; found 316.1095.

6.2.1.4 N,N-dimethyl-5-(piperazin-1-ylsulfonyl)naphthalen-1-amine (**4**)

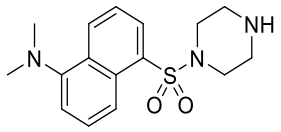

Compound **4** was synthesized using general procedure 6.1.1.2. Yielded 76 % of compound as a green solid. ^{1}H NMR (400 MHz, $CDCl_3$) δ 8.57 (d, J = 8.5 Hz, 1H), 8.45 (d, J = 8.7 Hz, 1H), 8.20 (d, J = 7.4 Hz, 1H), 7.54-7.51 (m, 2H), 7.19 (d, J = 7.4 Hz, 1H), 3.15 (m, 4H), 2.88 (s, 6H), 2.87 (m, 4H), ^{13}C NMR (100 MHz, $CDCl_3$) δ 151.9, 132.8, 130.8, 130.8, 130.7, 130.3, 128.1, 123.3, 120.0, 115.4, 46.7, 45.7, 45.6; HRMS (ESI-QTOF) m/z [M + H]+ calcd for $C_{16}H_{22}N_3O_2S$ 320.1433; found 320.1373.

6.2.1.5 tert-butyl 4-benzoylpiperazine-1-carboxylate (**4.1**)

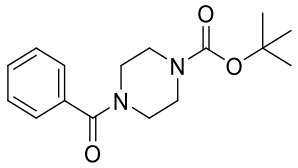

Compound **4.1** was synthesized using general procedure 6.1.1.4. Yielded 63 % of compound as a white powder. ^{1}H NMR (400 MHz, $CDCl_3$) δ 7.43 – 7.37 (m, 5H), 3.82 – 3.64 (m, 2H), 3.57 – 3.32 (m, 6H), 1.46 (s, 9H); ^{13}C NMR (100 MHz, $CDCl_3$) δ 170.6, 154.6, 135.5, 129.9, 128.6, 127.0, 80.4, 47.5, 44.1, 43.7, 28.4; HRMS (ESI-QTOF) m/z [M + Na]+ calcd for $C_{16}H_{22}N_2O_3Na$ 313.1528; found 313.1508.

6.2.1.6 tert-butyl 4-(1-naphthoyl)piperazine-1-carboxylate (**4.2**)

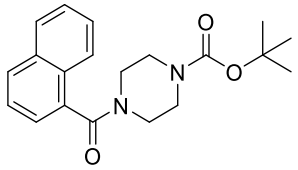

Compound **4.2** was synthesized using general procedure 6.1.1.4. Yielded 82 % of compound as a clear, colourless oil. ^{1}H NMR (400 MHz, $CDCl_3$) δ 7.87-7.78 (m, 3H), 7.51-7.38 (m, 4H), 3.96-3.81 (m, 2H), 3.56 (m, 2H), 3.29-3.14 (m, 4H), 1.43 (s, 9H), ^{13}C NMR (100 MHz, $CDCl_3$) δ 169.7, 154.6, 133.9, 133.6, 129.6, 129.5, 128.6, 127.3, 126.7, 125.3, 124.7, 123.9, 80.5, 47.1, 41.8, 28.5; HRMS (ESI-QTOF) m/z $[M + Na]^+$ calcd for $C_{20}H_{24}N_2O_3Na$ 363.1685; found 363.1696.

6.2.1.7 tert-butyl 4-(2-naphthoyl)piperazine-1-carboxylate (**4.3**)

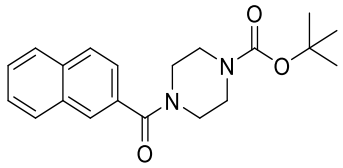

Compound **4.3** was synthesized using general procedure 6.1.1.4. Yielded 78 % of compound as a clear, colourless oil. ^{1}H NMR (400 MHz, $CDCl_3$) δ 7.88-7.82 (m, 4H), 7.52-7.44 (m, 3H), 3.75 (m, 2H), 3.45 (m, 6H), 1.44 (s, 9H), ^{13}C NMR (100 MHz, $CDCl_3$) δ 170.8, 154.7, 133.9, 132.9, 132.8, 128.6, 128.5, 127.9, 127.4, 127.1, 126.9, 124.3, 80.5, 28.5; HRMS (ESI-QTOF) m/z $[M + Na]^+$ calcd for $C_{20}H_{24}N_2O_3$ 363.1685; found 363.1678.

6.2.1.8 (S)-3-acrylamido-2-(((benzyloxy)carbonyl)amino)propanoic acid (**5**)

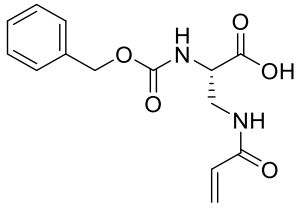

Compound **5** was synthesized using general procedure 6.1.1.1. Yielded 62 % of compound as a clear, colourless oil. ^{1}H NMR (400 MHz, CD_3OD) δ 7.37-7.27 (m, 5H), 6.22-6.20 (m, 2H), 5.67-5.64 (m, 1H), 5.09-5.08 (m, 2H), 4.38-4.35 (m, 1H), 3.77-3.73 (m, 1H), 3.59-3.54 (m, 1H), ^{13}C NMR (100 MHz, CD_3OD) δ 173.4, 168.8, 158.5, 138.1, 131.7, 129.4, 129.0, 128.8, 127.1, 67.7, 55.5, 41.7; HRMS (ESI-TOF) m/z $[M + Na]^+$ calcd for $C_{14}H_{16}N_2O_5Na$ 315.0957; found 315.0945.

6.2.1.9 (S)-4-acrylamido-2-(((benzyloxy)carbonyl)amino)butanoic acid (**6**)

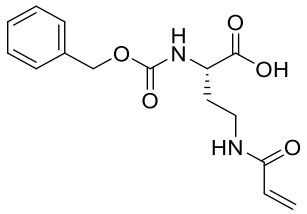

Compound **6** was synthesized using general procedure 6.1.1.1. Yielded 64 % of compound as a clear, colourless oil. ^{1}H NMR (400 MHz, $CDCl_3$) δ 9.44 (br s, 1H), 7.26-7.19 (m, 5H), 7.08-7.03 (m, 1H), 6.18-6.13 (d, *J* = 16.9 Hz, 1H), 6.06-6.00 (dd, *J* = 16.9 Hz, *J* = 10.4 Hz, 1H), 5.98-5.95 (m, 1H), 5.54-5.52 (d, *J* = 10.4 Hz, 1H), 4.99 (s, 2H), 4.28-4.24 (m, 1H), 3.57-3.51 (m, 1H), 3.07-3.02 (m, 1H), 2.05-1.97 (m, 1H), 1.80-1.71 (m, 1H), ^{13}C NMR (100 MHz, $CDCl_3$) δ 174.2, 167.2, 156.8, 136.1, 130.4, 128.7, 128.3, 128.1, 127.5, 67.3, 51.7, 36.2, 32.7, 29.3; HRMS (ESI-TOF) m/z $[M + Na]^+$ calcd for $C_{15}H_{18}N_2O_5Na$ 329.1113; found 329.1103.

6.2.1.10 (S)-5-acrylamido-2-(((benzyloxy)carbonyl)amino)pentanoic acid (**7**)

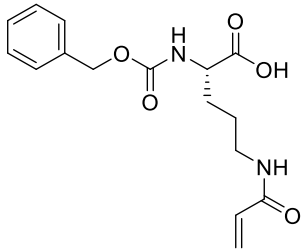

Compound **7** was synthesized using general procedure 6.1.1.1. Yielded 70 % of compound as a clear colourless oil. ^{1}H NMR (400 MHz, CD_3OD) δ 7.34-7.27 (m, 5H), 6.22-6.19 (m, 2H), 5.64-5.61 (m, 1H), 2.08 (s, 2H), 4.19-4.15 (m, 1H), 3.28-3.24 (t, *J* = 6.8 Hz, 2H), 1.93-1.83 (m, 1H), 1.74-1.57 (m, 3H), ^{13}C NMR (100 MHz, CD_3OD) δ 175.6, 168.1, 158.6, 138.1, 131.9, 129.4, 128.9, 128.7, 126.6, 67.6, 55.1, 39.9, 30.1, 26.8; HRMS (ESI-TOF) m/z $[M + Na]^+$ calcd for $C_{16}H_{20}N_2O_5Na$ 343.1270; found 343.1272.

6.2.1.11 (S)-6-acrylamido-2-(((benzyloxy)carbonyl)amino)hexanoic acid (**8**)

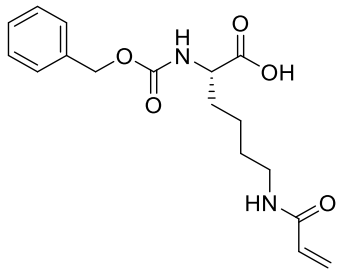

Compound **8** was synthesized using general procedure 6.1.1.1. Yielded 82 % of compound as a clear, colourless oil. Spectral data matched those from previously reported synthesis[144]. ^{1}H NMR (400 MHz, $CDCl_3$) δ 7.40 – 7.27 (m, 5H), 6.27 (dd, *J* = 17.0, *J* = 1.5 Hz, 1H), 6.07 (dd, *J* = 17.0, 10.3 Hz, 1H), 5.92 (s, 1H), 5.65 – 5.54 (m, 1H), 5.10 (d, *J* = 2.4 Hz, 2H), 4.36 (t, *J* = 7.0 Hz, 1H), 3.42 – 3.17 (m, 2H), 1.95 – 1.68 (m, 2H), 1.56 (q, *J* = 7.5 Hz, 2H), 1.48 – 1.33 (m, 2H).

6.2.2 Inhibitor synthesis

6.2.2.1 (S)-benzyl-(6-acrylamido-1-amino-1-oxohexan-2-yl)carbamate (**10**)

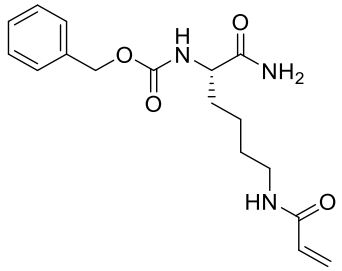

Compound **10** was prepared from ammonium chloride and compound **8** using general procedure 6.1.1.6. In this case, 2 equiv of DABCO was used in place of trimethylamine. Yielded 54% of desired compound as a white fluffy powder. mp 156-158 ˚C; $_{1}$H NMR (400 MHz, CD_3OD) δ 7.35-7.28 (m, 5H), 6.21-6.19 (m, 2H), 5.63-5.60 (m, 1H), 5.12-5.04 (m, 2H), 4.09-4.06 (m, 1H), 3.23 (t, *J* = 6.9 Hz, 1H), 1.83-1.78 (m, 1H), 1.69-1.61 (m, 1H), 1.56-1.53 (m, 2H), 1.42-1.40 (m, 2H), $_{13}$C NMR (100 MHz, CD_3OD) δ 177.7, 168.1, 158.5, 138.1, 132.0, 129.5, 129.0, 128.9, 126.5, 67.7, 56.1, 40.1, 32.9, 29.9, 24.2; HRMS (ESI-QTOF) m/z $[M + Na]^+$ calcd for $C_{17}H_{23}N_3O_4Na$ 356.1586; found 356.1554.

6.2.2.2 (S)-benzyl(6-acrylamido-1-((4-(5-(dimethylamino)naphthalene-1 -sulfonamido) butyl)amino)-1-oxohexan-2-yl)carbamate (**12**)

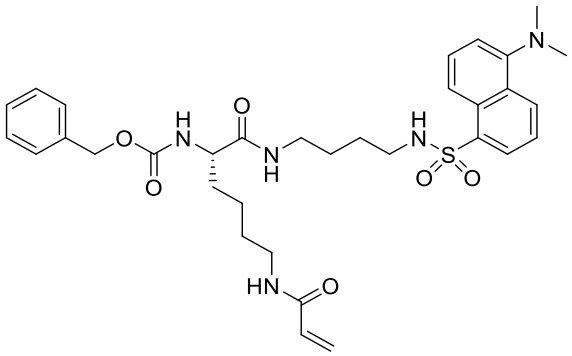

Compound **12** was prepared from N-(4-aminobutyl)-5-(dimethylamino)naphthalene-1-sulfonamide (**1**) and compound **8** using general procedure 6.1.1.7. This reaction yielded 56% of product as light green crystals. mp 54-56 ˚C; $_{1}$H NMR (400 MHz, $CDCl_3$) δ 8.51 (d, *J* = 8.4 Hz, 1H), 8.31 (d, *J* = 8.6 Hz, 1H), 8.18 (d, *J* = 7.3 Hz, 1H), 7.49-7.45 (m, 2H), 7.27 (m, 5H), 7.14 (d, *J* = 7.5 Hz, 1H), 6.68 (br s, 1H), 6.28 (br s, 1H), 6.23 (d, *J* = 16.8 Hz, 1H), 6.07 (m, 1H), 5.98 (br s, 1H), 5.88 (br s, 1H), 5.52 (d, *J* = 10.3 Hz, 1H), 5.03 (s, 2H), 4.10 (m, 1H), 3.25 (m, 2H), 3.10 (m, 2H), 2.85 (s, 6H), 2.81 (m, 2H), 1.78 (m, 1H), 1.64 (m, 1H), 1.50 (m, 2H), 1.40 (m, 6H), 1.23 (m, 1H), $_{13}$C NMR (100 MHz, $CDCl_3$) δ 172.3, 166.3, 156.6, 152.0, 136.4, 135.1, 131.0, 130.5, 130.0, 129.8, 129.6, 128.5, 126.7, 123.4, 119.2, 115.4, 67.2, 55.1, 45.6, 43.0, 39.0, 32.2, 29.0, 26.9, 26.6, 22.6; HRMS (ESI-QTOF) m/z $[M + Na]^+$ calcd for $C_{33}H_{43}N_5O_6SNa$ 660.2833; found 660.2842.

6.2.2.3 (S)-benzyl-(6-acrylamido-1-((3-(5-(dimethylamino)naphthalene-1-sulfonamido) propyl)amino)-1-oxohexan-2-yl)carbamate (**13**)

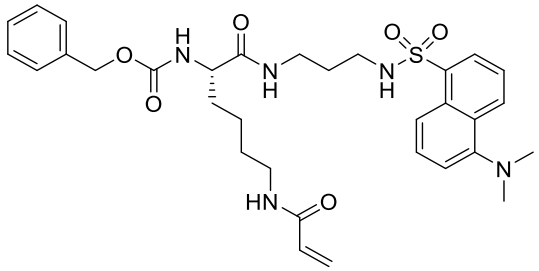

Compound **13** was prepared from N-(3-aminopropyl)-5-(dimethylamino)naphthalene-1-sulfonamide (**2**) and compound **8** using general procedure 6.1.1.7. This reaction yielded 49% of the product as light green crystals. mp 65-67 ˚C; $_{1}$H NMR (400 MHz, $CDCl_3$) δ 8.46-8.43 (d *J* = 8.5 Hz, 1H), 8.26-8.24 (d, *J* = 8.6 Hz, 1H), 8.14-8.12 (dd, *J* = 7.3 Hz, *J* = 1.2 Hz, 1H), 7.49-7.41 (m, 2H), 7.27-7.21 (m, 5H), 7.10-7.08 (d, *J* = 7.5 Hz, 1H), 6.61-6.59 (m, 1H), 6.18-6.13 (d, *J* = 16.9 Hz, 1H), 6.02-5.95 (dd, *J* = 16.9 Hz, 10.z Hz, 1H), 5.94-5.89 (m, 1H), 5.58-5.56 (d, *J* = 7.5 Hz, 1H), 5.49-5.46 (d, *J* = 10.2 Hz, 1H), 5.04-4.95 (m, 2H), 4.03-3.98 (m, 1H), 3.29-3.13 (m, 4H), 2.86-2.77 (m, 8H), 1.75-1.65 (m, 1H), 1.57-1.39 (m, 5H), 1.32-1.21 (m, 2H), $_{13}$C NMR (100 MHz, $CDCl_3$) δ 172.5, 166.0, 151.9, 136.2, 135.2, 130.7, 130.3, 129.9, 129.6, 129.2, 128.5, 128.3, 128.2, 128.1, 128.0, 126.6, 123.2, 119.0, 115.2, 67.0, 54.9, 45.4, 40.3, 38.6, 36.3, 31.7, 29.6, 28.9, 22.3; HRMS (ESI-QTOF) m/z $[M + Na]^+$ calcd for $C_{32}H_{41}N_5O_6SNa$ 646.2675; found 646.2657.

6.2.2.4 (S)-benzyl-(6-acrylamido-1-((2-(5-(dimethylamino)naphthalene-1-sulfonamido) ethyl)amino)-1-oxohexan-2-yl)carbamate (**14**)

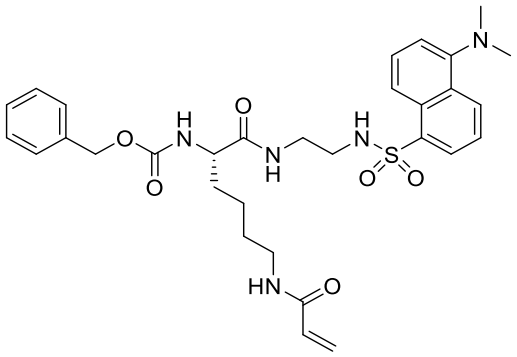

Compound **14** was prepared from N-(2-aminoethyl)-5-(dimethylamino)naphthalene-1-sulfonamide (**3**) and compound **8** using general procedure 6.1.1.7. This reaction yielded 51% of the product as a yellow/green sticky foam. ^{1}H NMR (400 MHz, $CDCl_3$) δ 8.50 (d, *J* = 8.5 Hz, 1H), 8.27 (d, *J* = 8.6 Hz, 1H), 8.15 (d, *J* = 7.1 Hz, 1H), 7.46 (m, 2H), 7.26 (m, 5H), 7.11 (d, *J* = 7.4 Hz, 1H), 6.55 (m, 1H), 6.50 (m, 1H), 6.21-6.16 (dd, *J* = 16.9 Hz, 1.5 Hz, 1H), 6.10-6.03 (dd, *J* = 10.0 Hz, 16.9 Hz, 1H), 5.95 (d, *J* = 7.4 Hz, 1H), 5.49-5.46 (dd, *J* = 10.0 Hz, 1.5 Hz, 1H), 5.04-5.01 (m, 2H), 4.09 (m, 1H), 3.25 (m, 4H), 2.96 (m, 2H), 2.83 (s, 6H), 1.75 (m, 1H), 1.64 (m, 1H), 1.47 (m, 2H), 1.34 (m, 2H), ^{13}C NMR (100 MHz, $CDCl_3$) δ 172.9, 166.3, 156.6, 136.3, 135.0, 130.9, 130.6, 129.7, 129.5, 128.7, 128.5, 128.4, 128.3, 126.7, 123.5, 119.2, 115.6, 67.3, 55.1, 45.6, 42.9, 39.5, 38.9, 32.0, 29.0, 22.6; HRMS (ESI-QTOF) m/z $[M + Na]^+$ calcd for $C_{31}H_{39}N_5O_6SNa$ 632.2519; found 632.2526.

6.2.2.5 (S)-benzyl-(6-acrylamido-1-(4-((5-(dimethylamino)naphthalen-1-yl)sulfonyl)piperazin-1-yl)-1-oxohexan-2-yl)carbamate (**15**, **VA4**).

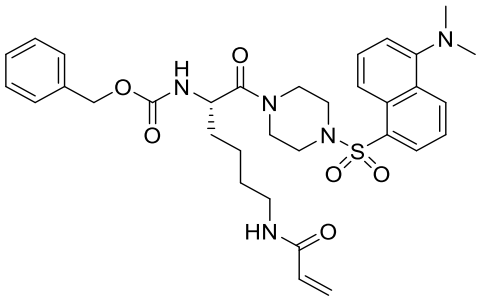

Compound **15** was prepared from N,N-dimethyl-5-(piperazin-1-ylsulfonyl)naphthalen-1-amine (**4**) and compound **8** using general procedure 6.1.1.7. This reaction yielded 38% of the product as a yellow/green sticky foam. mp 75-78 ˚C; $_{1}$H NMR (400 MHz, $CDCl_3$) δ 8.57 (d, *J* = 8.5 Hz, 1H), 8.32 (d, *J* = 8.7 Hz, 1H), 7.55-7.49 (m, 2H), 7.32-7.25 (m, 5H), 7.17 (d, *J* = 7.1 Hz, 1H), 6.23-6.19 (dd, *J* = 16.9 Hz, J = 1.5 Hz, 1H), 6.05-5.98 (dd, *J* = 16.9 Hz, *J* = 10.2 Hz, 1H), 5.70 (brs, 1H), 5.61-5.55 (m, 2H), 5.00 (s, 2H), 4.52-4.47 (m, 1H), 3.81-3.76 (m, 1H), 3.58-3.54 (m, 1H), 3.45-3.43 (m, 2H), 3.36-3.27 (m, 2H), 3.25-3.22 (m, 2H), 3.10-3.00 (m, 2H), 2.86 (s, 6H), 1.59-1.54 (m, 2H), 1.48-1.45 (m, 2H), 1.34-1.27 (m, 2H), $_{13}$C NMR (101 MHz, $CDCl_3$) δ 170.4, 165.7, 156.3, 152.0, 136.3, 132.3, 131.3, 131.0, 130.9, 130.4, 130.2, 128.7, 128.5, 128.3, 128.1, 126.5, 123.3, 119.4, 115.5, 67.1, 50.3, 45.7, 45.6, 45.4, 41.8, 39.1, 32.9, 29.9, 22.3; HRMS (ESI-QTOF) m/z [M + Na]+ calcd for $C_{33}H_{41}N_5O_6SNa$ 658.2675; found 658.2657.

6.2.2.6 (S)-benzyl (3-acrylamido-1-(4-((5-(dimethylamino)naphthalen-1-yl)sulfonyl)piperazin-1-yl)-1-oxopropan-2-yl)carbamate (**16**)

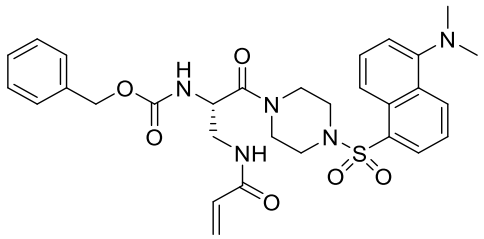

Compound **16** was prepared from N,N-dimethyl-5-(piperazin-1-ylsulfonyl)naphthalen-1-amine (**4**) and **5** using general procedure 6.1.1.7. This reaction yielded 32% of the final compound as a yellow/green sticky foam. mp 55-58 ˚C; $_{1}$H NMR (400 MHz, $CDCl_3$) δ 8.83-8.71 (m, 1H), 8.49-8.41 (m, 1H), 8.24-8.23 (d, *J* = 7.2 Hz, 1H), 7.66-7.54 (m, 2H), 7.36-7.26 (m, 6H), 6.27-6.15 (m, 2H), 6.04-5.95 (m, 1H), 5.88-5.84 (m, 1H), 5.61-5.59 (d, *J* = 10.2 Hz, 1H), 5.04 (s, 2H) , 4.76-4.70 (m, 1H), 3.73-3.56 (m, 5H), 3.38-3.15 (m, 5H), 2.99 (s, 6H), $_{13}$C NMR (100 MHz, $CDCl_3$) δ 168.3, 166.30, 156.3, 152.0, 136.1, 132.4, 131.2, 130.9, 130.3, 130.2, 128.6, 128.5, 128.4, 128.2, 127.2, 123.3, 119.4, 115.5, 67.3, 50.8, 45.6, 45.5, 45.3, 45.1, 42.6, 41.9 ; HRMS (ESI-QTOF) m/z $[M + Na]^+$ calcd for $C_{30}H_{35}N_5O_6SNa$ 616.2206; found 616.2194.

6.2.2.7 (S)-benzyl-(4-acrylamido-1-(4-((5-(dimethylamino)naphthalen-1-yl)sulfonyl)piperazin-1-yl)-1-oxobutan-2-yl)carbamate (**17**)

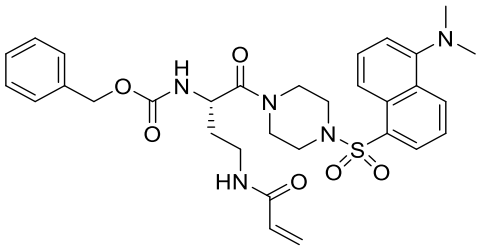

Compound **17** was prepared from N,N-dimethyl-5-(piperazin-1-ylsulfonyl)naphthalen-1-amine (**4**) and acrylamide **6** using general procedure 6.1.1.7. This reaction yielded 36% of the final compound as a yellow/green sticky foam. mp 65-67 ˚C; ^{1}H NMR (400 MHz, $CDCl_3$) δ 8.59-8.57 (d, *J* = 8.5 Hz, 1H), 8.32-8.29 (d, *J* = 8.7 Hz, 1H), 8.20-8.18 (d, *J* = 7.2 Hz, 1H), 7.56-7.52 (m, 2H), 7.19-7.18 (d, *J* = 7.5 Hz, 1H), 6.62-6.57 (m, 1H), 6.25-6.21 (d, *J* = 16.5 Hz, 1H), 6.11-6.05 (dd, *J* = 16.5 Hz, 10.2 Hz, 1 H), 5.90-5.88 (d, *J* = 7.8 Hz, 1H), 5.63-5.61 (d, *J* = 10.2 Hz, 1H), 5.06 (s, 2H), 4.59-4.49 (m, 1H), 3.75-3.67 (m, 2H), 3.58-3.50 (m, 1H), 3.41-3.33 (m, 2H), 3.28-3.10 (m, 4H), 3.01-2.92 (m, 1H), 2.88 (s, 6H), 1.97-1.87 (m, 1H), 1.56-1.45 (m, 1H), ^{13}C NMR (100 MHz, $CDCl_3$) δ 170.0, 165.8, 156.9, 152.0, 136.1, 132.3, 131.3, 130.9, 130.3, 130.2, 128.7, 128.5, 128.4, 128.1, 126.7, 123.3, 119.3, 115.6, 67.3, 48.5, 45.6, 45.5, 45.2, 45.1, 41.8, 35.6, 33.2; HRMS (ESI-QTOF) m/z $[M + H]^+$ calcd for $C_{31}H_{38}N_5O_6S$ 608.2543; found 608.2549.

6.2.2.8 (S)-benzyl-(5-acrylamido-1-(4-((5-(dimethylamino)naphthalen-1-yl)sulfonyl)piperazin-1-yl)-1-oxopentan-2-yl)carbamate (**18**)

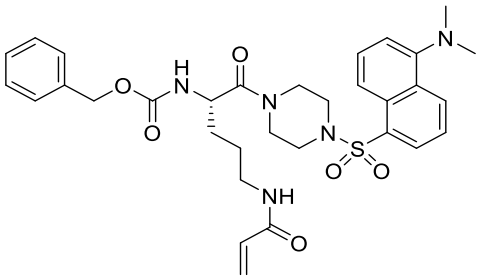

Compound **18** was prepared from N,N-dimethyl-5-(piperazin-1-ylsulfonyl)naphthalen-1-amine (**4**) and acrylamide **7** using general procedure 6.1.1.7. This reaction yielded 33% of the final compound as a yellow/green solid. mp 69-70 ˚C; $_1$H NMR (400 MHz, CDCl3) δ 8.53-8.51 (d, *J* = 8.5 Hz, 1H), 8.27-8.24 (d, *J* = 8.5 Hz, 1H), 8.14-8.12 (dd, *J* = 7.3, 1.0 Hz, 1H), 7.49-7.45 (m, 2H), 7.28-7.21 (m, 5H), 7.13-7.11 (d, *J* = 7.2 Hz, 1H), 6.19-6.15 (dd, *J* = 17.0, 1.3 Hz, 1H), 6.01-5.94 (dd, *J* = 17.0, 10.2 Hz, 1H), 5.89-5.84 (m, 1H), 5.60-5.57 (d, *J* = 8.4 Hz, 1H). 5.55-5.52 (dd, *J* = 10.2, 1.3 Hz, 1H), 4.97 (s, 2H), 4.55-4.50 (m, 1H), 3.51-3.37 (m, 3H), 3.32-3.18 (m, 4H), 3.11-2.98 (m, 3H), 2.82 (s, 6H), 1.58-1.42 (m, 4H), $_{13}$C NMR (100 MHz, CDCl$_3$) δ 170.3, 165.7, 156.3, 152.0, 136.2, 132.4, 131.3, 131.0, 130.9, 130.4, 130.2, 128.7, 128.5, 128.3, 128.2, 126.7, 123.3, 119.4, 115.5, 67.2, 50.2, 45.7, 45.5, 45.3, 41.9, 39.0, 31.2, 24.9; HRMS (ESI-QTOF) m/z [M + Na]+ calcd for $C_{32}H_{41}N_5O_6SNa$ 646.2675; found 646.2657.

6.2.2.9 (S)-benzyl-(1-(4-(1-naphthoyl)piperazin-1-yl)-6-acrylamido-1-oxohexan-2-yl)carbamate (**22, AA9**)

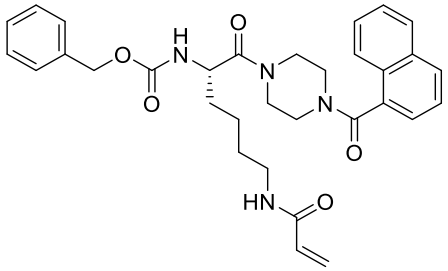

Compound **22** was prepared from Boc-deprotected **4.2** and compound **8** using general procedure 6.1.1.6. and 6.1.1.7. This reaction yielded 41% of the final compound as a white sticky foam. mp 59-62 ˚C; $_{1}$H NMR (500 MHz, $(CD_3)_2SO$) at 120 ºC) δ 7.99-7.96 (m, 2H), 7.84-7.81 (m, 2H), 7.59-7.54 (m, 3H), 7.46-7.44 (m, 2H), 7.35-7.26 (m, 4H), 6.74-6.72 (d, *J* = 7.5 Hz, 1H), 6.21-6.16 (dd, *J* = 17.1, 10.3 Hz, 1H), 6.05-6.01 (dd, *J* = 17.1, 2.1 Hz, 1H), 5.51-5.48 (dd, *J* = 10.3, 2.1 Hz, 1H), 5.04 (s, 1H), 4.46-4.41 (m, 1H), 3.63-3.38 (m, 8H), 3.16-3.12 (q, *J* = 6.85 Hz, 2 Hz), 1.71-1.56 (m, 2H), 1.51-1.44 (m, 2H), 1.39-1.29 (m, 2H), $_{13}$C NMR (100 MHz, $(CD_3)_2SO$) δ169.9, 167.8, 164.1, 155.0, 136.5, 133.5, 132.6, 131.7, 128.7, 128.2, 127.6, 127.5, 126.9, 126.8, 126.2, 125.6, 124.5, 123.9, 123.2, 123.1, 65.0, 50.3, 42.7, 37.8, 30.8, 28.2, 21.9; HRMS (ESI-QTOF) m/z $[M + Na]^+$ calcd for $C_{32}H_{36}N_4O_5Na$ 579.2584; found 579.2574.

6.2.2.10 (S)-benzyl(1-(4-(2-naphthoyl)piperazin-1-yl)-6-acrylamido-1-oxohexan-2-yl)carbamate (**23, AA10**).

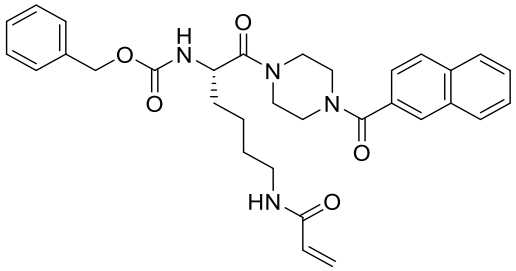

Compound **23** was prepared from Boc-deprotected **4.3** and compound **8** using general procedure 6.1.1.7. This reaction yielded 39% of the desired product as a white sticky foam. mp 60-63 ˚C; $_{1}$H NMR (300 MHz, $(CD_3)_2SO$ at 120 ˚C) δ 7.99-7.92 (m, 4H), 7.74 (br s, 1H), 7.60-7.48 (m, 3H), 7.33-7.23 (m, 5H), 7.06 (br s, 1H), 6.22-6.13 (dd, *J* = 17.2, 10.1 Hz, 1H), 6.06-5.99 (dd, *J* = 17.2, 2.4 Hz, 1H), 5.67 (s, 1H), 5.52-5.47 (dd, *J* = 10.1, 2.4 Hz, 1H), 5.02 (s, 2H), 4.46-4.38 (m, 1H), 3.63-3.46 (m, 8H), 3.14-3.07 (m, 2H), 1.65-1.53 (m, 2H), 1.49-1.39 (m, 2H), 1.36-1.25 (m, 2H), δ $_{13}$C NMR (75 MHz, $(CD_3)_2SO$) 170.9, 169.8, 165.1, 137.6, 133.7, 133.6, 132.8, 132.6, 128.7, 128.6, 128.5, 128.1, 128.0, 127.5, 127.1, 126.9, 124.8, 124.6, 66.0, 55.1, 51.2, 38.8, 31.7, 29.3, 23.1; HRMS (ESI-QTOF) m/z $[M + Na]^+$ calcd for $C_{32}H_{36}N_4O_5Na$ 579.2584; found 579.2557.

6.2.2.11 (S)-benzyl-(5-acrylamido-1-(4-benzoylpiperazin-1-yl)-1-oxopentan-2-yl)carbamate (**24**)

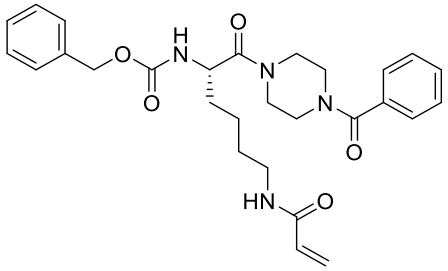

Compound **24** was prepared from Boc-deprotected **4.1** and compound **8** using general procedure 6.1.1.7. This reaction yielded 41% of the desired product as a white, sticky foam. mp 74-76 ˚C; $_{1}$H NMR (300 MHz, $(CD_3)_2SO$ at 80 ˚C) δ 7.73-7.65 (br s, 1H), 7.44-7.22 (m, 10 H), 7.05-6.98 (br s, 1H), 6.17-6.09 (dd, *J* = 17.1, 10.0 Hz, 1H), 6.01-5.95 (dd, *J* = 17.1, 2.3 Hz, 1H), 5.47-5.44 (dd, *J* = 10.0, 2.3 Hz, 1H), 4.97 (s, 2H), 4.41-4.36 (m, 1H), 3.55-3.36 (m, 8H), 3.09-3.02 (m, 2H), 1.61-1.49 (m, 2H), 1.44-1.33 (m, 2H), 1.32-1.20 (m, 2H), $_{13}$C NMR (75 MHz, $(CD_3)_2SO$ at 80 ˚C) δ 170.1, 168.9, 164.2, 136.7, 135.4, 131.7, 129.1, 127.9, 127.8, 127.2, 127.1, 126.4, 123.7, 65.1, 50.3, 37.9, 30.8, 28.3, 22.2; HRMS (ESI-QTOF) m/z $[M + Na]^+$ calcd for $C_{28}H_{34}N_4O_5Na$ 529.2427; found 529.2433.

6.3 Experimental section for Chapter 3

6.3.1 Enzyme activity assays (in vitro) for determining K_I and k_{inact}

6.3.1.1 Colorimetric transamidase activity assay

The activities of hTG1, hTG2, and hTG6 (recombinant proteins purchased from Zedira) were measured via a colorimetric assay using the chromogenic substrate Cbz-Glu(γ-p-nitrophenyl ester)Gly (**AL5**)[167]. The assay was conducted at 25 °C in 100 mM MOPS buffer (pH 6.5) containing 3.0 mM $CaCl_2$ and 50 μM EDTA. Enzymatic inhibition assays were run under Kitz and Wilson conditions[151] established for each transglutaminase isoform by varying the concentration of substrate to be 112 μM, 112 μM, and 436 μM **AL5** for hTG1, hTG2, and hTG6, respectively. A stock solution of **AL5** was prepared in DMSO such that the final concentration of this cosolvent was constant at 2.5% v/v. Stock solutions of the inhibitors were made in the buffer system described above. The reaction was initiated with the addition of 40−60 mU/mL of the respective enzyme (0.10 μM hTG1, 0.25 μM hTG2, or 0.32 μM hTG6). Product formation was monitored at 405 nm in a polystyrene 96-well microplate using a BioTek Synergy 4 plate reader. Monoexponential time-dependent inactivation was observed for all the inhibitors studied. Observed first-order rate constants of inactivation (k_{obs}) were determined from nonlinear regression fit to a monoexponential model (eq. 6.1) of the observed absorbance of the enzymatic hydrolysis product, *p*-nitrophenolate (pNP). These rate constants (k_{obs}) were in turn fit to a saturation kinetics model (eq. 6.2) by nonlinear regression, providing the kinetic parameters k_{inact} and K_I, as previously described by Stone and Hofsteenge[168]. A double reciprocal plot of eq 2 was applied when the observed rate constant of inactivation (k_{obs}) did not demonstrate saturation at high inhibitor concentrations or when solubility issues were encountered. Experiments were done in triplicate, and variation between repeats was less than 30%.

$$f(pNP) = [pNP]_0 + (plateau - [pNP]_0)(1 - e^{k_{obs}t}) \quad \text{eq. 6.1}$$

$$k_{obs} = \frac{k_{inact}[I]}{[I]+K_I(1+\frac{[S]}{K_M})} \quad \text{eq. 6.2}$$

6.3.1.2 Fluorescence isopeptidase activity assay

The isopeptidase activities of preactivated hTG3a and hFXIIIa (recombinant proteins purchased from Zedira) were measured via a fluorescence-based assay[43,162] using the commercially available peptidic FRET quenched probe **A101** from Zedira. Briefly, the final concentration in the reaction mixture contained 50 mM Tris (pH 7.0), 10mM $CaCl_2$, 100 mM NaCl, 2.8mM TCEP, 50 μM **A101**, and 14 mM H-Gly-OMe. The reaction was monitored at 25 °C using a BioTek Synergy 4 plate reader (Ex/Em: 318/413 nm). Enzymatic inhibition assays were run under Kitz and Wilson conditions[151], which were established for TG3a and FXIIa at a substrate (**A101**) concentration of 50 μM using enzyme concentrations of 0.17 μM and 0.11 μM for hTG3a and hFXIIIa, respectively.

6.3.2 GTP binding

6.3.2.1 In vitro GTP binding assay

GTP binding was measured using a method similar to that reported previously[159]. For all experiments, GTP binding was measured using 3 μM of the fluorescent, nonhydrolyzable GTP analogue BODIPY GTP-γ-S (Invitrogen), whose fluorescence increases when bound by protein.

hTG2 (8−10 μg) was incubated at 25 °C for 30 min with or without irreversible inhibitor (2 × K_I) with 3.0 mM $CaCl_2$ in 100 mM MOPS (pH = 6.54). The buffer was then exchanged at 4 °C to 100 mM MOPS (pH = 7.0), 1 mM EGTA, and 5 mM $MgCl_2$ to remove calcium and inhibitor using a 10 kDa molecular weight cut off membrane. The fluorescent GTP analog was then added to give a final concentration of 3.0 μM, and fluorescence was then measured on a microplate reader after 10 min of incubation (Ex/Em: 490/520 nm).

6.4 Experimental section for Chapter 4

Characterization data for intermediate/final compounds synthesized and used in Chapter 4 are described below. General procedures used for synthesis are denoted for each compound and any modifications will be described. Please note that some intermediates used in Chapter 4 are already described above for Chapter 3

6.4.1 Intermediate synthesis

6.4.1.1 tert-butyl (2-(1-naphthamido)ethyl)carbamate (**3.1**)

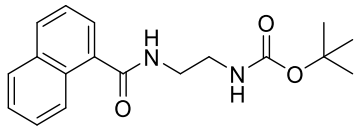

Compound **3.1** was prepared from commercially available N-Boc-ethylenediamine and 1-naphthoyl chloride using general procedure 6.1.1.4. This reaction yielded 76% of white solid product. ^{1}H NMR (400 MHz, $CDCl_3$) δ 8.26 – 8.20 (m, 1H), 7.84 – 7.75 (m, 2H), 7.51 – 7.43 (m, 3H), 7.33 – 7.25 (m, 1H), 7.04 – 6.92 (br s, 1H), 5.33 – 5.22 (br s, 1H), 3.55 – 3.45 (m, 2H), 3.34 – 3.25 (m, 2H), 1.36 (s, 9H), ^{13}C NMR (100 MHz, $CDCl_3$) δ 170.3, 156.9, 134.1, 133.6, 130.6, 128.2, 127.0, 126.3, 125.5, 125.1, 124.6, 79.6, 40.7, 40.4, 28.4; HRMS (ESI-QTOF) m/z [M + Na]$^{+}$ calcd for $C_{18}H_{22}N_2O_3Na$ 337.1528; found 337.1523.

6.4.1.2 tert-butyl (2-(naphthalene-1-sulfonamido)ethyl)carbamate (**3.2**)

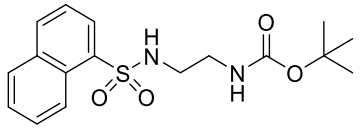

Compound **3.2** was prepared from commercially available N-Boc-ethylenediamine and 1-naphthalenesulfonyl chloride using general procedure 6.1.1.4. This reaction yielded 71% of white solid product. ^{1}H NMR (400 MHz, $CDCl_3$) δ 8.64-8.62 (d, *J* = 8.6 Hz, 1H), 8.23-8.21 (dd, *J* = 7.3, 1.2 Hz, 2H), 8.05-8.02 (d, *J* = 8.2 Hz, 1H), 7.92-7.90 (d, *J* = 7.6 Hz, 1H), 7.64-7.48 (m, 3H), 5.91-5.86 (m, 1H), 4.98-4.92 (m, 1H), 3.18-3.12 (m, 2H), 3.03-2.97 (m, 2H), 1.35 (s, 9H), ^{13}C NMR (100 MHz, $CDCl_3$) δ 156.5, 134.5, 134.4, 134.3, 129.6, 129.2, 128.5, 128.1, 127.0, 124.4, 124.2, 79.8, 43.7, 40.4, 28.4; HRMS (ESI-QTOF) m/z $[M + Na]^+$ calcd for $C_{17}H_{22}N_2O_4SNa$ 373.1198; found 373.1180.

6.4.1.3 tert-butyl-(2-((5-(dimethylamino)naphthalene)-1-sulfonamido)ethyl)carbamate (**3.3**)

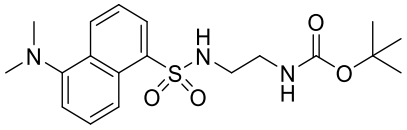

Compound **3.3** was prepared from commercially available N-Boc-ethylenediamine and dansyl chloride using general procedure 6.1.1.4. This reaction yielded 74% of yellow/green solid product. ^{1}H NMR (400 MHz, $CDCl_3$) δ 8.48-8.45 (d, *J* = 8.5 Hz, 1H), 8.27-8.24 (d, *J* = 8.6 Hz, 1H), 8.17-8.15 (dd, *J* = 7.3, 1.2 Hz, 1H), 7.48-7.41 (m, 2H), 7.10-7.08 (d, *J* = 7.5 Hz, 1H), 6.04 (br s, 1H), 5.10 (br s, 1H), 3.15-3.07 (m, 2H), 2.96-2.94 (m, 2H), 2.81 (s, 6H), 1.30 (s, 9H), ^{13}C NMR (100 MHz, $CDCl_3$) δ 156.3, 151.8, 134.6, 130.4, 129.8, 129.5, 129.3, 128.4, 123.1, 118.7, 115.2, 79.4, 45.3, 43.4, 40.2, 28.2; HRMS (ESI-QTOF) m/z $[M + Na]^+$ calcd for $C_{19}H_{27}N_3O_4SNa$ 416.1620; found 416.1617.

6.4.1.4 Benzyltert-butyl(3-((2-((5-(dimethylamino)naphthalene)-1-sulfonamido)ethyl)amino)-3-oxopropane-1,2-diyl)(S)-dicarbamate (**30.1**)

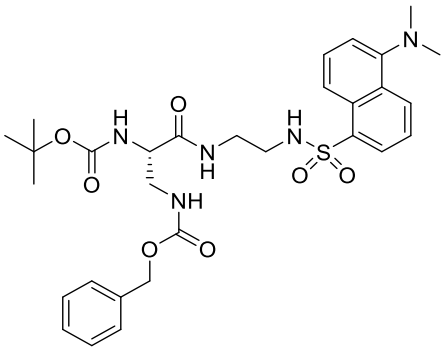

Compound **30.1** was prepared from Boc deprotected tert-butyl-(2-((5-(dimethylamino)naphthalene)-1-sulfonamido)ethyl)carbamate (**3.3**) and commercially available L-2,3-diaminopropionic acid (dicyclohexylammonium) salt using general amide coupling procedure 6.1.1.7, with 1 extra equivalence of Et_3N. Compound **3.3** was deprotected using general procedure 6.1.1.5. This reaction yielded 52 % of yellow-green sticky solid. ^1H NMR (400 MHz, $CDCl_3$) δ 8.51-8.48 (d, *J* = 8.5 Hz, 1H), 8.31-8.28 (d, *J* = 8.6 Hz, 1H), 8.18-8.16 (d, *J* = 7.1 Hz, 1H), 7.51-7.43 (m, 2H), 7.26-7.19 (m, 5H), 7.13-7.11 (d, *J* = 7.5 Hz, 1H), 6.40-6.36 (br s, 1H), 5.01 (s, 2H), 4.24-4.20 (bs s, 1H), 3.58-3.45 (m, 2H), 3.35-3.27 (m, 1H), 3.24-3.18 (m, 1H), 2.99-2.89 (m, 2H), 2.84 (s, 6H), 1.41 (s, 9H), ^{13}C NMR (100 MHz, $CDCl_3$) δ 171.0, 157.7, 152.1, 136.3, 130.6, 130.0, 129., 129.5, 128.6, 128.5, 18.3, 128.1, 123.3, 118.9, 115.4, 80.7, 67.3, 45.5, 43.1, 42.7, 39.9, 28.4; HRMS (ESI-QTOF) m/z $[M + H]^+$ calcd for $C_{30}H_{39}N_5O_7S$ 614.2648; found 614.2660.

6.4.1.5 tert-butyl-(S)-(3-amino-1-((2-(naphthalene-1-sulfonamido)ethyl)amino)-1-oxopropan-2-yl)carbamate (**30.2**)

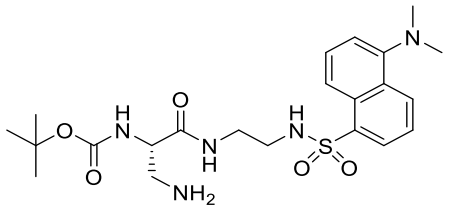

Compound **30.2** was prepared from compound **30.1** using general procedure 6.1.1.8. This reaction yielded 84% of yellow/green sticky solid. $_{1}$H NMR (400 MHz, $CDCl_3$) δ 8.49-8.47 (d, *J* = 8.5 Hz, 1H), 8.27-8.25 (d, *J* = 8.6 Hz, 1H), 8.16-8.14 (d, *J* = 7.3 Hz, 1H), 7.71-7.64 (br s, 1H), 7.50-7.42 (m, 2H), 7.12-7.10 (d, *J* = 7.4 Hz, 1H), 5.89-5.88 (br s, 1H), 4.09-4.08 (br s, 1H), 3.38-3.31 (m, 1H), 3.29-3.21 (m, 1H), 3.12-2.96 (m, 3H), 2.88-2.81 (m, 1H), 2.83 (s, 6H), 1.40 (s, 9H), $_{13}$C NMR (100 MHz, $CDCl_3$) δ 172.1, 155.9, 151.9, 135.0, 130.4, 129.9, 129.6, 129.2, 128.3, 123.2, 118.9, 115.3, 80.1, 55.6, 45.4, 43.9, 42.6, 39.5, 28.4; HRMS (ESI-QTOF) m/z [M + H]$^+$ calcd for $C_{22}H_{34}N_5O_5S$ 480.2281; found 480.2274.

6.4.1.6 tert-butyl-(S)-3-acetamido-4-(((S)-3-acrylamido-1-((2-((5-(dimethylamino)naphthalene)-1-sulfonamido)ethyl)amino)-1-oxopropan-2-yl)amino)-4-oxobutanoate (**30.3**)

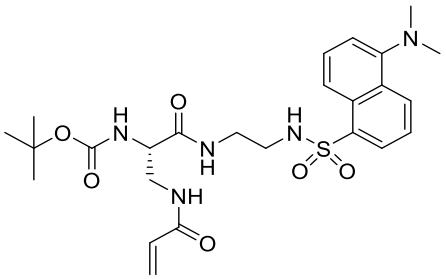

Compound **30.3** was prepared from compound **30.2** using general procedure 6.1.1.1. This reaction yielded 42% of yellow-green sticky oil. ^{1}H NMR (400 MHz, $CDCl_3$) δ 8.57-8.55 (d, *J* = 6.6 Hz, 1H), 8.52-8.49 (d, *J* = 8.5 Hz, 1H), 8.30-8.28 (d, *J* = 8.6 Hz, 1H), 8.18-8.16 (d, *J* = 7.3 Hz, 1H), 7.55-7.52 (br s, 1H), 7.53-7.45 (m, 2H), 7.25-7.20 (br s, 1H), 7.16-7.14 (d, *J* = 7.4 Hz, 1H), 7.08-7.06 (d, *J* = 6.7 Hz, 1H), 6.68-6.65 (m, 1H), 6.31-6.26 (dd, *J* = 16.9 Hz, 2.0 Hz, 1H), 6.24-6.17 (dd, *J* = 16.9 Hz, 9.6 Hz, 1H), 5.66-5.63 (dd, *J* = 9.6 Hz, 2.0 Hz, 1H), 4.65-4.58 (m, 1H), 4.46-4.40 (m, 1H), 3.86-3.78 (m, 1H), 3.72-3.63 (m, 1H), 3.43-3.33 (m, 1H), 3.25-3.16 (m, 1H), 3.08-3.01 (m, 1H), 2.86 (s, 6H), 2.87-2.80 (m, 1H), 2.10 (s, 3H), 1.43 (s, 9H), ^{13}C NMR (100 MHz, $CDCl_3$) δ 172.0, 171.3, 170.9, 170.7, 168.6, 151.9, 135.4, 130.4, 130.2, 130.0, 129.6, 129.1, 128.3, 127.8, 123.3, 119.2, 115.3, 82.3, 56.5, 51.1, 45.5, 42.8, 41.4, 39.9, 36.8, 28.2, 23.3; HRMS (ESI-QTOF) m/z $[M + Na]^+$ calcd for $C_{30}H_{42}N_6O_8S$ 669.2683; found 669.2661.

6.4.1.7 tert-butyl-(S)-3-acetamido-4-(((S)-3-acrylamido-1-((2-((5-(dimethylamino)naphthalene)-1-sulfonamido)ethyl)amino)-1-oxopropan-2-yl)amino)-4-oxobutanoate (**30.4**)

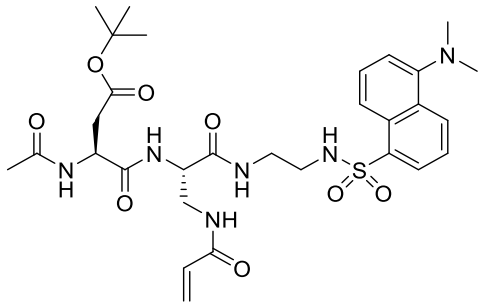

Compound **30.4** was prepared from Boc deprotected compound **30.3** and commercially available Ac-Asp(tBu)-OH using general amide coupling procedure 6.1.1.7. Compound **30.3** was deprotected using general procedure 1.1.1.5. This reaction yielded 45% of yellow/green sticky sticky foam. ^{1}H NMR (400 MHz, $CDCl_3$) δ 8.57-8.55 (d, *J* = 6.6 Hz, 1H), 8.52-8.49 (d, *J* = 8.5 Hz, 1H), 8.30-8.28 (d, *J* = 8.6 Hz, 1H), 8.18-8.16 (d, *J* = 7.3 Hz, 1H), 7.55-7.52 (br s, 1H), 7.53-7.45 (m, 2H), 7.25-7.20 (br s, 1H), 7.16-7.14 (d, *J* = 7.4 Hz, 1H), 7.08-7.06 (d, *J* = 6.7 Hz, 1H), 6.68-6.65 (m, 1H), 6.31-6.26 (dd, *J* = 16.9 Hz, 2.0 Hz, 1H), 6.24-6.17 (dd, *J* = 16.9 Hz, 9.6 Hz, 1H), 5.66-5.63 (dd, *J* = 9.6 Hz, 2.0 Hz, 1H), 4.65-4.58 (m, 1H), 4.46-4.40 (m, 1H), 3.86-3.78 (m, 1H), 3.72-3.63 (m, 1H), 3.43-3.33 (m, 1H), 3.25-3.16 (m, 1H), 3.08-3.01 (m, 1H), 2.86 (s, 6H), 2.87-2.80 (m, 1H), 2.10 (s, 3H), 1.43 (s, 9H), ^{13}C NMR (100 MHz, $CDCl_3$) δ 172.0, 171.3, 170.9, 170.7, 168.6, 151.9, 135.4, 130.4, 130.2, 130.0, 129.6, 129.1, 128.3, 127.8, 123.3, 119.2, 115.3, 82.3, 56.5, 51.1, 45.5, 42.8, 41.4, 39.9, 36.8, 28.2, 23.3; HRMS (ESI-QTOF) m/z [M + Na]$^{+}$ calcd for $C_{30}H_{42}N_6O_8S$ 669.2683; found 669.2661.

6.4.2 Inhibitor synthesis

6.4.2.1 Benzyl-(S)-(3-acrylamido-1-((2-((5-(dimethylamino)naphthalene)-1-sulfonamido) ethyl)amino)-1-oxopropan-2-yl)carbamate (**27**)

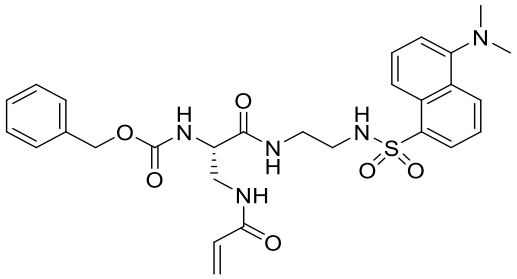

Compound **27** was prepared from Boc deprotected tert-butyl-(2-((5-(dimethylamino)naphthalene)-1-sulfonamido)ethyl)carbamate (**3.3**) and acrylamide (**5**) using general amide coupling procedure 6.1.1.7. Compound **3.3** was deprotected using general procedure 1.1.1.5. This reaction yielded 41 % of yellow/green solid. mp 51-53 ˚C; $_{1}$H NMR (400 MHz, $CDCl_3$) δ 8.52 – 8.49 (d, *J* = 8.5 Hz, 1H), 8.29 – 8.27 (d, *J* = 8.6 Hz, 1H), 8.17 – 8.15 (d, *J* = 7.3 Hz, 1H), 7.50 – 7.43 (m, 3H), 7.30 – 7.24 (m, 5H), 7.19 – 7.17 (m, 1H), 7.13 – 7.12 (d, *J* = 7.3 Hz, 1H), 6.71 (d, *J* = 6.6 Hz, 1H), 6.58 – 6.53 (m, 1H), 6.27 – 6.10 (m, 2H), 5.56 – 5.53 (d, *J* = 9.8 Hz, H), 5.07 – 5.02 (m, 2H), 4.36 – 4.32 (m, 1H), 3.71 – 3.68 (m, 2H), 3.35 – 3.20 (m, 2H), 3.02 – 2.94 (m, 2H), 2.85 (s, 6H), $_{13}$C NMR (100 MHz, $CDCl_3$) δ 171.3, 167.6, 156.8, 151.9, 136.2, 135.1, 130.5, 130.4, 130.0, 129.6, 129.2, 128.6, 128.4, 128.3, 128.2, 127.5, 123.3, 119.0, 115.4, 67.3, 56.3, 45.5, 42.6, 41.8, 39.9; HRMS (ESI-QTOF) m/z $[M + Na]^+$ calcd for $C_{28}H_{33}N_5O_6SNa$ 590.2049; found 590.2034.

6.4.2.2 Benzyl-(S)-(3-acrylamido-1-((3-((5-(dimethylamino)naphthalene)-1-sulfonamido) propyl)amino)-1-oxopropan-2-yl)carbamate (**26**)

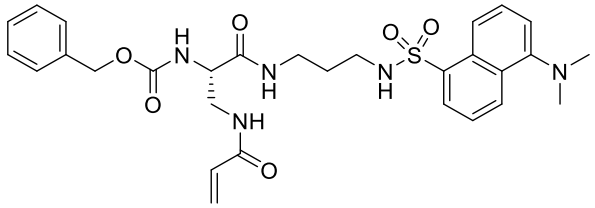

Compound **26** was prepared from N-(3-aminopropyl)-5-(dimethylamino)naphthalene-1-sulfonamide (**2**) and acrylamide (**5**) using general amide coupling procedure 6.1.1.7. This reaction yielded 45 % of yellow/green solid. mp 53-55 ˚C; ^{1}H NMR (400 MHz, $CDCl_3$) δ 8.51 – 8.48 (d, *J* = 8.5 Hz, 1H), 8.31 – 8.29 (d, *J* = 8.6 Hz, 1H), 8.19 – 8.16 (dd, *J* = 7.3, 1.1 Hz, 1H), 7.54 – 7.45 (m, 2H), 7.30 – 7.24 (m, 5H), 7.14 – 7.12 (d, *J* = 7.4 Hz, 1H), 7.09 – 7.05 (m, 1H), 6.93 – 6.89 (m, 1H), 6.86 – 6.82 (m, 1H), 6.42 – 6.38 (t, *J* = 6.5 Hz, 1H), 6.20 – 6.15 (dd, *J* = 16.9, 1.2 Hz, 1H), 6.00 – 5.93 (dd, *J* = 16.9, 10.2 Hz, 1H), 5.54 – 5.51 (d, *J* = 10.2 Hz, 1H), 5.07 – 4.99 (m, 2H), 4.33 – 4.27 (m, 1H), 3.70 – 3.55 (m, 2H), 3.30 – 3.16 (m, 2H), 2.87 – 2.79 (m, 8H), 1.58 – 1.48 (m, 2H), ^{13}C NMR (100 MHz, $CDCl_3$) δ 171.0, 167.6, 156.8, 151.9, 136.0, 135.1, 130.3, 130.0, 129.8, 129.5, 129.3, 128.5, 128.3, 128.2, 128.1, 127.5, 123.3, 119.1, 115.3, 67.2, 56.6, 45.4, 42.1, 40.1, 36.5, 29.6; HRMS (ESI-QTOF) m/z $[M + Na]^+$ calcd for $C_{29}H_{35}N_5O_6SNa$ 604.2206; found 604.2212.

6.4.2.3 Benzyl-(S)-(3-acrylamido-1-((4-((5-(dimethylamino)naphthalene)-1-sulfonamido) butyl)amino)-1-oxopropan-2-yl)carbamate (**25**)

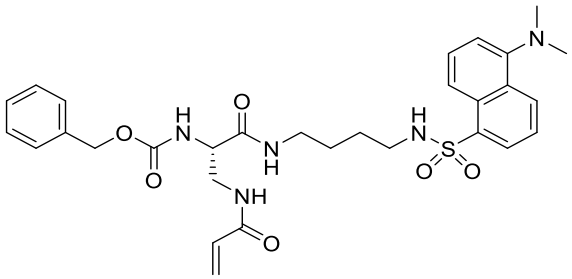

Compound **25** was prepared from *N-(4-aminobutyl)-5-(dimethylamino)naphthalene-1-sulfonamide* (**1**) and acrylamide (**5**) using general amide coupling procedure 6.1.1.7. This reaction yielded 42 % of yellow/green oil. ^{1}H NMR (400 MHz, $CDCl_3$) δ 8.53 – 8.51 (d, *J* = 8.5 Hz, 1H), 8.33 – 8.31 (d, *J* = 8.6 Hz, 1H), 8.19 – 8.16 (dd, *J* = 7.3, 1.1 Hz, 1H), 7.53 – 7.48 (m, 2H), 7.34 – 7.27 (m, 5H), 7.16 – 7.14 (d, *J* = 7.4 Hz, 1H), 7.01 – 6.91 (m, 2H), 6.81 – 6.75 (m, 1H), 6.28 – 6.23 (dd, *J* = 16.9, 1.0 Hz, 1H), 6.15 – 6.08 (dd, *J* = 16.8, 10.2 Hz, 1H), 5.82 – 5.78 (m, 1H), 5.62 – 5.59 (d, *J* = 10.2 Hz, 1H), 5.09 (s, 2H), 4.33 – 4.28 (m, 1H), 3.78 – 3.71 (m, 1H), 3.66 – 3.57 (m, 1H), 3.19 – 3.08 (m, 2H), 2.87 (s, 6H), 2.86 – 2.81 (m, 2H), 1.44 – 1.38 (m, 4H), ^{13}C NMR (100 MHz, $CDCl_3$) δ 170.5, 167.8, 157.1, 152.1, 136.2, 135.0, 130.5, 130.3, 130.1, 129.8, 129.7, 128.7, 128.5, 128.4, 128.3, 127.7, 123.4, 119.1, 115.4, 67.4, 56.8, 45.6, 42.9, 38.8, 26.7, 26.6; HRMS (ESI-QTOF) m/z $[M + Na]^+$ calcd for $C_{30}H_{37}N_5O_6SNa$ 618.2362; found 618.2369.

6.4.2.4 Benzyl(S)-(3-acrylamido-1-((2-(naphthalene-1-sulfonamido)ethyl)amino)-1-oxopropan-2-yl)carbamate (**28**)

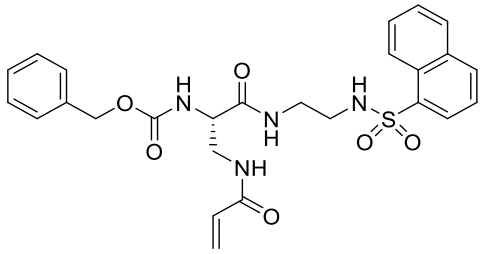

Compound **28** was prepared from Boc deprotected tert-butyl (2-(naphthalene-1-sulfonamido)ethyl)carbamate (**3.2**) and acrylamide (**5**) using general amide coupling procedure 6.1.1.7. Compound **3.2** was deprotected using general procedure 6.1.1.5. This reaction yielded 52 % of white solid. mp 84-87 ˚C; ^{1}H NMR (400 MHz, $(CD_3)_2SO$) δ 8.69-8.66 (d, *J* = 8.6 Hz, 1H), 8.25-8.22 (d, *J* = 8.3 Hz, 1H), 8.18-8.12 (m, 2H), 8.12-8.02 (m, 3H), 7.76-7.64 (m, 3H), 7.37-7.27 (m, 5H), 7.24-7.18 (br s, 1H), 6.22-6.15 (dd, *J* = 17.1, 10.0 Hz, 1H), 6.07-6.03 (dd, *J* = 17.1, 1.9 Hz, 1H), 5.57-5.53 (dd, *J* = 10.1, 1.9 Hz, 1H), 5.08-4.98 (m, 2H), 4.11-4.04 (m, 1H), 3.44-3.38 (m, 2H), 3.17-3.02 (m, 2H), 2.88-2.76 (m, 2H), ^{13}C NMR (100 MHz, $(CD_3)_2SO$) δ 169.9, 165.3, 155.7, 136.8, 135.4, 133.9, 133.7, 131.4, 128.9, 128.4, 128.3, 127.8, 127.7, 127.6, 127.5, 126.8, 125.4, 124.6, 124.5, 79.1, 65.6, 54.9, 41.5, 40.5, 38.7; HRMS (ESI-QTOF) m/z $[M + Na]^+$ calcd for $C_{26}H_{28}N_4O_6SNa$ 547.1627; found 547.1626.

6.4.2.5 Benzyl-(S)-(1-((2-(1-naphthamido)ethyl)amino)-3-acrylamido-1-oxopropan-2-yl)carbamate (**29**)

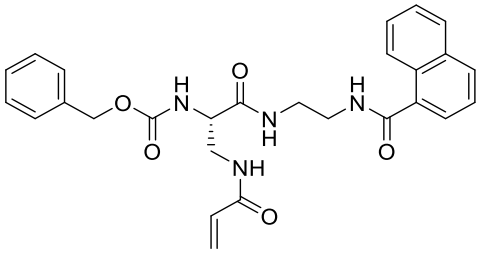

Compound **29** was prepared from Boc deprotected tert-butyl (2-(1-naphthamido)ethyl)carbamate (**3.1**) and acrylamide (**5**) using general amide coupling procedure 6.1.1.7. Compound **3.1** was deprotected using general procedure 6.1.1.5. This reaction yielded 51 % of white solid. mp 71-74 ˚C; $_{1}$H NMR (400 MHz, $(CD_3)_2SO$) δ 8.49-8.44 (m, 1H), 8.24-8.13 (m, 3H), 8.02-7.95 (m, 2H), 7.67-7.63 (m, 1H), 7.58-7.50 (m, 3H), 7.37-7.28 (m, 6H), 6.22-6.15 (dd, *J* = 17.0, 10.1 Hz, 1H), 6.07-6.02 (dd, *J* = 17.1, 2.2 Hz, 1H), 5.55-5.52 (dd, *J* = 10.1, 2.2 Hz, 1H), 5.05-4.94 (m, 2H), 4.15-4.09 (m, 1H), 3.47-3.35 (m, 4H), 3.31-3.24 (m, 2H), $_{13}$C NMR (100 MHz, $(CD_3)_2SO$) δ 169.9, 168.6, 165.2, 155.6, 136.7, 134.6, 132.9, 131.3, 129.7, 129.6, 128.2, 127.9, 127.6, 127.5, 126.5, 126.0, 125.4, 125.3, 125.1, 124.8, 65.4, 54.9, 40.5, 38.5; HRMS (ESI-QTOF) m/z [M + Na]$^+$ calcd for $C_{27}H_{28}N_4O_5Na$ 511.1957; found 511.1965.

6.4.2.6 5-(N-(2-((S)-2-((S)-2-acetamido-3-carboxypropanamido)-3-acrylamidopropanamido) ethyl) sulfamoyl)-N,N-dimethylnaphthalen-1-aminium (**30**)

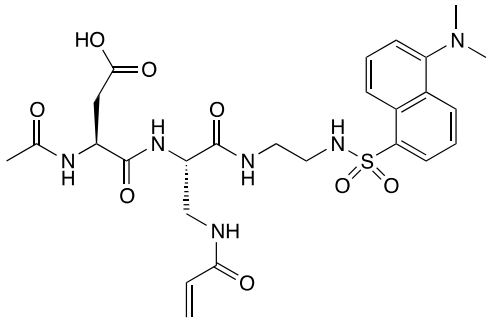

Compound **30** was prepared by deprotecting the tertbutyl ester of compound **30.4** using a solution of 5% v/v of TFA in $CHCl_3$. Reaction was complete in 3 hours and verified by TLC. The $CHCl_3$ was removed under reduced pressure. A 40:60 solution of acetone:hexane was added to product and solution was sonicated, then solvents removed under reduced pressure (this was repeated 3 times). One equivalence of HCl was added using an aqueous 1 M HCl solution. Product was dried under reduced pressure to afford a yellow/green sticky foam with a yield of 64%. ^{1}H NMR (400 MHz, CD_3OD) δ 8.63-8.61 (d, *J* = 7.3 Hz, 1H), 8.52-8.50 (d, *J* = 8.7 Hz, 1H), 8.28-8.26 (d, *J* = 7.3 Hz, 1H), 7.77-7.67 (m, 3H), 6.23-6.20 (m, 2H), 5.68-5.62 (m, 1H), 4.61-4.54 (m, 1H), 4.31-4.25 (m, 1H), 3.76-3.66 (m, 1H), 3.51-3.41 (m, 1H), 3.32-3.29 (m, 1H), 3.24-3.16 (m, 2H), 3.20 (s, 6H), 3.02-2.94 (m, 2H), 2.88-2.71 (m, 2H), 2.03 (s, 3H), ^{13}C NMR (100 MHz, CD_3OD) δ 174.4, 174.3, 173.7, 171.9, 169.3, 146.9, 146.8, 137.9, 131.8, 130.8, 129.3, 129.1, 128.8, 127.6, 126.4, 124.8, 118.7, 56.0, 52.1, 46.9, 43.0, 41.7, 40.7, 36.3, 22.8; HRMS (ESI-QTOF) m/z $[M + H]^+$ calcd for $C_{26}H_{35}N_6O_8S^+$ 591.2232; found 591.2301.

6.4.3 Inhibition kinetics – Ki mathematics

Experimentally, the K_i will be determined by taking the negative x-intercept of our normalized Dixon plot, which associates the initial rate of enzymatic activity (v_0) over initial rate with inhibitor (v_i) with the concentration of inhibitor corrected for substrate competition ([I]/α). Mathematically, the K_i value can be isolated from the linear equation of a Dixon plot, which is written as follows:

$$\frac{v_0}{v_i} = \frac{K_M}{V_{max}[S]K_i}[I] + \frac{K_M + [S]}{V_{max}[S]}$$

Using the value of the plot's slope and the y-intercept (which equals 1, since it is the ratio of v_0/v_i in the absence of inhibitor), we can find the negative value of the x-intercept. The manipulation is as follows:

$$x - intercept = \frac{-\frac{K_M + [S]}{V_{max}[S]}}{\frac{K_M}{V_{max}[S]K_i}}$$

With further algebraic manipulation, we obtain the following:

$$x - intercept = -K_i(1 + \frac{[S]}{K_M}) = -K_i\alpha$$

The error on each individual IC_{50} value, determined by a triplicate experiment, is taken by propagating the errors from the linear regression, namely S_b and S_m as obtained from the Microsoft Excel LINEST function.

$$\delta K_i\alpha = K_i\alpha \times \sqrt{(\frac{S_b}{b})^2 + (\frac{S_m}{m})^2}$$

6.4.4 Enzyme activity assays (in vitro) for determining K_i

6.4.4.1 Colorimetric transamidase activity assay

The activity of hTG2 was measured via our colorimetric assay using the chromogenic substrate Cbz-Glu(γ-p-nitrophenyl ester)Gly (**AL5**)[167]. The assay was conducted in the same buffer conditions as reported in section 6.3.1.1. The hTG2 inhibition assay was run in the presence of 112 μM substrate (**AL5**) taken from a stock solution prepared in DMSO such that the final concentration of this co-solvent was constant at 2.5% v/v. Stock solutions of the inhibitors were made using assay buffer solution. The reaction was initiated with the addition of 40−60 mU/mL of hTG2 (0.25 μM). Product formation was monitored at 405 nm in a polystyrene 96-well microplate using a BioTek Synergy 4 plate reader. Initial slopes were measured for the enzymatic reaction in the presence and absence of inhibitors studied. Initial slopes were fit over a three-minute range. This range was verified to be linear after doing the fitting, to ensure that initial rates were being measured accurately. A range of 3 concentrations of inhibitor, along with one positive control (no inhibitor) were recorded in triplicate in order to generate our normalized Dixon plot and extrapolate a K_i value. Experiments were done in triplicate, and error between repeats was less than 30%.

6.4.4.2 Fluorescence isopeptidase activity assay

The isopeptidase activity of hFXIIIa (recombinant protein purchased from Zedira) was measured via a fluorescence-based assay[43,162] using the commercially available peptidic FRET quenched probe **A101** from Zedira. The assay was conducted in the same buffer conditions as reported in section 6.3.1.2. The reaction was monitored at 25 °C using a BioTek Synergy 4 plate reader (Ex/Em: 318/413 nm). The hFXIIIa inhibition assay was run in the presence of 50 μM substrate (**A101**) taken from a stock solution prepared in DMSO such that the final concentration of this co-solvent was constant at 2.5% v/v. Stock solutions of the inhibitors were made using assay buffer solution. The reaction was initiated with the addition of hFXIIIa (0.11 μM). Initial slopes were measured for the enzymatic reaction in the presence and absence of inhibitors studied. Initial slopes were fit over a three-minute range. This range was verified to be linear after doing the fitting, to ensure that initial rates were being measured accurately. A range of 3 concentrations of inhibitor, along with one positive control (no inhibitor) were recorded in triplicate in order to generate our normalized Dixon plot and extrapolate a K_i value. Experiments were done in triplicate, and error between repeats was less than 30%.

References

(1) Hughes, J. P.; Rees, S. S.; Kalindjian, S. B.; Philpott, K. L. Principles of Early Drug Discovery. *Br. J. Pharmacol.* **2011**, *162* (6), 1239–1249.

(2) Bertram, L.; Tanzi, R. E. Thirty Years of Alzheimer's Disease Genetics: The Implications of Systematic Meta-Analyses. *Nat. Rev. Neurosci.* **2008**, *9* (10), 768–778.

(3) Mikami, T.; Aoki, M.; Kimura, T. The Application of Mass Spectrometry to Proteomics and Metabolomics in Biomarker Discovery and Drug Development. *Curr. Mol. Pharmacol.* **2012**, *5* (2), 301–316.

(4) Creighton, C. J.; Fu, X.; Hennessy, B. T.; Casa, A. J.; Zhang, Y.; Gonzalez-Angulo, A. M.; Lluch, A.; Gray, J. W.; Brown, P. H.; Hilsenbeck, S. G.; et al. Proteomic and Transcriptomic Profiling Reveals a Link between the PI3K Pathway and Lower Estrogen-Receptor (ER) Levels and Activity in ER+ Breast Cancer. *Breast Cancer Res.* **2010**, *12* (3).

(5) Arsenault, R.; Griebel, P.; Napper, S. Peptide Arrays for Kinome Analysis: New Opportunities and Remaining Challenges. *Proteomics* **2011**, *11* (24), 4595–4609.

(6) Kurosawa, G.; Akahori, Y.; Morita, M.; Sumitomo, M.; Sato, N.; Muramatsu, C.; Eguchi, K. Comprehensive Screening for Antigens Overexpressed on Carcinomas via Isolation of Human MAbs That May Be Therapeutic. *Proc. Natl. Acad. Sci.* **2008**, *105* (20).

(7) Fleming, A. On the Antibacterial Action of Cultures of a Penicillium with Special Reference to Their Use in the Isolation of B. Influenzae. *Br. J. Exp. Pathol.* **1929**, *10* (3), 3–13.

(8) Chain, E.; Florey, H. W.; Gardner, A. D.; Heatley, N. G.; Jennings, M. A.; Orr-Ewing, J.; Sanders, A. G. Penicillin as a Chemotherapeutic Agent. *Lancet* **1940**, *236* (6104), 226–

228.

(9) Beutler, J. A. Natural Products as a Foundation for Drug Discovery. *Curr. Protoc. Pharmacol.* **2009**, *46* (9), 1–30.

(10) Markowicz, M.; Mikiciuk-olasik, E.; Symanski, P. Adaptation of High-Throughput Screening in Drug Discovery — Toxicological Screening Tests. *Int. J. Mol. Sci.* **2012**, *13* (1), 427–452.

(11) Hajduk, P. J.; Greer, J. A Decade of Fragment-Based Drug Design: Strategic Advances and Lessons Learned. *Nat. Rev. Drug Discov.* **2007**, *6* (3), 211–219.

(12) Zheng, W.; Thorne, N.; Mckew, J. C. Phenotypic Screens as a Renewed Approach for Drug Discovery. *Drug Discov. Today* **2013**, *18* (0), 1067–1073.

(13) Anderson, A. C. The Process of Structure-Based Drug Design. *Chem. Biol.* **2003**, *10* (9), 787–797.

(14) Keillor, J. W.; Clouthier, C. M.; Apperley, K. Y. P.; Akbar, A.; Mulani, A. Bioorganic Chemistry Acyl Transfer Mechanisms of Tissue Transglutaminase. *Bioorg. Chem.* **2014**, *57*, 186–197.

(15) Eckert, R. L.; Broome, A.; Ruse, M.; Rorke, E. A. Transglutaminase Function in Epidermis. *J. Invest. Dermatol.* **2005**, *124* (3), 481–492.

(16) Pinkas, D. M.; Strop, P.; Brunger, A. T.; Khosla, C. Transglutaminase 2 Undergoes a Large Conformational Change upon Activation. *PLOS Biol.* **2007**, *5* (12), 2788–2796.

(17) Khosla, C.; Klock, C. Regulation of the Activities of the Mammalian Transglutaminase Family of Enzymes. *Protein Sci.* **2012**, *21* (12), 1781–1791.

(18) Keillor, J. W.; Apperley, K. Y. P.; Akbar, A. Inhibitors of Tissue Transglutaminase. *Trends Pharmacol. Sci.* **2015**, *36* (1), 32–40.

(19) Liu, S.; Cerione, R. A.; Clardy, J. Structural Basis for the Guanine Nucleotide-Binding Activity of Tissue Transglutaminase and Its Regulation of Transamidation Activity. *Proc. Natl. Acad. Sci. U.S.A.* **2002**, *99* (5), 2743–2747.

(20) Stamnaes, J.; Pinkas, D. M.; Fleckenstein, B.; Khosla, C.; Sollid, L. M. Redox Regulation of Transglutaminase 2 Activity. *J. Biol. Chem.* **2010**, *285* (33), 25402–25409.

(21) Jin, X.; Stamnaes, J.; Klo, C.; Diraimondo, T. R.; Sollid, L. M.; Khosla, C. Activation of Extracellular Transglutaminase 2 by Thioredoxin. *J. Biol. Chem.* **2011**, *286* (43), 37866–37873.

(22) Kim, H. C.; Lewis, M. S.; Gorman, J. J.; Park, S. C.; Girard, J. E.; Folk, J. E.; Chung, S. Il. Protransglutaminase E from Guinea Pig Skin. *J. Biol. Chem.* **1990**, *265* (35), 21971–21978.

(23) Hitomi, K.; Kanehiro, S.; Ikura, K.; Maki, M. Characterization of Recombinant Mouse Epidermal-Type Transglutaminase (TGase 3): Regulation of Its Activity by Proteolysis and Guanine Nucleotides. *J. Biochem.* **1999**, *125* (6), 1048–1054.

(24) Jiang, W. G.; Ye, L.; Sanders, A. J.; Ruge, F.; Kynaston, H. G.; Ablin, R. J.; Mason, M. D. Prostate Transglutaminase (TGase-4 , TGaseP) Enhances the Adhesion of Prostate Cancer Cells to Extracellular Matrix, the Potential Role of TGase-Core Domain. *J. Transl. Med.* **2013**, *269* (11), 1–12.

(25) Dean, M. D. Genetic Disruption of the Copulatory Plug in Mice Leads to Severely Reduced Fertility. *PLOS Genet.* **2013**, *9* (1), 1–7.

(26) Aeschlimann, D.; Paulsson, M. Transglutaminases: Protein Cross-Linking Enzymes in Tissues and Body Fluids. *Thromb. Haemost.* **1994**, *71* (4), 402–415.

(27) Candi, E.; Paradisi, A.; Terrinoni, A.; Pietroni, V.; Oddi, S.; Cadot, B.; Jogini, V.;

Meiyappan, M.; Clardy, J.; Finazzi-agro, A.; et al. Transglutaminase 5 Is Regulated by Guanine – Adenine Nucleotides. *Biochem. J.* **2004**, *381* (4), 313–319.

(28) Cadot, B.; Rufini, A.; Pietroni, V.; Ramadan, S.; Guerrieri, P.; Melino, G.; Candi, E. Overexpressed Transglutaminase 5 Triggers Cell Death. *Amino Acids* **2004**, *26* (4), 405–408.

(29) Pigors, M.; Kiritsi, D.; Cobzaru, C.; Schwieger-briel, A.; Suarez, J.; Faletra, F.; Aho, H.; Makela, L.; Kern, J. S.; Bruckner-Tuderma, L.; et al. TGM5 Mutations Impact Epidermal Differentiation in Acral Peeling Skin Syndrome. *J. Invest. Dermatol.* **2012**, *132* (5), 2422–2439.

(30) Grenard, P.; Bates, M. K.; Aeschlimann, D. Evolution of Transglutaminase Genes : Identification of a Transglutaminase Gene Cluster on Human Chromosome 15q15. *J. Biol. Chem.* **2001**, *276* (35), 33066–33078.

(31) Thomas, H.; Beck, K.; Adamczyk, M.; Aeschlimann, P.; Langley, M.; Oita, R. C.; Thiebach, L.; Hils, M.; Aeschlimann, D. Transglutaminase 6 : A Protein Associated with Central Nervous System Development and Motor Function. *Amino Acids* **2013**, *44* (1), 161–177.

(32) Liu, Y.; Tang, B.; Lan, W. E. I.; Song, N.; Huang, Y.; Zhang, L.; Guan, W.; Shi, Y.; Ding, Y.; Wang, J. Distribution of Transglutaminase 6 in the Central Nervous System of Adult Mice. *Anat. Rec.* **2013**, *296* (10), 1576–1587.

(33) Kuramoto, K.; Yamasaki, R.; Shimizu, Y.; Tatsukawa, H.; Hitomi, K. Phage-Displayed Peptide Library Screening for Preferred Human Substrate Peptide Sequences for Transglutaminase 7. *Arch. Biochem. Biophys.* **2013**, *537* (1), 138–143.

(34) Muszbek, L.; Yee, V. C.; Hevessy, Z. Blood Coagulation Factor XIII : Structure and

Function. *Thromb. Res.* **1999**, *94* (5), 271–305.

(35) Muszbek, L.; Bereczky, Z.; Bagoly, Z.; Komaromi, I.; Katona, E. Factor XIII: A Coagulation Factor with Multiple Plasmatic and Cellular Functions. *Physiol. Rev.* **2011**, *91* (3), 931–972.

(36) Korsgren, C.; Lawlert, J.; Lambert, S.; Speichert, D.; Cohen, C. M. Complete Amino Acid Sequence and Homologies of Human Erythrocyte Membrane Protein Band 4 . 2. *Proc. Natl. Acad. Sci. U. S. A.* **1990**, *87* (2), 613–617.

(37) Eckert, R. L.; Kaartinen, M. T.; Nurminskaya, M.; Belkin, A. M.; Colak, G.; Johnson, G. V. W.; Mehta, K. Transglutaminase Regulation of Cell Function. *Physiol. Rev.* **2019**, *94* (2), 383–417.

(38) Peters, L. L.; Jindel, H. K.; Gwynn, B.; Korsgren, C.; John, K. M.; Lux, S. E.; Mohandas, N.; Cohen, C. M.; Cho, M. R.; Golan, D. E.; et al. Mild Spherocytosis and Altered Red Cell Ion Transport in Protein 4.2–Null Mice. *J. Clin. Invest.* **1999**, *103* (11), 1527–1537.

(39) Leblanc, A.; Gravel, C.; Labelle, J.; Keillor, J. W. Kinetic Studies of Guinea Pig Liver Transglutaminase Reveal a General-Base-Catalyzed Deacylation Mechanism. *Biochemistry* **2001**, *40* (28), 8335–8342.

(40) Cabras, T.; Inzitari, R.; Fanali, C.; Scarano, E.; Patamia, M.; Sanna, M. T.; Pisano, E.; Giardina, B.; Castagnola, M.; Messana, I. HPLC – MS Characterization of Cyclo-Statherin Q-37, a Specific Cyclization Product of Human Salivary Statherin Generated by Transglutaminase 2. *J. Seperation Sci.* **2006**, *29* (17), 2600–2608.

(41) Gross, M.; Whetzel, N. K.; Folk, J. E. Amine Binding Sites in Acyl Intermediates Transglutaminases. *J. Biol. Chem.* **1977**, *252* (11), 3752–3759.

(42) Parameswaran, K. N.; Lorand, L. New Thioester Substrates for Fibrinoligase (Coagulation

Factor XIIIa) and for Transglutaminase. Transfer of the Fluorescently Labeled Acyl Group to Amines and Alcohols. *Biochemistry* **1981**, *20* (13), 3703–3711.

(43) Kiraly, R.; Nemes, Z.; Fesüs, L.; Griffin, M.; Thangaraju, K.; Collighan, R.; Nagy, Z. Isopeptidase Activity of Human Transglutaminase 2: Disconnection from Transamidation and Characterization by Kinetic Parameters. *Amino Acids* **2015**, *48* (1), 31–40.

(44) Folk, J. E.; Cole, P. W. Structural Requirements of Specific Substrates for Guinea Pig Liver Transglutaminase. *J. Biol. Chem.* **1965**, *240* (7), 2951–2960.

(45) Chica, R. A.; Gagnon, P.; Keillor, J. W.; Pelletier, J. N. Tissue Transglutaminase Acylation: Proposed Role of Conserved Active Site Tyr and Trp Residues Revealed by Molecular Modeling of Peptide Substrate Binding. *Protein Sci.* **2004**, *13* (4), 979–991.

(46) Lai, T.-S.; Slaughter, T. F.; Peoples, K. A.; Hettasch, J. M.; Greenberg, C. S. Regulation of Human Tissue Transglutaminase Function by Magnesium-Nucleotide Complexes. *J. Biol. Chem.* **1998**, *273* (3), 1776–1781.

(47) Kiraly, R.; Csosz, E.; Kurtan, T.; Antus, S.; Szigeti, K.; Simon-Vecsei, Z.; Korponay-Szabo, I. R.; Keresztessy, Z.; Fesus, L. Functional Significance of Five Noncanonical Ca2+ -Binding Sites of Human Transglutaminase 2 Characterized by Site-Directed Mutagenesis. *FEBS J.* **2009**, *276* (23), 7083–7096.

(48) Begg, G. E.; Holman, S. R.; Stokes, P. H.; Matthews, J. M.; Graham, R. M.; Iismaa, S. E. Mutation of a Critical Arginine in the GTP-Binding Site of Transglutaminase 2 Disinhibits Intracellular Cross-Linking Activity. *J. Biol. Chem.* **2010**, *281* (18), 12603–12609.

(49) Nakaoka, H.; Perez, D. M.; Baek, K. J.; Das, T.; Husain, A.; Misono, K.; Im, M. J.; Graham, R. M. Gh: A GTP-Binding Protein with Transglutaminase Activity and Receptor Signaling Function. *Science (80-.).* **1994**, *264* (5165), 1593–1596.

(50) Mariani, P.; Carsughi, F.; Spinozzi, F.; Romanzetti, S.; Meier, G.; Casadio, R.; Bergamini, C. M. Ligand-Induced Conformational Changes in Tissue Transglutaminase : Monte Carlo Analysis of Small-Angle Scattering Data. *Biophys. J.* **2000**, *78* (6), 3240–3251.

(51) Caron, N. S.; Munsie, L. N.; Keillor, J. W.; Truant, R. Using FLIM-FRET to Measure Conformational Changes of Transglutaminase Type 2 in Live Cells. *PLoS One* **2012**, *7* (8), e44159–e44159.

(52) Clouthier, C. M.; Mironov, G. G.; Okhonin, V.; Berezovski, M. V; Keillor, J. W. Real-Time Monitoring of Protein Conformational Dynamics in Solution Using Kinetic Capillary Electrophoresis. *Angew. Chem. Int. Ed. Engl.* **2012**, *51* (50), 12464–12468.

(53) Pavlyukov, M. S.; Antipova, N. V; Balashova, M. V; Shakhparonov, M. I. Detection of Transglutaminase 2 Conformational Changes in Living Cell. *Biochem. Biophys. Res. Commun.* **2012**, *421* (4), 773–779.

(54) Sarkar, N. K.; Clarke, D. D.; Waelsch, H. An Enzymically Catalyzed Incorporation of Amines into Proteins. *Biochim. Biophys. Acta* **1957**, *25* (2), 451–452.

(55) Akimov, S. S.; Belkin, A. M. Cell Surface Tissue Transglutaminase Is Involved in Adhesion and Migration of Monocytic Cells on Fibronectin. *Blood* **2001**, *98* (5), 1567–1577.

(56) Akimov, S. S.; Krylov, D.; Fleischman, L. F.; Belkin, A. M. Tissue Transglutaminase Is an Integrin-Binding Adhesion Coreceptor for Fibronectin. *J. Cell Biol.* **2000**, *148* (4), 825–838.

(57) Walther, D. J.; Stahlberg, S.; Vowinckel, J. Novel Roles for Biogenic Monoamines : From Monoamines in Transglutaminase-Mediated Post-Translational Protein Modification to Monoaminylation Deregulation Diseases. *FEBS J.* **2011**, *278* (24), 4740–4755.

(58) Boroughs, L. K.; Antonyak, M. A.; Cerione, R. A. A Novel Mechanism by Which Tissue Transglutaminase Activates Signaling Events That Promote Cell Survival. *J. Biol. Chem.* **2014**, *289* (14), 10115–10125.

(59) Begg, G. E.; Carrington, L.; Stokes, P. H.; Matthews, J. M.; Wouters, M. A.; Husain, A.; Lorand, L.; Iismaa, S. E.; Graham, R. M. Mechanism of Allosteric Regulation of Transglutaminase 2 by GTP. *Proc. Natl. Acad. Sci. U.S.A.* **2006**, *103* (52), 19683–19688.

(60) Gundemir, S.; Monteagudo, A.; Akbar, A.; Keillor, J. W.; Johnson, G. V. W. The Complex Role of Transglutaminase 2 in Glioblastoma Proliferation. *Neuro. Oncol.* **2017**, *19* (2), 208–218.

(61) Hoffner, G.; Andre, W.; Vanhoutteghem, A.; Soues, S.; Djian, P. Transglutaminase-Catalyzed Crosslinking in Neurological Disease: From Experimental Evidence to Therapeutic Inhibition. *CNS Neurol. Disord. - Drug Targets* **2010**, *9* (2), 217–231.

(62) Bernassola, F.; Federici, M.; Corazzari, M.; Terrinoni, A.; Hribal, M. L.; De Laurenzi, V.; Ranalli, M.; Massa, O.; Sesti, G.; Irwin McLean, W. H.; et al. Role of Transglutaminase 2 in Glucose Tolerance: Knockout Mice Studies and a Putative Mutation in a MODY Patient. *FASEB J.* **2002**, *16* (11), 1371–1378.

(63) Scarpellini, A.; Huang, L.; Burhan, I.; Schroeder, N.; Funck, M.; Johnson, T. S.; Verderio, E. A. M. Syndecan-4 Knockout Leads to Reduced Extracellular Transglutaminase-2 and Protects against Tubulointerstitial Fibrosis. *J. Am. Soc. Nephrol.* **2014**, *25* (5), 1013–1027.

(64) Olsen, K. C.; Sapinoro, R. E.; Kottmann, R. M.; Kulkarni, A. A.; Iismaa, S. E.; Johnson, G. V. W.; Thatcher, T. H.; Phipps, R. P.; Sime, P. J. Transglutaminase 2 and Its Role in Pulmonary Fibrosis. *Am. J. Respir. Crit. Care Med.* **2011**, *184* (6), 699–707.

(65) Sollid, L. M. Molecular Basis of Celiac Disease. *Annu. Rev. Immunol.* **2000**, *18*, 53–81.

(66) Huang, L.; Xu, A. M.; Liu, W. Transglutaminase 2 in Cancer. *Am. J. Cancer Res.* **2015**, *5* (9), 2756–2776.

(67) Xia, J.; Siegel, M.; Bergseng, E.; Sollid, L. M.; Khosla, C. Inhibition of HLA-DQ2-Mediated Antigen Presentation by Analogues of a High Affinity 33-Residue Peptide from A2-Gliadin. *J. Am. Chem. Soc.* **2006**, *128* (6), 1859–1867.

(68) Dieterich, W.; Ehnis, T.; Bauer, M.; Donner, P.; Volta, U.; Riecken, E. O.; Schuppan, D. Identification of Tissue Transglutaminase as the Autoantigen of Celiac Disease. *Nat. Med.* **1997**, *3* (7), 797–801.

(69) Korponay-Szabo, I. R.; Halttunen, T.; Szalai, Z.; Laurila, K.; Kiraly, R.; Kovacs, J. B.; Fesus, L.; Maki, M. In Vivo Targeting of Intestinal and Extraintestinal Transglutaminase 2 by Coeliac Autoantibodies. *Gut* **2004**, *53* (5), 641–648.

(70) Sardy, M.; Odenthal, U.; Karpati, S.; Paulsson, M.; Smyth, N. Recombinant Human Tissue Transglutaminase ELISA for the Diagnosis of Gluten-Sensitive Enteropathy. *Clin. Chem.* **1999**, *45* (12), 2142–2149.

(71) Wynn, T. Cellular and Molecular Mechanisms of Renal Fibrosis. *Nat. Rev. Nephrol.* **2011**, *7* (12), 684–696.

(72) Shweke, N.; Boulos, N.; Jouanneau, C.; Vandermeersch, S.; Melino, G.; Dussaule, J. C.; Chatziantoniou, C.; Ronco, P.; Boffa, J. J. Tissue Transglutaminase Contributes to Interstitial Renal Fibrosis by Favoring Accumulation of Fibrillar Collagen through TGF-β Activation and Cell Infiltration. *Am. J. Pathol.* **2008**, *173* (3), 631–642.

(73) Huang, L.; Haylor, J. L.; Hau, Z.; Jones, R. A.; Vickers, M. E.; Wagner, B.; Griffin, M.; Saint, R. E.; Coutts, I. G. C.; El Nahas, A. M.; et al. Transglutaminase Inhibition Ameliorates Experimental Diabetic Nephropathy. *Kidney Int.* **2009**, *76* (4), 383–394.

(74) Daneshpour, N.; Griffin, M.; Collighan, R.; Perrie, Y. Targeted Delivery of a Novel Group of Site-Directed Transglutaminase Inhibitors to the Liver Using Liposomes: A New Approach for the Potential Treatment of Liver Fibrosis. *J. Drug Target.* **2011**, *19* (8), 624–631.

(75) Dvorak, H. F. Tumors: Wounds That Do Not Heal. *N. Engl. J. Med.* **1986**, *315* (26), 280–284.

(76) Li, H.; Fan, X.; Houghton, J. M. Tumor Microenvironment: The Role of the Tumor Stroma in Cancer. *J. Cell. Biochem.* **2007**, *101* (4), 805–815.

(77) Bussard, K. M.; Mutkus, L.; Stumpf, K.; Gomez-Manzano, C.; Marini, F. C. Tumor-Associated Stromal Cells as Key Contributors to the Tumor Microenvironment. *Breast Cancer Res.* **2016**, *18* (84), 1–11.

(78) Fisher, M. L.; Keillor, J. W.; Xu, W.; Eckert, R. L.; Kerr, C. Transglutaminase Is Required for Epidermal Squamous Cell Carcinoma Stem Cell Survival. *Mol. Cancer Res.* **2016**, *13* (7), 1083–1094.

(79) Assi, J.; Srivastava, G.; Matta, A.; Chang, M. C.; Walfish, P. G.; Ralhan, R. Transglutaminase 2 Overexpression in Tumor Stroma Identifies Invasive Ductal Carcinomas of Breast at High Risk of Recurrence. *PLoS One* **2013**, *8* (9), e74437.

(80) Mehta, K.; Fok, J.; Miller, F. R.; Koul, D.; Sahin, A. A. Prognostic Significance of Tissue Transglutaminase in Drug Resistant and Metastatic Breast Cancer. *Clin. Cancer Res.* **2004**, *10* (23), 8068–8076.

(81) Yuan, L.; Siegel, M.; Choi, K.; Khosla, C.; Miller, C. R.; Jackson, E. N.; Piwnica-Worms, D.; Rich, K. M. Transglutaminase 2 Inhibitor, KCC009, Disrupts Fibronectin Assembly in the Extracellular Matrix and Sensitizes Orthotopic Glioblastomas to Chemotherapy.

Oncogene **2007**, *26* (18), 2563–2573.

(82) Dyer, L. M.; Schooler, K. P.; Ai, L.; Klop, C.; Qiu, J.; Robertson, K. D.; Brown, K. D. The Transglutaminase 2 Gene Is Aberrantly Hypermethylated in Glioma. *J. Neurooncol.* **2011**, *101* (3), 429–440.

(83) Eckert, R. L.; Kerr, C.; Fisher, M. L.; Boucher, S.; Hornyak, T.; Adhikary, G.; Bickenbach, J. R.; Rorke, E. A.; Vemuri, M.; Xu, W.; et al. Identification of a Population of Epidermal Squamous Cell Carcinoma Cells with Enhanced Potential for Tumor Formation. *PLoS One* **2013**, *8* (12), e84324.

(84) Eckert, R. L.; Fisher, M. L.; Grun, D.; Adhikary, G.; Xu, W.; Kerr, C. Transglutaminase Is a Tumor Cell and Cancer Stem Cell Survival Factor. *Mol. Carcinog.* **2015**, *54* (10), 947–958.

(85) Khanna, M.; Chelladurai, B.; Gavini, A.; Li, L.; Shao, M.; Courtney, D.; Turchi, J. J.; Matei, D.; Meroueh, S. Targeting Ovarian Tumor Cell Adhesion Mediated by Tissue Transglutaminase. *Mol. Cancer Ther.* **2011**, *10* (4), 626–636.

(86) Huang, S. P.; Liu, P. Y.; Kuo, C. J.; Chen, C. L.; Lee, W. J.; Tsai, Y. H.; Lin, Y. F. The Gαh-PLCδ1 Signaling Axis Drives Metastatic Progression in Triple-Negative Breast Cancer. *J. Hematol. Oncol.* **2017**, *10* (1), 1–13.

(87) Mehta, K. Biological and Therapeutic Significance of Tissue Transglutaminase in Pancreatic Cancer. *Amino Acids* **2009**, *36* (4), 709–716.

(88) Yu, C.; Cao, Q.; Chen, P.; Yang, S.; Gong, X.; Deng, M.; Ruan, B.; Li, L. Tissue Transglutaminase 2 Exerts a Tumor-Promoting Role in Hepatitis B Virus-Related Hepatocellular Carcinoma. *Tumor Biol.* **2016**, *37* (12), 16269–16274.

(89) Kausar, T.; Sharma, R.; Hasan, M. R.; Tripathi, S. C.; Saraya, A.; Chattopadhyay, T. K.;

Gupta, S. D.; Ralhan, R. Clinical Significance of GPR56, Transglutaminase 2, and NF-KB in Esophageal Squamous Cell Carcinoma. *Cancer Invest.* **2011**, *29* (1), 42–48.

(90) Sarang, Z.; Tóth, B.; Balajthy, Z.; Köröskényi, K.; Garabuczi, É.; Fésüs, L.; Szondy, Z. Some Lessons from the Tissue Transglutaminase Knockout Mouse. *Amino Acids* **2009**, *36* (4), 625–631.

(91) Folk, J. E.; Cole, P. W. Transglutaminase: Mechanistic Features of the Active Site as Determined by Kinetic and Inhibitor Studies. *Biochim. Biophys. Acta* **1966**, *122* (2), 244–264.

(92) Okauchi, M.; Xi, G.; Keep, R. F.; Hua, Y. Tissue-Type Transglutaminase and the Effects of Cystamine on Intracerebral Hemorrhage-Induced Brain Edema and Neurological Deficits. *Brain Res.* **2009**, *1249*, 229–236.

(93) Folk, J. E.; Connellan, J. M. Mechanism of the Inactivation of Guinea Pig Liver Transglutaminase by 5,5'-Dithiobis(2-Nitrobenzoic Acid). *J. Biol. Chem.* **1970**, *244* (12), 3173–3181.

(94) Case, A.; Stein, R. L. Kinetic Analysis of the Interaction of Tissue Transglutaminase with a Nonpeptidic Slow-Binding Inhibitor. *Biochemistry* **2007**, *46* (4), 1106–1115.

(95) Duval, E.; Case, A.; Stein, R. L.; Cuny, G. D. Structure-Activity Relationship Study of Novel Tissue Transglutaminase Inhibitors. *Bioorganic Med. Chem. Lett.* **2005**, *15* (7), 1885–1889.

(96) Schaertl, S.; Prime, M.; Wityak, J.; Dominguez, C.; Munoz-Sanjuan, I.; Pacifici, R. E.; Courtney, S.; Scheel, A.; MacDonald, D. A Profiling Platform for the Characterization of Transglutaminase 2 (TG2) Inhibitors. *J. Biomol. Screen.* **2010**, *15* (5), 478–487.

(97) Klock, C.; Jin, X.; Choi, K.; Khosla, C.; Madrid, P. B.; Spencer, A.; Raimundo, B. C.;

Boardman, P.; Lanza, G.; Griffin, J. H. Acylideneoxoindoles: A New Class of Reversible Inhibitors of Human Transglutaminase 2. *Bioorganic Med. Chem. Lett.* **2011**, *21* (9), 2692–2696.

(98) Lee, D.; Long, S. A.; Adams, J. L.; Chan, G.; Vaidya, K. S.; Francis, T. A.; Kikly, K.; Winkler, J. D.; Sung, C. M.; Debouck, C.; et al. Potent and Selective Nonpeptide Inhibitors of Caspases 3 and 7 Inhibit Apoptosis and Maintain Cell Functionality. *J. Biol. Chem.* **2000**, *275* (21), 16007–16014.

(99) Keillor, J. W.; Chica, R. A.; Chabot, N.; Vinci, V.; Pardin, C.; Fortin, E.; Gillet, S. M. F. .; Nakano, Y.; Kaartinen, M. T.; Pelletier, J. N.; et al. The Bioorganic Chemistry of Transglutaminase — from Mechanism to Inhibition and Engineering. *Can. J. Chem.* **2008**, *86* (4), 271–276.

(100) Song, M.; Hwang, H.; Im, C. Y.; Kim, S. Y. Recent Progress in the Development of Transglutaminase 2 (TGase2) Inhibitors: Miniperspective. *J. Med. Chem.* **2017**, *60* (2), 554–567.

(101) Choi, K.; Siegel, M.; Piper, J. L.; Yuan, L.; Cho, E.; Strnad, P.; Omary, B.; Rich, K. M.; Khosla, C. Chemistry and Biology of Dihydroisoxazole Derivatives: Selective Inhibitors of Human Transglutaminase 2. *Chem. Biol.* **2005**, *12* (4), 469–475.

(102) Klöck, C.; Herrera, Z.; Albertelli, M.; Khosla, C. Discovery of Potent and Specific Dihydroisoxazole Inhibitors of Human Transglutaminase 2. *J. Med. Chem.* **2014**, *57* (21), 9042–9064.

(103) Dafik, L.; Albertelli, M.; Stamnaes, J.; Sollid, L. M.; Khosla, C. Activation and Inhibition of Transglutaminase 2 in Mice. *PLoS One* **2012**, *7* (2), e30642.

(104) Keillor, J. W.; Chica, R. A.; Chabot, N.; Vinci, V.; Pardin, C.; Fortin, E.; Gillet, S. M. F.

G.; Nakano, Y.; Kaartinen, M. T.; Pelletier, J. N.; et al. The Bioorganic Chemistry of Transglutaminase — from Mechanism to Inhibition and Engineering. *Can. J. Chem.* **2008**, *86* (4), 271–276.

(105) Carrell, N. A.; Erickson, H. P.; McDonagh, J. Electron Microscopy and Hydrodynamic Properties of Factor XIII Subunits. *J. Biol. Chem.* **1989**, *264* (1), 551–556.

(106) Yee, V. C.; Pedersen, L. C.; Le Trong, I.; Bishop, P. D.; Stenkamp, R. E.; Teller, D. C. Three-Dimensional Structure of a Transglutaminase: Human Blood Coagulation Factor XIII. *Proc. Natl. Acad. Sci. U.S.A.* **2006**, *91* (15), 7296–7300.

(107) Gupta, S.; Biswas, A.; Akhter, M. S.; Krettler, C.; Reinhart, C.; Dodt, J.; Reuter, A.; Philippou, H.; Ivaskevicius, V.; Oldenburg, J. Revisiting the Mechanism of Coagulation Factor XIII Activation and Regulation from a Structure/Functional Perspective. *Sci. Rep.* **2016**, *6*, 1–16.

(108) Muszbek, L.; Ádány, R.; Mikkola, H. Novel Aspects of Blood Coagulation Factor XIII. I. Structure, Distribution, Activation, and Function. *Crit. Rev. Clin. Lab. Sci.* **1996**, *33* (5), 357–421.

(109) Richardson, V. R.; Cordell, P.; Standeven, K. F.; Carter, A. M. Substrates of Factor XIII-A: Roles in Thrombosis and Wound Healing. *Clin. Sci.* **2012**, *124* (3), 123–137.

(110) Da-Yu, S.; Shu-Jie, W. Advances of Coagulation Factor XIII. *Chin. Med. J. (Engl).* **2017**, *130* (2), 219–233.

(111) Kim, H.; Ahn, M.; Choi, S.; Kim, M.; Sim, K. B.; Kim, J.; Moon, C.; Shin, T. Potential Role of Fibronectin in Microglia/Macrophage Activation Following Cryoinjury in the Rat Brain: An Immunohistochemical Study. *Brain Res.* **2013**, *1502*, 11–19.

(112) Bae, H. B.; Zmijewski, J. W.; Deshane, J. S.; Zhi, D.; Thompson, L. C.; Peterson, C. B.;

Chaplin, D. D.; Abraham, E. Vitronectin Inhibits Neutrophil Apoptosis through Activation of Integrin-Associated Signaling Pathways. *Am. J. Respir. Cell Mol. Biol.* **2012**, *46* (6), 790–796.

(113) Soendergaard, C.; Kvist, P. H.; Seidelin, J. B.; Nielsen, O. H. Tissue-Regenerating Functions of Coagulation Factor XIII. *J. Thromb. Haemost.* **2013**, *11* (5), 806–816.

(114) Dardik, R.; Loscalzo, J.; Eskaraev, R.; Inbal, A. Molecular Mechanisms Underlying the Proangiogenic Effect of Factor XIII. *Arterioscler. Thromb. Vasc. Biol.* **2005**, *25* (3), 526–532.

(115) Ehman, E. C.; Johnson, G. B.; Villanueva-meyer, J. E.; Cha, S.; Leynes, A. P.; Eric, P.; Larson, Z.; Hope, T. A. Newly-Recognized Roles of Factor XIII in Thrombosis. *Semin. Thromb. Haemost.* **2017**, *46* (5), 1247–1262.

(116) Fadoo, Z.; Mechant, Q.; Abdur-Rahman, K. New Developments in the Management of Congenital Factor XIII Deficiency. *J. Blood Med.* **2013**, *4*, 65–73.

(117) Kohler, H. P.; Ichinose, A.; Seitz, R.; Ariens, R. A. S.; Muszbek, L. Diagnosis and Classification of Factor XIII Deficiencies. *J. Thromb. Haemost.* **2011**, *9* (7), 1404–1406.

(118) Ageno, W. Arterial and Venous Thrombosis: Clinical Evidence for Mechanistic Overlap. *Blood* **2014**, *124*, SCI-3.

(119) La Corte, A. L. C.; Philippou, H.; Arins, R. A. S. *Role of Fibrin Structure in Thrombosis and Vascular Disease*, 1st ed.; Elsevier Inc., 2011; Vol. 83.

(120) Bagoly, Z.; Koncz, Z.; Hársfalvi, J.; Muszbek, L. Factor XIII, Clot Structure, Thrombosis. *Thromb. Res.* **2012**, *129* (3), 382–387.

(121) Duval, C.; Ali, M.; Chaudhry, W. W.; Ridger, V. C.; Ariëns, R. A. S.; Philippou, H. Factor XIII A-Subunit V34L Variant Affects Thrombus Cross-Linking in a Murine Model

of Thrombosis. *Arterioscler. Thromb. Vasc. Biol.* **2016**, *36* (2), 308–316.

(122) Bereczky, Z.; Katona, E.; Muszbek, L. Fibrin Stabilization (Factor XIII), Fibrin Structure and Thrombosis. *Pathophysiol. Haemost. Thromb.* **2003**, *33* (5–6), 430–437.

(123) Muszbek, L.; Bereczky, Z.; Bagoly, Z.; Shemirani, A.; Katona, E. Factor XIII and Atherothrombotic Diseases. *Semin. Thromb. Hemost.* **2010**, *36* (01), 018–033.

(124) Bohm, M.; Kühl, T.; Hardes, K.; Coch, R.; Arkona, C.; Schlott, B.; Steinmetzer, T.; Imhof, D. Synthesis and Functional Characterization of Tridegin and Its Analogues: Inhibitors and Substrates of Factor XIIIa. *ChemMedChem* **2012**, *7* (2), 326–333.

(125) Sugimura, Y.; Hosono, M.; Wada, F.; Yoshimura, T.; Maki, M.; Hitomi, K. Screening for the Preferred Substrate Sequence of Transglutaminase Using a Phage-Displayed Peptide Library. *J. Biol. Chem.* **2006**, *281* (26), 17699–17706.

(126) Freund, K. F.; Doshi, K. P.; Gaul, S. L.; Claremon, D. A.; Remy, D. C.; Baldwin, J. J.; Pitzenberger, S. M.; Stern, A. M. Transglutaminase Inhibition by 2-[(2-Oxopropyl)Thio]Imidazolium Derivatives: Mechanism of Factor XIIIa Inactivation. *Biochemistry* **1994**, *33* (33), 10109–10119.

(127) Leidy, E. M.; Stern, A. M.; Friedman, P. A.; Bush, L. R. Enhanced Thrombolysis by a Factor XIIIa Inhibitor in a Rabbit Model of Femoral Artery Thrombosis. *Thromb. Res.* **1990**, *59* (1), 15–26.

(128) Leung-Toung, R.; Tam, T. F.; Wodzinska, J. M.; Zhao, Y.; Lowrie, J.; Simpson, C. D.; Karimian, K.; Spino, M. 3-Substituted Imidazo[1,2-d][1,2,4]-Thiadiazoles: A Novel Class of Factor XIIIa Inhibitors. *J. Med. Chem.* **2005**, *48* (7), 2266–2269.

(129) Iwata, Y.; Tago, K.; Kiho, T.; Kogen, H.; Fujioka, T.; Otsuka, N.; Suzuki-Konagai, K.; Ogita, T.; Miyamoto, S. Conformational Analysis and Docking Study of Potent Factor

XIIIa Inhibitors Having a Cyclopropenone Ring. *J. Mol. Graph. Model.* **2000**, *18* (6), 591–599.

(130) Stieler, M.; Weber, J.; Hils, M.; Kolb, P.; Heine, A.; Büchold, C.; Pasternack, R.; Klebe, G. Structure of Active Coagulation Factor-Xiii Triggered by Calcium Binding: Basis for the Design of next-Generation Anticoagulants. *Angew. Chemie - Int. Ed.* **2013**, *52* (45), 11930–11934.

(131) Keillor, J. W. *Transglutaminases: Multiple Functional Modifiers and Targets for New Drug Discovery*; Hitomi, K., Kojima, S., Fesus, L., Eds.; Springer: Tokyo, 2015.

(132) Copeland, R. A. *Evaluation of Enzyme Inhibitors in Drug Discovery: A Guide for Medicinal Chemists and Pharmacologist*; Hoboken, NJ, USA, 2013.

(133) Baillie, T. A. Targeted Covalent Inhibitors for Drug Design. *Angew. Chemie Int. Ed.* **2016**, *55* (43), 13408–13421.

(134) Lonsdale, R.; Ward, R. A. Structure-Based Design of Targeted Covalent Inhibitors. *Chem. Soc. Rev.* **2018**, *47* (11), 3816–3830.

(135) Shibata, Y.; Chiba, M. The Role of Extrahepatic Metabolism in the Pharmacokinetics of the Targeted Covalent Inhibitors Afatinib, Ibrutinib, and Neratinib S. *Drug. Metab. Dispos.* **2015**, *43* (3), 375–384.

(136) Mah, R.; Thomas, J. R.; Shafer, C. M. Bioorganic & Medicinal Chemistry Letters Drug Discovery Considerations in the Development of Covalent Inhibitors. *Bioorg. Med. Chem. Lett.* **2014**, *24* (1), 33–39.

(137) Herman, S. E. M.; Montraveta, A.; Niemann, C. U.; Mora-Jensen, H.; Gulrajani, M.; Krantz, F.; Mantel, R.; Smith, L. L.; McClanahan, F.; Harrington, B. K.; et al. The Bruton's Tyrosine Kinase (BTK) Inhibitor Acalabrutinib Demonstrates Potent on-Target

Effects and Efficacy in Two Mouse Models of Chronic Lymphocytic Leukemia. *Clin. Cancer Res.* **2017**, *23* (11), 2831.

(138) Hausch, F.; Halttunen, T.; Mäki, M.; Khosla, C. Design, Synthesis, and Evaluation of Gluten Peptide Analogs as Selective Inhibitors of Human Tissue Transglutaminase. *Chem. Biol.* **2003**, *10* (3), 225–231.

(139) Pardin, C.; Gillet, S. M. F. G.; Keillor, J. W. Synthesis and Evaluation of Peptidic Irreversible Inhibitors of Tissue Transglutaminase. *Bioorg. Med. Chem.* **2006**, *14* (24), 8379–8385.

(140) Marrano, C.; de Macédo, P.; Gagnon, P.; Lapierre, D.; Gravel, C.; Keillor, J. Synthesis and Evaluation of Novel Dipeptide-Bound 1,2,4-Thiadiazoles as Irreversible Inhibitors of Guinea Pig Liver Transglutaminase. *Bioorg. Med. Chem.* **2002**, *9* (12), 3231–3241.

(141) Halim, D.; Caron, K.; Keillor, J. W. Synthesis and Evaluation of Peptidic Maleimides as Transglutaminase Inhibitors. *Bioorg. Med. Chem. Lett.* **2007**, *17* (2), 305–308.

(142) de Macédo, P.; Marrano, C.; Keillor, J. W. Synthesis of Dipeptide-Bound Epoxides and α,β-Unsaturated Amides as Potential Irreversible Transglutaminase Inhibitors. *Bioorg. Med. Chem.* **2002**, *10* (2), 355–360.

(143) de Macédo, P.; Marrano, C.; Keillor, J. W. A Direct Continuous Spectrophotometric Assay for Transglutaminase Activity. *Anal. Biochem.* **2000**, *285* (1), 16–20.

(144) Wityak, J.; Prime, M. E.; Brookfield, F. A.; Courtney, S. M.; Erfan, S.; Johnsen, S.; Johnson, P. D.; Li, M.; Marston, R. W.; Reed, L.; et al. SAR Development of Lysine-Based Irreversible Inhibitors of Transglutaminase 2 for Huntington's Disease. *ACS Med. Chem. Lett.* **2012**, *3* (12), 1024–1028.

(145) Al-Jallad, H. F.; Myneni, V. D.; Piercy-Kotb, S. A.; Chabot, N.; Mulani, A.; Keillor, J.

W.; Kaartinen, M. T. Plasma Membrane Factor XIIIA Transglutaminase Activity Regulates Osteoblast Matrix Secretion and Deposition by Affecting Microtubule Dynamics. *PLoS One* **2011**, *6* (1), e15893–e15893.

(146) Fisher, M. L.; Kerr, C.; Adhikary, G.; Grun, D.; Xu, W.; Keillor, J. W.; Eckert, R. L. Transglutaminase Interaction with A6/B4-Integrin Stimulates YAP1-Dependent ΔNp63α Stabilization and Leads to Enhanced Cancer Stem Cell Survival and Tumor Formation. *Cancer Res.* **2016**, *76* (24), 7265–7276.

(147) Kerr, C.; Szmacinski, H.; Fisher, M. L.; Nance, B.; Lakowicz, J. R.; Akbar, A.; Keillor, J. W.; Lok Wong, T.; Godoy-Ruiz, R.; Toth, E. A.; et al. Transamidase Site-Targeted Agents Alter the Conformation of the Transglutaminase Cancer Stem Cell Survival Protein to Reduce GTP Binding Activity and Cancer Stem Cell Survival. *Oncogene* **2017**, *36* (21), 2981–2990.

(148) Lipinski, C. A.; Lombardo, F.; Dominy, B. W.; Feeney, P. J. Experimental and Computational Approaches to Estimate Solubility and Permeability in Drug Discovery and Development Settings1PII of Original Article: S0169-409X(96)00423-1. The Article Was Originally Published in Advanced Drug Delivery Reviews 23 (1997) 3. *Adv. Drug Deliv. Rev.* **2001**, *46* (1), 3–26.

(149) Veber, D. F.; Johnson, S. R.; Cheng, H.-Y.; Smith, B. R.; Ward, K. W.; Kopple, K. D. Molecular Properties That Influence the Oral Bioavailability of Drug Candidates. **2002**.

(150) Folk, J. E.; Cole, P. W. Mechanism of Action of Guinea Pig Liver Transglutaminase. *J. Biol. Chem.* **1966**, *241* (23), 5518–5525.

(151) Kitz, R.; Wilson, I. B. Esters of Methanesulfonic Acid as Irreversible Inhibitors of Acetylcholinesterase. *J. Biol. Chem.* **1962**, *237* (10).

(152) Akbar, A.; McNeil, N. M. R.; Albert, M. R.; Ta, V.; Adhikary, G.; Bourgeois, K.; Eckert, R. L.; Keillor, J. W. Structure–Activity Relationships of Potent, Targeted Covalent Inhibitors That Abolish Both the Transamidation and GTP Binding Activities of Human Tissue Transglutaminase. *J. Med. Chem.* **2017**, *60* (18), 7910–7927.

(153) Veber, D. F.; Johnson, S. R.; Cheng, H.-Y.; Smith, B. R.; Ward, K. W.; Kopple, K. D. Molecular Properties That Influence the Oral Bioavailability of Drug Candidates. *J. Med. Chem.* **2002**, *45* (12), 2615–2623.

(154) Marrano, C.; de Macédo, P.; Keillor, J. W. Evaluation of Novel Dipeptide-Bound α,β-Unsaturated Amides and Epoxides as Irreversible Inhibitors of Guinea Pig Liver Transglutaminase. *Bioorg. Med. Chem.* **2001**, *9* (7), 1923–1928.

(155) Lorand, L.; Graham, R. M. Transglutaminases: Crosslinking Enzymes with Pleiotropic Functions. *Nat. Rev. Mol. Cell Biol.* **2003**, *4* (2), 140–156.

(156) Im, M.; Riek, R. P.; Graham, R. M. A Novel Guanine Nucleotide-Binding Protein Coupled to the A1-Adrenergic Receptor. *J. Biol. Chem.* **1990**, *265* (31), 18952–18960.

(157) Fisher, M. L.; Adhikary, G.; Xu, W.; Kerr, C.; Keillor, J. W.; Eckert, R. L. Type II Transglutaminase Stimulates Epidermal Cancer Stem Cell Epithelial-Mesenchymal Transition. *Oncotarget* **2015**, *6* (24), 20525–20539.

(158) Mironov, G. G.; Clouthier, C. M.; Akbar, A.; Keillor, J. W.; Berezovski, M. V. Simultaneous Analysis of Enzyme Structure and Activity by Kinetic Capillary Electrophoresis-MS. *Nat. Chem. Biol.* **2016**, *12* (11), 918–922.

(159) McEwen, D. P.; Gee, K. R.; Kang, H. C.; Neubig, R. R. Fluorescent BODIPY-GTP Analogs: Real-Time Measurement of Nucleotide Binding to G Proteins. *Anal. Biochem.* **2001**, *291* (1), 109–117.

(160) Folk, J. E. and Cole, P. W. Identification of a Functional Cysteine Essential for the Activity of Guinea Pig Liver Transglutaminse. *J. Biol. Chem.* **1966**, *241* (1), 3238–3240.

(161) Hall, D. M. S.; Brooks, S. A. In Vitro Invasion Assay Using Matrigel™: A Reconstituted Basement Membrane Preparation; Humana Press, New York, NY, 2014; pp 1–11.

(162) Pasternack, R.; Specker, E.; Hunfeld, A.; Dodt, J.; Seitz, R.; Oertel, K.; Reiff, C. A Highly Sensitive Fluorometric Assay for Determination of Human Coagulation Factor XIII in Plasma. *Anal. Biochem.* **2007**, *367* (2), 152–158.

(163) Ufer, M. Comparative Pharmacokinetics of Vitamin K Antagonists: Warfarin, Phenprocoumon and Acenocoumarol. *Clin. Pharmacokinet.* **2005**, *44* (12), 1227–1246.

(164) Garcia, D.; Libby, E.; Crowther, M. A. New Oral Anticoagulants. *Am. Soc. Hematol.* **2010**, *115* (1), 1–133.

(165) Mulani, A. Synthesis and Evaluation of Peptidic Probes for Tissue Transglutaminase and Factor XIII, University of Ottawa, PhD Thesis, 2014.

(166) Yoshino, M.; Murakami, K. A Graphical Method for Determining Inhibition Constants. *J. Enzyme Inhib. Med. Chem.* **2009**, *24* (6), 1288–1290.

(167) Leblanc, A.; Gravel, C.; Labelle, J.; Keillor, J. W. Kinetic Studies of Guinea Pig Liver Transglutaminase Reveal a General-Base-Catalyzed Deacylation Mechanism. *Biochemistry* **2001**, *40* (28), 8335–8342.

(168) Stone, S. R.; Hofsteenge, J. Specificity of Activated Human Protein C. *Biochem. J.* **2015**, *230* (2), 497–502.

Appendices

Appendix I

NMR spectra of final compounds

Compound 10

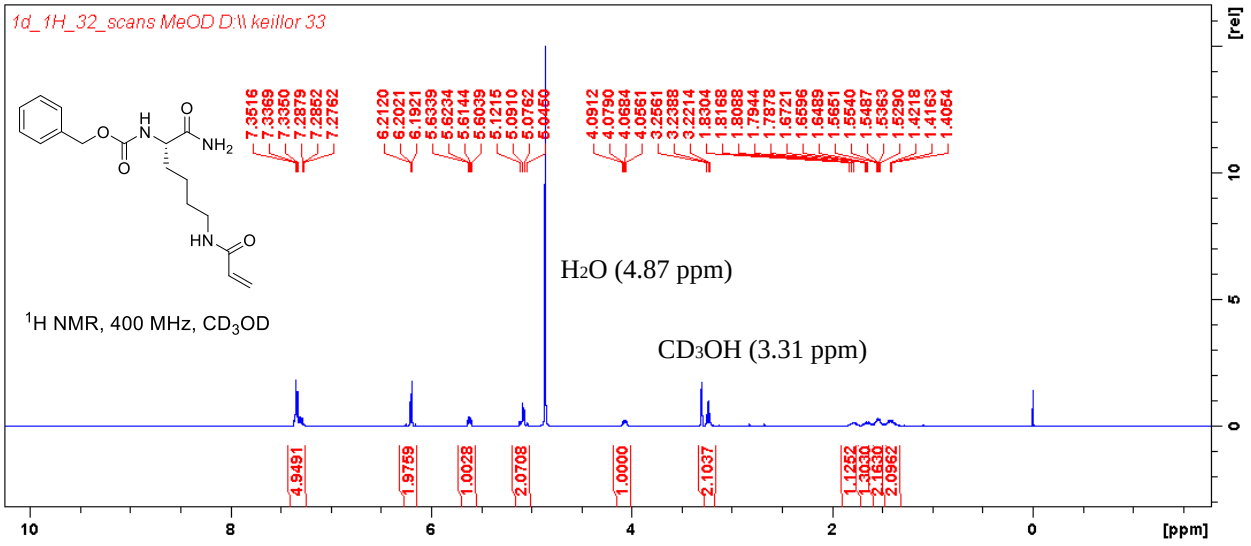

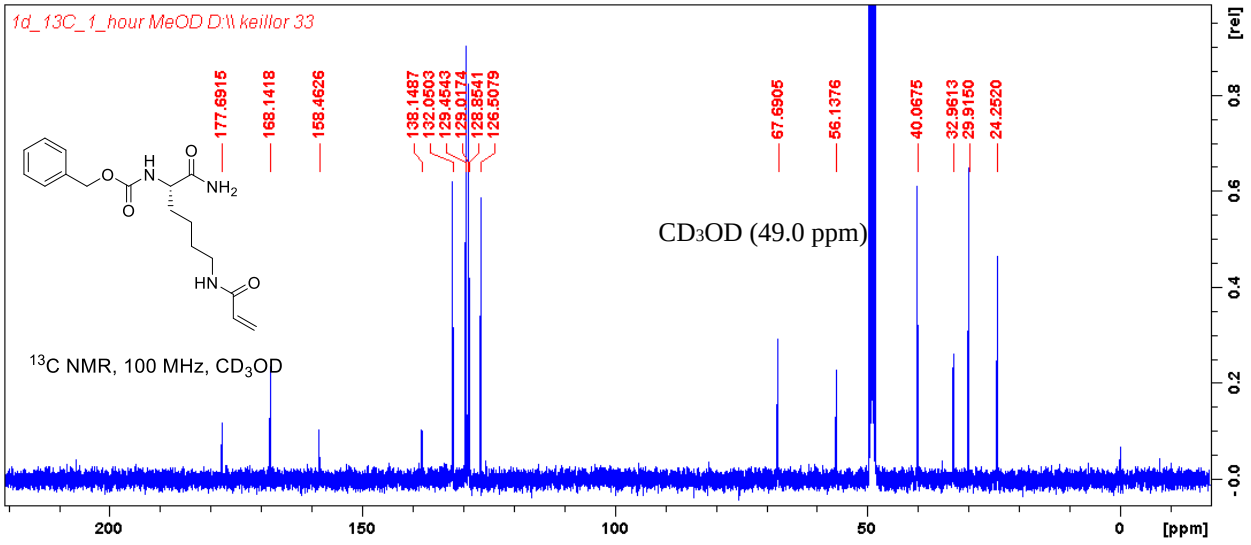

Compound 12

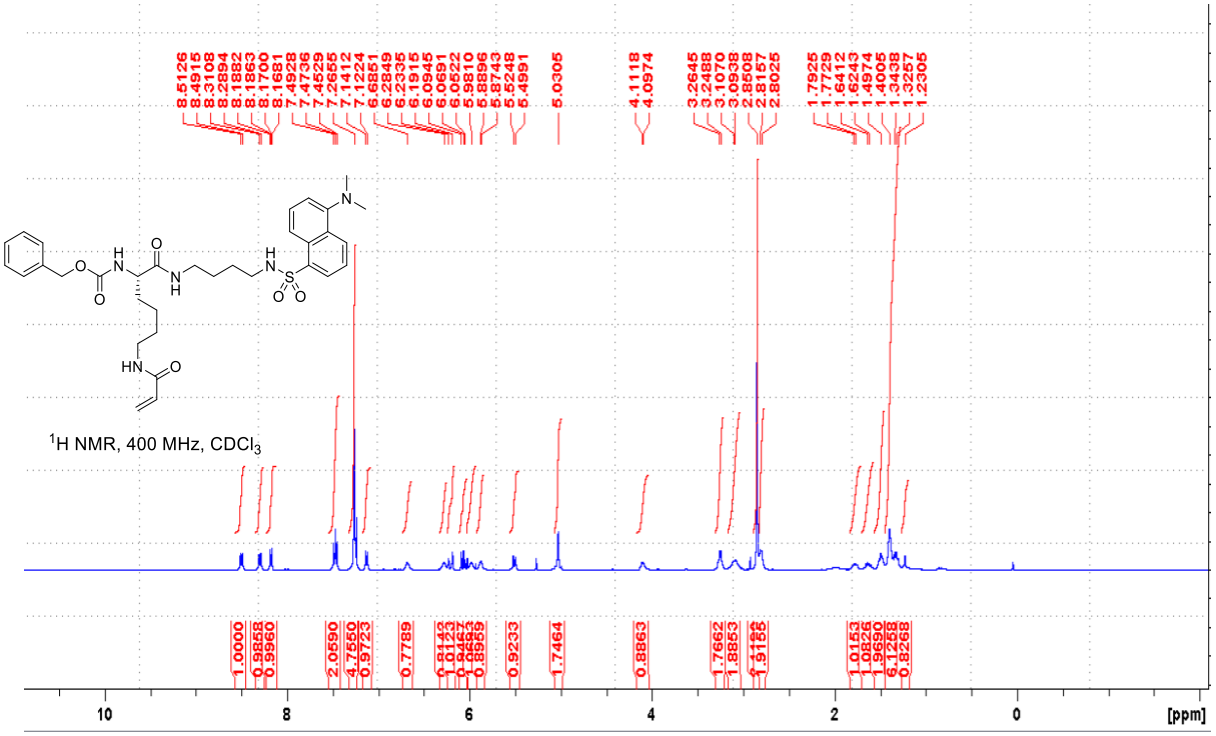
8.5126
8.4915
8.3108
8.2894
8.1882
8.1863
8.1700
8.1681
7.4928
7.4736
7.4529
7.2655
7.1412
7.1224
6.6851
6.2849
6.2335
6.1915
6.0945
6.0691
6.0522
5.9810
5.8896
5.8743
5.5248
5.4991
5.0305
4.1118
4.0974
3.2645
3.2488
3.1070
3.0938
2.8508
2.8157
2.8025
1.7925
1.7729
1.6412
1.6243
1.4674
1.4005
1.3438
1.3257
1.2305
1.0000
0.9858
0.9960
2.0590
4.7550
0.9723
0.7789
0.8142
1.0127
1.0662
0.8959
0.9233
1.7464
0.8863
1.7662
1.8853
6.1185
1.9188
1.0152
1.0826
1.9690
6.1256
0.8268
10
8
6
4
2
0
[ppm]
^{1}H NMR, 400 MHz, CDCl$_3$

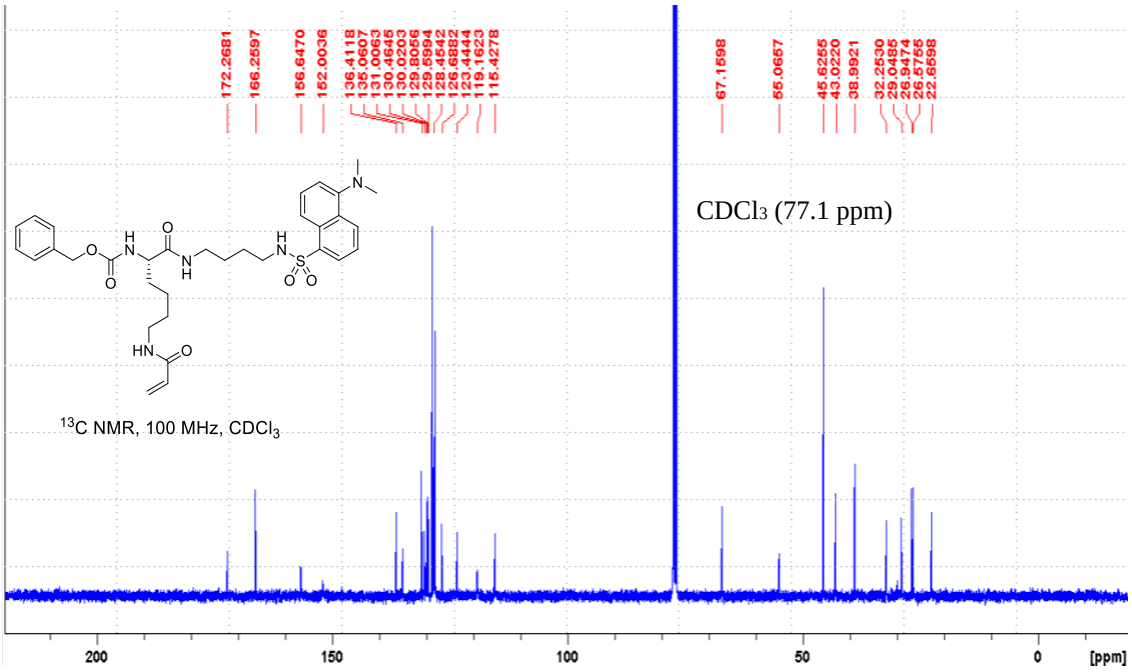
172.2681
166.2597
156.6470
152.0036
136.4118
135.0607
131.0063
130.4645
130.0203
129.8066
129.5994
128.4542
123.4444
119.1623
115.4278
67.1598
55.0657
45.6255
43.0220
38.9921
32.2530
29.0485
28.9474
26.5765
22.8598
CDCl3 (77.1 ppm)
200
150
100
50
0
[ppm]
^{13}C NMR, 100 MHz, CDCl$_3$

Compound 13

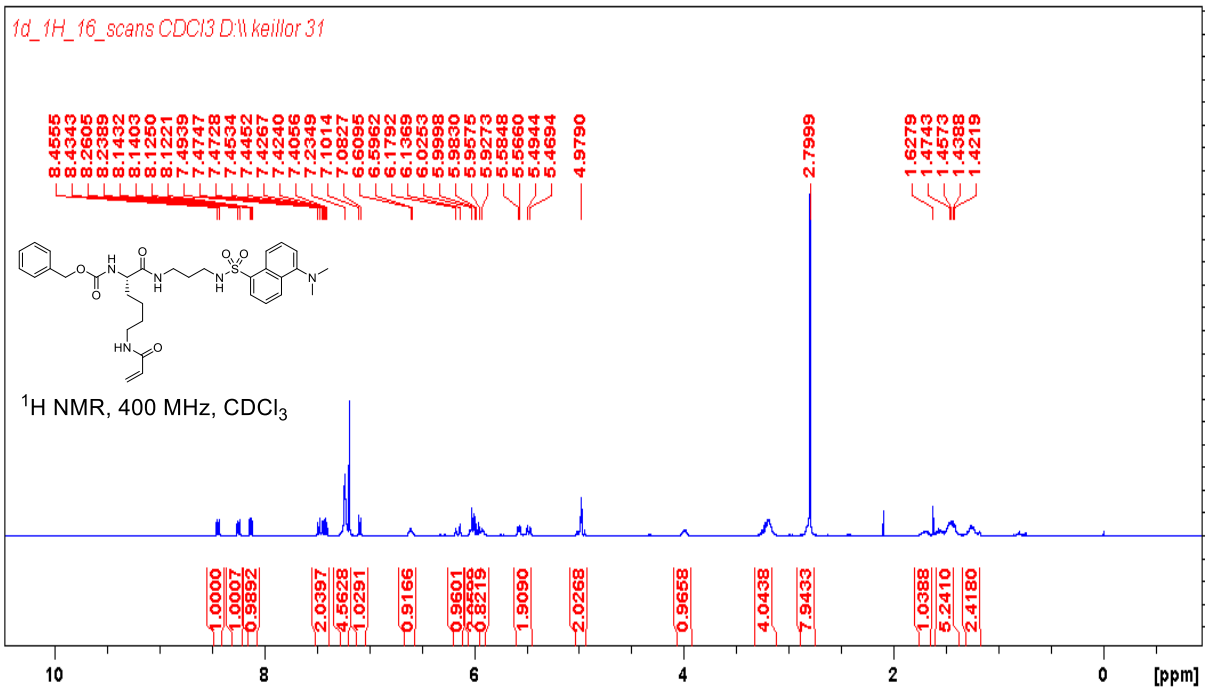
1d_1H_16_scans CDCl3 D:\\ keillor 31
8.4555
8.4343
8.2605
8.2389
8.1432
8.1403
8.1250
8.1221
7.4939
7.4747
7.4728
7.4534
7.4452
7.4267
7.4240
7.4056
7.2349
7.1014
7.0827
6.6095
6.5962
6.1792
6.1369
6.0253
5.9998
5.9830
5.9575
5.9273
5.5848
5.5660
5.4944
5.4694
4.9790
2.7999
1.6279
1.4743
1.4573
1.4388
1.4219
1H NMR, 400 MHz, CDCl3
1.0000
1.0007
0.9892
2.0397
4.5628
1.0291
0.9166
0.9601
0.8216
1.9090
2.0268
0.9658
4.0438
7.9433
1.0388
5.2410
2.4180
10
8
6
4
2
0
[ppm]

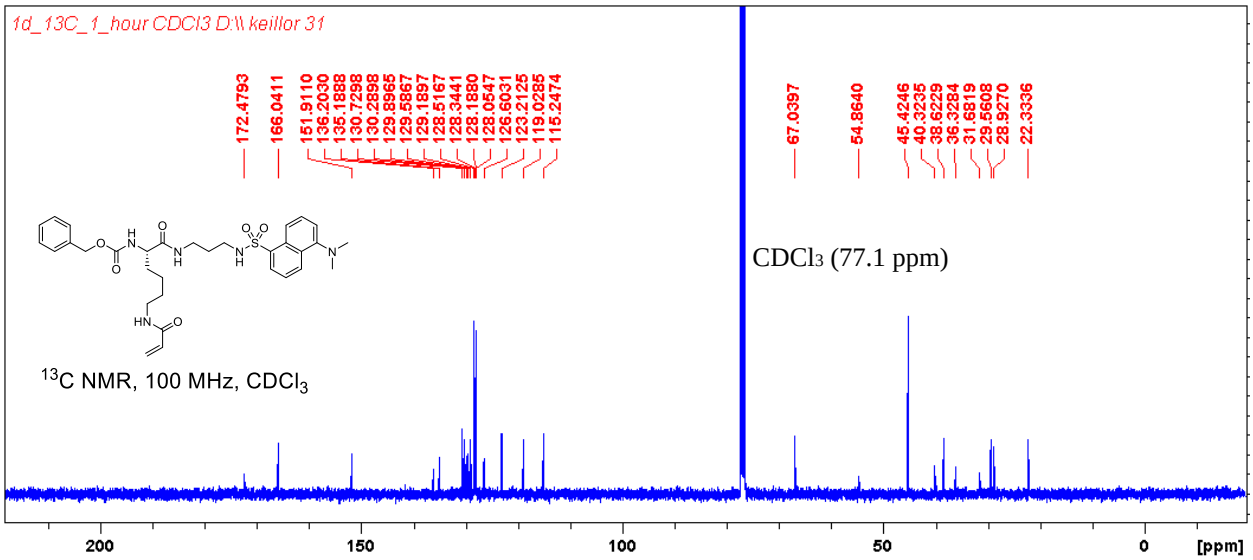
1d_13C_1_hour CDCl3 D:\\ keillor 31
172.4793
166.0411
151.9110
136.2030
135.1888
130.7298
130.2898
129.8965
129.5867
129.1897
128.5167
128.3441
128.1880
128.0547
126.6031
123.2125
119.0285
115.2474
67.0397
54.8640
45.4246
40.3235
38.6229
36.3284
31.6819
29.5608
28.9270
22.3336
CDCl3 (77.1 ppm)
13C NMR, 100 MHz, CDCl3
200
150
100
50
0
[ppm]

Compound 14

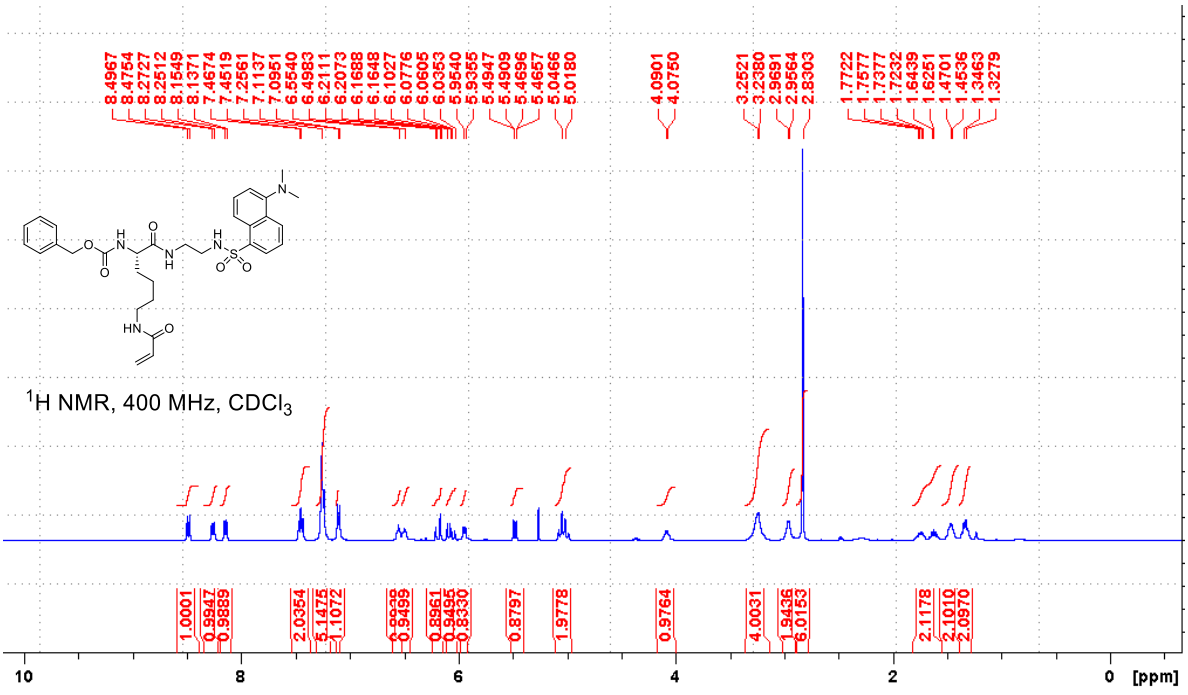
8.4967
8.4754
8.2727
8.2512
8.1549
8.1371
7.4674
7.4519
7.2561
7.1137
7.0951
6.5540
6.4983
6.2111
6.2073
6.1688
6.1648
6.1027
6.0776
6.0605
6.0353
5.9540
5.9355
5.4947
5.4909
5.4696
5.4657
5.0466
5.0180
4.0901
4.0750
3.2521
3.2380
2.9691
2.9564
2.8303
1.7722
1.7577
1.7377
1.7232
1.6439
1.6251
1.4701
1.4536
1.3463
1.3279
1H NMR, 400 MHz, CDCl3
1.0001
0.9947
0.9889
2.0354
5.1475
1.1072
0.9499
0.8961
0.9495
0.8330
0.8797
1.9778
0.9764
4.0031
1.9436
6.0153
2.1178
2.1010
2.0970
10
8
6
4
2
0
[ppm]

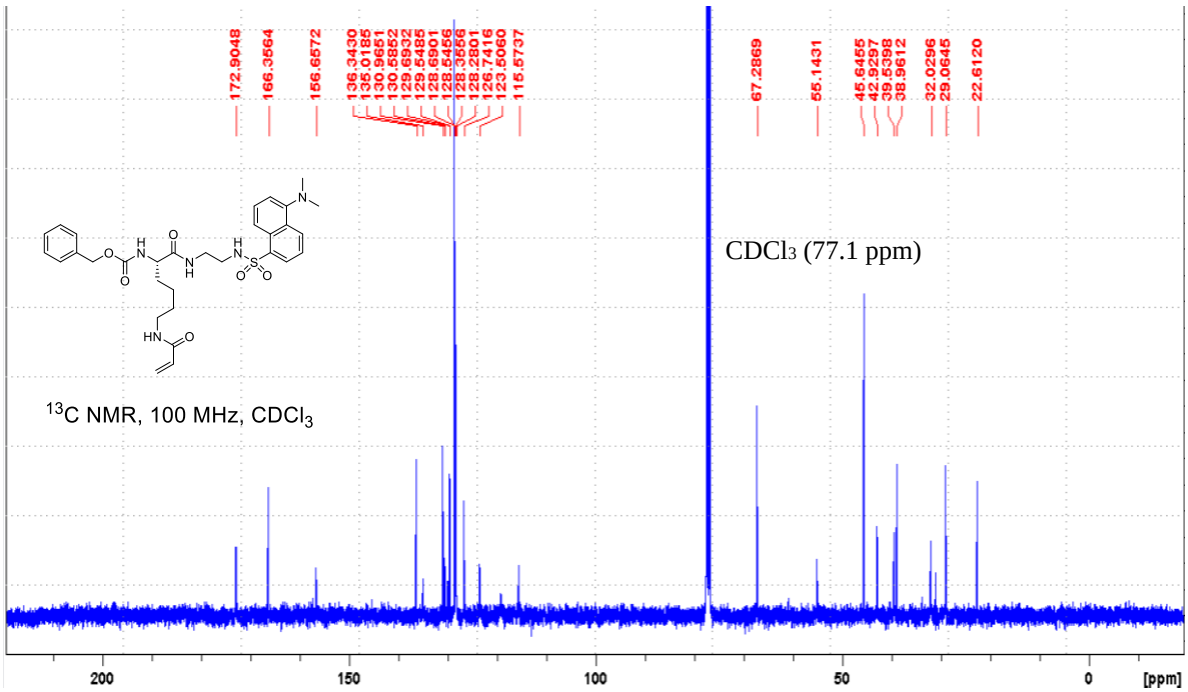
172.9048
166.3564
156.6572
136.3430
135.0185
130.9651
130.5852
129.6932
129.5485
128.6901
128.5456
128.3656
128.2801
126.7416
123.6060
115.5737
67.2869
55.1431
45.6455
42.9297
39.5398
38.9612
32.0296
29.0645
22.6120
CDCl3 (77.1 ppm)
13C NMR, 100 MHz, CDCl3
200
150
100
50
0
[ppm]

Compound 15

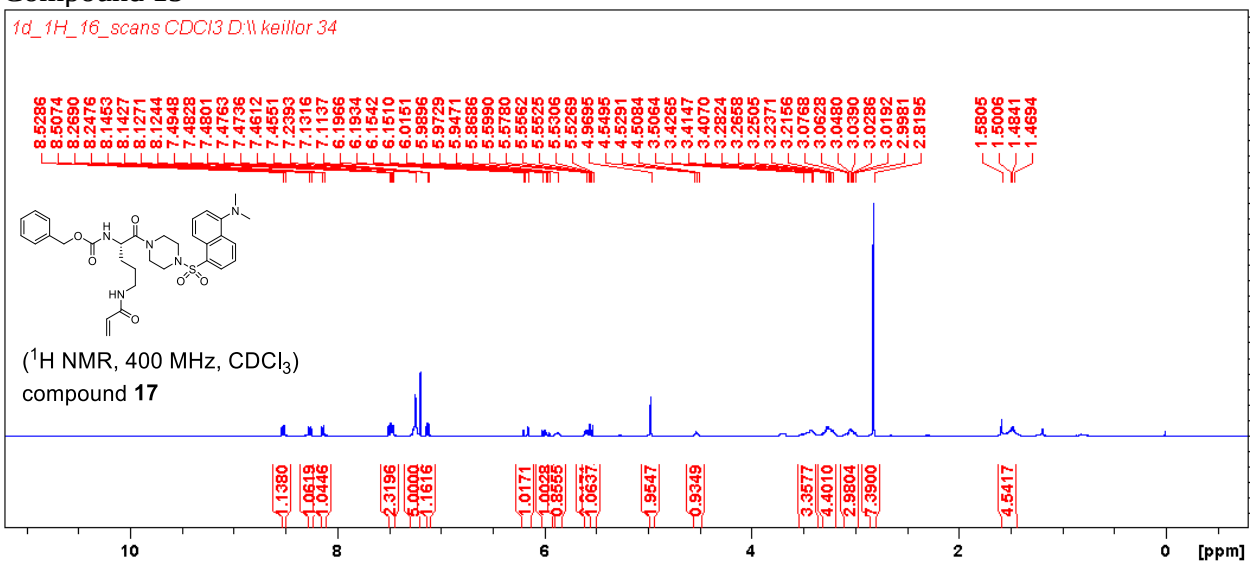
1d_1H_16_scans CDCl3 D:\\ keillor 34
(1H NMR, 400 MHz, CDCl3)
compound 17
[ppm]

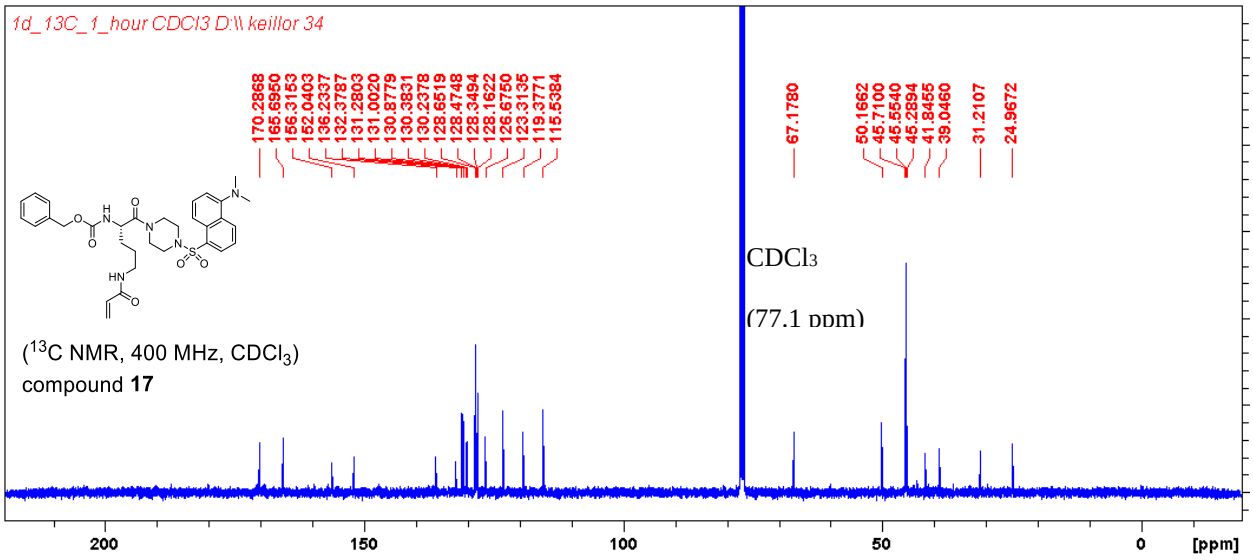
1d_13C_1_hour CDCl3 D:\\ keillor 34
CDCl3
(77.1 ppm)
(13C NMR, 400 MHz, CDCl3)
compound 17
[ppm]

Compound 16

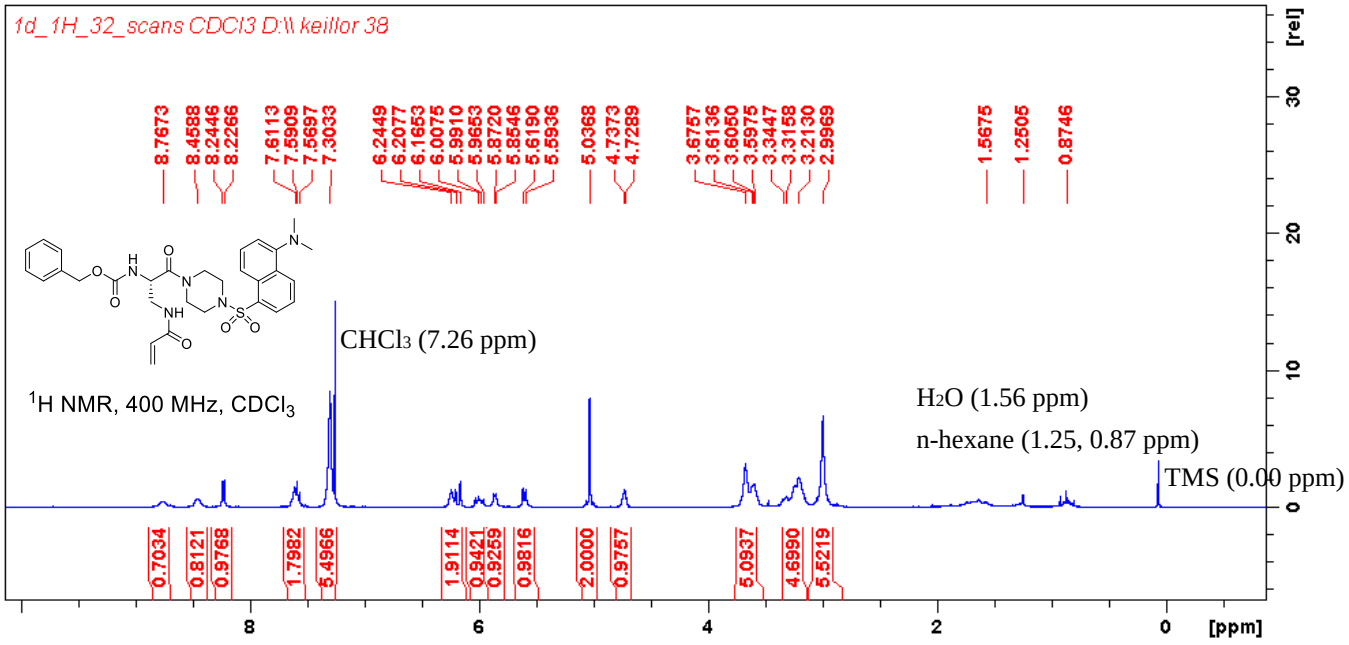
1d_1H_32_scans CDCl3 D:\\ keillor 38
8.7673
8.4588
8.2446
8.2266
7.6113
7.5909
7.5697
7.3033
6.2449
6.2077
6.1653
6.0075
5.9910
5.9653
5.8720
5.8546
5.6190
5.5936
5.0368
4.7373
4.7289
3.6757
3.6136
3.6050
3.5975
3.3447
3.3158
3.2130
2.9969
1.5675
1.2505
0.8746
CHCl3 (7.26 ppm)
1H NMR, 400 MHz, CDCl3
H2O (1.56 ppm)
n-hexane (1.25, 0.87 ppm)
TMS (0.00 ppm)
0.7034
0.8121
0.9768
1.7982
5.4966
1.9114
0.9421
0.9259
0.9816
2.0000
0.9757
5.0937
4.6990
5.5219
[rel]
[ppm]

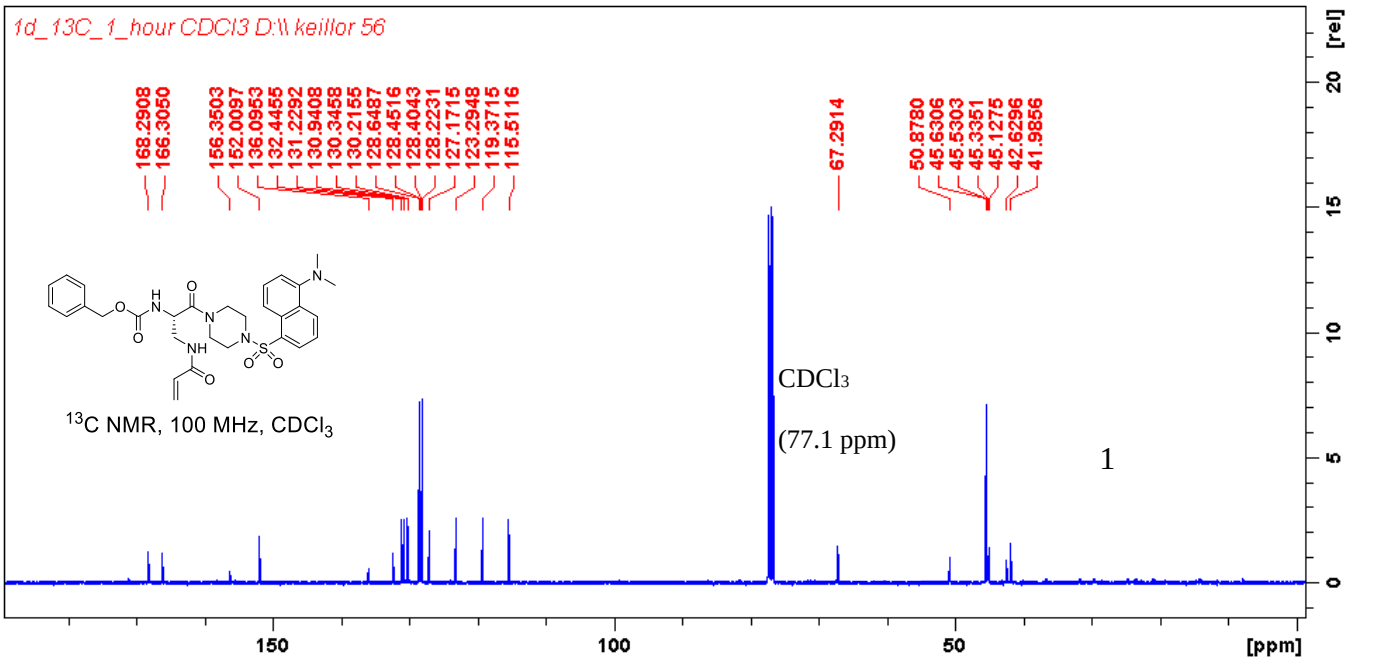
1d_13C_1_hour CDCl3 D:\\ keillor 56
168.2908
166.3050
156.3503
152.0097
136.0953
132.4455
131.2292
130.9408
130.3458
130.2155
128.6487
128.4516
128.4043
128.2231
127.1715
123.2948
119.3715
115.5116
67.2914
50.8780
45.6306
45.5303
45.3351
45.1275
42.6296
41.9856
13C NMR, 100 MHz, CDCl3
CDCl3
(77.1 ppm)
1
[rel]
[ppm]

Compound 17

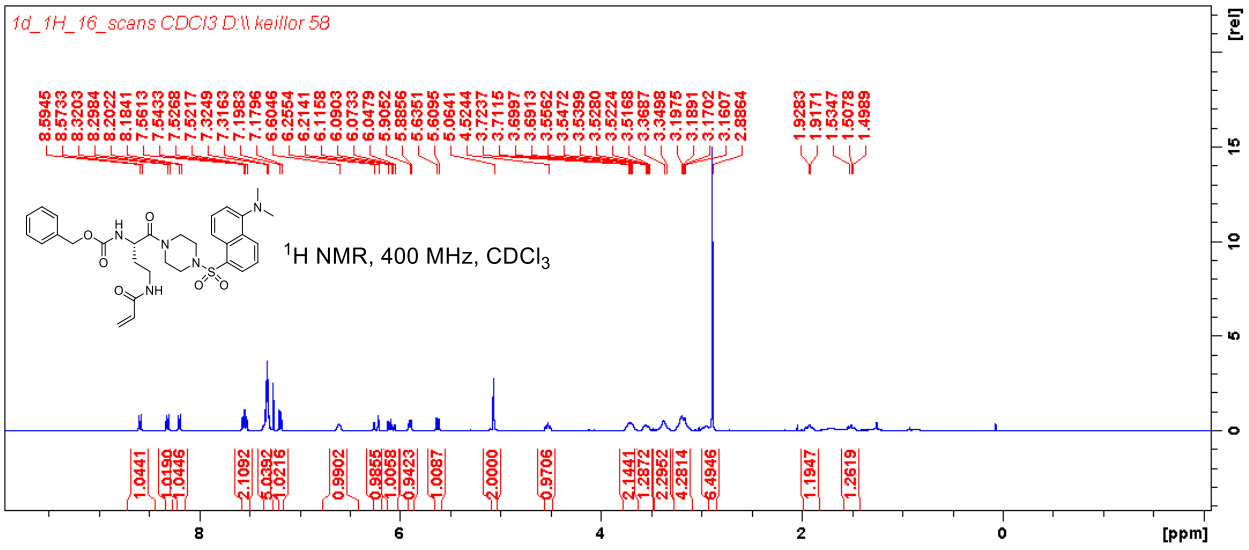
1d_1H_16_scans CDCl3 D:\\ keillor 58
^{1}H NMR, 400 MHz, $CDCl_3$
[rel]
[ppm]

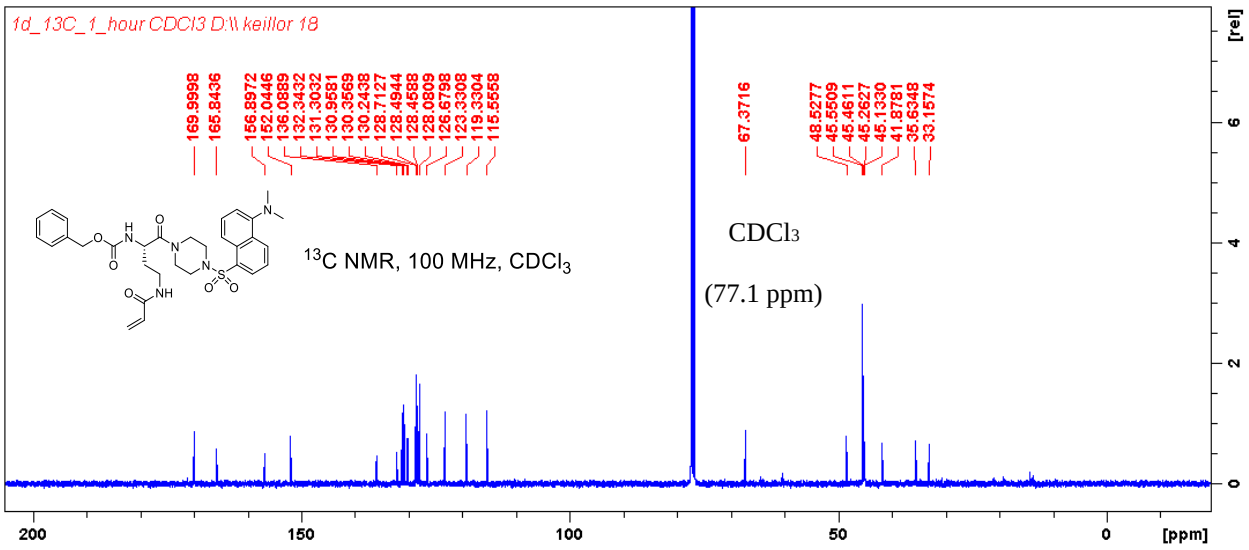
1d_13C_1_hour CDCl3 D:\\ keillor 18
^{13}C NMR, 100 MHz, $CDCl_3$
$CDCl_3$
(77.1 ppm)
[rel]
[ppm]

Compound 18

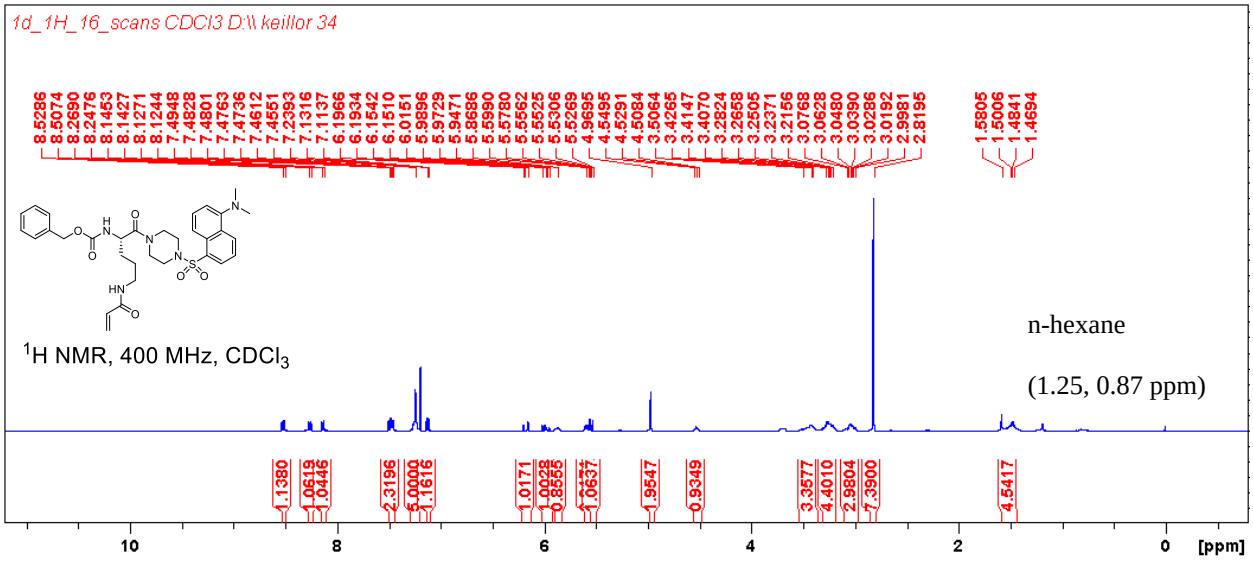
1d_1H_16_scans CDCl3 D:\\ keillor 34
8.5286
8.5074
8.2690
8.2476
8.1453
8.1427
8.1271
8.1244
7.4948
7.4828
7.4801
7.4763
7.4736
7.4612
7.4551
7.2393
7.1316
7.1137
6.1966
6.1934
6.1542
6.1510
6.0151
5.9896
5.9729
5.9471
5.8686
5.5990
5.5780
5.5562
5.5525
5.5306
5.5269
4.9695
4.5495
4.5291
4.5084
3.5064
3.4265
3.4147
3.4070
3.2824
3.2658
3.2505
3.2371
3.2156
3.0768
3.0628
3.0480
3.0390
3.0286
3.0192
2.9981
2.8195
1.5805
1.5006
1.4841
1.4694
1H NMR, 400 MHz, CDCl3
n-hexane
(1.25, 0.87 ppm)
1.1380
1.0619
1.0446
2.3196
6.0000
1.1616
1.0171
1.0028
0.8555
1.0637
1.9547
0.9349
3.3577
4.4010
2.9804
7.3900
4.5417
10
8
6
4
2
0
[ppm]

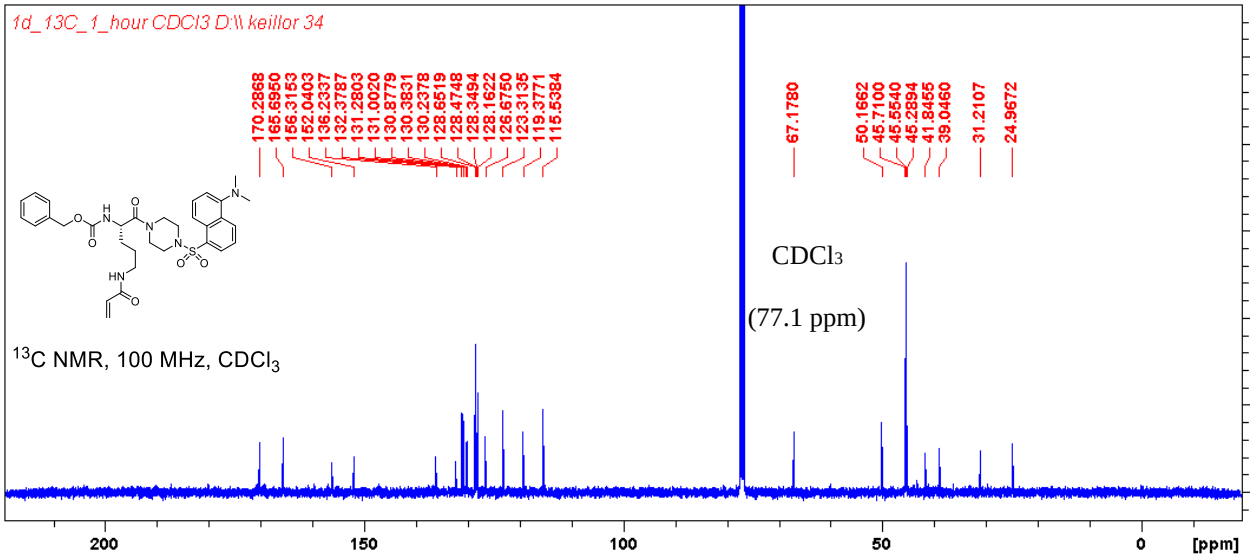
1d_13C_1_hour CDCl3 D:\\ keillor 34
170.2868
165.6950
156.3153
152.0403
136.2337
132.3787
131.2803
131.0020
130.8779
130.3831
130.2378
128.6519
128.4748
128.3494
128.1622
126.6750
123.3135
119.3771
115.5384
67.1780
50.1662
45.7100
45.5540
45.2894
41.8455
39.0460
31.2107
24.9672
13C NMR, 100 MHz, CDCl3
CDCl3
(77.1 ppm)
200
150
100
50
0
[ppm]

Compound 22

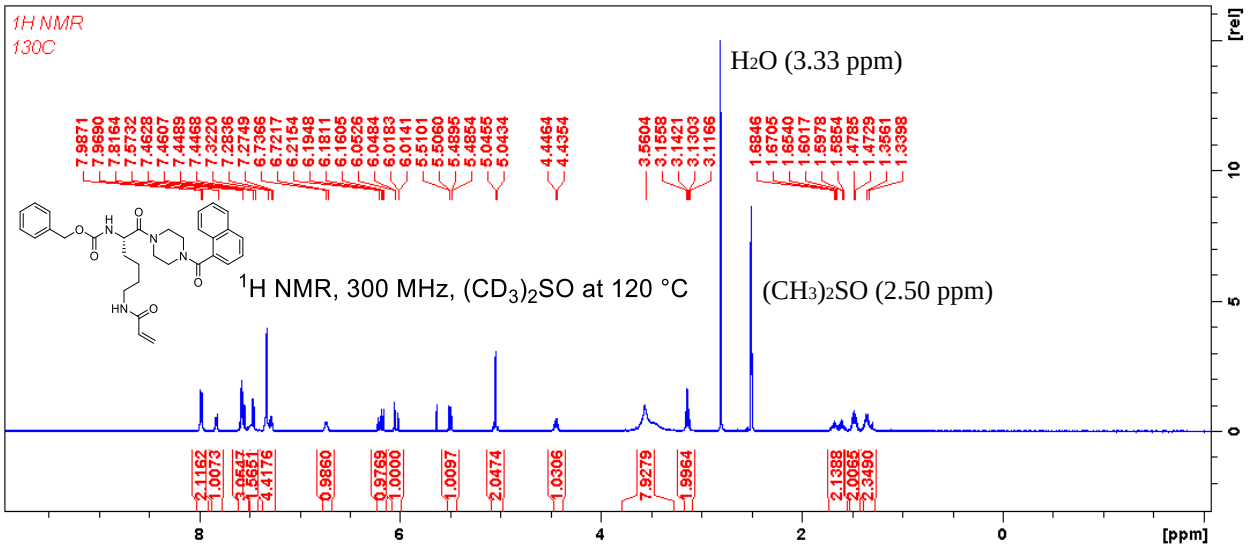
1H NMR
130C
H2O (3.33 ppm)
(CH3)2SO (2.50 ppm)
1H NMR, 300 MHz, (CD3)2SO at 120 °C
[rel]
[ppm]

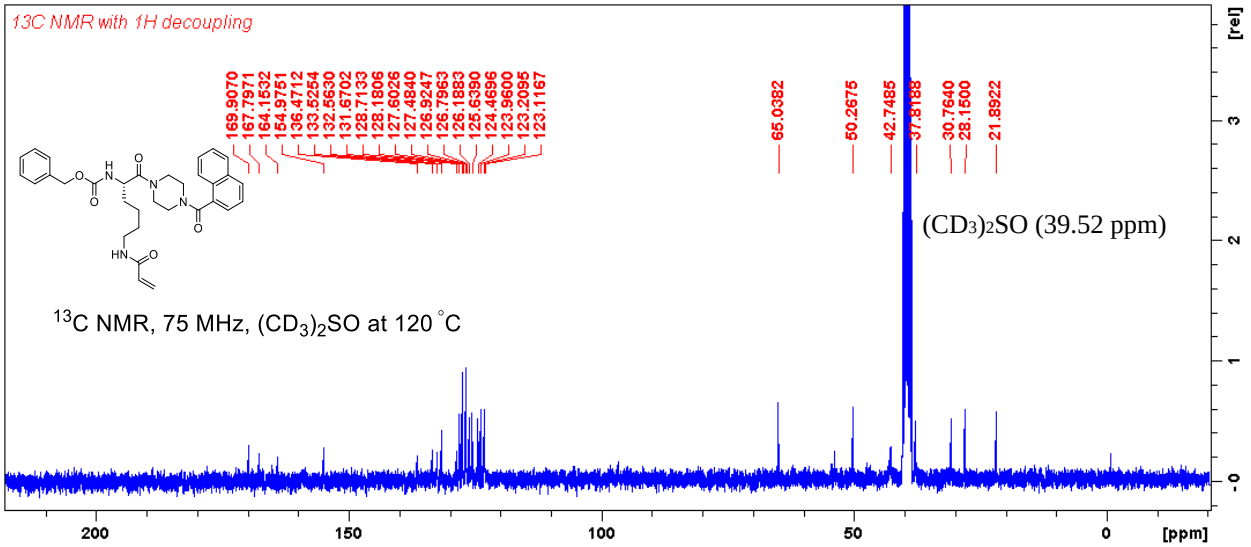
13C NMR with 1H decoupling
(CD3)2SO (39.52 ppm)
13C NMR, 75 MHz, (CD3)2SO at 120 °C
[rel]
[ppm]

Compound 23

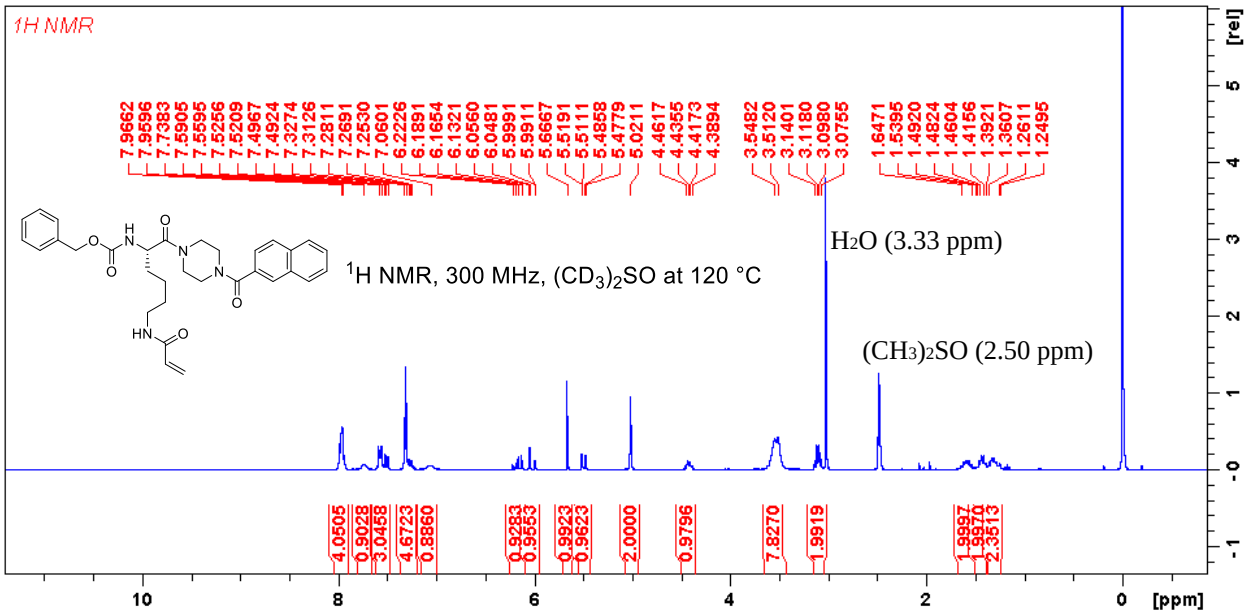
1H NMR
7.9662 7.9596 7.7383 7.5905 7.5595 7.5256 7.5209 7.4967 7.4924 7.3274 7.3126 7.2811 7.2691 7.2530 7.0601 6.2226 6.1891 6.1654 6.1321 6.0560 6.0481 5.9991 5.9911 5.6667 5.5191 5.5111 5.4858 5.4779 5.0211 4.4617 4.4355 4.4173 4.3894 3.5482 3.5120 3.1401 3.1180 3.0980 3.0755 1.6471 1.5395 1.4920 1.4824 1.4604 1.4156 1.3921 1.3607 1.2611 1.2495
H2O (3.33 ppm)
(CH3)2SO (2.50 ppm)
1H NMR, 300 MHz, (CD3)2SO at 120 °C
4.0505 0.9028 3.0456 4.6723 0.8860 0.9283 0.9553 0.9923 0.9623 2.0000 0.9796 7.8270 1.9919 1.9997 1.9970 2.3513
[rel]
[ppm]

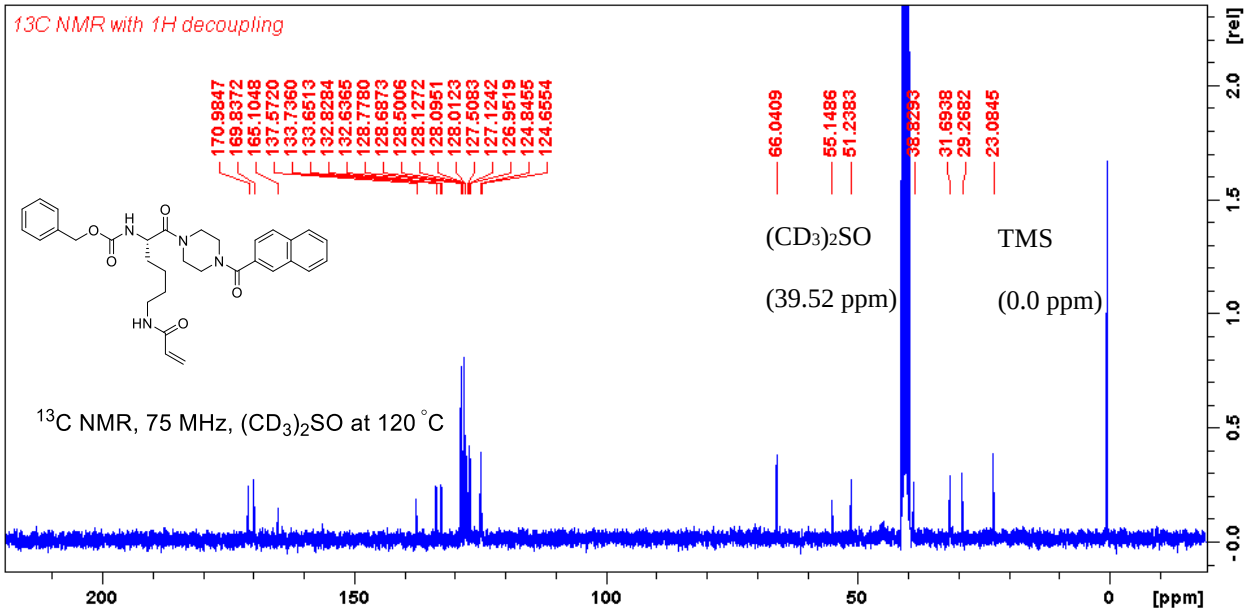
13C NMR with 1H decoupling
170.9847 169.8372 165.1048 137.5720 133.7360 133.6513 132.8284 132.6365 128.7780 128.6873 128.5006 128.1272 128.0951 128.0123 127.5083 127.1242 126.9519 124.8455 124.6554
66.0409 55.1486 51.2383 39.5233 31.6938 29.2682 23.0845
(CD3)2SO
(39.52 ppm)
TMS
(0.0 ppm)
13C NMR, 75 MHz, (CD3)2SO at 120 °C
[rel]
[ppm]

Compound 24

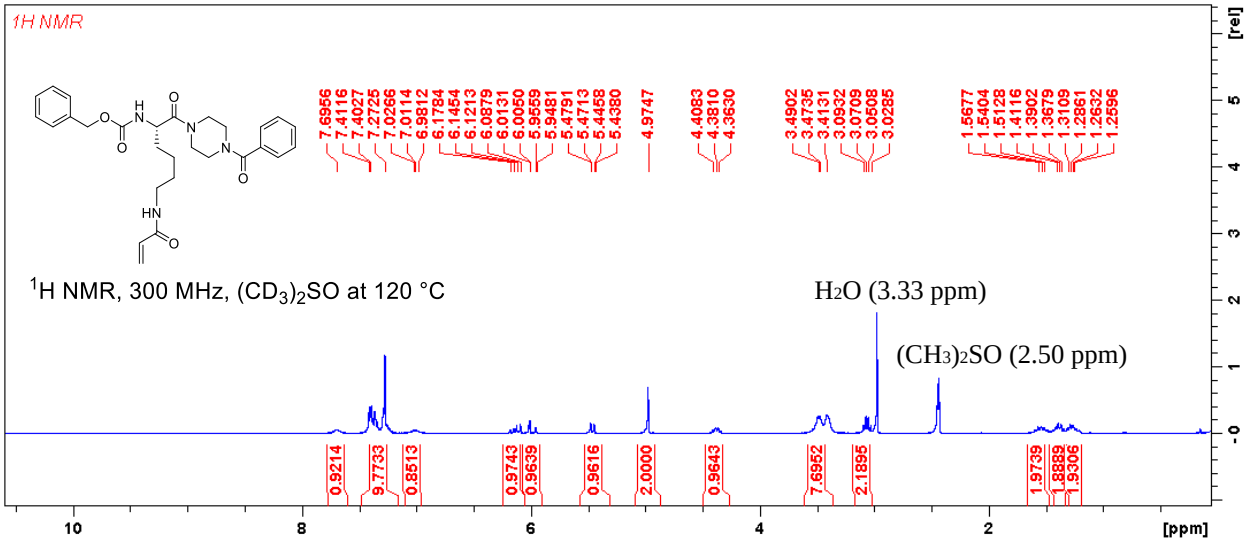
1H NMR
7.6956
7.4116
7.4027
7.2725
7.0266
7.0114
6.9812
6.1784
6.1454
6.1213
6.0879
6.0131
6.0050
5.9559
5.9481
5.4791
5.4713
5.4458
5.4380
4.9747
4.4083
4.3810
4.3630
3.4902
3.4735
3.4131
3.0932
3.0709
3.0508
3.0285
1.5677
1.5404
1.5128
1.4116
1.3902
1.3679
1.3109
1.2861
1.2632
1.2596
[rel]
1H NMR, 300 MHz, (CD3)2SO at 120 °C
H2O (3.33 ppm)
(CH3)2SO (2.50 ppm)
0.9214
9.7733
0.8513
0.9743
0.9639
0.9616
2.0000
0.9643
7.6952
2.1895
1.9739
1.8889
1.9306
10
8
6
4
2
[ppm]

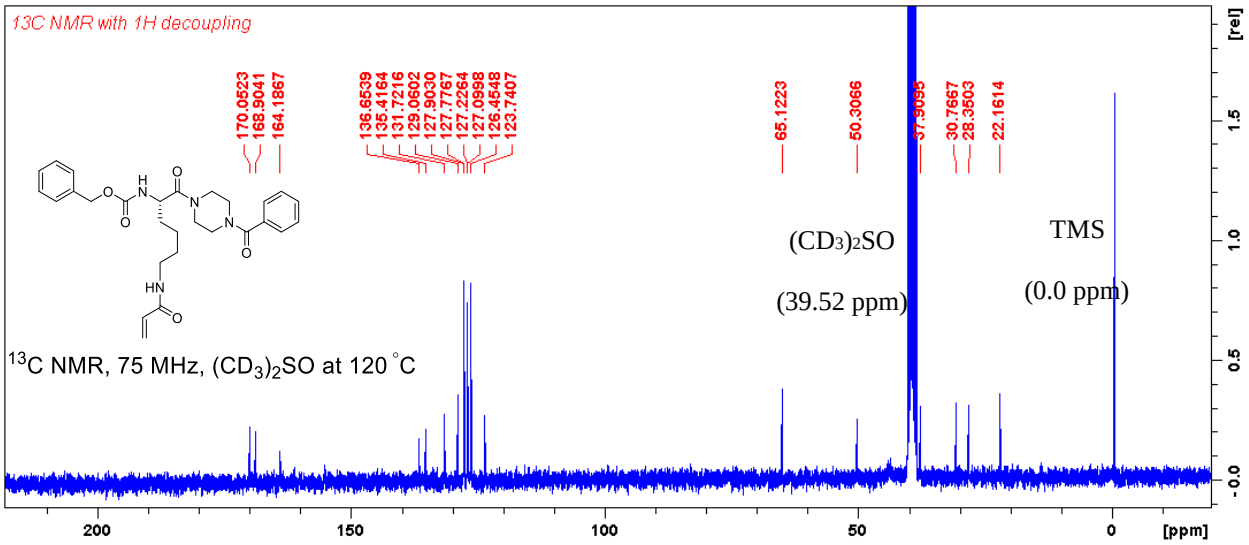
13C NMR with 1H decoupling
170.0523
168.9041
164.1867
136.6539
135.4164
131.7216
129.0602
127.9030
127.7767
127.2264
127.0988
126.4548
123.7407
65.1223
50.3066
37.9095
30.7667
28.3503
22.1614
[rel]
(CD3)2SO
(39.52 ppm)
TMS
(0.0 ppm)
13C NMR, 75 MHz, (CD3)2SO at 120 °C
200
150
100
50
0
[ppm]

Compound 27

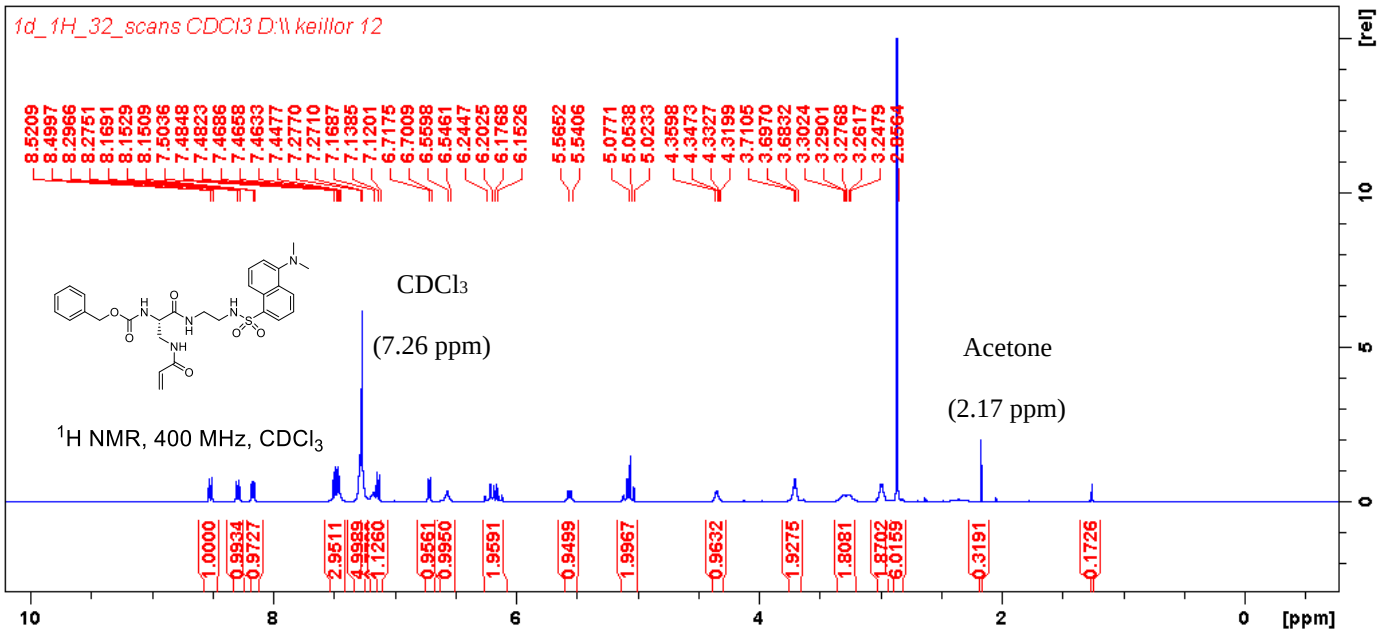
1d_1H_32_scans CDCl3 D:\\ keillor 12
CDCl3
(7.26 ppm)
Acetone
(2.17 ppm)
1H NMR, 400 MHz, CDCl3
[rel]
[ppm]

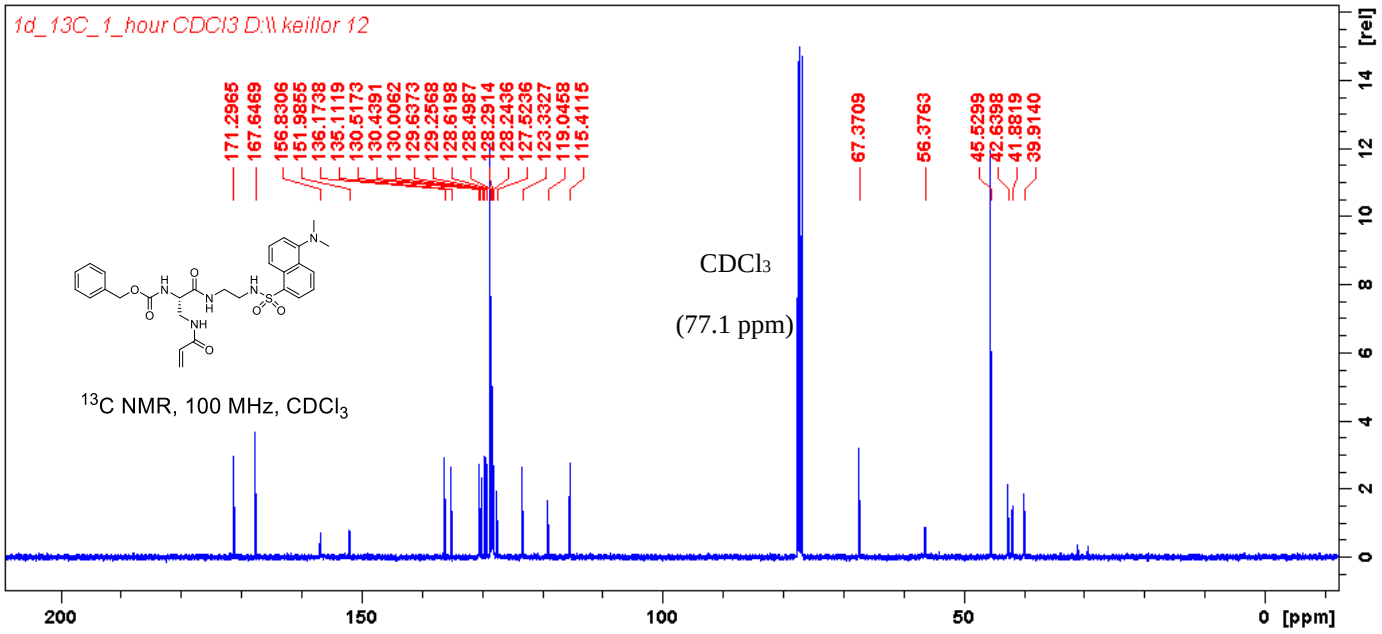
1d_13C_1_hour CDCl3 D:\\ keillor 12
CDCl3
(77.1 ppm)
13C NMR, 100 MHz, CDCl3
[rel]
[ppm]

Compound 26

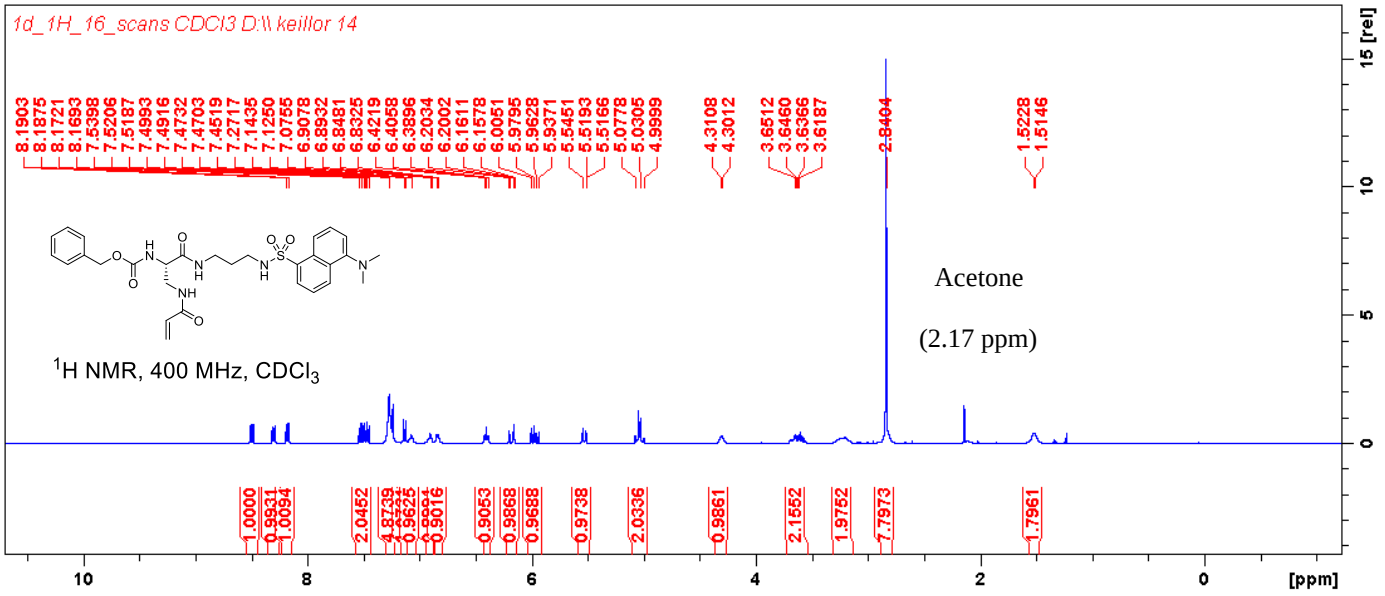
1d_1H_16_scans CDCl3 D:\\ keillor 14
8.1903
8.1875
8.1721
8.1683
7.5398
7.5206
7.5187
7.4993
7.4916
7.4732
7.4703
7.4519
7.2717
7.1435
7.1250
7.0755
6.9078
6.8932
6.8481
6.8325
6.4219
6.4058
6.3896
6.2034
6.2002
6.1611
6.1578
6.0051
5.9795
5.9628
5.9371
5.5451
5.5193
5.5166
5.0778
5.0305
4.9999
4.3108
4.3012
3.6512
3.6460
3.6366
3.6187
2.8404
1.5228
1.5146
Acetone
(2.17 ppm)
1H NMR, 400 MHz, CDCl3
1.0000
0.9831
1.0094
2.0452
4.8739
0.9625
0.9804
0.9016
0.9053
0.9868
0.9688
0.9738
2.0336
0.9861
2.1552
1.9752
7.7973
1.7961
10
8
6
4
2
0
[ppm]
15 [rel]
10
5
0

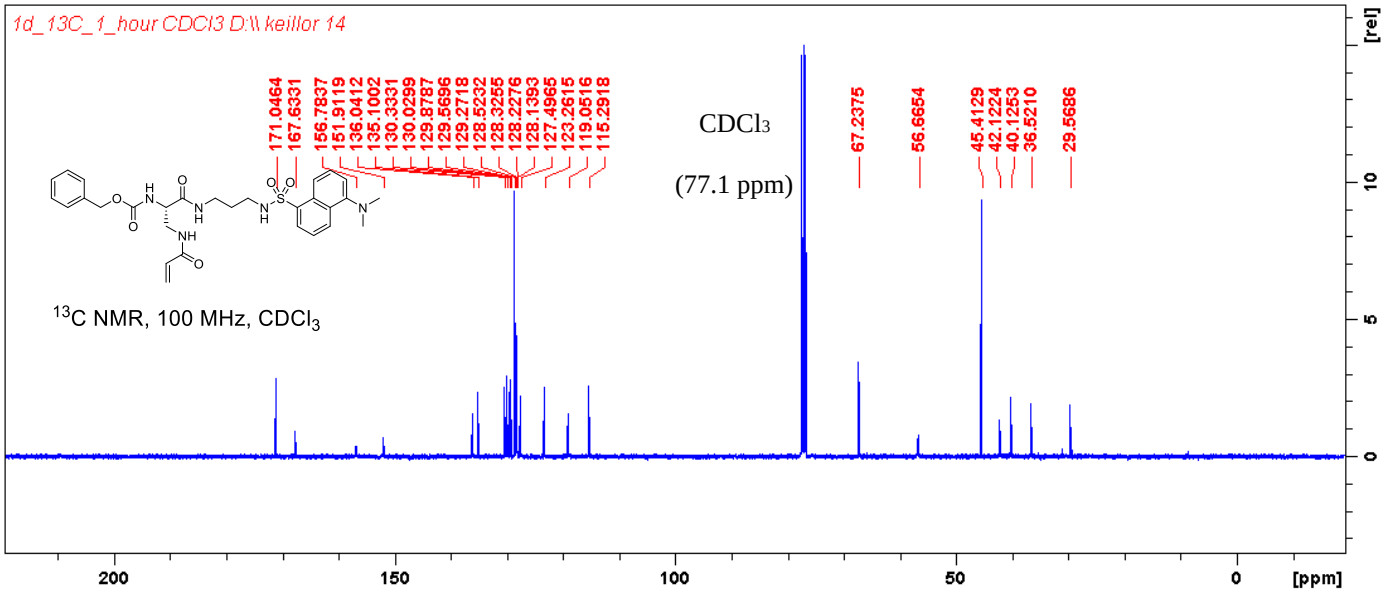
1d_13C_1_hour CDCl3 D:\\ keillor 14
171.0464
167.6331
156.7837
151.9119
136.0412
135.1002
130.3331
130.0299
129.8787
129.5696
129.2718
128.5232
128.3255
128.2276
128.1393
127.4965
123.2615
119.0516
115.2918
CDCl3
(77.1 ppm)
67.2375
56.6654
45.4129
42.1224
40.1253
36.5210
29.5686
13C NMR, 100 MHz, CDCl3
200
150
100
50
0
[ppm]
[rel]
10
5
0

Compound 25

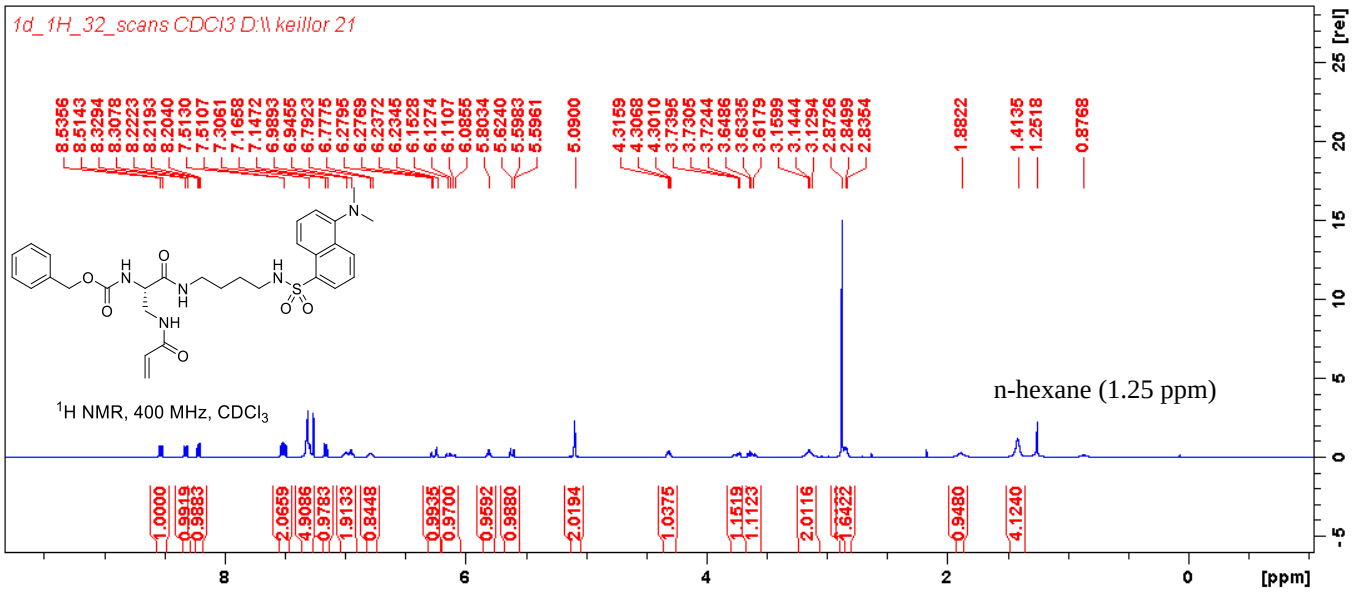
1d_1H_32_scans CDCl3 D:\\ keillor 21
8.5356
8.5143
8.3294
8.3078
8.2223
8.2193
8.2040
7.5130
7.5107
7.3061
7.1658
7.1472
6.9893
6.9455
6.7923
6.7775
6.2795
6.2769
6.2372
6.2345
6.1528
6.1274
6.1107
6.0855
5.8034
5.6240
5.5983
5.5961
5.0900
4.3159
4.3068
4.3010
3.7395
3.7305
3.7244
3.6486
3.6335
3.6179
3.1599
3.1444
3.1294
2.8726
2.8499
2.8354
1.8822
1.4135
1.2518
0.8768
n-hexane (1.25 ppm)
1H NMR, 400 MHz, CDCl3
1.0000
0.9919
0.9883
2.0659
4.9086
0.9783
1.9133
0.8448
0.9535
0.9700
0.9592
0.9880
2.0194
1.0375
1.1519
1.1123
2.0116
1.6422
0.9480
4.1240
[ppm]
[rel]

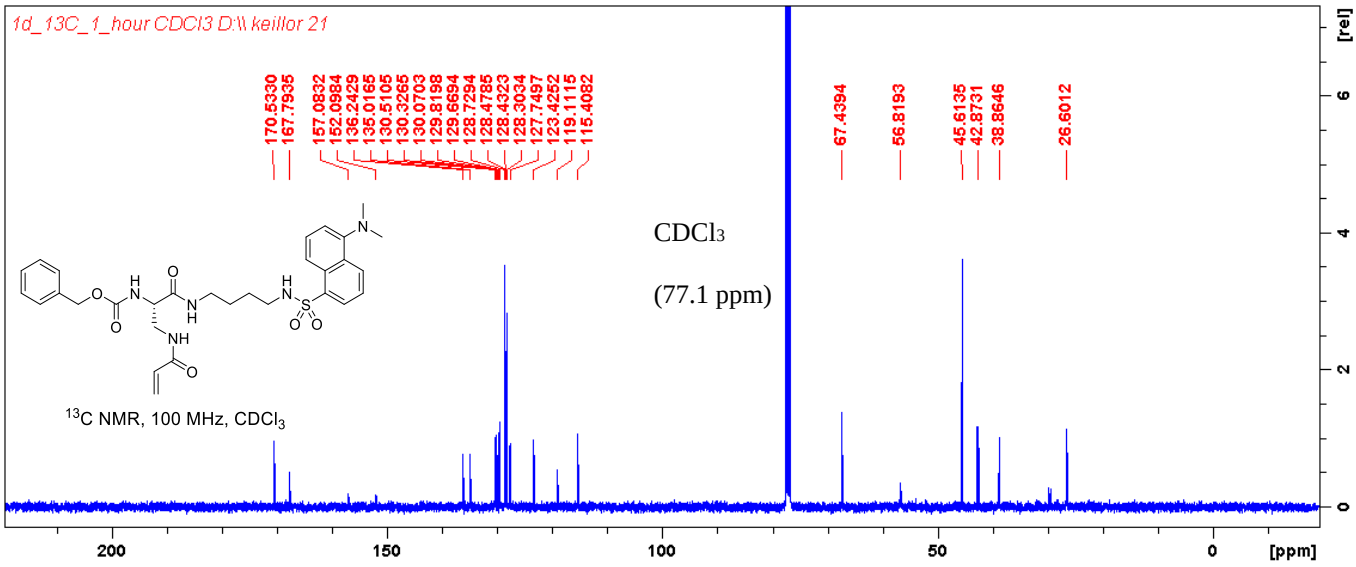
1d_13C_1_hour CDCl3 D:\\ keillor 21
170.5330
167.7935
157.0832
152.0984
136.2429
135.0165
130.5105
130.3265
130.0703
129.8198
129.6694
128.7294
128.4785
128.4323
128.3034
127.7497
123.4252
119.1115
115.4082
67.4394
56.8193
45.6135
42.8731
38.8646
26.6012
CDCl3
(77.1 ppm)
13C NMR, 100 MHz, CDCl3
[ppm]
[rel]

Compound 28

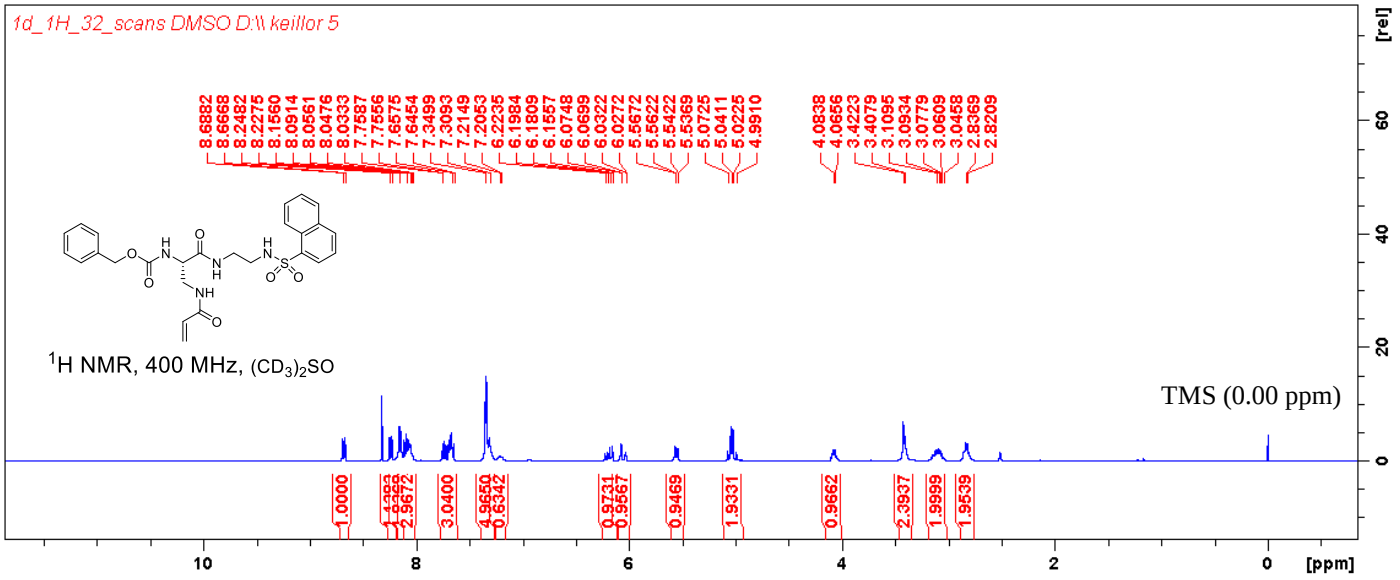
1d_1H_32_scans DMSO D:\\ keillor 5
8.6882
8.6668
8.2482
8.2275
8.1560
8.0914
8.0561
8.0476
8.0333
7.7587
7.7556
7.6575
7.6454
7.3499
7.3093
7.2149
7.2053
6.2235
6.1984
6.1809
6.1557
6.0748
6.0699
6.0322
6.0272
5.5672
5.5622
5.5422
5.5369
5.0725
5.0411
5.0225
4.9910
4.0838
4.0656
3.4223
3.4079
3.1095
3.0934
3.0779
3.0609
3.0458
2.8369
2.8209
1H NMR, 400 MHz, (CD3)2SO
TMS (0.00 ppm)
1.0000
1.4393
2.9672
3.0400
4.9650
0.6342
0.9731
0.9567
0.9469
1.9331
0.9662
2.3937
1.9999
1.9539
10
8
6
4
2
0
[ppm]
[rel]

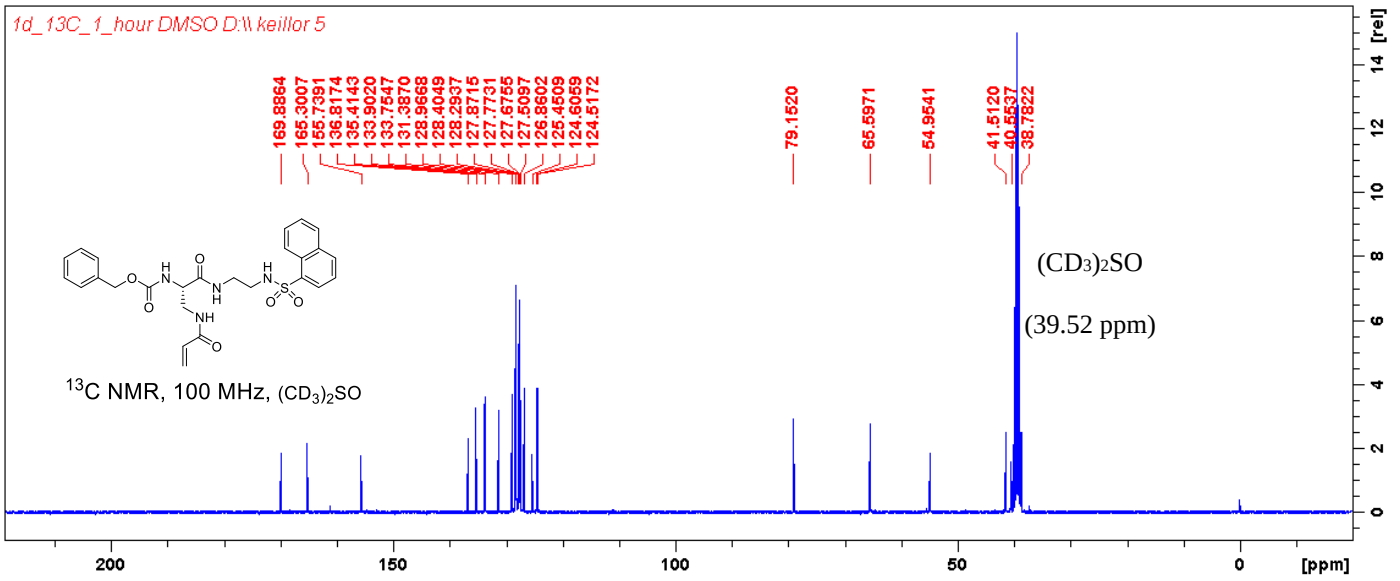
1d_13C_1_hour DMSO D:\\ keillor 5
169.8864
165.3007
155.7391
136.8174
135.4143
133.9020
133.7547
131.3870
128.9668
128.4049
128.2937
127.8715
127.7731
127.6755
127.5097
126.8602
125.4509
124.6059
124.5172
79.1520
65.5971
54.9541
41.5120
40.5537
38.7822
13C NMR, 100 MHz, (CD3)2SO
(CD3)2SO
(39.52 ppm)
200
150
100
50
0
[ppm]
[rel]

Compound 29

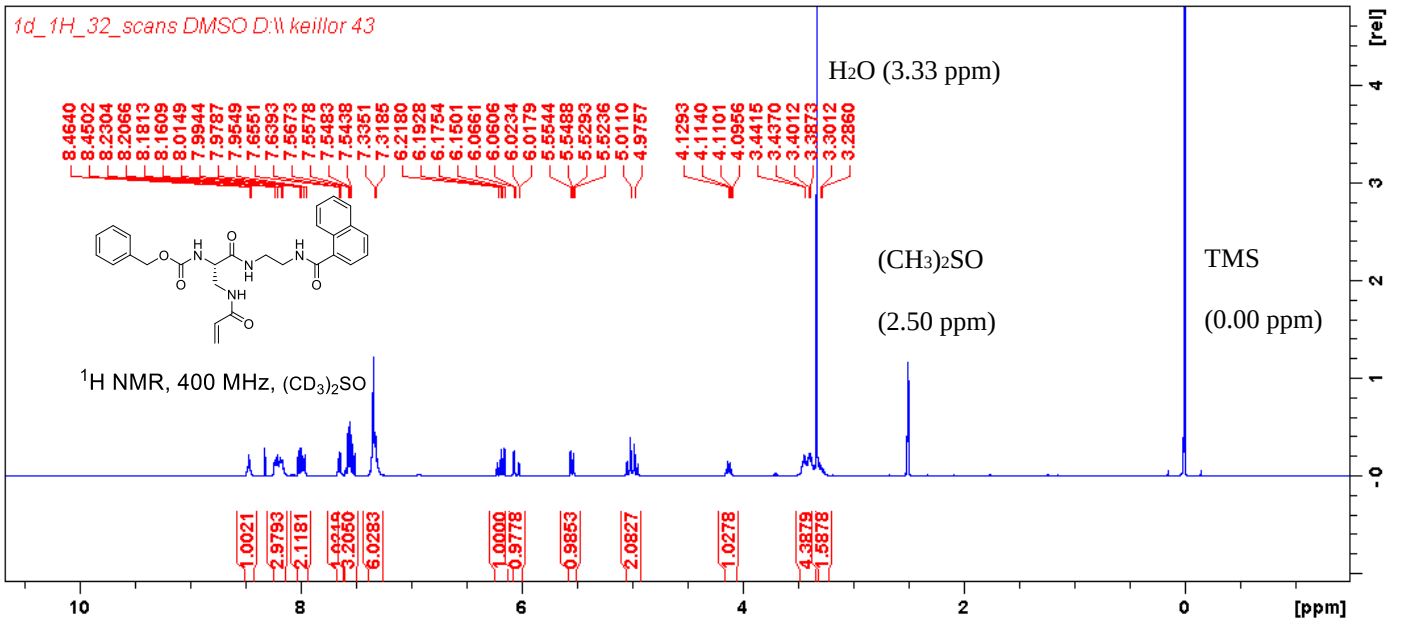
1d_1H_32_scans DMSO D:\\ keillor 43
H2O (3.33 ppm)
(CH3)2SO
(2.50 ppm)
TMS
(0.00 ppm)
1H NMR, 400 MHz, (CD3)2SO
[rel]
[ppm]

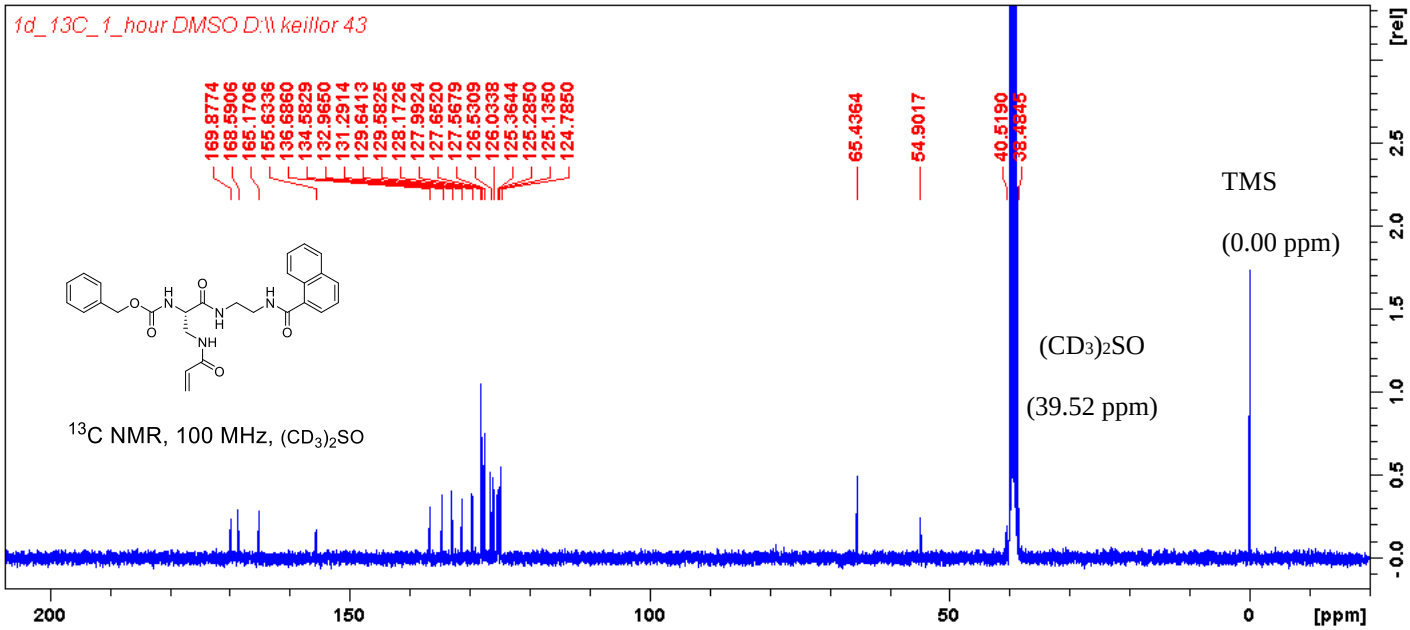
1d_13C_1_hour DMSO D:\\ keillor 43
TMS
(0.00 ppm)
(CD3)2SO
(39.52 ppm)
13C NMR, 100 MHz, (CD3)2SO
[rel]
[ppm]

Compound 30

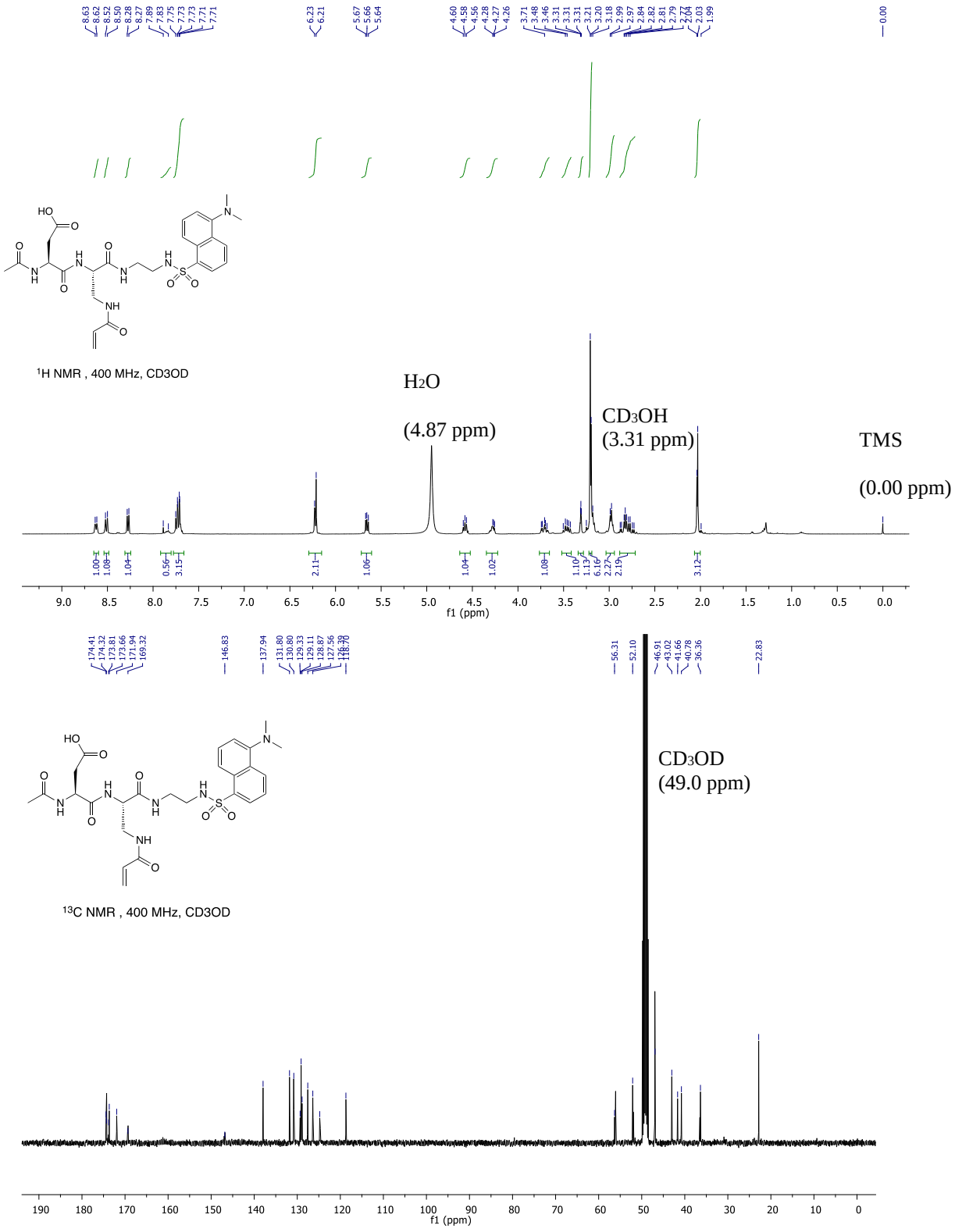
^{1}H NMR , 400 MHz, CD3OD
H2O
(4.87 ppm)
CD3OH
(3.31 ppm)
TMS
(0.00 ppm)
f1 (ppm)
^{13}C NMR , 400 MHz, CD3OD
CD3OD
(49.0 ppm)
f1 (ppm)

Appendix II

Determination of kinetic parameters for AL5 as substrate

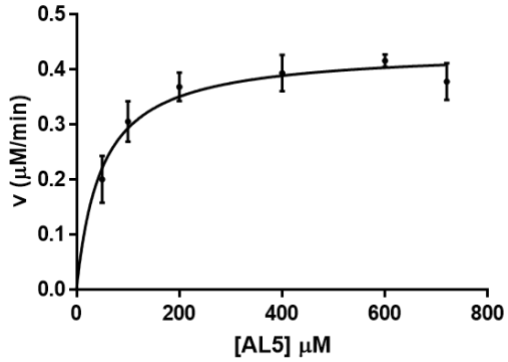

K_M (μM) = 48.6 ± 10.3

k_{cat} (min^{-1}) = 4.37 ± 0.18

k_{cat}/K_M ($\mu M^{-1}\ min^{-1}$) = 0.08 ± 0.02

Figure S1. Michaelis-Menten analysis of **AL5** with hTG1.

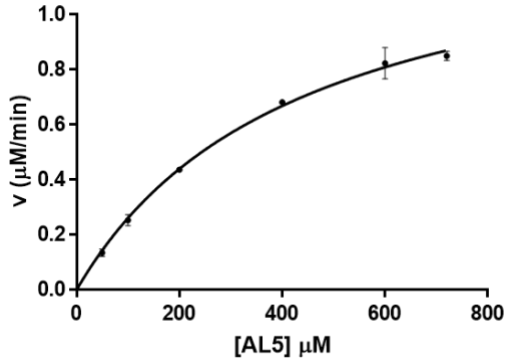

K_M (μM) = 434.6 ± 37.8

k_{cat} (min^{-1}) = 13.9 ± 0.58

k_{cat}/K_M ($\mu M^{-1}\ min^{-1}$) = 0.03 ± 0.003

Figure S2. Michaelis-Menten analysis of **AL5** with hTG6.

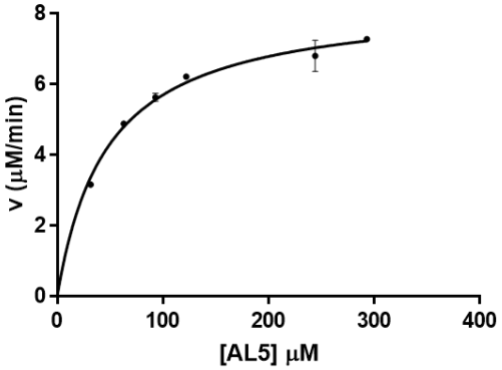

K_M (μM) = 47.2 ± 4.7

k_{cat} (min^{-1}) = 35.6 ± 0.96

k_{cat}/K_M ($\mu M^{-1}\ min^{-1}$) = 0.71 ± 0.07

Figure S3. Michaelis-Menten analysis of **AL5** with hTG2.

Appendix III

k_{obs} vs [I] data from the colorimetric AL5 assay

Structure of inhibitor (I)	k_{obs} vs [I] plot
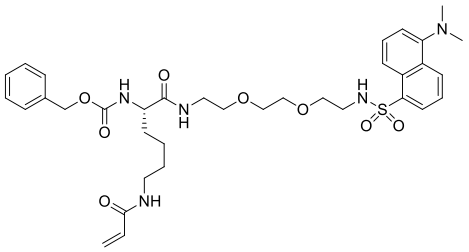 NC9	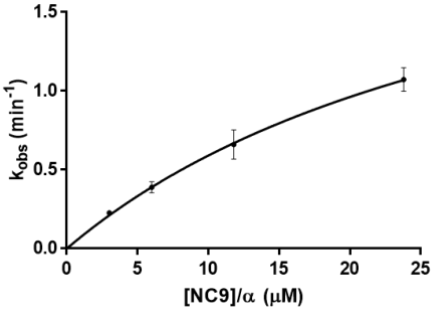
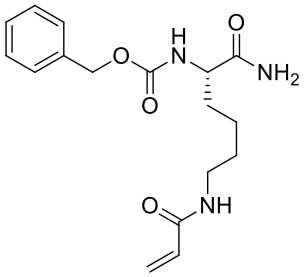 Compound 10	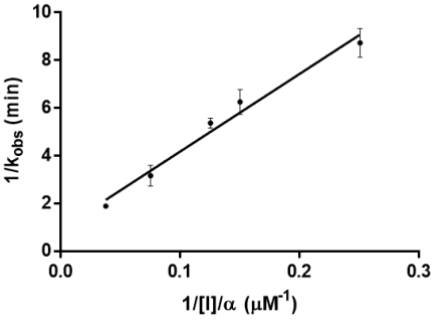
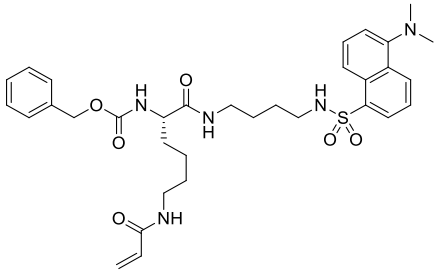 Compound 12	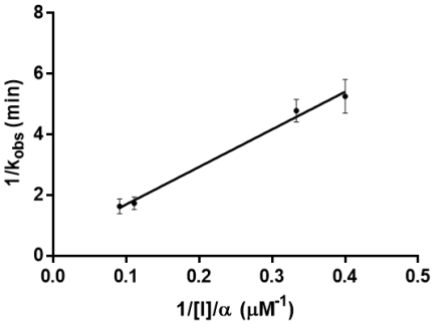

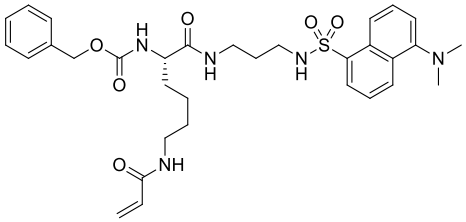

Compound 13

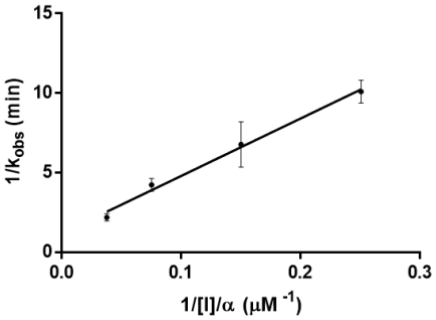

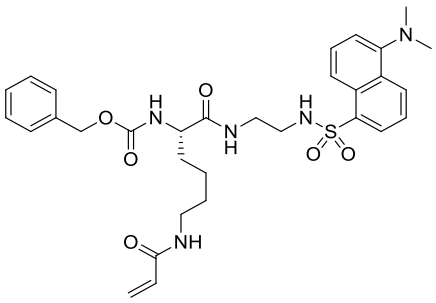

Compound 14

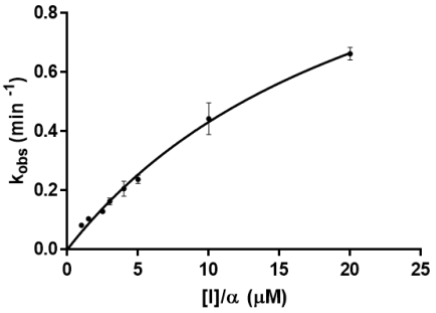

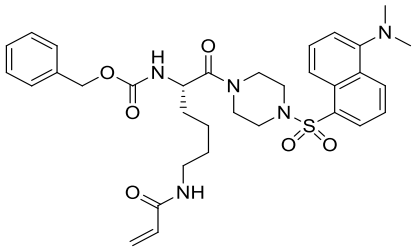

Compound 15 (VA4)

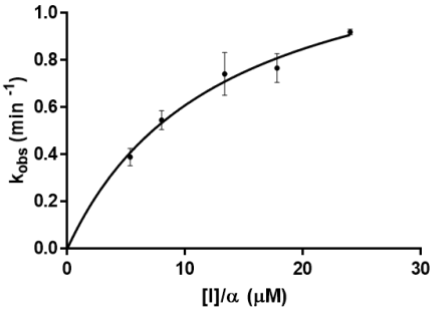

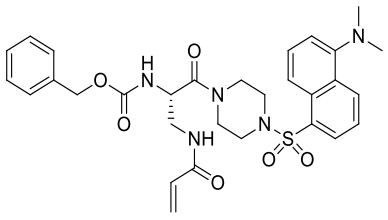

Compound 16

No inhibition detected at 18 μM of inhibitor; see Figure 3.3

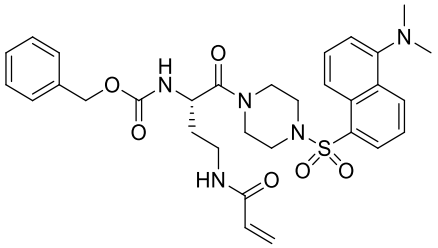

Compound 17

No inhibition detected at 18 μM of inhibitor; see Figure 3.3

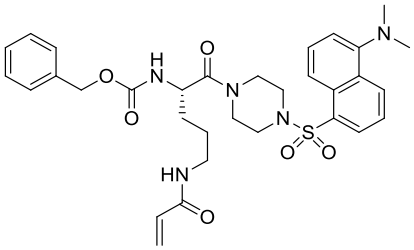

Compound 18

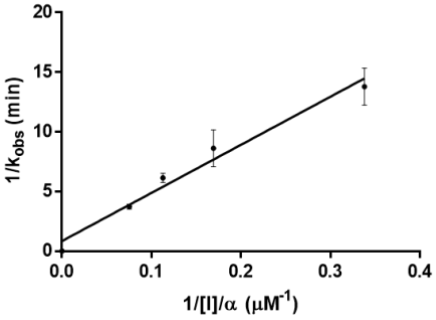

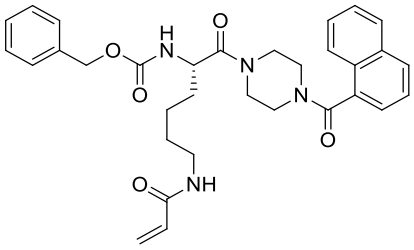

Compound 22 (AA9)

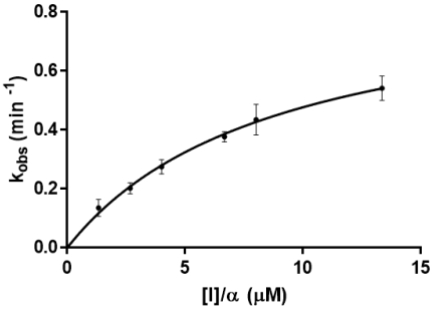

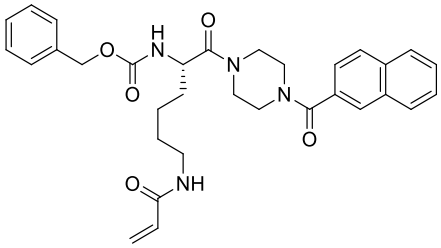

Compound 23 (AA10)

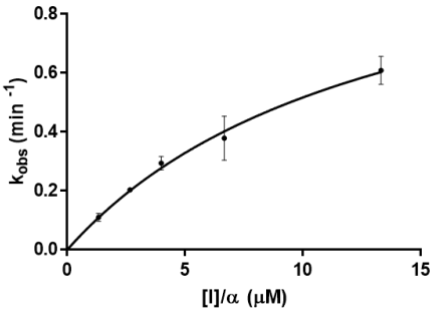

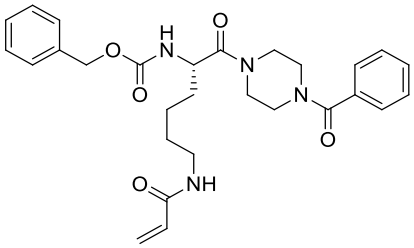

Compound 24

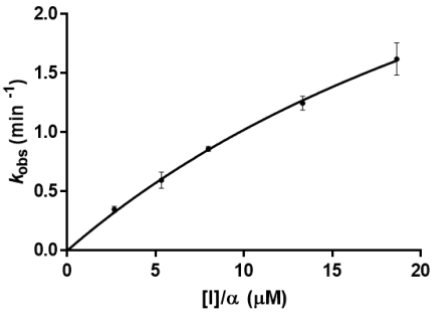

Appendix IV

GTP Binding Assay Results

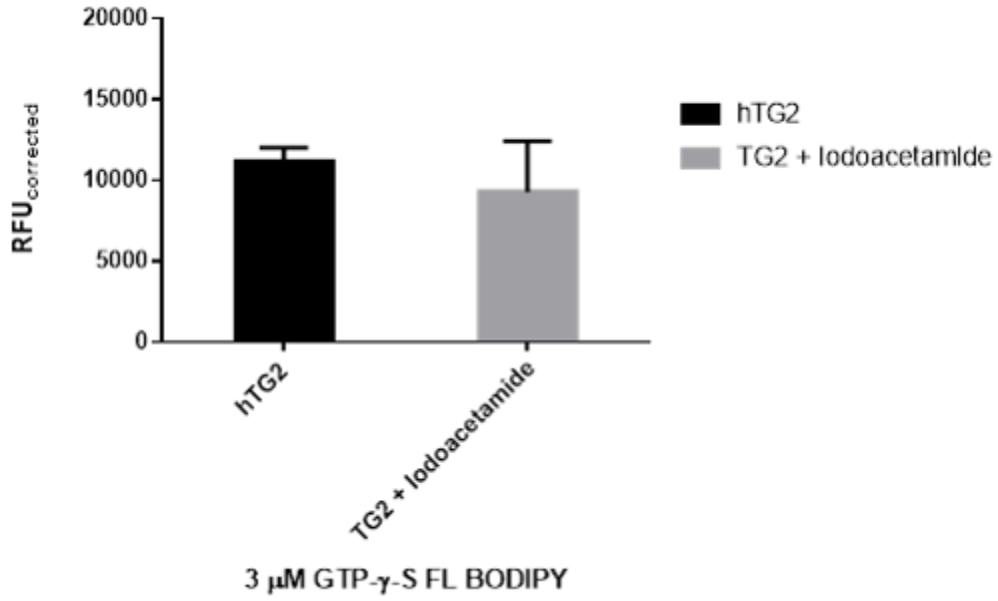

Figure S4. Iodoacetamide, a non-selective inhibitor of acyltransferases, does not abolish the GTP binding ability of hTG2.

Appendix V

TGase isoform selectivity results

I) Determination of inhibition rate constant (k_{obs}) for inactivation of hTG1

A

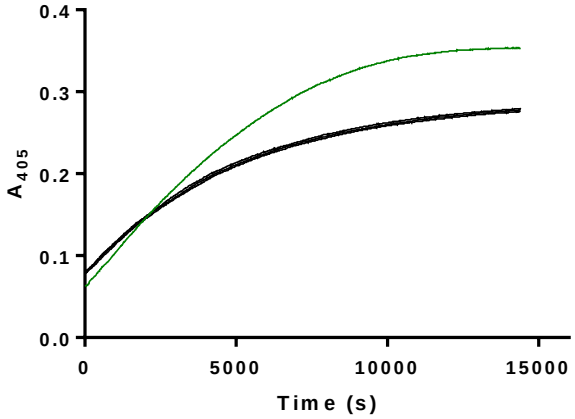

B

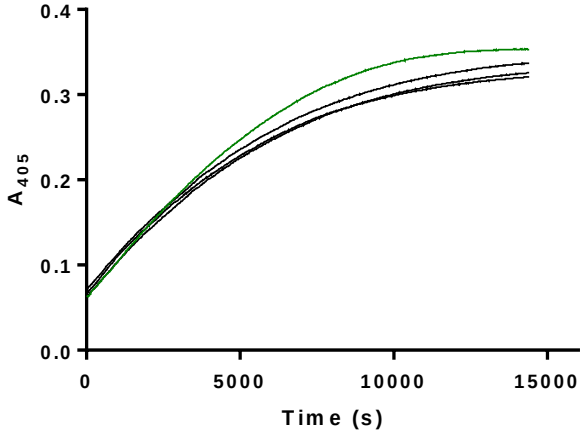

Figure S5. Time-dependent inactivation curves of hTG1 with substrate **AL5** (112 µM). Green line represents 0 µM of inhibitor. Black lines represent 20 µM **VA4** (A) and **NC9** (B).

II) Determination of inhibition rate constant (k_{obs}) for inactivation of hTG3a

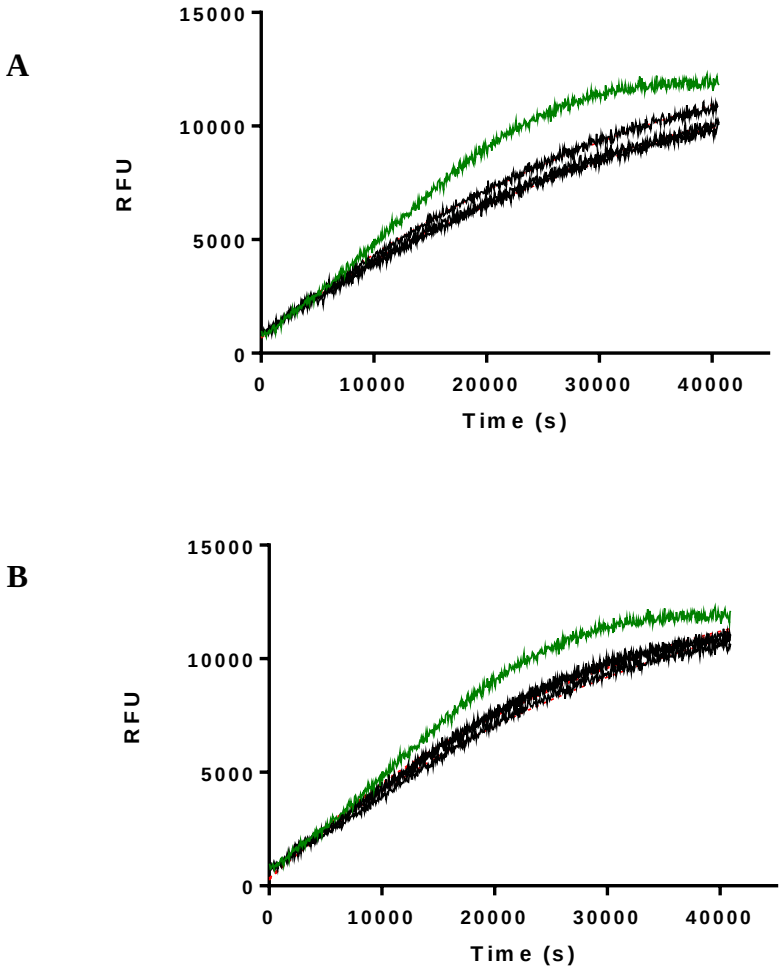

Figure S6. Time-dependent inactivation curves of hTG3a with substrate **A101** (50 µM). Green line represents 0 µM of inhibitor. Black lines represent 39 µM **VA4** (A) and **NC9** (B).

III) Determination of inhibition rate constant (k_{obs}) for inactivation of hTG6

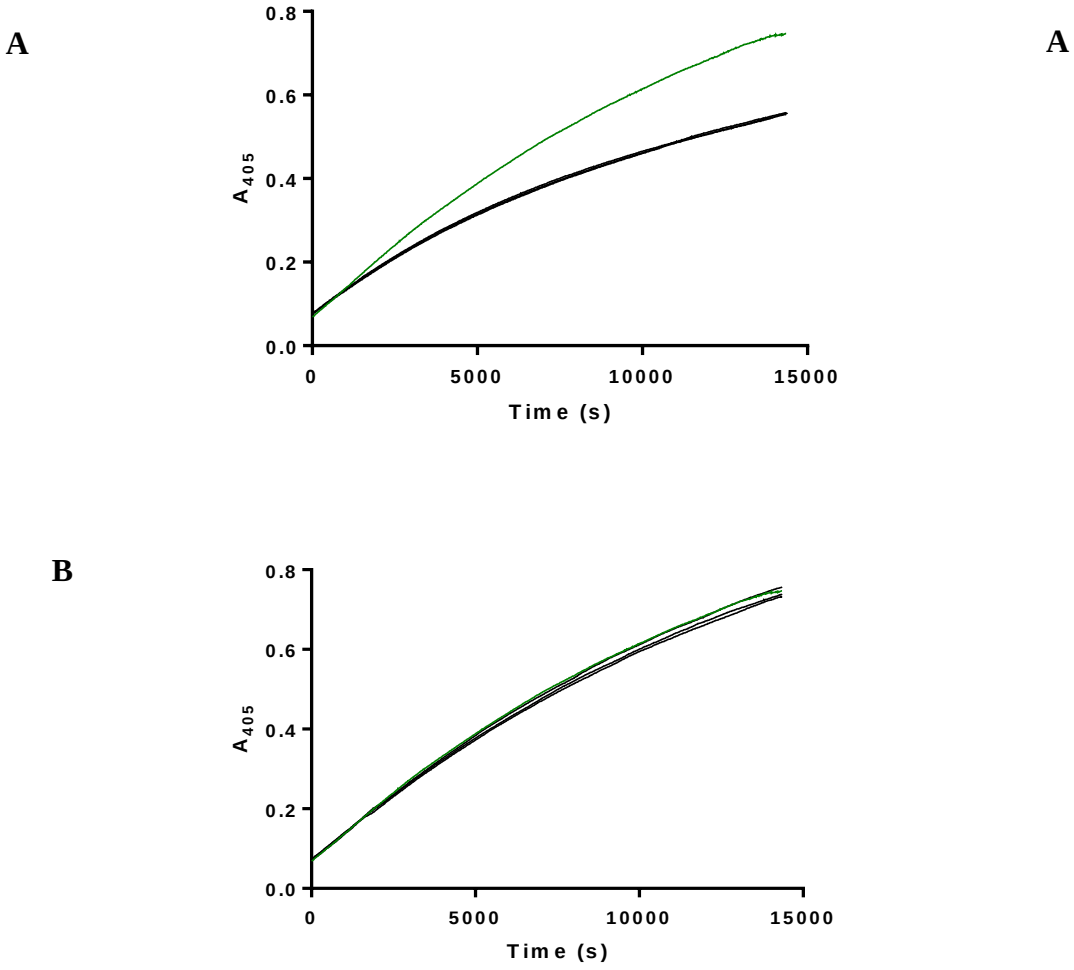

Figure S7. Time-dependent inactivation curves of hTG1 with substrate **AL5** (436 µM). Green line represents 0 µM of inhibitor. Black lines represent 12 µM **VA4** (A) and **NC9** (B).

IV) Determination of inhibition rate constant (k_{obs}) for inactivation of FXIIIa

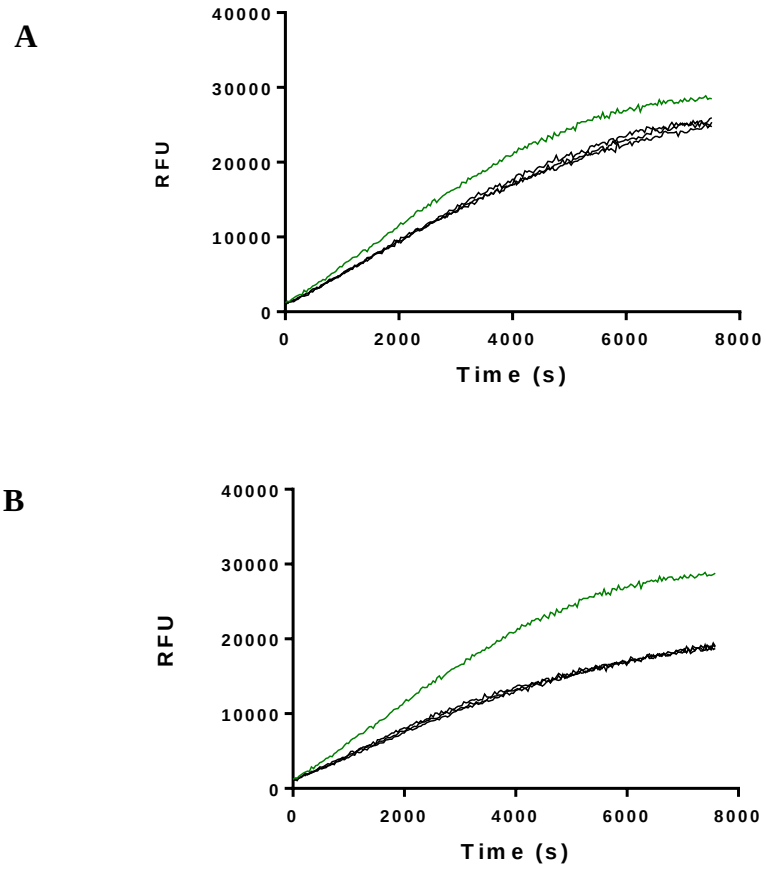

Figure S8. Time-dependent inactivation curves of FXIIIa with substrate **A101** (50 μM). Green line represents 0 μM of inhibitor. Black lines represent 28 μM **VA4** (A) and **NC9** (B).

Appendix VI

Normalized Dixon plots results for hTG2 and hFXIIIa

Structure of inhibitor (I)	v_0/v vs [I]/α plot
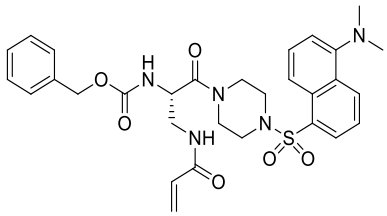 Compound 16	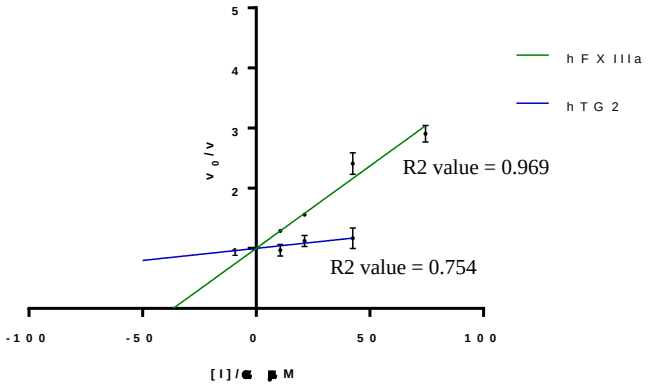

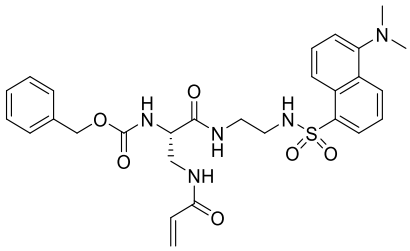

Compound 27

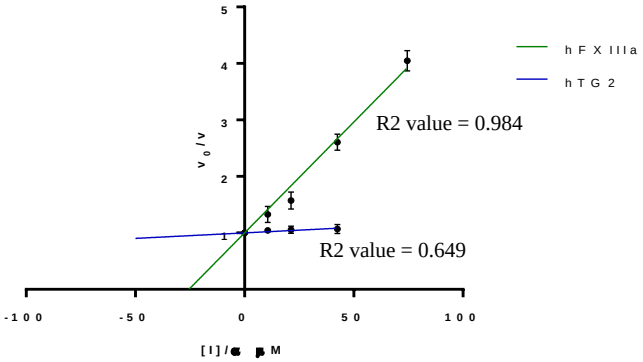

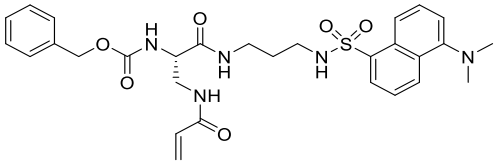

Compound 26

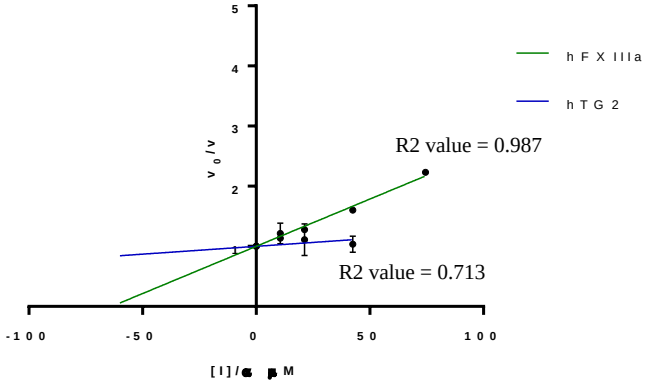

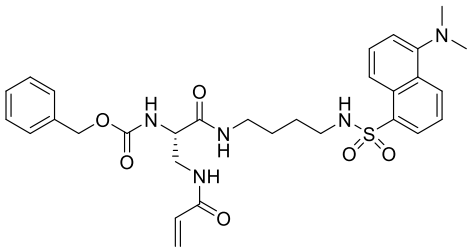

Compound 25

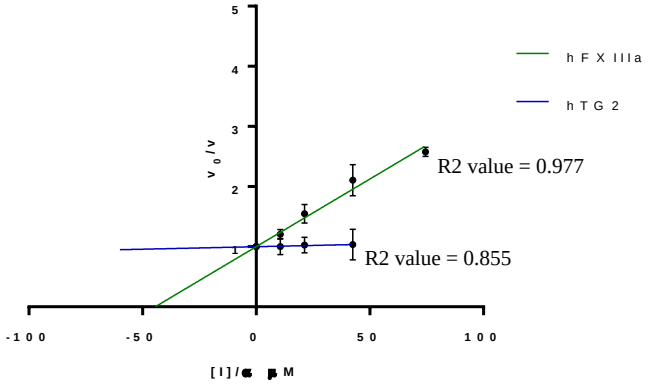

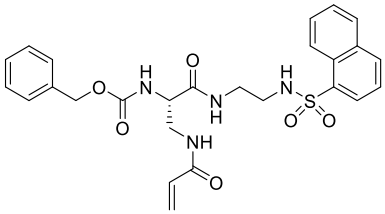

Compound 28

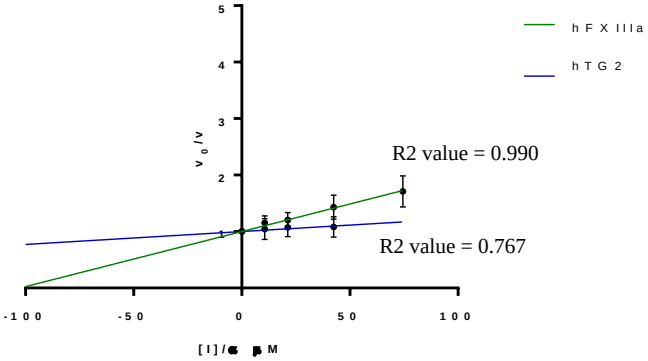

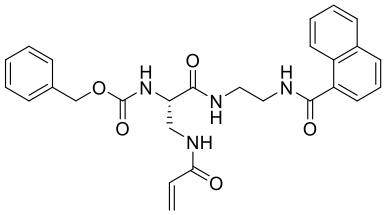

Compound 29

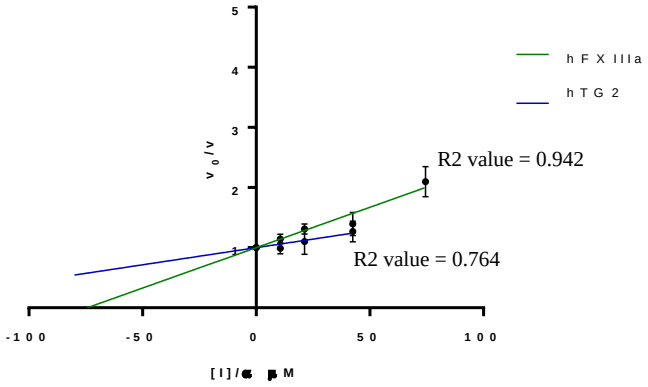

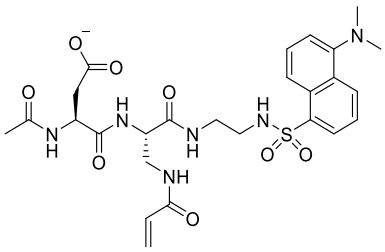

Compound 30